Design and fabrication of a climate-controlled lysimeter and testing of new controlled-release fertilisers

A thesis presented in partial fulfilment of the

requirements for the degree of

Doctor of Philosophy (PhD)

In

Agricultural Engineering and Environmental Sciences

at Massey University, Palmerston North,

New Zealand

Abhiram Gunaratnam

2021

ABSTRACT

Pastoral agriculture is the backbone of the New Zealand (NZ) economy and nearly 9 million hectares of land (33% of the total land area in NZ) is under pastoral farming. The higher and continuous applications of readily available N fertilisers to pastoral land use increase nitrogen (N) losses, which degrade the water and air quality. Controlled-release fertilisers (CRFs) have been shown to be an effective strategy to mitigate N losses in many parts of the world. This study was undertaken to develop different CRF formulations and test their effect on ryegrass under a simulated climate condition.

A new controlled-environment lysimeter system was designed and fabricated, since lysimeter designs available in the literature are not suitable to conduct a controlled-environment study. The lysimeter was permanently capped to provide a confined space for controlling the microclimate of ryegrass, and equipped with sensors to monitor the environmental variables. An environmental controlling unit (ECU) was designed to emulate a climate model and control the environmental variables in the lysimeter. Taranaki region's (spring season of the year 2013) climate model was selected to emulate in this design. The ECU modifies the ambient air according to the climate model and circulates it through 40 lysimeters using air conduits and distributors. The ryegrass was grown for three months under simulated climate conditions, and DM yield was measured. In addition, microclimate temperature, relative humidity (RH), evapotranspiration and drainage of each lysimeter during the experimental period were recorded. The performance of the ECU was tested by comparing the observed temperature and RH values of the plant proximity with setpoints of the climate model. In addition, the performance of the lysimeter system on recreating the climate model was tested by comparing the observed drainage, evapotranspiration, and DM yield values with the estimated values derived from the climate model. The root-mean-square error (RMSE) of temperature was 1.96 °C day^{-1}, which was marginally higher than the targeted temperature variation range of 1 °C day^{-1}. However, the RMSE of RH was 4.45% day^{-1}, which was within the targeted fluctuation range of 5% day^{-1}. These observations showed that the ECU satisfactorily controlled the environmental variables as per the climate model. The observed drainage,

evapotranspiration and total DM yield were within the estimated values; 525 mm, 104 mm and 2167 kg-DM ha^{-1}, respectively. These results revealed that the selected Taranaki climate model was successfully emulated in the newly developed lysimeter system design.

A low-cost, simple lysimeter soil retriever (LSR) design was fabricated to retrieve the soil, and its performance was examined. The soil moisture influenced the retrieval process, where lower disturbances for soil block structure and roots were observed for soil with high moisture (28%) than low moisture (13%). The linear actuator used in this design was powerful enough to perform soil retrieval and showed consistent performance after 80 soil columns were retrieved. Force given by the linear actuator did not damage the lysimeter body, but was sufficient to push the soil column out of the lysimeter. Therefore, this design is suitable to retrieve soil blocks from mini (<100 kg) and small (100-1000 kg) lysimeters.

Different forms of CRFs were developed by coating urea with epoxy-lignite (Epox) or polyester-lignite (Poly) polymer composites. Each composite was coated three or five times, and therefore four CRFs were formulated depending on the type of composite and coating thickness; Epox3, Epox5, Poly3, and Poly5. The complete release of urea took place at 144, 408, 120 and 175 hours for Epox3, Epox5, Poly3 and Poly5, respectively, in water. Increasing the coating thickness prolonged the duration of urea release for both composites. Although no cracks were identified in all the CRF coatings, micropores were seen under high magnification in the scanning electron microscopy (SEM) images. The interactions between lignite and polymer were demonstrated using Fourier Transform Infrared Spectroscopy (FTIR) analysis. The lignite dominated in all coatings compared to the polymer, and lignite compositions were 2.1 to 5.3-fold higher than polymers in CRFs. The Epox5 showed overall better performance than other formulations.

The CRF formulations which showed more controlled-release characteristics in water; Epox5 and Poly5, were selected to study their performance on ryegrass against urea and diammonium phosphate (DAP) in the climate-controlled lysimeter system. The total DM yield, root DM distribution, herbage N recovery and nitrogen utilisation efficiencies (NUE) were not significantly different between

N treatments. Although N_2O emission and nitrate leaching losses were not significantly different between N treatments, the values were very low in comparison to the values obtained in similar studies reported in the literature. An investigation was carried out to find out the reason for these observed low N_2O and nitrate levels with different hypotheses. The only hypothesis tested that showed a significant relationship with these observed results; the high iron content of sand could have decreased the nitrate in leachate and N_2O emission. In this study, a 2 x 4 factorial design was used with two types of sand (low and high iron sand) and four N levels (0, 50, 100 and 200 kg-N ha^{-1}). It was found that high iron sand significantly lowered ($P<0.05$) the nitrate leaching at all N levels compared to low iron sand, except for the 0 kg-N ha^{-1} treatment. The N_2O emission was significantly lower ($P<0.05$) for high iron sand than low iron sand, only at the 200 kg-N ha^{-1} application level. These observations support the hypothesis, that iron is involved in nitrate reduction and the possible mechanism was dissimilatory nitrate reduction (DNR) pathway.

A new controlled-release fertiliser (Ver-1) was developed by Verum Group Ltd using lignite and urea. In this study, the effectiveness of two different types of CRFs (Epox5 and Ver-1) and two levels of iron application (239 and 478 kg-$FeSO_4$ ha^{-1}) on controlling N losses were tested in lysimeters where ryegrass was grown. The Epox5 and Ver-1 significantly ($P<0.05$) reduced N leaching losses by 37% and 47%, respectively, whereas only Epox5 significantly ($P<0.05$) increased N_2O emission compared to the urea treatment. Iron treatments were not effective in controlling N losses, which suggests that the expected DNR pathway was not prominent in this study. The DM yield and NUE were not significantly increased by CRFs and iron applications compared to the urea treatment. The hierarchical clustering analysis revealed that Ver-1 was the best treatment for controlling N leaching losses.

Future research is recommended to investigate (a) the mechanism which underlies the reduction of nitrate in high iron content sand, (b) the effectiveness of iron application on N leaching losses on different soils, and (c) the performance of new CRFs formulations (Epox5 and Ver-1) at the field level.

ACKNOWLEDGEMENTS

I'm sincerely thankful to the Ministry of Business, Innovation and Employment (MBIE) for the financial support for this study and for awarding the Doctoral scholarship for pursuing a PhD attached to Massey University, New Zealand.

I'm highly obligated to Uva Wellassa University, Sri Lanka for granting me the study leave for conducting my PhD studies.

I'm pleased to extend my gratitude to my primary supervisor, Dr Miles Grafton, for recruiting me as a PhD candidate, his excellent supervision, support to improve my writing skills, advice, and guidance throughout my doctoral study.

It is my pleasure to express my gratefulness to my co-supervisor, Dr Paramsothy Jeyakumar, for his great supervision, confidence boost, advice, scientific inputs, moral support, and helped to improve my writing skills. Apart from supervision, as a compatriot, his support during my difficulties and downtimes were invaluable.

I'm also grateful to my co-supervisor, Dr Peter Bishop, for his supervision, kind words, guidance for laboratory work, technical advice, valuable comments and inputs for my PhD research work and thesis.

I must be thankful to my co-supervisor, Prof Clive Davies, for the supervision, advice, appreciation for my hard work and critical comments on the research and thesis which have enriched the quality of this work.

I'm very much grateful to my co-supervisor Dr Murray McCurdy for his supervision during my research work in Verum Group, Lower Hutt, who gave a helping hand with my research work during my visit to my home country, being a mentor and gave me freedom for my research work and space for my research ideas.

I thank all the Verum Group staff members who gave moral support to me during my research there. I express my special thanks to Rod Brown, Ben Rumsey, Simon Zhang, and Trevor Dine for their assistance in several research activities.

Thank you to Mr Ian Furkert and Mr Bob Toes for their technical support in the laboratory analysis. I acknowledged the administrative support given by Fiona Bardell, Sharon Wright and Tara Penketh.

I’m thankful to the Kathleen Spragg Agricultural Research Trust for granting me the scholarship to participate in the APSIM workshop in Australia.

I’m indeed thankful to the Sri Lankan community in Lower Hutt and Palmerston North for helping me in various ways, especially for their hospitality. My special thanks to Jayamohan & Valarmathy, Jeyakumar & Vitheky, Sivarajan & Malar and Suthakaran & Vanajah for supporting my stay in New Zealand.

Lastly, but most importantly, I express my immense gratitude to my family members. I’m indebted to my lovely wife Briyangari, who took all the responsibility to look after my daughter from the age of three weeks in my absence and supported me in all possible ways to keep me on PhD track in the long three-year separation. My little princess Kiruthanja was always an inspiration for me and her sweet words helped me to overcome all kinds of stress. I extend my gratitude to my parents, parents-in-law, sister, brother-in-law, niece and nephew for their support throughout my PhD career.

TABLE OF CONTENTS

LIST OF FIGURES

LIST OF TABLES

Chapter 1

Introduction

1.1. Overview of the study and Justification

Meeting the increasing food demand that results from an increasing world population is a challenge as there is limited farming land to produce food on. More intensive agriculture has provided the solution to date, to a large extent, however, the use of high inputs with advanced management practices in intensive farming creates adverse environmental effects (Fenemor and Robb, 2001; Hubbard et al., 2004). For example, higher fertilisation input rates under intensive farming lead to nutrient loss to the environment. These often contaminate water resources and release greenhouse gases (GHG) to the atmosphere when application rates exceed the plant attenuation ability and carrying capacity of the farmland.

Sheep, beef and dairy cattle are the key pastoral farming systems in New Zealand, where 31.9% of the total land area is used for sheep and beef farming followed by dairying at 9.8% (Stats NZ, 2018). In the last few decades due to the intensification of the pastoral farming sector (mainly in the dairy sector), fertiliser and supplementary feed input rates have increased significantly. Dairy farmers are incentivised to apply high nitrogen application rates to increase milk solids income by providing good quality pasture for the animals (Harris et al., 1996). For instance, nitrogen fertiliser application in New Zealand has increased 4-fold during the period from 1990 to 2015 (Fertilizer Association - New Zealand, 2019). In addition to synthetic nitrogen fertilisers, biological fixation of nitrogen by legume-pasture based farming systems (Brock et al., 1989; Goh and Bruce, 2005), excreta from animal (urine and dung) and effluent application (Saggar et al., 2004) are other sources of nitrogen to the farmland. However, increasing nitrogen fertilisation can increase the pasture yield only up to the economic optimum level and anything beyond that potentially increases losses (Cameron et al., 2013).

The major losses of nitrogen fertilisers occur through leaching (nitrate-NO_3^-), volatilisation (ammonia-NH_3) and denitrification (nitrous oxide-N_2O, nitric oxide-NO and nitrogen-N_2) (Oenema, 2006; Schipper et al., 2010; Stevenson et al., 2010). The nitrogen leaching losses may eventually end up in water bodies and degrade the quality of drinking water which risks human health (Höring and Chapman, 2004), and incurs higher maintenance costs to enhance the quality of water resources (Dell, 2006; MacGibbon et al., 2010). A nationwide study reported that Waikato, Manawatu-Wanganui and Canterbury regions showed the highest nitrate leaching losses at nearly 35, 20 and 20 million kg-NO_3-N yr^{-1}, respectively (Dymond et al., 2013). Dairying has been identified as the main source of nitrogen losses to fresh and coastal water (Scarsbrook and Melland, 2015).

New Zealand holds the third position for per capita GHG emissions worldwide since the ratio between livestock and human population is very high (Luo et al., 2019). In New Zealand, the agriculture sector is the largest contributor to nitrous oxide emissions, wherein animal excreta and N-fertilisers account for 80% and 14% of agricultural emissions, respectively (de Klein and Ledgard, 2005). The New Zealand government has set a goal to achieve a carbon zero state by 2050 (Ministry for the Environment, 2018). As a result, the dairy industry is facing an enormous challenge to mitigate the environmental consequences while sustaining high productivity. Hence, increasing nitrogen use efficiency (NUE) is an immediate task to control nitrogen losses and their negative environmental effects (Shaviv and Mikkelsen, 1993).

The inefficiency of fertiliser use is associated with a lack of synchronisation of plant demand and supply. Conventional nitrogen fertilisers release surplus amounts of ammonium or nitrate to the soil in a short period from the application which are not fully utilised by the plant. The excess of ammonium is potentially volatile and nitrate leaches as it is highly mobile due to its high solubility and low affinity to soil. Controlled-release-nitrogen fertilisers (CRNFs) prolong the release time of nitrogen to the soil thus have the potential to improve the NUE and minimise the losses. Although CRNFs are tested often on field crops such as maize (Diez et al., 1994), potato (Zvomuya et al., 2003), vegetables (Simonne and Hutchinson, 2005), only a few attempts have been made to test the

performance of CRNFs on pasture in other countries (Bowman and Paul, 1991; Shaviv, 1996; Garcia et al., 1997) and in New Zealand (Steele and Dawson, 1980; Bishop et al., 2008; Edmeades, 2015). For example, polyurethane-coated-controlled-release urea (5 and 7% coating) significantly increased the dry matter yield and NUE of Italian ryegrass while reducing nitrate leaching losses by nearly 78% compared to urea in a field trial (Bishop et al., 2008). Two slow-releasing fertilisers; Isobutylidenediurea and Organiform, were tested on ryegrass and they did not significantly increase the ryegrass DM yield compared to a single application of urea (Steele and Dawson, 1980).

Controlled environment lysimeter studies have been conducted in greenhouses or phytotrons as there are no climate-controlled lysimeter systems available. However, the studies under greenhouse or phytotron consume a high amount of energy since the climate controls a large space. Further, exactly emulating a climate and precisely controlling the microclimate to each experimental unit is very difficult with these facilities. Controlling the temperature in a greenhouse is challenging because the spatial variation of temperature across the greenhouse is high (Bucklin et al., 1993; Ganguly and Ghosh, 2011). Therefore, a climate-controlled lysimeter system for iterative testing of new controlled-release fertiliser formulations is essential with a simple climate-controlled mechanism. This study aimed to develop a climate-controlled lysimeter system and test the new controlled-release fertilisers in comparison to standard nitrogen fertilisers on pastoral land use in New Zealand.

1.2 Research focus and thesis structure

The overall objective of this research was to develop an innovative climate-controlled lysimeter system for testing new CRF formulations on ryegrass in comparison with other commercially available standard N fertilisers.

The specific objectives of the study were as follows;

1. To design and develop a new lysimeter system that can emulate a climate model for iterative testing of newly developed controlled-release fertilisers under a controlled environment (Chapter 3).
2. To evaluate the performance of the newly developed lysimeter system in emulating a challenging climate model in terms of temperature, relative humidity, drainage, evapotranspiration and dry matter yield (Chapter 3).
3. To develop a simple and low-cost lysimeter soil retriever design to retrieve the soil blocks from the lysimeter with minimum disturbances (Chapter 4).
4. To develop and characterise polymer-lignite composite coated controlled-release nitrogen fertiliser formulations (Chapter 5).
5. To compare the performance of newly developed controlled-release nitrogen fertilisers against the commercially available conventional nitrogen fertilisers (Chapter 6 and 7).

Chapter 2

Literature review

2.1. Environmental consequences of N fertiliser application and possible mitigations

2.1.1. Nitrogen losses through N-cycle

Nitrogen, phosphorus, potassium, calcium, magnesium and sulphur are the major essential plant nutrients. Nitrogen is important for vegetative plant growth and its uptake is in comparably large quantities (Haygarth and Jarvis, 2002). The natural level of nitrogen in the soil is very limited, 1 mg-N kg^{-1} or less (Novoa and Loomis, 1981). Additional nitrogen supplements need to be provided for plants to get the maximum growth rates and yields to their genetic potential. However, a major portion of the applied N-fertilisers is lost to the environment (20 - 70% of the applied amount) due to their high mobility in soil (Naz and Sulaiman, 2016). As a result, conventional N-fertilisers show poor nitrogen utilization efficiency (NUE).

A better understanding of the N-cycle helps to improve the NUE and minimise the losses to the environment. The nitrogen losses take place through volatilisation, erosion, runoff, leaching and denitrification process (Cameron et al., 2013) (Figure 2.1). Ammonia volatilises from the soil, and agricultural practices contribute 14% of total NH_3 released in New Zealand (Bishop and Manning, 2010). Many factors such as atmospheric and soil temperature, pH, ammonium concentration and cation exchange capacity of soil contribute to the rate of ammonium volatilisation (Cameron et al., 2013).

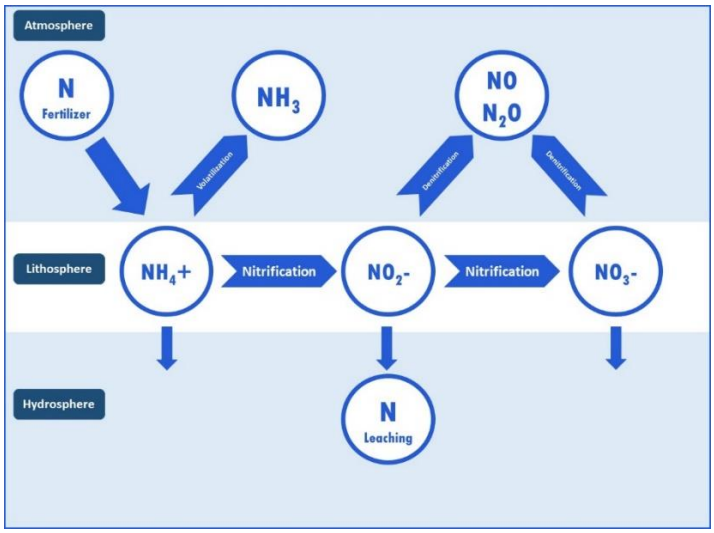

Figure 2.1. The fate of nitrogen fertiliser in ecosphere.

Nitrite (NO_2^-) and Nitrate (NO_3^-) ions are the products of the nitrification process in which ammonium ions are oxidized to nitrite and then finally to nitrate. The second reaction rate is higher than first, thus nitrite rarely presents in soil (Cameron et al., 2013). The negatively charged nitrate ion is repulsed by negatively charged soil minerals. The main binding sites for nitrate in the soils are Al and Fe oxy-hydroxides. However, this is very weak under most NZ soil pH conditions (5-7). Therefore, a limited amount of NO_3^- ions bind with clay minerals and organic compounds in the soil, and the majority of the nitrate is in soil solution (Shuford et al., 1977). Once a rainfall or irrigation event occurs, the nitrates in soil solution transit through the soil profile and reach the groundwater or any other surface water bodies. This leaching process is influenced by the NO_3^- ion concentration of soil (amount of nitrogen applied to the soil and nitrification rate), amount of drainage, season and climate, and soil texture and structure (Cameron et al., 2013). Nitrate leaching losses are usually greatest during late autumn, winter and early spring months when plant uptake of nitrate is low and drainage of water is high (Wild and Cameron, 1980). The contribution of ammonium ions to nitrogen leaching loss is minimal when compared to nitrate as positively charged ammonium has more affinity to the soil minerals and organic matter.

Elevated levels of nitrate in drinking water can be harmful to humans via food chain, and may cause methemoglobinemia (blue baby disease) (Greer and

Shannon, 2005). A high rate of leaching of nitrate into streams or lakes contributes to eutrophication. Nutrient release from grazing pasture lands is particularly high, discharging 5 to 10 times more nutrient compared to other croplands and forest lands (Harris and Clark, 1996). Di and Cameron (2000) produced a semi-empirical model for New Zealand that found urea application rates have to be below 390-392 kg-N ha^{-1} for cut and carry and 62-192 kg-N ha^{-1} for grazed pastures, to avoid nitrogen concentrations in drainage water reaching critical drinking water hazard standard level of 11.3 mg-N L^{-1}. In addition to the losses of leached nitrogen , gaseous losses occur through both nitrification and denitrification processes.

Denitrification reactions are carried out by heterotrophic bacteria through several enzymatic pathways. The denitrification of nitrate and nitrite produces nitrogen (N_2), nitrous oxide (N_2O) and nitric oxide (NO) gases. This process is favoured by anaerobic conditions and high soil carbon content (an energy source for microbes); however, the end products depend on the availability of oxygen. The increasing anaerobic condition promotes the release of N_2 gas, but less anaerobic condition favours the release of NO (Hahn and Junge, 1977). Nitrous oxide is one of the main contributor to the greenhouse effect (300 times greater global warming potential than CO_2) and depletes the ozone layer (Cameron et al., 2013). Agricultural activities contribute to 62% of the total N_2O emissions globally, around 4.2 Tg-N yr^{-1} (Thomson et al., 2012). The denitrification process is governed by the soil characteristics such as temperature, oxygen level, moisture, pH, available nitrogen and organic matter content (Chirinda et al., 2011; Cameron et al., 2013). The release of N_2O gases from New Zealand pastoral soils is shown in Table 2.1.

Table 2.1. The selected recent studies for the N leaching losses and N_2O emissions from pastoral soil applied with conventional N-fertilisers in New Zealand (N/A – not available).

Fertiliser	Application rate (kg-N ha^{-1})	Soil type	Type of pasture	Leaching losses	N_2O emission (kgN_2O-N ha^{-1})	Location in New Zealand	Reference
Urea	50	Pukemutu silt loam	Ryegrass & white clover mix	N/A	1 – 3.74 kg- N ha^{-1} measurement $period^{-1}$	Invercargill.	Smith et al. (2008)
Urea	400 kg-N ha^{-1} yr^{-1}	course loamy, mixed mesic	Ryegrass & white clover mix	10 kg-N ha^{-1} yr^{-1}		Lincoln	Silva et al. (2005)
Urea	50	Pukemutu argillic-mottled Fragic Pallic soil	Ryegrass & white clover mix	7.1 – 15.5 kg-N ha^{-1} yr^{-1}	N/A	Invercargill	Monaghan et al. (2009)
Urea	100, 200 & 400 kg-N ha^{-1} yr^{-1}	Fleming silt loam	N/A	34, 46 & 56 kg-N/ha, respective for N application rate	N/A	Edendale	Monaghan et al. (2000)
Urea	150	Horotiu sandy loam	Ryegrass & white clover mix	0.1315 kg-N ha^{-1}	2.4	Hamilton	Zaman et al. (2008)
DAP	150	Horotiu sandy loam	Ryegrass & white clover mix	0.702 kg-N ha^{-1}	2.2	Hamilton	Zaman et al. (2008)
Urea	150	Tokomaru silt loam	Italian ryegrass	~ 7 kg-N ha^{-1}	N/A	Palmerston North	Bishop et al. (2008)
Urea	50	Kowhai silt loam soil	Ryegrass & white clover mix	N/A	0 - 0.78	Hamilton	Luo et al. (2007)
Urea	50	Horotiu silt loam	Ryegrass & white clover mix	N/A	0.451	Waikato	Van der Weerden et al. (2016)
Urea	50	Karapoti fine sandy loam	Ryegrass & white clover mix	N/A	0.78	Manawatu	Van der Weerden et al. (2016)
Urea	50	Templeton fine sandy loam	Ryegrass & white clover mix	N/A	0.094	Canterbury	Van der Weerden et al. (2016)
Urea	50	Wingatui deep silt loam	Ryegrass & white clover mix	N/A	0.003	Otago	Van der Weerden et al. (2016)

Since urea is the primary N-fertiliser source in New Zealand, a number of studies were reported on the effect of urea application on leaching and gaseous losses (Table 2.1). However, nitrogen losses with the application of di-ammonium phosphate (DAP) have not been extensively studied (Zaman et al., 2008).

The results of different studies with the same application rate of urea showed that the leaching losses and nitrous oxide emission depend on climate condition and soil characteristics (Table 2.1). For example, different studies conducted at different sites; Hamilton (Zaman et al., 2008) and Palmerston North (Bishop et al., 2008), with 150 kg-N ha^{-1} urea application rate exhibited different leaching losses. The highest leaching losses were observed in Palmerston North study where the total drainage (116 mm) was higher than Hamilton study (33.14 mm) and free drainage lysimeters used in Palmerston North study induced more drainage. Similarly, a study conducted at four different sites (Waikato, Manawatu, Canterbury and Otago) with a same urea application rate (50 kg-N ha^{-1}) produced different N_2O emission ranged from 0.003 - 0.78 kg-N_2O-N ha^{-1}. These results indicated that leaching losses are not only influenced by the fertilisation rate but also depend on multiple factors such as soil and climate. However, many studies (conducted at the same site) proved that increasing N-fertiliser application rate increases the risk of potential leaching losses (Ledgard et al., 1996; Monaghan et al., 2000; Wachendorf et al., 2004) and nitrous oxide emission (Petersen et al., 2004; Bell et al., 2016).

2.1.2. The economic optimum level of N fertiliser application rate for ryegrass

Fertilisers applied to arable and pastoral situations are not fully utilised by the crops. A significant part of the unused fertiliser is retained in the soil as residual nitrogen that is susceptible to leaching and volatilisation loss in subsequent seasons. Every crop has an economic optimum level of N application that is enough to get the optimum yield of its genetic potential, when other factors are not limiting growth. Further application beyond this level decreases the economic return and fertiliser use efficiency. For example, a study conducted in Netherlands

(Lantinga et al., 1999) showed that the economic optimum level of N application rate for ryegrass was around 550 kg-N ha^{-1} and the corresponding yield was around 15 ton-DM ha^{-1} (Figure 2.2).

Mitchell (1963) established a theoretical maximum dry matter production from a ryegrass and clover pasture at 22.5 tonnes DM ha^{-1}. Improved pasture cultivars, trialled by Crush et al. (2006) found that diploid and tetraploid cultivars produced similar quantities of dry matter, little over 17 tonnes DM ha^{-1} on average for each of the four years the trial continued. High dry matter yields are possible only in high fertility pastures, failure to maintain fertility will result in high yielding grasses being replaced by low yielding species, which will replace them in low fertility situations.

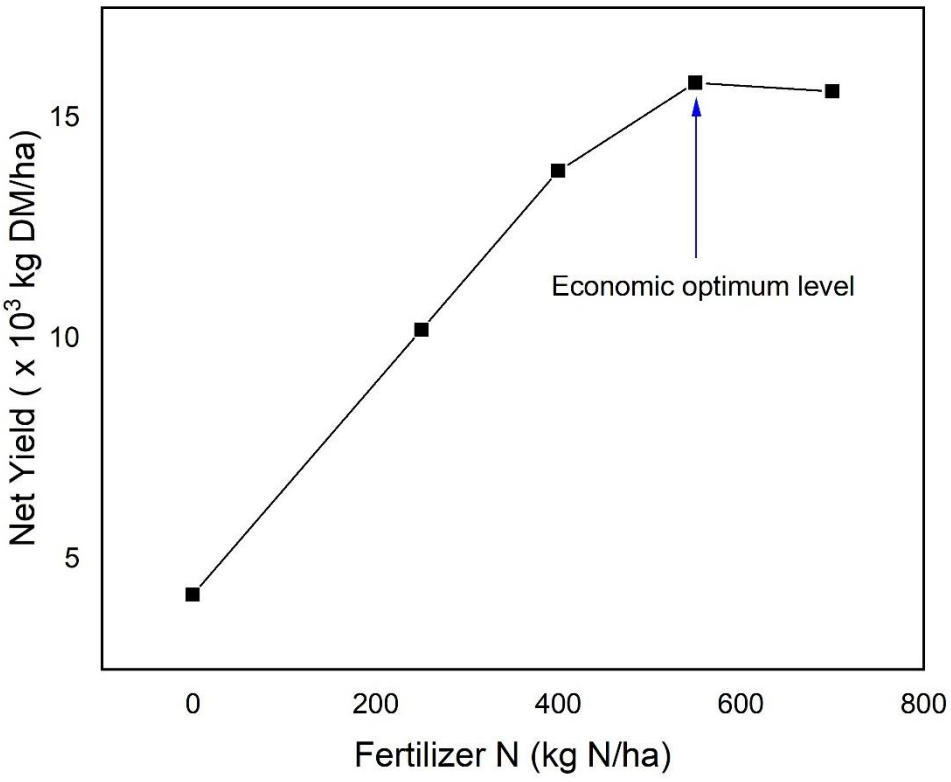

Figure 2.2. The effect of N-fertiliser on the net yield of ryegrass on sandy soil. The yield increased up to 550 kg-N ha^{-1} (economic optimum level), then decreased beyond that (adapted from Lantinga et al. (1999)).

In a Scottish study, 23 different nitrogen rates from 0 to 897 kg-N ha^{-1} were applied on ryegrass with clover (RGC) and without clover mix (RG) and DM yields were measured over a three year period (Reid, 1972). Both RG and RGC showed a linear DM yield increment for nitrogen application rates up to 336 kg-N ha^{-1} for the first two years and 280 kg-N ha^{-1} for the third year. The RGC showed significantly higher yield than RG for all three years. Beyond these N-levels, the yield responses were small and curvilinear, and for high application rates, no significant yield differences were observed between RG and RGC. The nitrogen response of both RG and RGC decreased over the period and the author suggested to apply 140 kg-N ha^{-1} to get a consistent annual DM yield.

2.1.3. The environmental and health impacts of nitrogen losses

Anthropogenic reactive nitrogen loading is the primary element in polluting groundwater drinking water sources. Nitrate (NO_3^-) contamination of lakes and groundwater is a growing problem in New Zealand (Burden, 1982; Spalding and Exner, 1993). The NO_3-N from fertilisers and urine patches may be washed off and through the soil profile by excess irrigation or by rain and contaminate water bodies. Whereas, leached NO_3^- ions through the vadose zone to groundwater reservoirs may pollute drinking water. High concentrations of NO_3^- in drinking water can cause methemoglobinemia (blue baby disease), hypertension, infant mortality, goitre, stomach cancer, thyroid disorder, cytogenetic defects, (Sahoo et al., 2016) and birth defects, and nitrite may act as a carcinogenic agent. High loading rates of nitrate into streams or lakes contributes to eutrophication. Due to this degradation of water quality, many waterbodies have reached unacceptable condition for drinking and recreational purposes (Cameron et al., 2002).

The Water Research Center (2020) in the USA recommended that nitrate concentrations of 10 mg L^{-1} or above (equivalent to 44.3 mg-NO_3^- L^{-1}) in drinking water is not suitable for human consumption. In New Zealand, the corresponding drinking water standard for nitrate is 11.3 mg L^{-1} (McLay et al., 2001). The nitrate trigger value (the management action taken level) for Upland and Lowland rivers are 167 and 444 µg-N L^{-1}, respectively. A study in the Waikato region with 88

drinking water sites reported that 9% of these water resources had already reached levels above the standard nitrate level (McLay et al., 2001).

Apart from health risk for humans, poor water quality impacts on livestock health as well. For optimum production and high fertility, good quality water is important for livestock (Anzecc, 2000). A high concentration of nitrate-N in water can cause loss of appetite (Shukla and Saxena, 2018) and can even be fatal (Anzecc, 2000). The threshold level of nitrate in livestock drinking water is 400 mg L^{-1}, however, any level beyond 1500 mg L^{-1} is toxic for livestock. The nitrite threshold level for livestock is 30 mg L^{-1} (Anzecc, 2000).

2.1.4. Different approaches for controlling the nitrogen losses and associated environmental consequences

A reduction in nitrogen losses to the environment and improvements to NUE are interrelated concepts. The strategies used to improve NUE by increasing nitrogen assimilation by plants minimise the losses. A number of approaches have been used to improve NUE. They can be broadly categorised as good management practices, fertiliser types, fertilisation methods and time of application (Trenkel, 2010; Liu et al., 2015).

There are several mitigation tools available under good management practices; incorporating the fertiliser closer to the root zone, using foliar application of nitrogen fertiliser, minimising or avoiding fertiliser application in a wet spell to avoid leaching and denitrification losses, delaying fertiliser application until a substantial canopy is developed, growing fallow crops to minimise the accumulation of nitrogen in the soil, and applying fertiliser at the correct amount and correct time to synchronise the crop demand and application (Humphreys et al., 1988; De Datta et al., 1989; Strong et al., 1992; McLenaghen et al., 1996). Split applications of nitrogen fertiliser (the required amount of nitrogen for the plant is applied as several portions) is another approach to reduce nitrogen losses. A granular or prill form of fertiliser application rather than a powder form reduces the contacted surface area with water, and limits the solubility of fertiliser (Trenkel, 2010).

The typical plant growth and nutrient intake curves are sigmoid curves (Shoji et al., 1991). An ideal fertiliser has to release the nutrient at the rate of plant intake (sigmoid pattern) which increases the NUE and reduces the residual nutrient in the soil which has a potential to leach in subsequent season (Figure 2.3) (Shoji et al., 1991; Trenkel, 2010). This concept was used to develop enhanced efficiency nitrogen fertilisers (EENF). This group of fertilisers includes stabilized nitrogen fertiliser, controlled-release fertilisers (CRF) and slow-release fertilisers (SRF). Stabilized N fertilisers such as urease and nitrification inhibitors inhibit the functional mechanisms of certain soil microbes or enzymes to enhance the availability of their N sources. Urease inhibitors (UI) slow down the hydrolysis rate of urea when it is applied to the soil. For example, N-(n-butyl) thiophosphoric tri-amide (NBPT) and phenylphosphorodiamidate used as UI. Nitrification inhibitors slow down the nitrification processes, and control the formation of nitrate and nitrite ions. The following nitrification inhibitors are used in commercial agriculture: nitrapyrin (2-chloro-6-trichloromethyl-pyridine, trade name N-Serve or Instinct), dicyandiamide (DCD), and DMPP (3,4-dimethylpyrazole phosphate, trade name ENTEC) (Trenkel, 2010; Franzen, 2011). However, slow-release and controlled-release fertilisers are functionally different to stabilized nitrogen fertiliser. These two fertiliser types reduce the release rate of active fertiliser compounds and match the release with the plant uptake. There are many controlled-released N fertilisers developed and marketed (Trenkel, 2010).

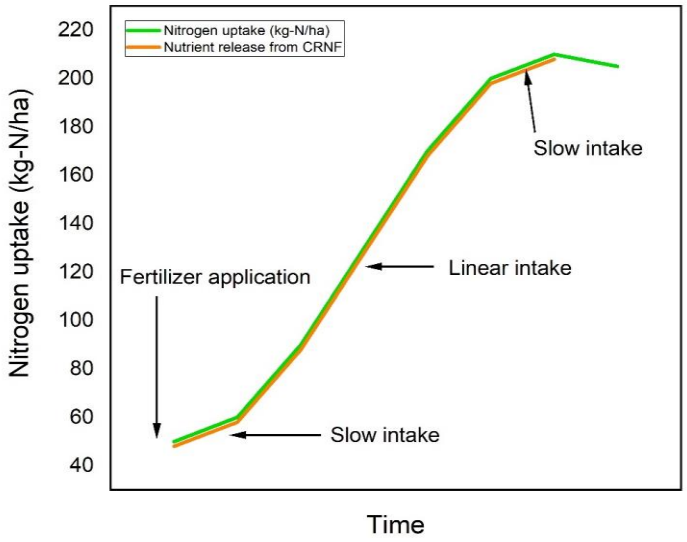

Figure 2.3. The 'ideal fertiliser': the nutrient release is synchronised with the crop's nutrient requirements (adapted from Trenkel (2010)).

2.2. Controlled and slow-release fertiliser

2.2.1. Controlled release and slow-release urea fertiliser

There is no clear definition for controlled release fertiliser (CRF) or slow-release fertiliser (SRF). The slow-release or controlled-release urea fertiliser allows the urea to release slowly in a delayed manner compared to the conventional form of urea in order to synchronise the sequential needs of plants for nutrients.

Notwithstanding that the terms slow and controlled-release fertilisers are used synonymously in literature, they differ in solubility and release pattern (Shaviv, 2001; Trenkel, 2010). The nutrient release of a slow-releasing fertiliser is unpredictable and the release pattern is influenced by the soil type and climatic conditions. Whereas, the nutrient release pattern, rate and duration of a controlled release fertiliser are predictable and can be manipulated during the fertiliser production process (Liu et al., 2015). Some examples of slow-release nitrogen fertilisers (SRNFs) are; urea-formaldehyde, crotonylidendiurea (CDU), isobutylene diurea (IBDU) and methylene Urea. Since these SRNFs take a long time to chemically decompose to release nitrogen, the plants do not receive the nutrient immediately after application (Trenkel, 2010). These SRNFs fertilisers were in peak demand in the mid-nineties. However, due to the delayed initial response of SRNFs, CRNFs took their place in the market (Trenkel, 2010).

According to the Standard of the European Standardization Committee (CEN), a CRF should not release more than 15% of the active substance (plant-available form of nutrient) within 24 hours of application, the maximum release of 75% in 28 days and at least 75% release within the specified time period (Trenkel, 2010).

2.2.2. The nutrient release mechanism, release pattern and fundamental mathematical models of CRF

The general mechanism of active ingredient release by a coated CRF involves several steps (Figures 2.4 and 2.5). The first step occurs when the CRF granule makes contact with water, which begins to diffuse through the membrane into the granule. The intrusion of water is further facilitated by the degradation of the coating material over time. The urea inside the granule dissolves in water which creates an osmotic pressure that swells and cracks the coating. As a result, urea diffuses from the membrane and enters the soil solution. In some cases, the membrane tensile strength is not sufficient to withhold the build-up of osmotic pressure, this can rupture and release the urea suddenly (not in a controlled manner) which is known as ‘failure release’ or ‘catastrophic release’. In addition to this, degradation of coating material due to chemical reactions (chemical degradation), biological activity (biodegradation) and hydrolysis may also contribute to failure release. Some CRNFs showed ‘stalling’ or ‘lock off’ N behaviour in which the granules stop releasing the fertiliser after a certain time as insufficient osmotic pressure is developed in the granules. The possible reasons for this are; the moisture level is insufficient to penetrate the membrane to dissolve the fertiliser and the membrane is too strong to release the fertiliser or there is a lack of available osmotic pressure to crack the membrane. Both burst (failure) and stalling release reduce the efficiency of CRNFs.

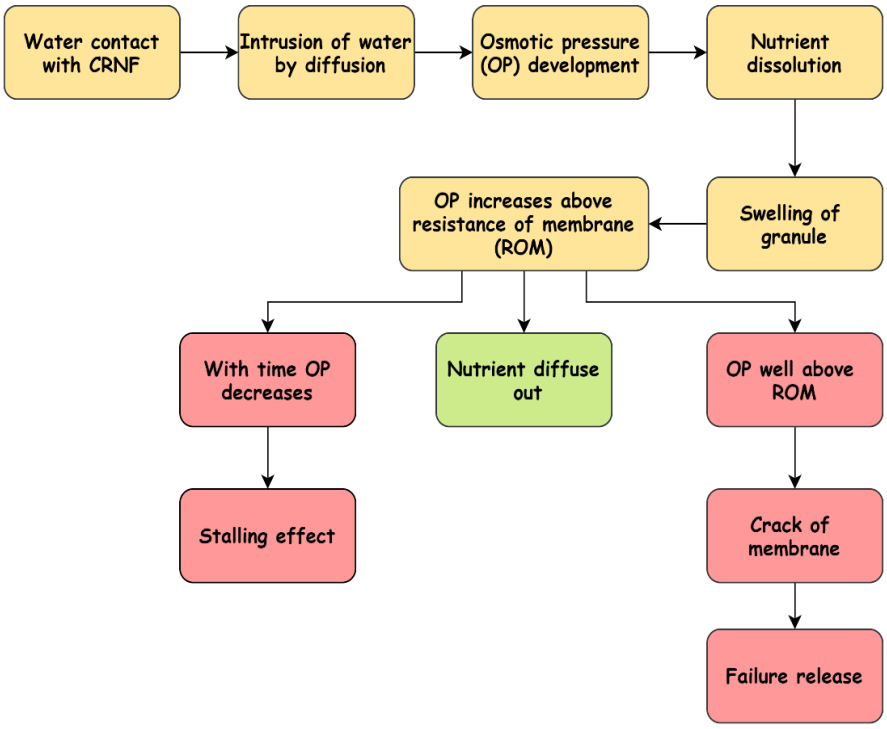

Figure 2.4. Controlled-release fertiliser nutrient releasing mechanism at different scenarios. The different colours are used to show variation in release behaviours. The green and red colour shaded text box shows the normal (expected) and unfavourable release behaviour of CRNFs, respectively.

In the nutrient releasing mechanism, three different phases of nutrient release were identified: lag phase, linear phase and decay phase. During the lag phase, the nutrient release is very slow as the movement of water into the coated granule is minimal, immediately after it contacts water. In the linear phase, water intrusion is completed and nutrient is completely dissolved in water. The nutrient is releasing out of the granule at a constant rate due to the concentration gradient. The nutrient release rate again decreases in the decay phase as a result of a lower concentration gradient and lack of nutrient availability inside the coating (Shaviv, 2001).

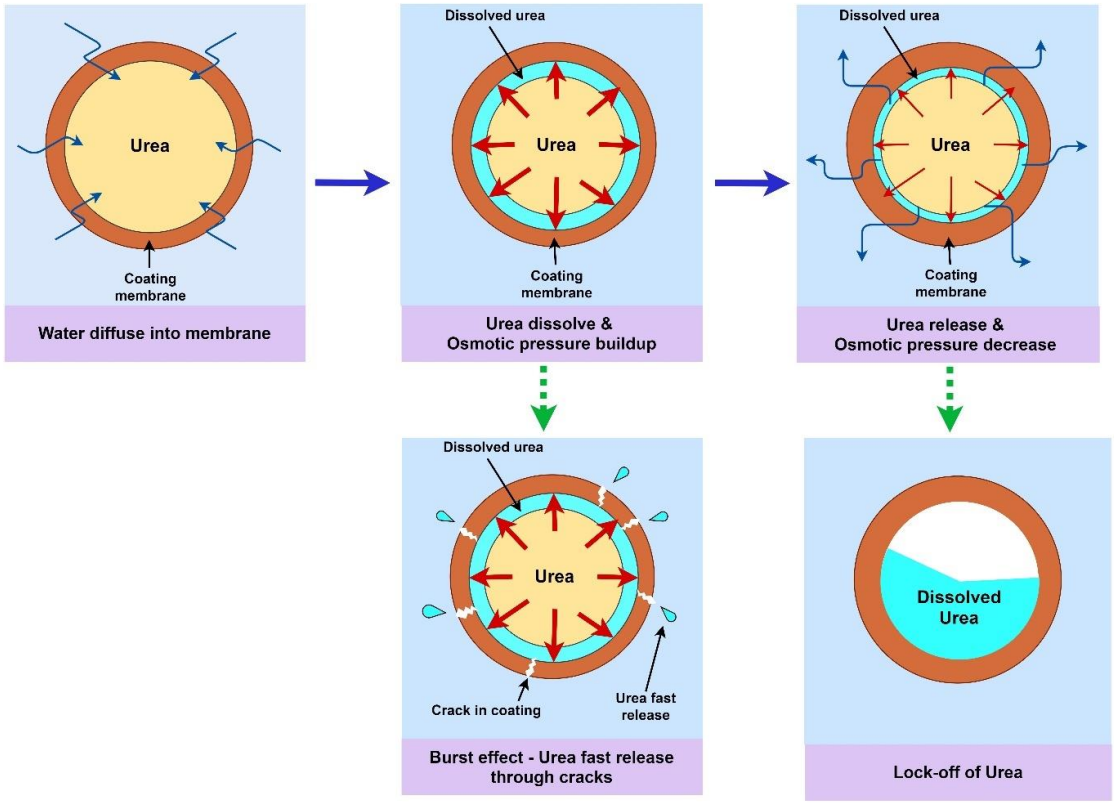

Figure 2.5. The schematic diagram of normal release, burst release and lock-off (stalling effect) of urea from a coated controlled-release fertiliser. The normal release follows the blue-solid line and failure releases follows green-broken line.

A CRNF should have a known nutrient release pattern and release rate (Sempeho et al., 2014). The CRNFs show three different nutrient releasing patterns; parabolic, sigmoidal and linear release. The linear and sigmoidal release patterns are synchronised better with the plant nutrient uptake (Shaviv, 2001). Temperature has an influence on the denaturing of the coating material and microbial activity, so can alter the nutrient release rates and release patterns of a CRNF. Further, the higher the temperature the lower the duration of nutrient release (Figure 2.6).

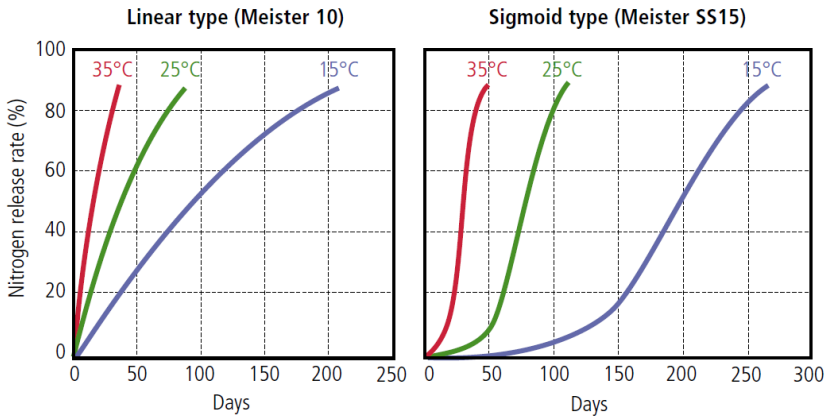

Figure 2.6. The linear and sigmoid pattern of nutrient release of Meister®-controlled-release fertiliser (Trenkel, 2010). The releasing pattern changes with the temperature for both types of CRF.

Understanding the nutrient release behaviour aids in precise formulation and application of CRFs. Different empirical and semi-empirical mathematical models have been published to simulate the nutrient release rate and pattern (Shaviv, 2001). The Korsmeyer–Peppas model and Peppas–Sahlin model are the fundamental mathematical models used to interpret the non-linear nutrient release of the polymer-coated CRFs.

The Korsmeyer–Peppas model characterises the CRF membrane and nutrient solution using swelling component and swelling rate.

$$Q_t = k\, t^n$$

Where Qt, t, n and k are fraction of solvent release, time, distinctive constant (swelling rate) and diffusion exponent, respectively.

The Fick's diffusion theory explains that solvent movement takes place from high to low concentration gradient. Based on Fick's diffusion theory, the swelling behaviour of coating membrane is classified into four groups; case I or Fickian diffusion transport (0.45<n), non-Fickian transport (0.45<n<0.89), case II transport (n=0.89) and case III (n>0.89) (Dash et al., 2010).

The Peppas–Sahlin Model is governed by the diffusion and coating relaxation mechanism (Peppas and Sahlin, 1989). The first and second terms of the equation describes the Fickian diffusion and case II relaxation of the coating membrane, respectively.

$$Q_t = k_1 t^m + k_2 t^{2m}$$

Where Qt is the fraction of solution release, t is time, m is Fickian diffusion component, k_1 and k_2 are Fickian and relaxation kinetic constants, respectively.

2.2.3. Classification of controlled-release fertiliser

Controlled-release fertilisers are classified into three groups based on the material used for coating and the interaction of coating with the urea granule (Trenkel, 2010; Azeem et al., 2014). The classification of the CRF is shown in Figure 2.7.

2.2.3.1. *Organic compounds used for coating*

Natural and artificial organic compounds have been used as coating materials in controlled-release fertilisers. Animal manure, sewage sludge and industrial organic wastes are examples of natural organic compounds (Azeem et al., 2014). Urea formaldehyde (UF), isobutyledene-diurea (IBDU), urea acetaldehyde and cyclo diurea (CDU) are examples of synthetic organic materials (Figure 2.7) (Azeem et al., 2014). Urea formaldehyde is a biologically decomposing material and IBDU and CDU are chemically decomposing materials. All these fertilisers are a chemical modification of urea and functioning as slow-release fertilisers. These organic fertilisers take a long time to break down and release urea. Therefore, urea release from chemically modified urea fertilisers does not match with plant nutrient uptake (Trenkel, 2010) which has decreased the use of these fertilisers as a CRF (Hähndel and Jürgens-Gschwind, 1986; Goertz, 2000).

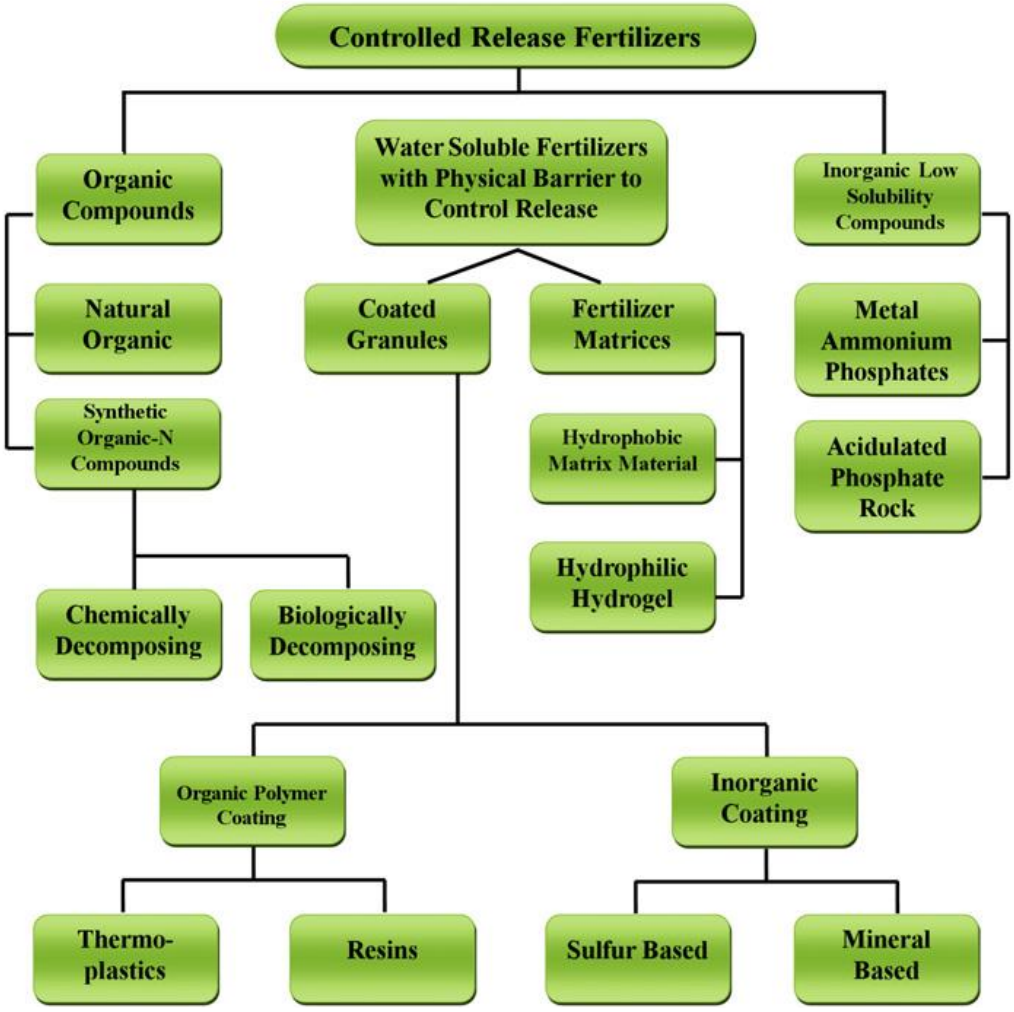

Figure 2.7. Classification of controlled-release fertilisers (Azeem et al., 2014).

2.2.3.2. *Physical barriers used to control the release*

Hydrophobic polymers are used as physical barriers which minimise the contact of fertiliser with water and decrease the release rate. They are grouped as organic and inorganic encapsulating materials (Figure 2.7). Sulphur and minerals ($CaCO_3$ and $MgCO_3$) are examples of inorganic materials used to encapsulate urea. Commercial production of CRF started with sulphur coated urea fertiliser in 1960s by the Tennessee Valley Authority (Azeem et al., 2014). The failure release of urea was observed through the cracks of sulphur coating. Therefore, wax materials (sealant) were applied on top of sulphur coatings to overcome this issue

(Blight et al., 1978). This modification has prolonged the release of urea by 25% up to 28 days compared to granular urea. Other inorganic coating materials used for CRF are zinc oxide (ZnO) (Irfan et al., 2018), calcium oxide (CaO) and metal ammonium phosphates (Mg NH_4PO_4) (Azeem et al., 2014). The organic polymers used for coating are categorized as thermoplastics and resins (Figure 2.7). Hydrophobic materials (polyolefines, rubber, etc.) and gel-forming polymers or hydrogels (superabsorbent) are used in matrix type fertilisers (Azeem et al., 2014).

2.2.4. Advantages and Disadvantages of CRFs

2.2.4.1. *Advantages of using CRFs*

The major advantages of using CRFs include:

- The CRF can potentially control the loss of nutrient by 20 - 30% through minimising the leaching, runoff and volatilisation and enhance fertiliser efficiency (Trenkel, 2010).
- It reduces the harmful effect of excess application of fertiliser to the plant for example; leaf burning, scotching, toxicity, osmotic pressure stress, etc.
- CRF reduces the environmental consequences of N losses such as eutrophication, water contamination, greenhouse gas emission, the salinity of soil, etc.
- It reduces the labour in the split application of fertiliser. Eliminating extra applications of fertiliser saves the farmer between 15 and 23 NZ$/hectare broadcasting expense (Liu et al., 2011).
- Sulphur coated urea decreases the soil pH which is suitable for alkaline soil. However, these CRFs are less suitable because most of New Zealand soils are acidic.
- CRF considerably reduces the total cost of pasture production, and thereby, increases the profit margin in the farming system.

2.2.4.2. *Disadvantages of using CRFs*

- Cost of the CRF is much higher than for conventional fertilisers. For example, the price was 975 NZ$ per ton for environmentally smart nitrogen (ESN) (44% N) versus 720 NZ$ per ton for urea (46% N) (Ruark, 2012).
- Most of the polymers used in CRF are non-biodegradable which could pollute the environment. The time taken for the complete degradation of the polymer-coated fertilisers has not been reported in the literature.
- Cracks and burst to CRF coatings could release the nutrient very rapidly. This is likely to effect performance of CRF in the field.
- Usually, the nitrogen percentage of a CRF is lower than conventional N fertilisers.
- Nutrient deficiencies may occur if nutrients are not released as predicted because of low temperatures, flooded or droughty soil, and poor soil microbe activity.

2.2.5. The performance of controlled-release fertiliser on ryegrass

Controlled-release nitrogen fertilisers are widely used in field crops and horticultural crops; however, very limited information is available on testing of CRNFs on ryegrass and these are summarized in Table 2.2. The CRNFs showed differential responses on ryegrass based on the type and characteristics of CRFs, application rate, climate and soil conditions (Trenkel, 2010). For instance, few studies have reported that CRNFs tested on ryegrass caused a decline in the DM yield compared to urea application for the entire experimental period (Bowman and Paul, 1991) or at least at the end of the experimental period (Bishop et al., 2008). However, CRNFs have shown to increase the DM yield and NUE in some field and pot trials (Volk and Horn, 1975; Vallejo et al., 1993). Nevertheless, it is well documented that CRNFs effectively control nitrogen leaching losses (Easton and Petrovic, 2004; Bishop et al., 2008). However, none of the studies has examined the nitrous oxide emission behaviour of CRNFs on ryegrass pasture and no studies have tested the effect of CRNFs on either monolithic or repacked lysimeters.

Table 2.2. Performance of selected controlled-release or slow-release-nitrogen fertilisers (CRNF or SRNF) on ryegrass.

CRNF/ SRNF	Experiment type	Application rate	DM yield	NUE improvement (kg DM kg^{-1})	Leaching loss control	Country	Reference
Polyurethane coated urea (5 & 7%)	Field trial	50 & 150	NSI	22–24	SI	NZ	Bishop et al. (2008)
Dicyandiamide coated Urea (10% coating)	Field trial	50 & 150	NSI	12–15	SI	NZ	Bishop et al. (2008)
Coron	Greenhouse (NSCS)	84	SD (30%)	N/A	N/A	USA	Bowman and Paul (1991)
N-Sure	Greenhouse (NSCS)	84	SD (30%)	N/A	N/A	USA	Bowman and Paul (1991)
Nitrazine	Greenhouse (NSCS)	84	SD (40%)	N/A	N/A	USA	Bowman and Paul (1991)
Lesco sulfur-coated urea	Field trial	50 & 100	N/A	N/A	NSI	USA	Easton and Petrovic (2004)
Floranid Komplett (FK)	Pot experiment	300 mg N/pot	SI	SI	SI	Spain	Vallejo et al. (1993)
CDU (crotonylidendiurea)	Pot experiment	300 mg N/pot	NSI	NSI	NSI	Spain	Vallejo et al. (1993)
Triabon (CDU+Urea)	Pot experiment	300 mg N/pot	SI	SI	SI	Spain	Vallejo et al. (1993)
Lignin coated urea CRFs (16 – 34%)	Pot experiment		SI	SI	SI	Spain	Garcia et al. (1998)
Ureaform	Field plot trial	3 kg-N/season	N/A	SI	N/A	USA	Volk and Horn (1975)
IBDU	Field plot trial	3 kg-N/season	N/A	SI	N/A	USA	Volk and Horn (1975)
SCU	Field plot trial	3 kg-N/season	N/A	SI	N/A	USA	Volk and Horn (1975)

SI - Significantly improved
SD - Significantly decreased
NSI - No significant improved
NSCS - Nutrient solution culture system
N/A - Not available

Bishop et al. (2008) have conducted a six-month field study to assess the effectiveness of polyurethane-coated-controlled-release urea (PCU, 5 & 7% coating) and dicyandiamide-coated urea (DCU, 10% coating) against conventional urea fertiliser at two different application rates; 50 and 150 kg-N ha^{-1}. The dry matter (DM) yield of ryegrass for both CRNFs did not significantly differ from the urea treatment (Table 2.2). They also found that CRNFs showed a negative growth response in the last trial month (November), due to the stalling effect caused by a lack of soil surface moisture. However, both CRNFs showed better nitrogen use efficiency (NUE) and decreased leaching compared to urea application.

Bowman and Paul (1991) have studied the uptake of three CRNFs (Coron, N-Sure and Nitrazine) by ryegrass in a nutrient solution culture system under greenhouse conditions. Coron and N-Sure have decreased the DM yield by 30% and Nitrazine by 40% compared to urea at 84 kg-N ha^{-1} application rate (Table 2.2). Easton and Petrovic (2004) have tested sulphur coated urea (SCU) against readily available urea (RAU) and found that at both 50 and 100 kg-N ha^{-1} application rates, SCU controlled the N losses better than RAU in the first year. Nevertheless, in the second year, it did not show promising results.

In a pot experiment, the performance of three different SRNFs (Floranid Komplett ® (FK), Triabon ® (TR) and crotonylidendiurea (CDU)) were tested on ryegrass in terms of DM yield, N uptake and N leaching (Vallejo et al., 1993). The composition of the first two CRNFs are; FK that contains isobutylendiurea (IBDU), urea, nitrate and ammonium, and TR which contains CDU, urea and ammonium. It was found that FK showed the best performance of all, followed by TR for DM yield and N uptake (Table 2.2). The CDU fertiliser performance for the same parameters was only comparable to the control treatment which had not received any nitrogen. Whereas the leaching losses were in the following order; TR> CDU> FK.

In another study, urea-based lignin coated fertiliser with different coating percentages (16 -34%) were formulated and evaluated in a pot trial with ryegrass for 75 days (Garcia et al., 1998) (Table 2.2). The 18 and 34% lignin coating with linseed oil seal showed higher DM yield compared to ones without sealant. They

also found that increasing coating thickness increased nitrogen uptake and decreased leaching losses.

Volk and Horn (1975) conducted a field plot study to evaluate different SRNF (Ureaform, IBDU and SCU) for the total nitrogen captured by different types of turf-grasses, including ryegrass (Table 2.2). They found that SCU gave a good response for summer application followed by IBDU. However, for winter response, IBDU was superior to the other fertilisers.

The performance of a newly developed CRF needs to be analysed in terms of controlling the nutrient losses as well as its agronomic performance. For a complete analysis of nitrogen fertilisers, leaching losses, gaseous losses (nitrous oxide and ammonia), the residual nutrient in soil and growth responses of the crop need to be analysed. Therefore, a lysimeter is essential to study all types of nutrient losses with respect to temporal and special variation. Lysimeters provide accurate and additional information with the support of sensors in real time. This allows interpreting the data closer to a realistic scenario.

2.3. Lysimeters

A soil solution sampling technique is a common way of testing the quality and quantity of contaminants in the vadose zone. In addition to the lysimeter technique, displacement method, sampling drainage flow and bored well sampling have been used for soil solution sampling (Boulding and Ginn, 2003; Fares et al., 2009). However, there is no standard method for sampling soil solutes. In the displacement method, the chemical (for example nitrate, phosphate, colloids, etc.) which is the subject of investigation is sent through a packed soil column, (which mimics the natural soil layers) and the collected leachate at the bottom boundary is analysed (Fares et al., 2009). The borehole sampling method is used to study the solute movement in the vadose zone through collection of water samples at different bore well depths (Boulding and Ginn, 2003). In the sampling drainage flow method, the leachates are collected from the constructed drainage and analysed (Wilson et al., 2018). Although, these methods have their own advantages and disadvantages (Fares et al., 2009), all these methods have been used by researchers. However, lysimeters have become a common method for studying the soil solute movement in the vadose zone (Litaor, 1988) and the only method to measure all hydrological components.

2.3.1. Systematic classification of lysimeters

2.3.1.1. *Pan Lysimeter*

A pan lysimeter (zero tension lysimeter) is made of a conical shaped water receiver filled with coarse particles or highly water penetrating materials (Figure 2.8). The absence of a side wall of a pan lysimeter allows the collection of both percolating and seepage water. The solutes moving through the soil matrix accumulate and form a saturation zone at the bottom boundary. When it saturates only solutes drip into the pan lysimeter due to the gravitational force. In other words, discharge of solute is possible only if the soil exceeds field capacity (Fares et al., 2009). The tension at the interface of soil and coarse particles of the pan lysimeter is equal to the atmospheric pressure (not a negative suction similar to

a continuous soil matrix). Therefore, this only drains the macropores solutes, not the micropores solutes. This does not represent the natural soil continuum, where negative suction tension is always present due to the unsaturated porous soil in successive layers.

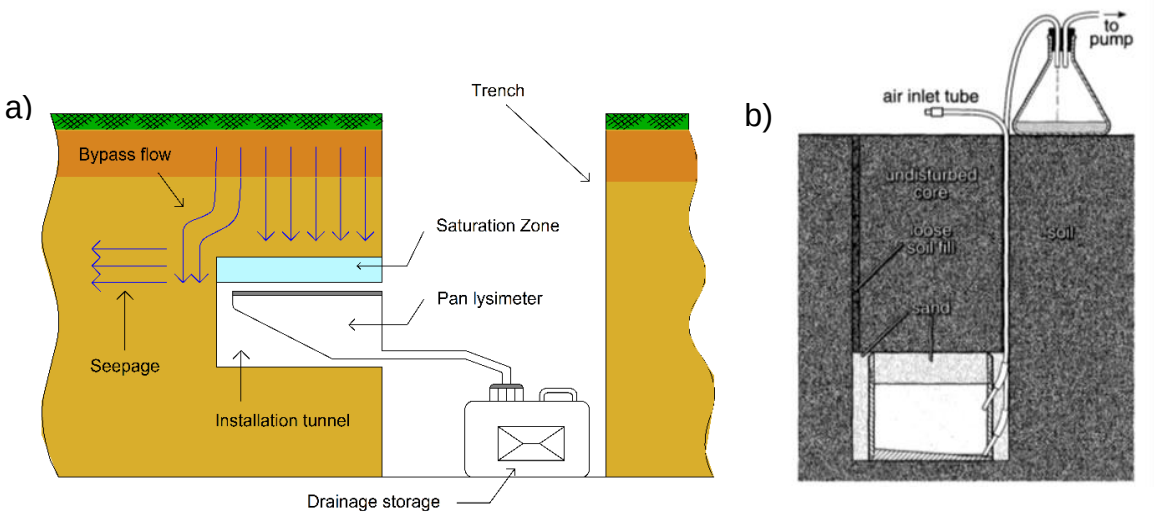

Figure 2.8. (a) Schematic diagram of a pan lysimeter illustrates the bypass flow of drainage and (b) a modified design of a pan lysimeter (Thompson and Scharf, 1994).

Pan lysimeter collection efficiency (CE) is very low (under sampling), less than 10% which often doesn't yield a sufficient sample for analysis (Radulovich and Sollins, 1987). This is attributed to the developed saturation zone at the bottom boundary. The saturation zone leads to bypass flux (divergence of flux away from the pan lysimeter) and redistributes the solutes from the saturated zone towards surrounding low moisture soil (high matrix tension) via seepage flow (Figure 2.8-a). These losses can't be avoided since there is no divergence control (sidewall) in the pan lysimeter. The collection efficiency of a pan lysimeter depends on the size of the catchment, soil type (hydraulic properties and soil moisture level) and spatial variation of soil (degree of heterogeneity). The larger the pan-lysimeter size, the better the representative of the soil heterogeneity and lower the variability. The heterogeneity of the soil forms a network of flow channels (preferential flow) and increases the CE (Robison et al., 2004).

Improved designs to the pan lysimeter increases the collection efficiency to a certain extent. Jordan (1968) suggested the placement of glass wool on a mesh on top of the pan lysimeter and filing the pan with coarse sand could improve the CE. Radulovich and Sollins (1987) have improved the design by increasing the catchment size to 2500 cm^2 and pushing the rim of the pan lysimeter into the soil which increased the CE to 17% and 36% for grassland and forest, respectively. However, increasing the catchment size is not always possible especially when the structural stability of the soil is low. Since one side of the installation tunnel is standing without physical support, it can collapse particularly during heavy rainfall. Therefore, Jemison and Fox (1992) used a steel support with pressure-treated lumber under the ceiling to give mechanical support to avoid collapse of the ceiling. Instead of this, Way et al. (2011) made a top and two sides open steel box to support the soil ceiling for a sandy loam soil (that has low structural stability). The box was pressed into the soil using an especially designed hydraulic jack-guiding frame facility while one of the open sides facing the soil. Once it is fully inserted into the soil, the soil inside the box was removed manually to construct a tunnel to place the wick sampler. Although this method is laborious, it eliminates the risk of peri and post operational soil collapses. Also, it was reported that there was no evidence to show that this method alters the soil bulk density or the water flow paths.

The pan lysimeters can be successfully used in a saturated soil compared to a dry soil due to the lack of capillary connection between soil column and lysimeter. Therefore, the water can move backward (from bottom to top boundary) during evapotranspiration in a dry soil. The pan lysimeter works well for coarse-texture soils and moderately drained soil types.

A modified design and different installation method of a pan lysimeter was proposed by Thompson and Scharf (1994) for the colloidal collection from soil (Figure 2.8-b). It is a fully enclosed cylindrical container with a slopping bottom floor for water collection and sand filled on a mesh at the top surface to receive the drainage water. Two ports, air inlet tube and drainage sampling tubes are connected at the side wall of the cylinder. The air inlet tube equalizes the pressure by removing and sucking air when water drains into the container and drainage sample collection, respectively. The installation method is completely different

from the conventional ‘trench and horizontal installation tunnel’ practice. In this method, an undisturbed soil core was excavated and then the pan lysimeter was placed in the excavated pit. Finally, after trimming the soil core to the remaining size of the pit, it was carefully placed on top of the lysimeter and loose soil and sand were used to fill the gaps. This is an intermediate approach of a field lysimeter and a pan lysimeter setup.

2.3.1.2. *Flux meter and Capillary wick sampler*

The flux meter is made of a funnel on which a frayed wick is spread and filled with soil as shown in Figure 2.9. A convergence ring (a small side wall) is connected above the funnel to prevent the divergence of flux. The length of the convergence ring depends on the research question, flux flow rate and soil type (Gee et al., 2002). Flux meters are commonly used to study water and solute movements in disturbed soil (Frisbee et al., 2010).

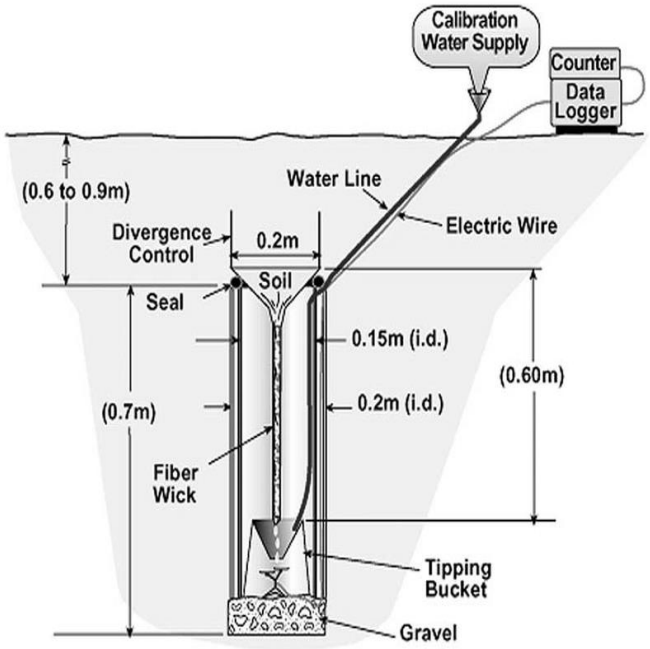

Figure 2.9. Schematic diagram of a typical flux meter (Gee et al., 2002).

The capillary wick sampler is similar to a flux meter; however, the sidewall is extended to the full length of the soil column as shown in Figure 2.10. The bottom boundary of a capillary wick sampler is connected to frayed wick material. In general, fibreglass and rock wool are used as wicking material. These wick materials show capillary action since they are made of porous substances. Therefore, the wick exerts a capillary suction force on the bottom boundary of soil, this prevents the issues related to saturation (Mertens et al., 2007). As a result, the leachate collection efficiency of a wick sampler is always equal or greater than 100% (Abdulkareem et al., 2015).

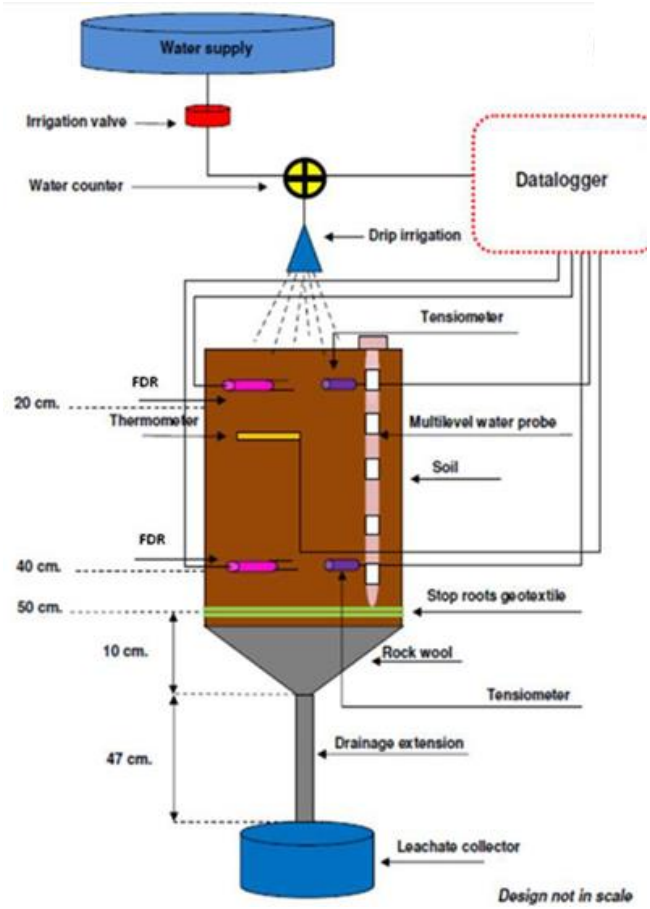

Figure 2.10. The schematic diagram of the lysimeter (rock wool used as the wicking material) (Mantovani et al., 2013).

The wick has to be preheated at 400°C for at least 3 hours to remove any organic residues that may convert the wick to a hydrophobic state and to avoid the retention of soil colloids (Knutson and Selker, 1994; Czigány et al., 2005). The

recommended wick length is between 0.6 and 1.0 m (Gee et al., 2002), however, it can be shortened if sought to mimic tile drains. A lengthy wick needs to be avoided in lysimeters since it leads to over-sampling of solutes during wet seasons, or under-sampling during dry seasons (Mertens et al., 2007).

Generally, fibreglass wick materials do not alter the chemical composition of the leachate (Gee et al., 2002). However, a study has reported that pH, alkalinity and concentration of ions (Ca, Mg, P and Al) of leachate were altered while working with acid-forest soil. It was also reported that the possible causes for this were leaching and weathering of wick material due to the acidic nature of the forest soil (Goyne et al., 2000).

2.3.1.3. *Suction cup lysimeters*

A suction cup lysimeter (SCL) is a well-developed method for leachate collection (Singh et al., 2018). It is named in several ways in the literature. For example: porous tube, deep pressure vacuum lysimeter, vacuum extractor, porous candle, porous cup, or suction cup (Abdulkareem et al., 2015). The main components of SCL are porous cup, sample collector and vacuum generator (Figure 2.11). A negative pressure is created in the ceramic cup by the vacuum generator. As a consequence of that, the soil solution moves into the porous cup and it is collected in a leachate collector. The materials used for the fabrication of suction cups are membranes, ceramic materials, synthetic and sintered materials (Abdulkareem et al., 2015).

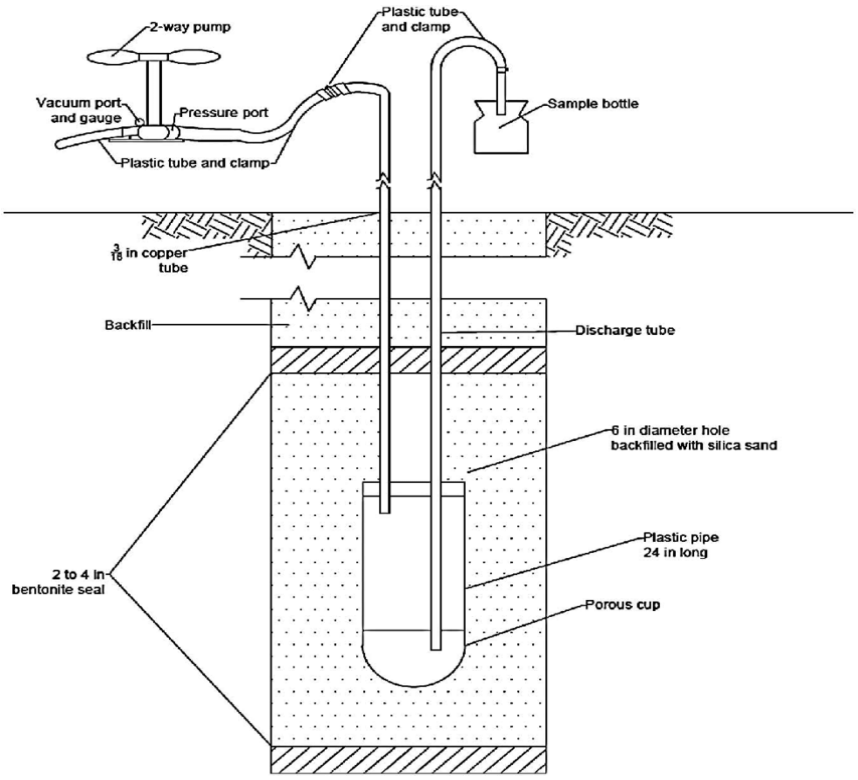

Figure 2.11. The schematic diagram of a suction cup lysimeter (Kreith, 1999).

The SCL is more popular because of the simple installation process with little disturbance to the soil. It allows continuous collection of solutes from different depths of a soil profile (Grossmann and Udluft, 1991). The SCL can collect leachate from a soil with moisture below the field capacity (Litaor, 1988). However, there are several issues with SCL which are listed below;

a. The leachate collected by SCL does not represent the real collection rate of an ideal undisturbed field condition. It was reported that SCL has over sampled the soil solutes due to the excess-negative pressure application (Abdulkareem et al., 2015).
b. The deposition of solids (phosphates and aluminium hydroxyl sulphate) on the porous cup block the pores which prevent the solute movement into it (Hansen and Harris, 1975).
c. The sorption of soil solutes by the porous cup can affect the adsorption and desorption rates of the solutes (Hansen and Harris, 1975) that can alter the concentration of the chemicals in soil solutes (Grossmann and Udluft, 1991).

d. The soil solutes sampling area is unclear in this method since the suction cup can draw water from a far distance.
e. The suction applied by the vacuum creator can be sustained for only a few days (2-3 days). Therefore, it is necessary to apply the vacuum periodically.

2.3.1.4. *Drainage lysimeters*

The drainage lysimeter (field lysimeter) is the oldest lysimeter and widely used in field studies (Singh et al., 2018). This lysimeter has a cylindrical body filled with soil which is subjected to the study. The bottom of the soil matrix is packed with coarse materials (stone, gravel and sand) which increases the drainage and prevents water saturation (Figure 2.12). The drainage lysimeters are large in size, both height and width (Singh et al., 2018). These lysimeters are extensively used to study water balance, ET, water flux measurements, and developing crop response and hydrological models (Abdou and Flury, 2004; Chen et al., 2008).

The annular gap between the soil matrix and inner surface of a monolithic lysimeter should be sealed with a material (which does not react with soil and water) to minimise the preferential flow. Generally, wax or petroleum gel are used as a sealing material. This improves the matrix flow of the lysimeter (Wilson et al., 2018).

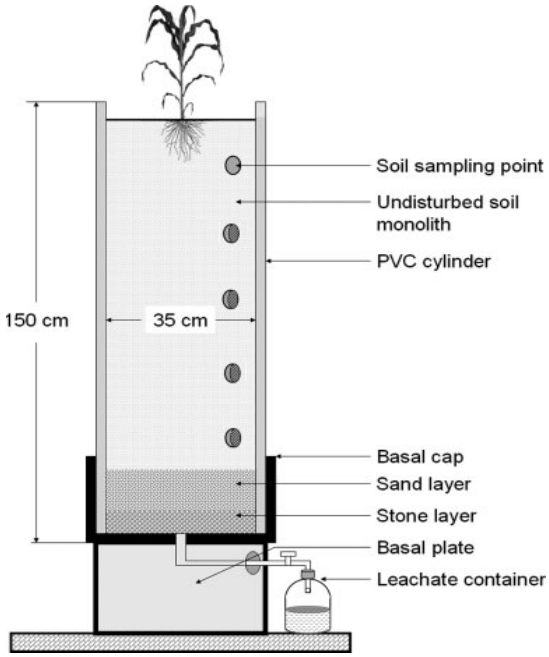

Figure 2.12. The schematic diagram of a basic drainage lysimeter (Islam et al., 2011).

Current lysimeter designs and practices are more suitable to conduct a research study under field or laboratory conditions. With existing lysimeter designs, a study under controlled environment can only be possible under a greenhouse or in a controlled growing space. However, the spatial variation of environmental parameters in the study area reduces the reliability of these methods. Hence, controlling the soil and climate variables to every single treatment or replicate level is not possible. Consequently, it is crucial to design a lysimeter which can control environmental parameters more precisely up to a single treatment level. This can be achieved with the support of sensors since they allow the lysimeter to monitor and control the climatic parameters.

2.3.2. Instrumentation of lysimeter

Lysimeters have been equipped with different sensors to collect additional data and improve the precision of information (Pütz et al., 1998). For example, sensors are used to measure weight change of lysimeters, soil temperature, soil moisture content and soil matric potential. The precipitation and evapotranspiration can be measured using a weighable lysimeter (López-Urrea et al., 2006). The counter-weight weighing system was used to measure the weight changes in lysimeters, however, the external disturbances (wind) lowered the precision (Howell et al., 1995; Nolz et al., 2009). Therefore, more precise load cells have replaced the counter-weight weighing system. The advantages of load cell lysimeters are continuous monitoring, high precision, automatic data logging and wide range of weight selections. The weight range of a load cell lysimeter is varied from 50 to 6000 kg and the resolution is 10 g or 0.01 mm precipitation (Mueller et al., 2013). These lysimeters are suitable for measuring all types of precipitation such as rain, dew, frost and snow (Mueller et al., 2013). The shear gauge used in load cells is temperature sensitive which is a disadvantage to the load cell measuring system. However, it can be overcome through a temperature correction algorithm (Sear et al., 2000).

Soil temperature is one of the important parameters which influences chemical reactions and microbial activity of the soil. The temperature sensors are useful to maintain the natural temperature gradient of a soil profile. Different temperature transducers (LM 35, HydraProbe, etc.) and thermocouples are used for this purpose (Liu et al., 2011).

The soil moisture sensors are used in lysimeters to measure the moisture content of soil at different depths, to identify the moisture front movement with respect to each rainfall event and to schedule an irrigation system (automated irrigation system). The common sensors used in soil moisture measurement are Time Domain Reflectometry (TDR) probe, Neutron scattering (NS) probe and capacitive moisture sensors (ATMOS 14, EC-5, 5TE, 5TM, 10HS, etc.) (Mueller et al., 2013).

2.4. Summary and knowledge gaps

The nitrogen losses through leaching and gaseous form impose a threat to the environment and human health. In New Zealand, total nitrogen fertiliser use has increased significantly since the 1990s which has been linked to the nitrate contamination of water bodies and nitrous oxide emission. Controlled-release fertiliser is one of the strategies, which is widely applied in horticultural crop to control the release rate of the nutrient. However, the application of CRF to grazed pastures is uncommon, mainly due to the increased cost of CRFs compared to urea and limited knowledge is available on CRF efficiency in pastoral land use globally.

Polymer-coated CRF is the widely applied CRF type in which a physical barrier controls the release of nutrient. The recent interest in CRF formulation is to make composite polymer coatings by adding fillers to decrease the polymer percentage in the coating and to gain the good characteristics of the fillers. Lignite could be a potential filler which has low hydrophilicity and may be useful in decreasing the tackiness of a polymer coating. Lignite matrix type fertilisers found in the literature showed better control of nutrient release compared to uncoated urea. However, a polymer-lignite composite membrane CRF has not been produced yet.

A lysimeter is a widely accepted tool for measuring the solute movement through the vadose zone. To date, a lysimeter system design which can control the environmental variables is not available. Lysimeter studies under controlled environment have been conducted in a greenhouse or under confined space. However, precise control of the microenvironment of plants is not possible using these techniques. In this study, the newly developed fertilisers need to be tested in iterative trials and under the same controlled environment regardless of the changes in the outside environment. Therefore, an advanced lysimeter system design is required which can control the environment variables close to the selected climate model.

The soil analysis in incremental depth gives detailed information of the chemical movements in the soil profile and root distribution at various depths in a lysimeter. However, manual soil excavation and sectioning is laborious and it is difficult to

achieve the precise soil block size. The designs available in the literature are only suitable for retrieving the soil from a large lysimeter. A simple and low-cost lysimeter soil retriever design is required to retrieve the soil from a small to medium size lysimeter.

2.5. Research Objectives

The following objectives have been designed based on the identified research gaps in the literature.

The hypothesis of this study was that newly developed climate-controlled lysimeter systems can emulate a climate model satisfactorily. New controlled-release fertiliser/s can control the nitrogen losses without detrimental impact on ryegrass yield compared to standard N fertilisers under a selected climate model. This study was carried out with the following objectives;

1. To design and develop a new lysimeter system which can emulate a climate model in order to study the performance of the newly developed controlled-release fertilisers on ryegrass under specific controlled environmental conditions.
2. To evaluate the performance of an environmental controlling unit by comparing observed temperature and relative humidity values with set points, and performance of the lysimeter system in terms of reproducing the climate model using ryegrass yield, leachate and evapotranspiration.
3. To design and develop a low-cost lysimeter soil retriever (LSR) to remove undisturbed soil columns and evaluate the performance of LSR using two different moisture level soil blocks.
4. To develop a new polymer-lignite membrane coated urea controlled-release fertiliser and study the urea releasing characteristic, and it’s physical and chemical properties.
5. To measure and compare the performance of new CRFs developed by Verum Group against the commercially available conventional nitrogen fertilisers in a controlled environment in lysimeters.

6. To determine the effect of iron (II) sulphate dosage levels on denitrification, controlling leaching losses, nitrous oxide emission and ryegrass dry matter yield.

Chapter 3

An innovative lysimeter system design for a climate control study

3.1. Introduction

A lysimeter is a widely used tool to study the movement of agrochemicals through the vadose zone and to estimate the evapotranspiration of crops. The basic types of lysimeters are pan lysimeters, suction cup lysimeters, drainage lysimeters and capillary-wick lysimeters or flux meters (Weihermüller et al., 2007). Although these lysimeters have been used for solute transport studies under different soil and climatic conditions, there is no single lysimeter described in literature which can work well under all these conditions.

The existing lysimeter designs used in many research studies do not have the capability to conduct experiments in a controlled environment. A greenhouse or growth chamber setup is required to conduct a controlled environment study with the existing lysimeter designs. Although numerous lysimeter studies were conducted under greenhouse-experimental conditions, many limitations need to be underpinned. For example, high energy is required for maintaining a constant microclimate in a large confined space, difficulties in controlling the disease spread from one lysimeter to another, and maintaining the specific growth factors to an individual lysimeter. The spatial and temporal variation of microclimates in greenhouses can minimise the accuracy of the study. Many studies reported that the temperature gradient at the plant level considerably changes across the greenhouse and the trend of the gradient is very difficult to predict (Bucklin et al., 1993; Teitel et al., 2010; Ganguly and Ghosh, 2011). These erratic microclimate changes induce infections or diseases and cause adverse effects on the plant physiological activities that lead to low-quality products (Soni et al., 2005). Therefore, a more reliable lysimeter design that can control the climate variables to an individual experimental unit is crucial.

The lysimeter experiments involved with collecting greenhouse gases are temporarily capped using a chamber, but not for controlling the microclimate of plants. However, designing a lysimeter with permanent capping allows the climate variables to be manipulated, in a small confined space, so that it can be more effective compared to a large space in a greenhouse. In addition, capping permits individual control over the plant growth factors. An environmental variable monitoring and controlling system (ECU) needs to couple with the capped lysimeter to precisely control the main climate variables of temperature and relative humidity (RH).

Different methods have been employed in greenhouses for controlling temperature and RH. Heaters and heat exchangers are generally being used to increase the temperature, whereas evaporative cooling, forced air cooling, heat exchangers and refrigeration are being used to cool down the air temperature (Liu et al., 2000). Four basic types of humidification methods are being used in greenhouse and growth chamber studies; pan humidifier, wetted elements, atomizers, and steam humidifiers (Liu et al., 2000). Dehumidification is achieved through refrigerating the air below the dew point temperature. In commercial greenhouses, an evaporative cooling technique using wetted pads coupled with fans is the common way of controlling temperature and maintaining the required level of moisture in the air. However, pan and atomizer methods are less accurate in controlling RH and regular maintenance is needed to overcome fouling when using the wet pad humidification method. Therefore, a packed bed humidification column is an appropriate solution to overcome these issues. In this design, a chiller and air heaters can be used to change the air temperature. In addition, the system should be equipped with sensors to monitor the variables of RH, air temperature, soil temperature, weight and soil moisture.

The lysimeter system in the present study allows for iterative fertiliser testing trials to optimize the performance of newly developed, controlled-release fertiliser (CRF) formulations, under consistent climate conditions. Therefore, a study was undertaken to design and develop a lysimeter system, with the objective of controlling the environmental variables, at each lysimeter, with minimum spatial and temporal variation. In this chapter, a new design of a lysimeter system is proposed to conduct the research study, under a controlled environment. A

detailed description of the lysimeter design and ECU are discussed. The performance of ECU was tested by comparing the observed temperature and RH with setpoints. Further, the performance of the proposed lysimeter system design was compared against estimated data of evapotranspiration, leachate volume and dry matter yield of ryegrass in order to prove the suitability of the design.

3.2. Materials and Methods

3.2.1. The mechanical design

3.2.1.1. *The structure of the lysimeter*

The new lysimeter design has two main structural components; cap and lysimeter body (Figure 3.1). The novelty of the new design is the addition of a permanent cap to the lysimeter which provides a confined space to control environmental variables when it is coupled to an ECU. The diameter and length of the cap were 20 and 25 cm, respectively. It was made of a cylindrical body (PVC), two flanges and a roof plate (PVC). An airtight environment was ensured in the cap enclosure by employing a rubber O-ring in between the top flange and roof plate. Two barbed plastic male hose tails (20 mm) were threaded on the body of the cap in opposite directions at 2.5 cm from both flanges, to facilitate the circulation of conditioned air derived from the ECU through the cap (Figure 3.1). The bottom hose tails were connected to the air-line whilst the top hose was exposed to the environment. A gas collection port was made of silicon tube with a valve on the roof plate to enable the greenhouse gas collection (Figure 3.1).

The lysimeter body was a PVC pipe, 45 cm in length, 20 cm in diameter and 2.77 mm thick. The top and bottom flanges were plastic welded at either end of the lysimeter body. The bottom end of the body was attached to a cone plate that sloped towards the drainpipe to facilitate the leachate movement downward (Figure 3.1). A fibreglass wick was attached to the bottom boundary of the soil matrix to provide the capillary suction. The top 10 cm of the wick was frayed and spread radially on the cone plate and the rest of the 20 cm length was directed

through the drainage tube, functioning as a hanging water column. A fibreglass cloth was glued to the bottom flange of the lysimeter body (on top of the frayed wick) to stop soil leaching and to increase the contact between the soil matrix and wick. The fibreglass wick and cloth were preheated at 400 °C for 4 hours to remove organic residues (Knutson et al., 1993). An O-ring was placed in between the plates to prevent the leachate leaking through (Figure 3.1).

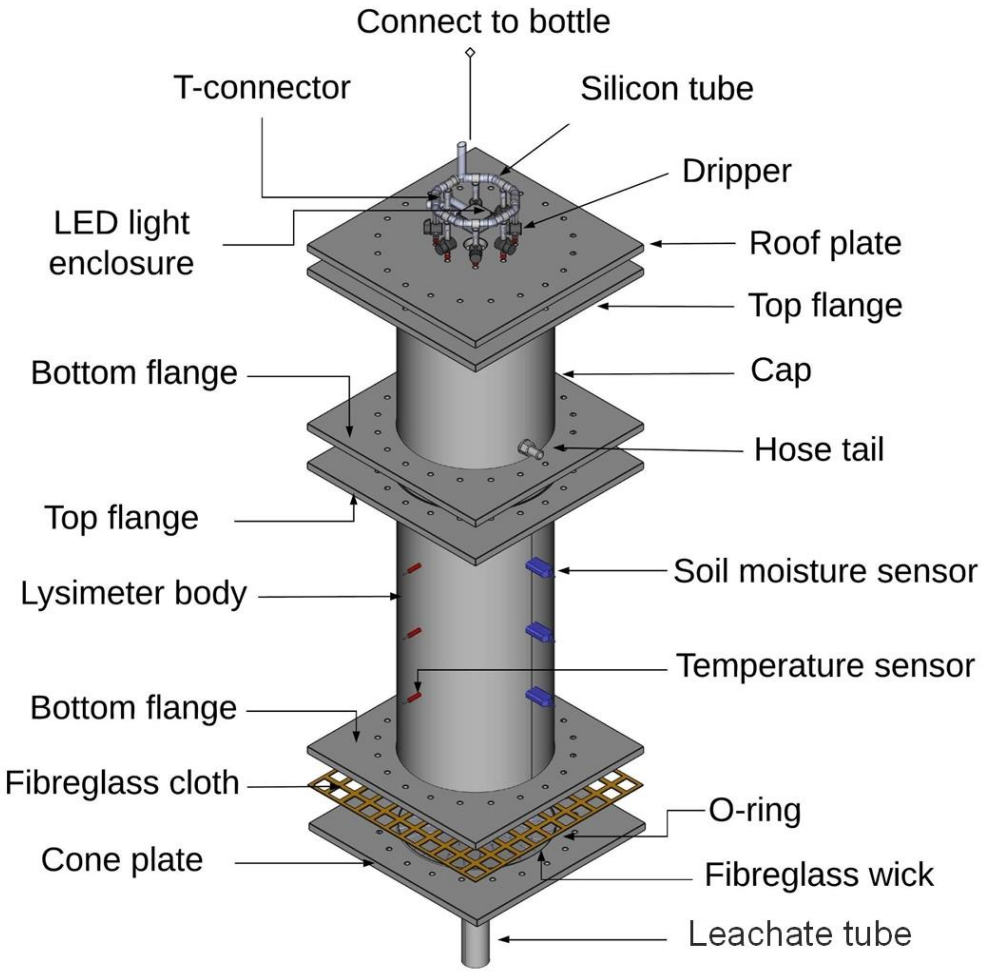

Figure 3.1. The 3D schematic diagram of the new lysimeter design (exploded view).

A dripping irrigation system was designed to create the artificial rainfall events of the selected climate model (Figure 3.2). In this design, eight T-connectors were placed in a circular arrangement and were joined together using silicon tubes

(Figure 3.2-a). The vertical end of each T-connector was connected to a variable flowrate emitter (Figure 3.2-b). One end of the first T-connector was connected to a water bottle (1000 ml capacity) through the silicon tube. An in-line valve connected to this silicon tube was used to control the water flow from the bottle at 350-375 ml hr^{-1} to emulate a normal rainfall intensity. The measured volume of water was manually filled in the bottle according to the rainfall event in the climate model on respective days.

An LED-chip-on-board light (Bridgelux® Gen 7 Vero®) was used as an artificial light source which can deliver 450 µmol $m^{-2}s^{-1}$ of photosynthetic photon flux density (PPFD) at 500 mA drive current. It was glued to a water-cooling block made of aluminium alloy using a thermal adhesive. Both LED and cooling block assemblies were placed in a 3D printed plastic enclosure and mounted to the outer surface of the roof plate (Figure 3.2-a). The roof plate has a circular cut at the centre which allows the light to pass into the cap (Figure 3.2-b). A transparent acrylic sheet was fitted to the roof-plate underneath the LED light to protect it from water or moisture damage.

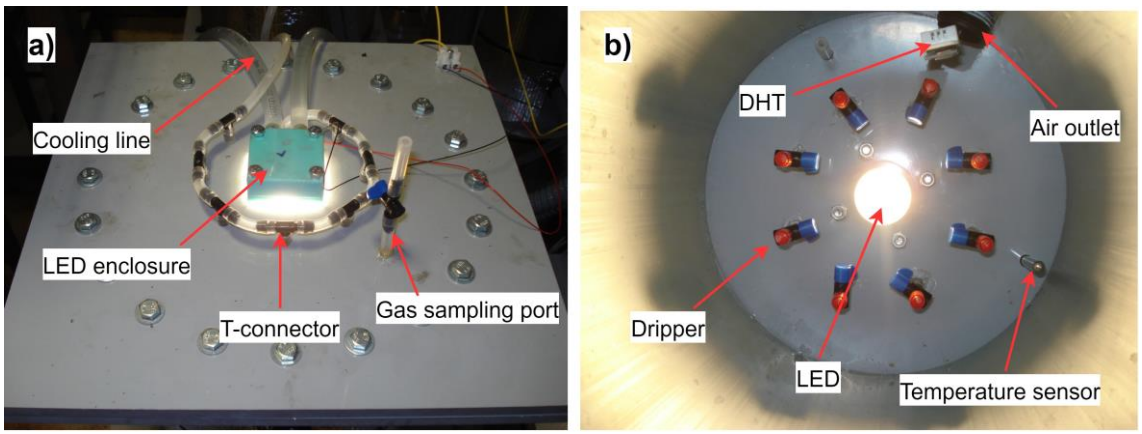

Figure 3.2. The instrumentation of lysimeter cap; (a) outside and (b) inside view of the lysimeter cap.

A constant-current LED driver for each lysimeter bank (ELG-150-C500B, Mean Well, Taiwan) was used to maintain the constant current flow to the LED system. The smart relay (Zelio Logic, Schneider Electric, France) was programmed with

weekly LED operational hours that was used to control the on/off cycle of LED lights. A water-cooling system was used in this study and eight LED lights were connected in series (Figure 3.3). The cooling system removes the dissipated heat from the LED and assures the working temperature of the LED was around 25°C to obtain the targeted lumens. A flow switch was used to protect the LED from burn-out if the water supply failed. It only allows the current flow to the LED when there was water flow in the cooling system (Figure 3.3). A similar LED system was used in all five lysimeter banks.

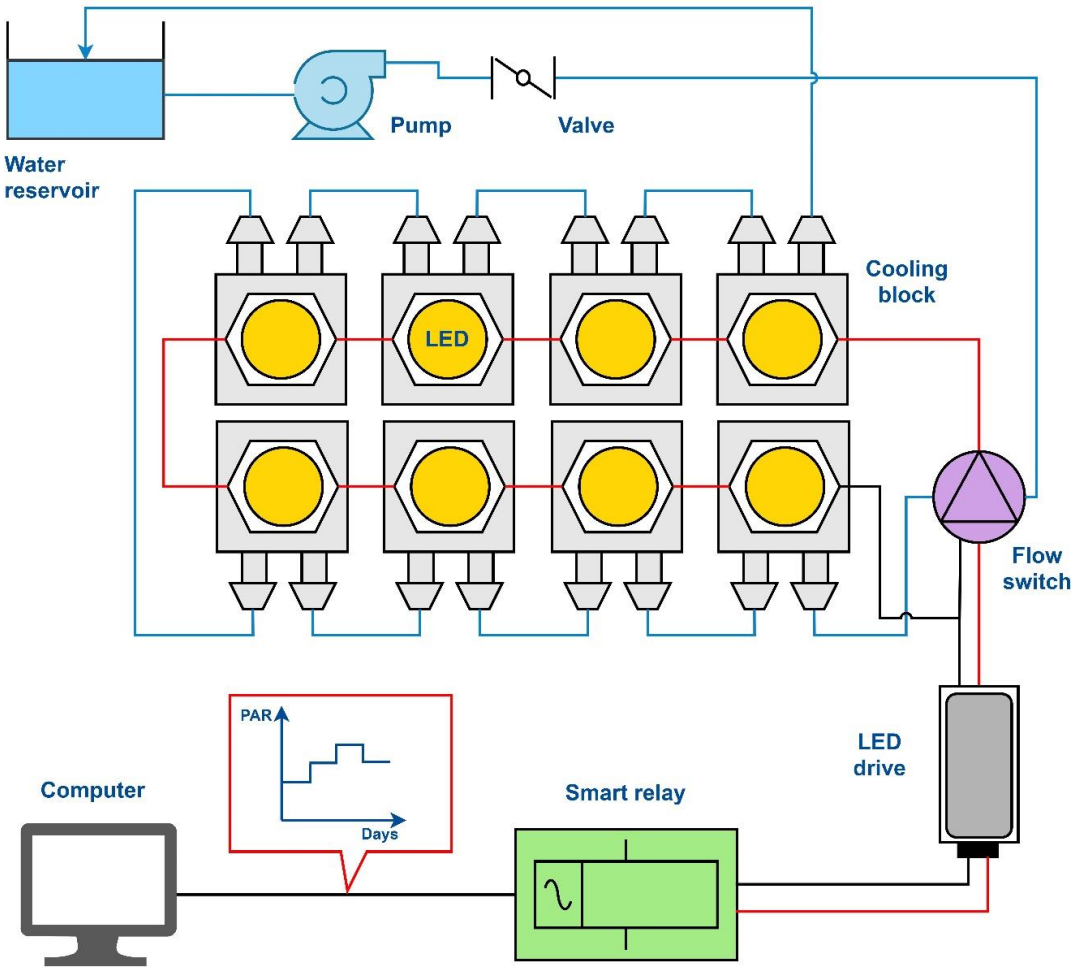

Figure 3.3. The schematic diagram of electrical (black and red colour lines) and cooling system (blue colour line) of the LED light system used in a lysimeter bank.

3.2.1.2. *The metal support frame and load cell arrangement*

A rigid metal frame served as the support to anchor 8 lysimeters in a 2 x 4 arrangement (Figure 3.4). The rear end of the load cell was affixed to the beam of the frame. In this design, the lysimeters were rested on three-point support in which one of the contact points was a load cell and the other two were height-adjustable screws (Figure 3.5). The three points were adjusted to the horizontal plane using a level before the lysimeter was placed on the stand.

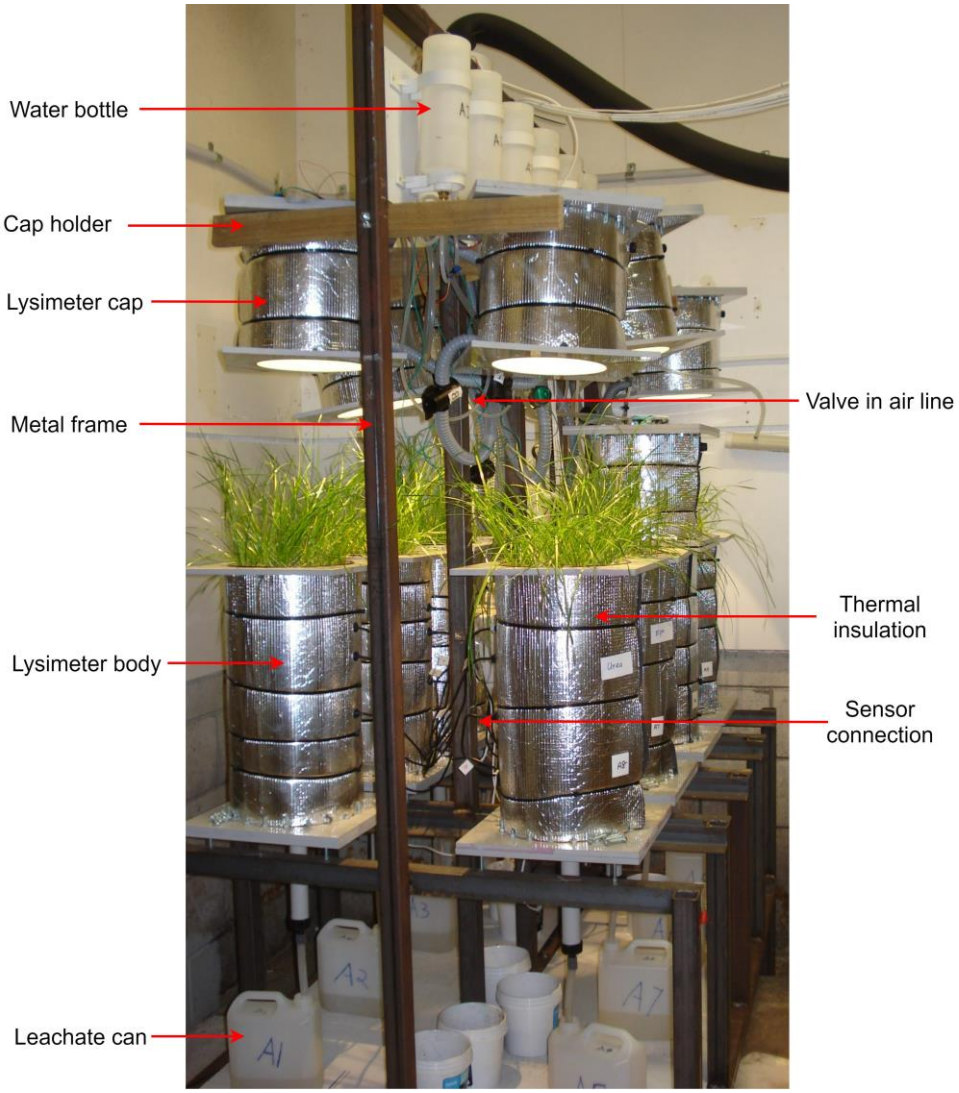

Figure 3.4. The arrangement of eight lysimeters (2 x 4 arrangement) on the metal support frame of a lysimeter bank. This image was taken after the cap was removed from the lysimeter body during the first grass clipping.

Figure 3.5. The side view of load cell assembly and lysimeter resting position on the load cell.

3.2.1.3. *The data acquisition system*

The lysimeter and ECU were equipped with different sensors to monitor and control the soil and environmental variables (Table 3.1). A DHT22 (Adafruit Industries, New York, NY) sensor was positioned near the air inlet and outlet port of the lysimeter cap to measure the temperature and RH changes that take place during the air circulation through the cap (Table 3.1). Another temperature sensor; DS18B20 (Adafruit Industries, New York, NY) was placed in the cap to measure the temperature changes of the middle part of the cap (Table 3.1). Three temperature (DS18B20) and soil moisture sensors (EC 5, Decagon Devices) were placed in three different depths of the soil profile (5, 10 and 20 cm) and positioned horizontally using a cable gland (Table 3.1). The precision of DS18B20 sensors was tested against a platinum point temperature probe and was within the rated range of ± 0.5°C (Table 3.1). Soil moisture sensors were calibrated in the respective soils they were used in (either sand or topsoil).

A 50 kg bending-beam type load cell was used to measure the weight changes of the lysimeter. The load cell was given 5 V of excitation voltage through an external power supply. The load cell was capable to measure to 5 g of its full 50 kg load capacity. All the load cells were calibrated separately using the 6 points calibration method (Misra et al., 2011) and a linear relationship was obtained for

loading and unloading of the weights. An HX711 module (Adafruit Industries, New York, NY) (24-bit resolution) was used to amplify and convert analogue signals to digital.

Table 3.1. The specifications and features of the sensors used in the lysimeter and environmental controlling unit.

Sensor	**Parameter**	**Reading range**	**Accuracy**	**Features**
DHT22	Temperature	-40 to 80 °C	± 0.5 °C	-
	RH	0 to 100% RH	± 2% RH	
DS18B20	Temperature	-10 to 85 °C	±0.5 °C	Water proof
EC-5	Soil moisture	0 to 60% VWM	± 1-2%	-
Load cell	Weight change	0 to 50 kg	2 mV/V ± 10%	IP65 & Temperature compensated

The architecture of the sensor connection is shown in Figure 3.6. The Arduino Mega 2560 (Adafruit Industries, New York, NY) was used as the data logger and it was programmed to gather readings from all sensors in 5-minute intervals. The data were stored with real-time values in an SD card using the data logger shield (Adafruit Industries, New York, NY) and on a computer.

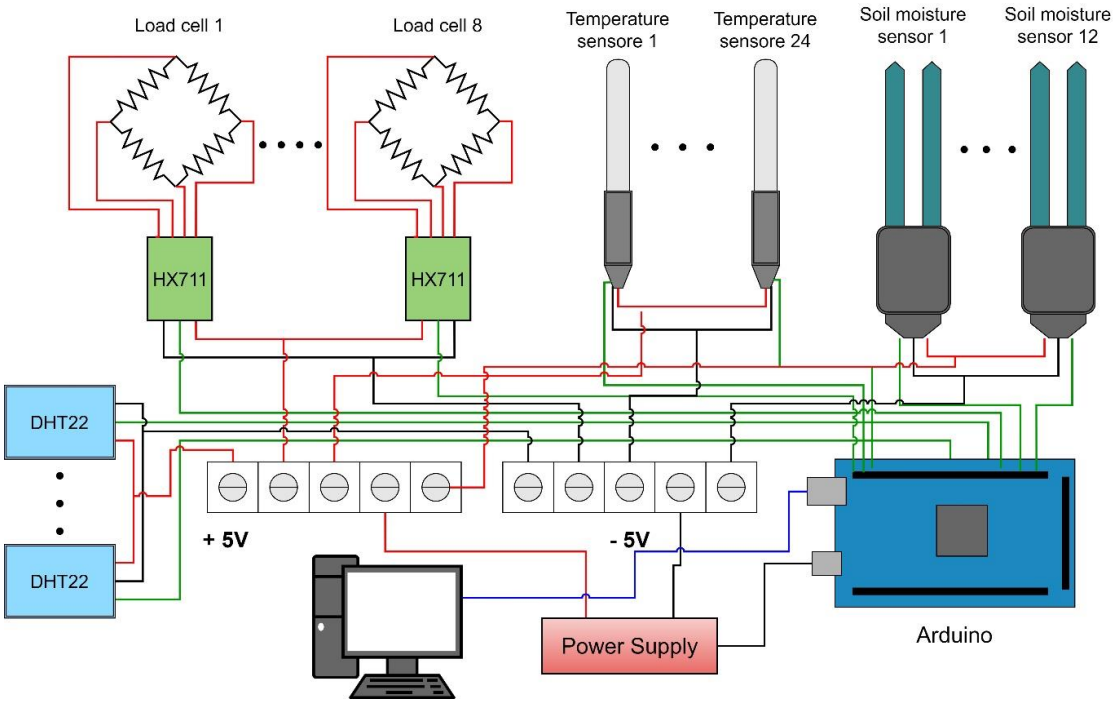

Figure 3.6. The architecture of the sensors and data logging system of a lysimeter bank.

3.2.2. Setup the lysimeter for the experiment

3.2.2.1. *Soil packing in lysimeter*

The soil column height was determined as 40 cm, which could provide enough space for root development for perennial ryegrass (average root depth was 30 cm) and the remaining depth of soil (10 cm) serves as the buffer zone. The top 10 cm of the soil profile was composed of Manawatu fine sandy loam (bulk density 1.18 g cm^{-3}) and the rest with washed builders' sand (bulk density 1.63 g cm^{-3}). The Manawatu fine sandy loam soil was excavated from Dairy 1 farm, Massey University, Palmerston North. The washed builders sand bought in packets from Bunnings, Lower Hutt and the origin of the soil is unknown. The soil packing was performed with soil segments each of 5-cm depth, which has a minimal distortion of hydraulic properties (Gunaratnam et al., 2020). The predetermined weight of the soil (using the bulk density and volume of 5 cm segment) was transferred to the lysimeter and gently compressed using a rammer to the 5 cm marked level. The soil surface was scarified after filling each

segment to maintain the hydraulic conductivity throughout the soil profile (Plummer et al., 2004).

3.2.2.2. *Ryegrass establishment and treatment application*

The perennial ryegrass (*Lolium perenne* L.) seedlings were grown in seedling trays under LED grow light (Solar system 550, California LightWorks) in a grow tent. At the three weeks stage, grass seedlings were transplanted into the lysimeter at a rate of 10 seedlings per lysimeter. During this period, the soil moisture level was maintained at around 70% of the field capacity.

Following the transplanting, seedlings were grown to the mature stage (full development of canopy and root) under the LED grow light in a grow tent for three months. During this period, ryegrass was irrigated to maintain the soil at around 70% field capacity level. The nutrients present in the soil were leached out by applying several (4 to 5) pore volumes of water through the soil matrix before the experimental period started in order to isolate and test the fertiliser effect on N losses and agronomic parameters. The grass was clipped at the end of every month at a height of 5 cm from the soil surface level to induce tiller formation and emulate natural grazing. After the 1st clipping, 'Nitrophoska Extra' (Ravensdown) fertiliser was applied to the seedlings at the rate of 50 kg-N ha^{-1}. This fertiliser contains N, P, K, S, Mg and Ca in 12: 5.2: 14: 8: 1.2: 3.8 ratios (and trace elements). At the end of the stabilization period, the grass was clipped and the soil moisture level was brought to 100% on the starting day of the experiment. The lysimeters were fertilised with urea at a rate of 200 kg-N ha^{-1}. Then caps were placed on the lysimeter and they were fastened with nuts and bolts to maintain an airtight enclosure.

3.2.3. Climate model

The performance of the lysimeter system design was tested with an emulated climate model. For this, the climate regime of the Taranaki region (spring season of 2013; September to November) was selected since it is one of the most productive dairying regions in New Zealand with high annual rainfall patterns. A

climate station named Stratford EWS (Agent No. 23872, Lat. -39.33726°, Long. 174.30487°, Elev. 300 m) in the Taranaki region was selected for this study and the complete and comprehensive range of climatic variables of this station were interrogated from the National Institute of Water and Atmospheric Research's (NIWA) climate database.

The daily rainfall values were adopted for the experiment in the climate model. However, weekly average values were considered for other climate variables (temperature, RH and PAR hours) due to the practical difficulties of altering the lysimeter climate on a daily basis (Figure 3.7). This three-month (spring season from September to November) climate model includes 48 rainfall events which were artificially created using the irrigation system. The temperature and daylight (PAR hours) of the climate model increased with time whereas RH showed a random small variation (as the model was a 90-day September to December climate in the Southern hemisphere) (Figure 3.7).

The air-flow rate was maintained at a constant rate for the total span of the experimental period (not changed weekly). The air circulation system was designed to remove the maximum potential evapotranspiration (MPET) of the climate model and it was calculated using the Penman-Monteith equation (Allen et al., 1998). According to the climate model, the MPET was 270.76 g-H_2O day^{-1} and it occurred in the 11^{th} week. The absolute humidity of the air for this week was 2.5 g kg-dry-air^{-1}. The number of total lysimeter cap volume changes need to remove this MPET was calculated by dividing MPET by absolute humidity and it was 108.31 volume changes. The ET takes place only during the LED operation time (PAR hours) and it was 12 hours for the 11^{th} week. The evapotranspiration during the night time was neglected for air flow calculations. Therefore, the number of volume changes per hour to remove the MPET was calculated by dividing total volume changes by PAR hours and it was 9.02 volume changes per hour. The total air flow rate for an hour was calculated by multiplying the lysimeter cap volume (9420 cm^3) by the number of volume changes per hour (9.02 times). This was 85027 cm^3 hr^{-1} and this airflow was maintained at a constant rate throughout the experiment. An air blower a little above this capacity was selected for the experiment and the exact flow rate was adjusted by bleeding excess air through a valve. The air velocity at each lysimeter bank distributor was measured

using a handheld anemometer and it measured as 0.12 m s^{-1}. By using the cross-sectional area of the air circulating tubes, the flow rate in to each lysimeter bank was calculated and it was 0.15 ± 0.01 m^3 hr^{-1}.

The photosynthetically active radiation (PAR) emitted from the LED was measured using a full spectrum PAR meter (Apogee Instruments, USA). The weekly average solar radiation (MJ m^{-2}) was converted to PAR and the LED operating PAR hours were calculated by dividing solar PAR by LED PAR. The weekly average operational hours (PAR hours) were provided by the LED light for the growing ryegrass (Figure 3.7).

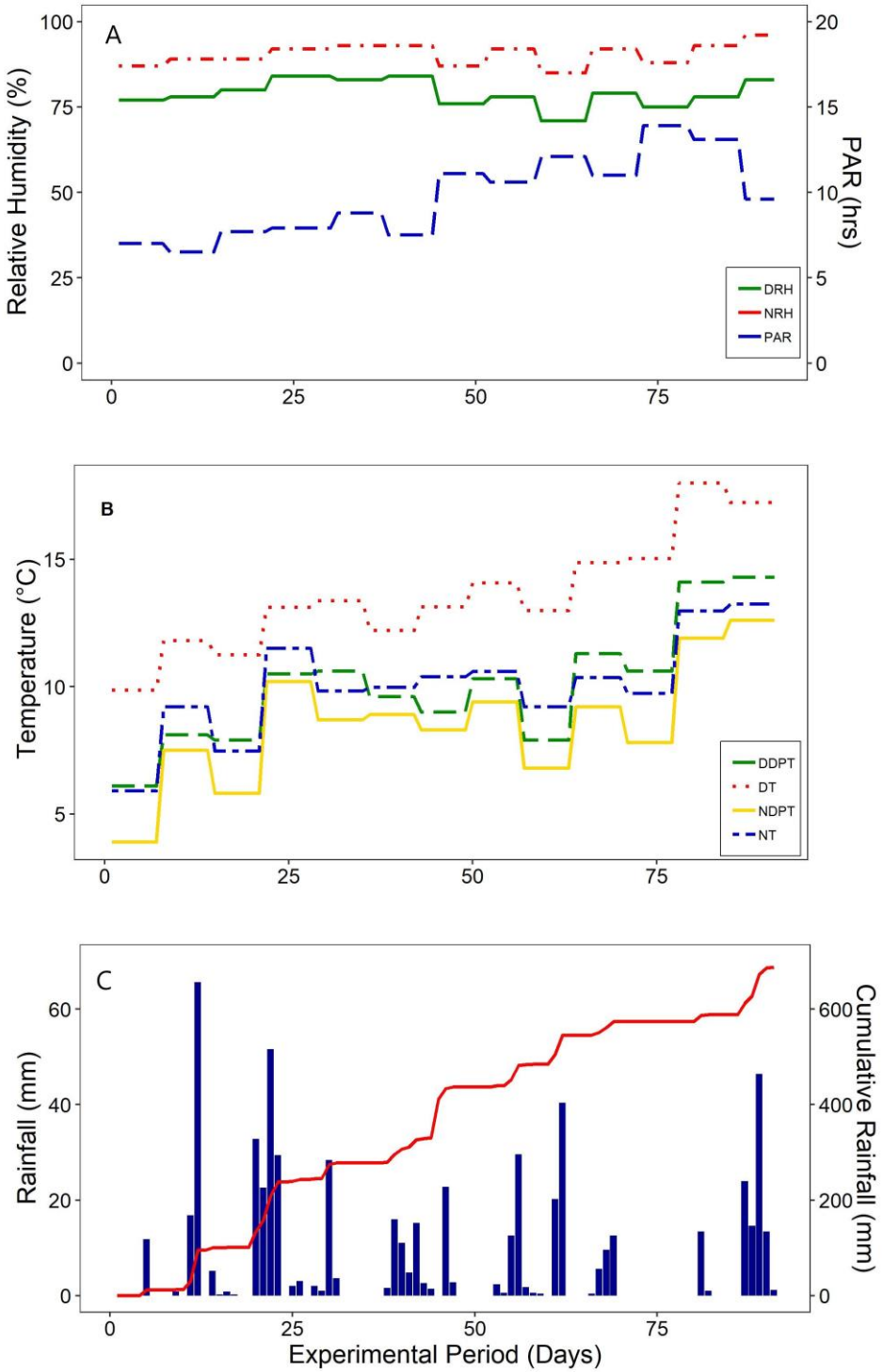

Figure 3.7. The climate regime of Taranaki region for the year 2013 (September to November); (A) weekly average of day (DRH) and night relative humidity (NRH) and photosynthetically active radiation (PAR), (B) weekly average of day (DT) and night temperature (NT) and day (DDPT) and night (NDPT) dew point temperature, and (C) daily rainfall and cumulative rainfall.

3.2.4. Environmental controlling unit

An environment controlling unit (ECU) was designed to control the environmental parameters (Figure 3.8); weekly average temperature and RH in the growing space (lysimeter cap) as per the climate model. The dew point temperatures of the climate model were ranged between 3.9 and 14.3 °C, wherein most of the values were lower than the ambient temperature of the laboratory. Hence, a humidification column was incorporated into the system which allows simultaneous cooling and humidification or dehumidification.

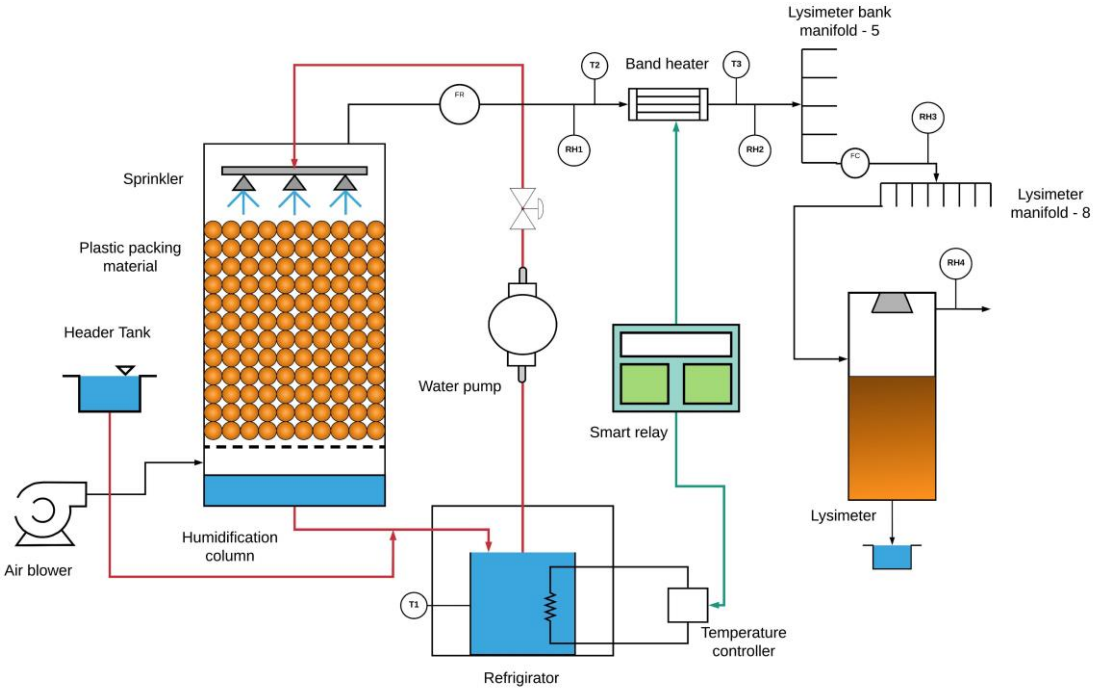

Figure 3.8. The schematic diagram of environmental controlling unit coupled with lysimeter: temperature sensor (T), relative humidity sensor (RH), flow control valve (FC) and flow meter (FR).

3.2.4.1. *Humidification column – Design 1*

The packed-bed humidification column was packed with plastic packing material to a height of 290 mm (Figures 3.9 & 3.10-a). An air-blower was used to feed the outside air through the humidification column. The circulated water through the humidification column was pre-refrigerated using a chiller to bring down the temperature to the dew point (Figure 3.10-b). A temperature controller was connected to the refrigerator to maintain the water temperature at the dew point (fluctuation limit of ±0.5 °C) with on-off control. A smart relay fed with the weekly average dew point temperature values regulated the temperature controller (Figure 3.10-c). The refrigerated water was pumped into the column using a 12 V DC pump and sprayed on top of the packed bed using an array of drippers arranged in a circular pattern (Figure 3.9). The water drips down through the packed bed to the reservoir.

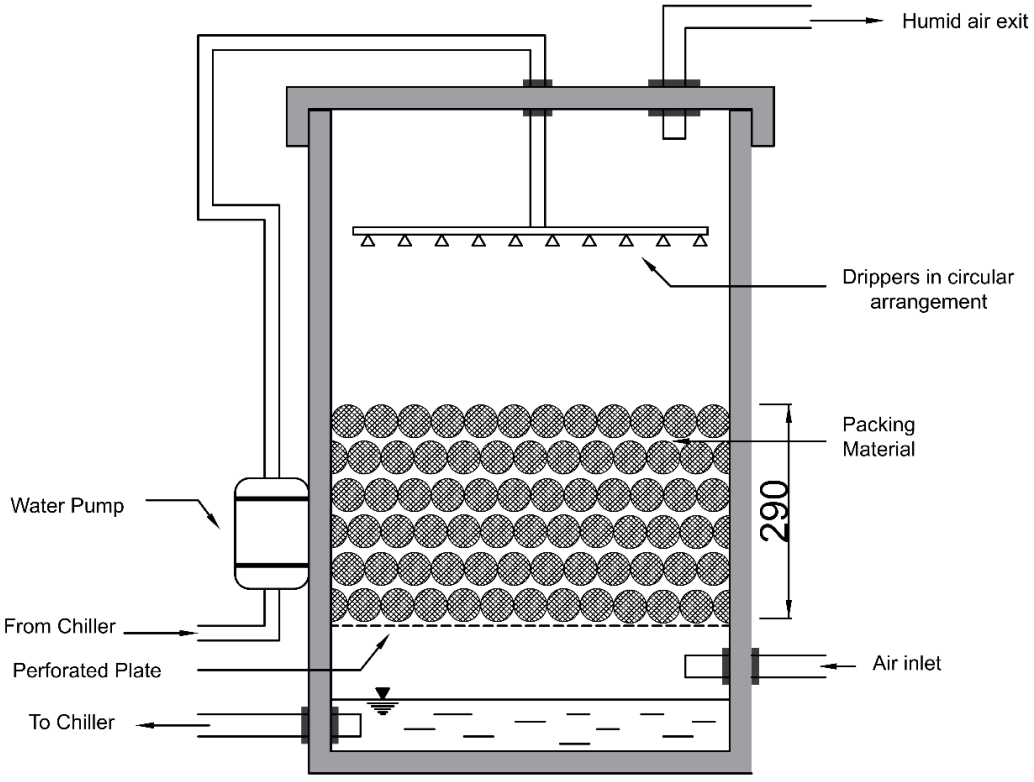

Figure 3.9. The schematic diagram of the humidification column design 1 used in fertiliser testing trial 1.

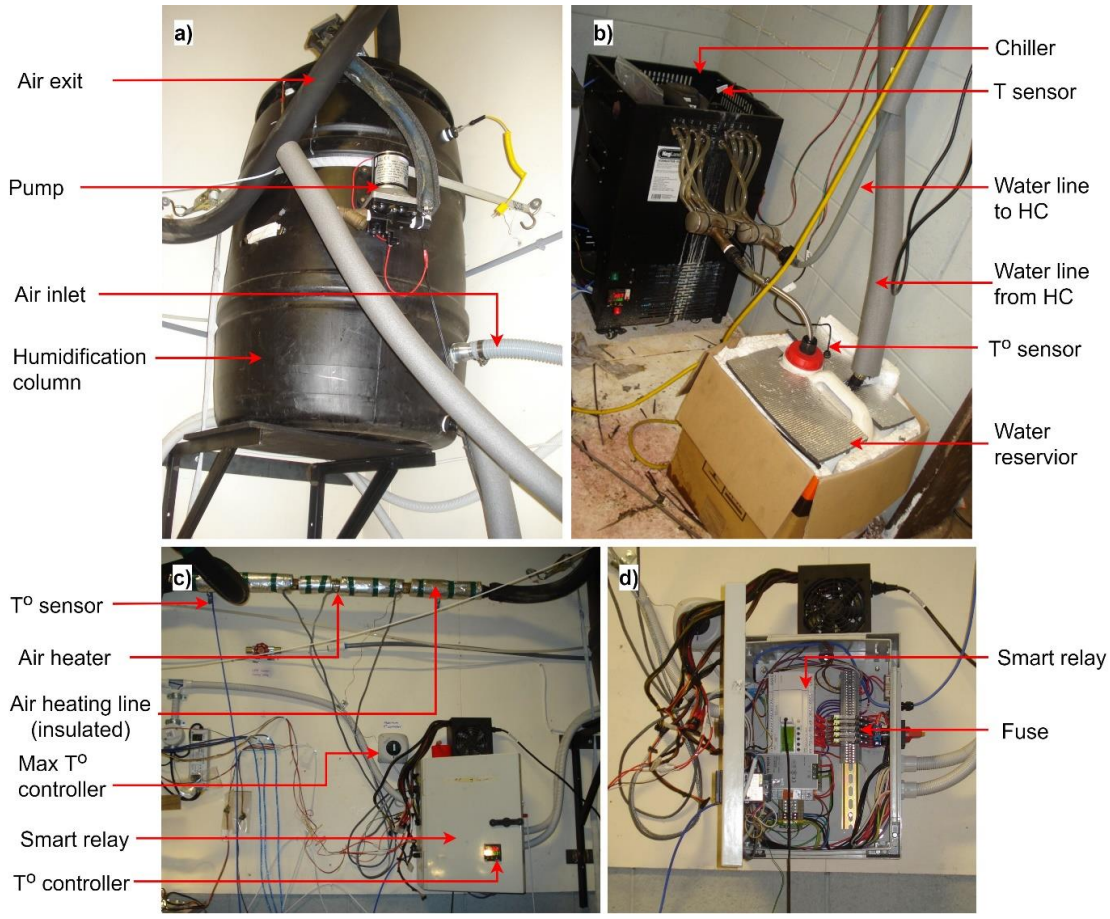

Figure 3.10. The components of the environmental controlling unit; (a) humidification column (HC), (b) chiller and water reservoir, (c) air-heating unit and temperature controllers, and (d) smart relay unit.

3.2.4.2. *Humidification column – Design 2*

In humidification column design 2, there were three major changes made to design 1. First, the packed bed height was increased to 500 mm. Second, all the water circulating lines and airlines were insulated to minimise thermal exchanges. Third, the circular drippers were replaced by a perforated pan. This pan has several air vents to minimise the airflow resistance and maintains a moderate airflow rate (Figure 3.11). The water inflow rate from the chiller to the perforated pan was higher than water dripping rate through pan holes thus a thin water film was maintained for spreading water over the pan uniformly. This helps to drip the water uniformly on the packing material.

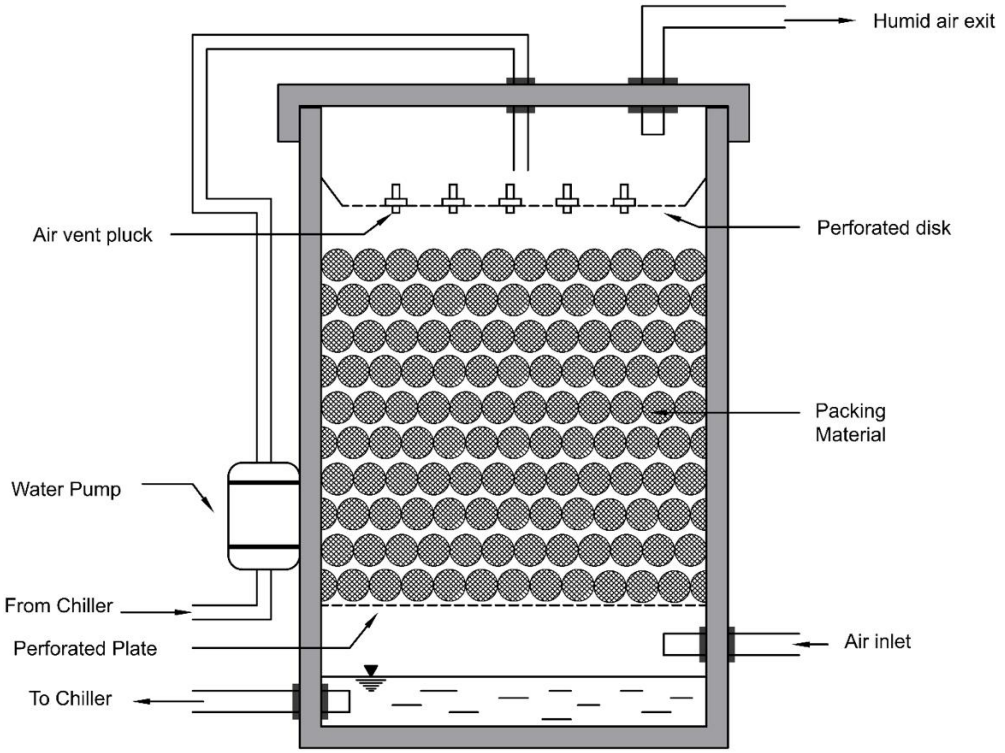

Figure 3.11. The schematic diagram of the humidification column design 2 used in fertiliser testing trial 2.

The function of the ECU is summarized in Figure 3.12. The saturated air (100% RH) leaves the humidification column at the dew point temperature. At this stage, airflow rate, temperature and RH of the humid air were measured. Subsequently, the air temperature was elevated to the dry-bulb temperature of the climate model using an air heater. A platinum thermocouple was fixed at the air exit point of the air heater to measure the heated air temperature and send the signals to the temperature controller. Based on the feedback from the thermocouple, the temperature controller controls the air temperature within ±1 °C of the set temperature value. For the safe operation of the air heater, a high limit temperature controller (HLTC) was connected and the maximum operational temperature was set to 100 °C. In case of a malfunction in the heater, the HLTC shuts down the heating system to avoid fire hazards. Thereafter, the heated air was distributed to five lysimeter banks using a 5-port manifold and then dispensed for eight lysimeters in a lysimeter bank using another 8-port manifold (Figure 3.13).

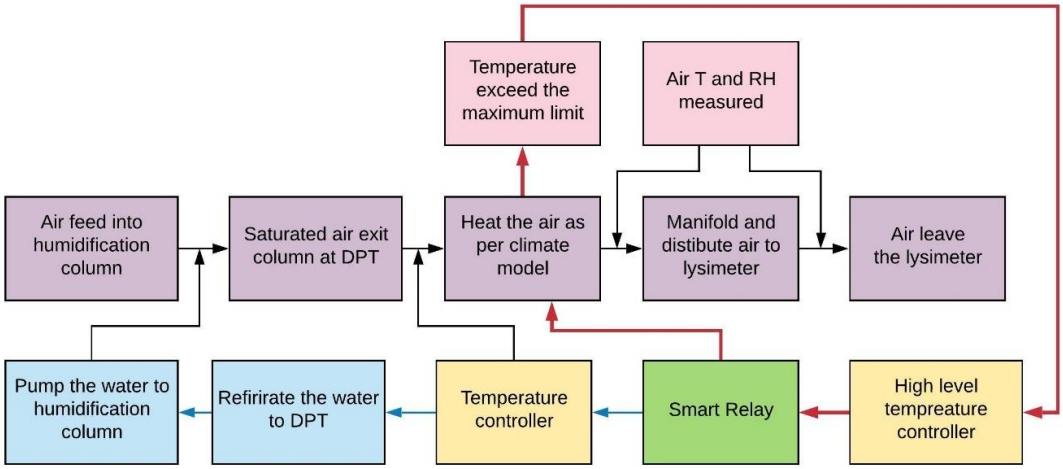

Figure 3.12. The process flow diagram of the environment controlling unit (ECU).

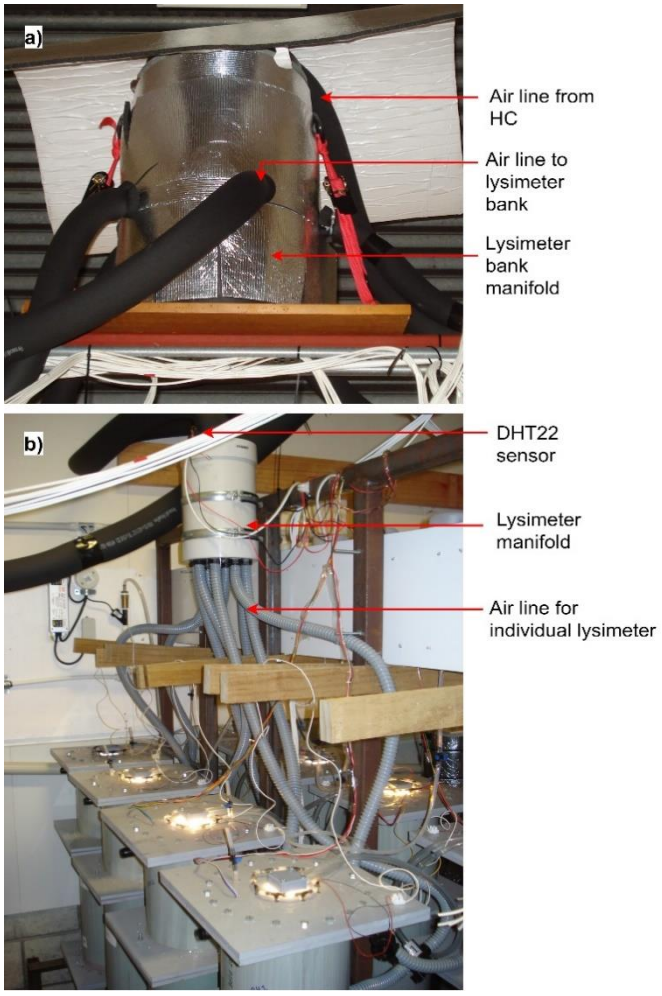

Figure 3.13. (a) Lysimeter bank manifold and (b) lysimeter manifold, which distributes air to five lysimeter banks and eight lysimeters, respectively.

3.2.5. The assessment of environment controlling unit's performance

The performance of the ECU was assessed by comparing the observed temperature and RH of microclimate in plant proximity against the targeted temperature and RH as per the climate model. The allowable fluctuation limit of temperature and RH was ±1°C day^{-1} and ±5% day^{-1}, respectively, from the targeted values.

3.2.6. The assessment of lysimeter system's performance

The success of recreating a climate model in a lysimeter system can be measured using metrological parameters and the growth of a crop under a particular climate condition. So, measured values of drainage, evapotranspiration and dry matter yield from the lysimeter experiment were compared with estimated values derived from the climate model.

3.2.6.1. *The observed and estimated evapotranspiration*

The observed evapotranspiration was calculated using weight change data obtained from load cells using a water balance method.

The estimated evapotranspiration was calculated using the following method. The reference evapotranspiration (ET_o in mm day^{-1}) was calculated using the FAO-56 version of the Penman-Monteith equation (Allen et al., 1998). The ET_o calculated for the weekly average values since these values were emulated in the lysimeter study.

$$ET_0 = \frac{0.408 \times \Delta \times (R_n - G) + \gamma \frac{900}{T + 273} \times U_2 (e_s - e_a)}{\Delta + \gamma (1 + 0.34\, U_2)}$$

Where R_n net radiation at the crop surface [MJ m^{-2} day^{-1}], G soil heat flux density [MJ m^{-2} day^{-1}], T mean daily air temperature at 2 m height [°C], U_2 wind speed at 2 m height [m s^{-1}], e_s saturation vapour pressure [kPa], e_a actual vapour pressure

[kPa], e_s - e_a saturation vapour pressure deficit [kPa], Δ slope vapour pressure curve [kPa °C^{-1}] and ɣ psychrometric constant [ɣ ≈ 66 Pa K^{-1}].

The estimated evapotranspiration (ET_e in mm day^{-1}) was calculated using a crop coefficient approach based on the FAO guidelines (Allen et al., 1998).

$$ET_e = K_c \times ET_o$$

The crop coefficient (K_c is a dimensionless parameter) for perennial ryegrass under a rotational grazing system was derived from a developed relationship between K_c and grass height, h (KC et al., 2018).

$$K_c = 0.02h + 0.38$$

The crop adjusted Kc values for the first four weeks were 0.5, 0.6, 0.7 and 0.8, respectively. These values were well matched with the prescribed values for initial, mid and end values of crop coefficient derived by Allen et al. (1998).

3.2.6.2. *The observed and estimated drainage*

The observed drainage (D_o) was measured after every drainage event using electronic balance and values were averaged.

The estimated drainage (De) was calculated using the water balance equation.

$$D_e = I - ET_e - S - R$$

In our experiment, the runoff (R) was zero since the lysimeter wall restricts the sideways movement of ponding water thus irrigation (I) was only directed downward. At the commencement of the experiment, all the lysimeters were brought to field capacity. Therefore, the change of the soil water storage (S) was zero when the experiment was started.

3.2.6.3. *The observed and estimated dry matter yield*

The ryegrass swards were clipped at 5 cm height at the end of each month for three months. The dry weights were obtained and the average was calculated. The DM yield was estimated using climate-driven, soil fertility dependent, pasture

production model developed based on New Zealand conditions (Moir et al., 2000). This model correlates the DM yield of pasture with ET and assumes the proportionality constant (k) depends on the soil fertility. The values for k ranged from 11 to 19 kg-DM ha^{-1} for high and low soil fertilities, respectively.

$$G = k \times ET_e$$

Where G is pasture DM yield (kg-DM ha^{-1}), k is proportionality constant (kg-DM ha^{-1} mm^{-1}) and ET_e is estimated evapotranspiration (mm). The ET was moderate given that the emulated climate condition in this study was spring. Therefore, the middle proportionality constant value (k = 15) was applied to estimate DM yield.

3.2.7. Data Analysis

The observed and targeted climate variables (temperature and RH) and observed and estimated values of evapotranspiration, drainage and dry matter yield of perennial ryegrass were compared using Root Mean Squared Error (RMSE), linear regression statistics (Person r, slope and R^2) and Mean Bias Error (MBE) as follows;

$$RMSE = \sqrt{\frac{1}{n}\sum_{i=1}^{n}(E_i - O_i)^2}$$

$$MBE = \frac{1}{n}\sum_{i=1}^{n}(E_i - O_i)$$

Where Ei and Oi are estimated and observed values, respectively; n is number of samples.

All analysis were performed in R 3.5.1 (R Core Team, 2019).

3.3. Results and Discussion

3.3.1. Temperature and Relative Humidity

The daily mean values of day and night temperature for the span of the experimental period is shown in Figure 3.14. The actual day and night temperature values were significantly ($P<0.05$) and positively correlated ($r = 0.783$) with the targeted temperature values of the climate model. The MRSE for total daily temperature value was 1.96°C day^{-1}, which was larger than the allowable fluctuation limit of 1°C day^{-1} (Table 3.2). The day (DT) and night temperature (NT) values were broken down and analysed separately to investigate the individual contribution for the variation. Both day and night temperature values were significantly ($p<0.05$) correlated with targeted values. However, lower Pearson correlation coefficient ($r_{DT} = 0.77 > r_{NT} = 0.621$) and higher RMSE (DT = 1.56 < NT = 2.3°C day^{-1}) showed that NT was deviated more highly than DT in relation to the allowable fluctuation limit (Table 3.2). The lower temperature limit of the chiller used in the ECU was 6°C and therefore, low NT values were not achieved successfully. On these days a higher night ambient temperature is recorded (Figure 3.14). The monthly temperature breakdown showed that the targeted temperature was successfully attained in the 3rd month (RMSE = 0.85 < 1°C day^{-1}) compared to the first two months. The lower Pearson correlation coefficient ($r = 0.565$) and higher RMSE (1.96°C day^{-1}) suggest that the greatest deviation of temperature was experienced in the 2nd month when compared to the other two months.

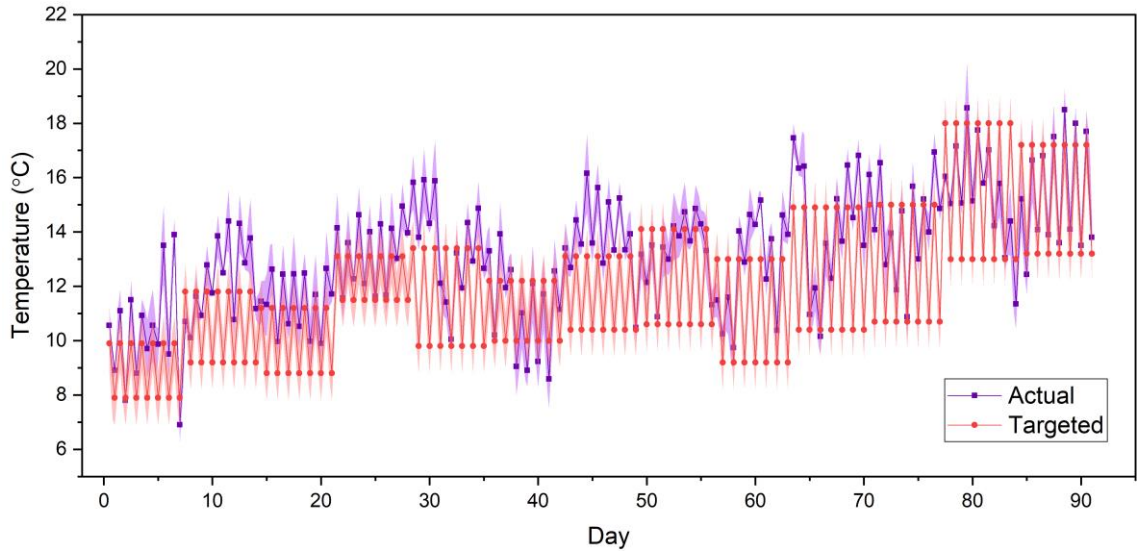

Figure 3.14. The daily average values of day and night temperature; actual temperature in growing space (lysimeter cap) and targeted temperature according to the climate model. The purple shade indicates the standard deviation of actual temperature (n=5) and the red shade indicates the targeted temperature range (±1°C).

Table 3.2. The summary of the statistical analysis between actual and targeted temperature.

Parameter	**RMSE** (°C day^{-1})	**MBE** (°C day^{-1})	**Pearson r**	**Significance**
Total daily values	1.96	1.19	0.783	P<0.05
Day Temperature (DT)	1.56	0.66	0.77	P<0.05
Night Temperature (NT)	2.30	1.72	0.621	P<0.05
1st Month Temperature	1.90	1.54	0.815	P<0.05
2nd Month Temperature	1.96	0.84	0.565	P<0.05
3rd Month Temperature	0.85	0.89	0.727	P<0.05

The RH changes of the growing space (lysimeter cap) are shown in Figure 3.15. The daily day and night average RH values were significantly (P<0.05) and positively correlated (r = 0.664) with targeted RH. The RMSE of total daily average RH (4.45% day^{-1}) was within the targeted fluctuation range of 5% day^{-1}. The night RH (NRH) deviated highly compared to day RH (DRH), from the

targeted values (Table 3.3). The RMSE of DRH was within the targeted RH fluctuation range, whereas NRH was higher by 0.6% day^{-1}. The higher Pearson correlation (r = 0.885) and lower RMSE value (4.4% day^{-1}) indicated that the targeted RH was achieved successfully in the 3rd month compared to the other two months (Table 3.3).

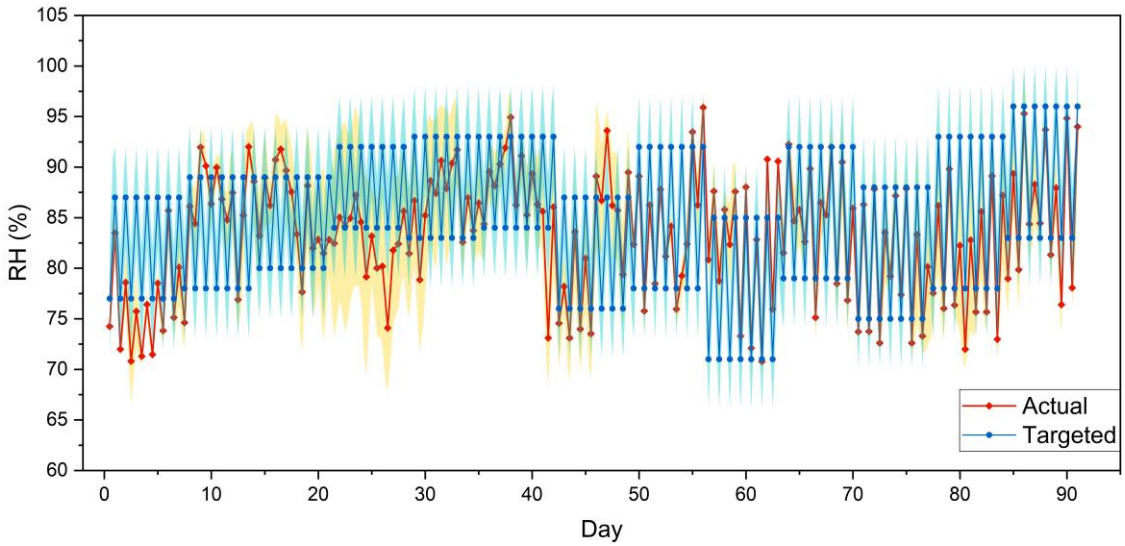

Figure 3.15. The daily average value of day and night RH; actual RH in growing space (lysimeter cap) and targeted RH according to the climate model. The yellow shade indicates the standard deviation of actual RH (n=5) and blue shade indicates the targeted RH range (± 5%).

Table 3.3. The summary of the statistical analysis between actual and targeted RH.

Parameter	**RMSE** (RH% day^{-1})	**MBE** (RH% day^{-1})	**Pearson r**	**Significance**
Total daily RH values	4.45	-1.34	0.664	P<0.05
Day RH (DRH)	4.29	1.00	0.468	P<0.05
Night RH (NRH)	5.60	-3.68	0.68	P<0.05
1st Month RH	6.27	-2.06	0.41	P<0.05
2nd month RH	5.40	0.24	0.664	P<0.05
3rd month RH	4.40	-2.09	0.855	P<0.05

In general, the temperature and RH of the growing space were satisfactorily controlled using the ECU. The growing environment in five lysimeter banks (totally 40 lysimeters) was controlled by one centralised humidification column and chiller. This increased the air-distribution line length, which allowed more heat exchange between the air-line and the outside environment. An individual humidification column for each bank would shorten the air-line and decrease the heat exchange. Furthermore, the thermal load from the air, sent to all five lysimeter banks was harder to manage by the low-capacity single chiller used in this experiment. Hence, either a chiller with a high cooling capacity or an individual chiller for each lysimeter bank is essential for maintaining the low NT of the climate model.

Although the insulation around the lysimeter body and cap mitigated the influence of the outside temperature, an active cooling mechanism is required to completely avoid it. Therefore, a thermally insulated cooling chamber around the lysimeter banks is recommended for future studies to maintain a consistent ambient temperature. In this study, a smart relay that can perform on-off control was used. This sent the programmed temperature to the chiller and air-heater, but did not adjust the climate variables of the growing space, using a feedback mechanism. However, for more precise control of environmental variables, a programmable logic controller (PLC) with a feedback control mechanism is required.

3.3.2. Drainage

The observed drainage (Do) for the total period of the experiment (91 days) was well within the range of estimated drainage (De) values (Figure 3.16). Although the number of estimated drainage events (25) were equal to the observed events, one unpredicted drainage event and one missed drainage event occurred (encircled in Figure 3.16). The expected drainage after a small rainfall event was not observed on the 33rd day. However, an unexpected drainage event was observed after moderate dry days on the 83rd day of the experiment. These mismatches were due to the imbalance of observed and estimated ET. Similar mismatch drainage events were reported in another study (Graham et al., 2019). It was observed that only 12 events matched with the estimated 25 drainage

events in terms of drainage volume, while 5 and 9 events were overestimated and underestimated, respectively. The cumulative De and Do were 525.15 ± 25 and 535.64 mm, respectively. The observed total drainage value was within the estimation, and this suggests that drainage was emulated well according to the climate model.

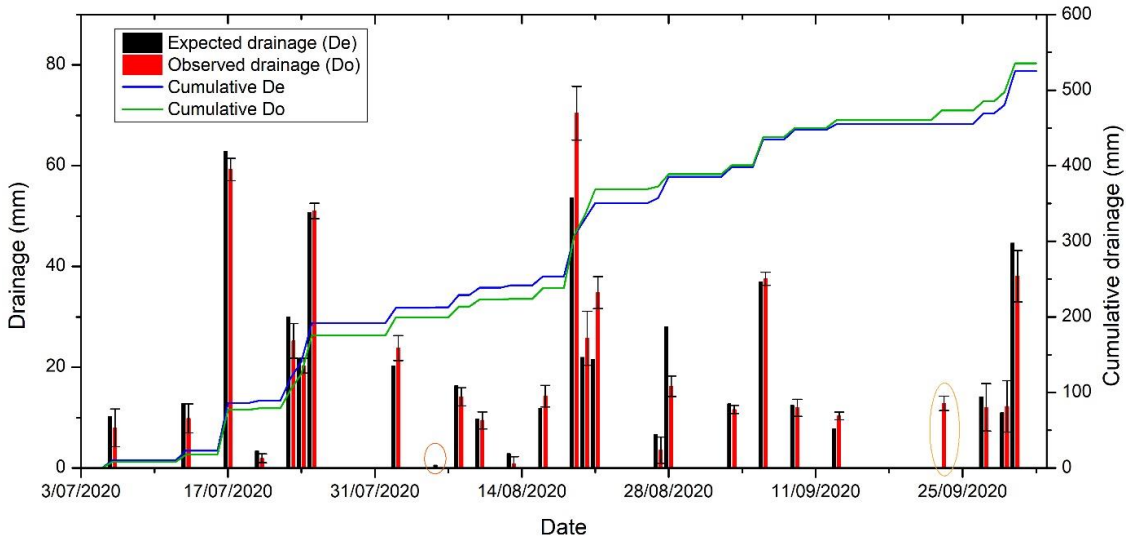

Figure 3.16. The sequential and cumulative observed and estimated drainage over 91 days of the experimental period. The error bars indicate standard deviation (n = 40). Unexpected drainage events are encircled in orange colour.

3.3.3. Evapotranspiration

The load cell sensitivity was sufficient to detect all hydrological components; rainfall, drainage, and evapotranspiration. The daily evapotranspiration was calculated by using changes in load cell readings, in association with a water balance method. The final weight of the lysimeter per day was calculated by performing the mean value of the last 30 minutes (12 data points) load cell measurement of that day (Figure 3.17).

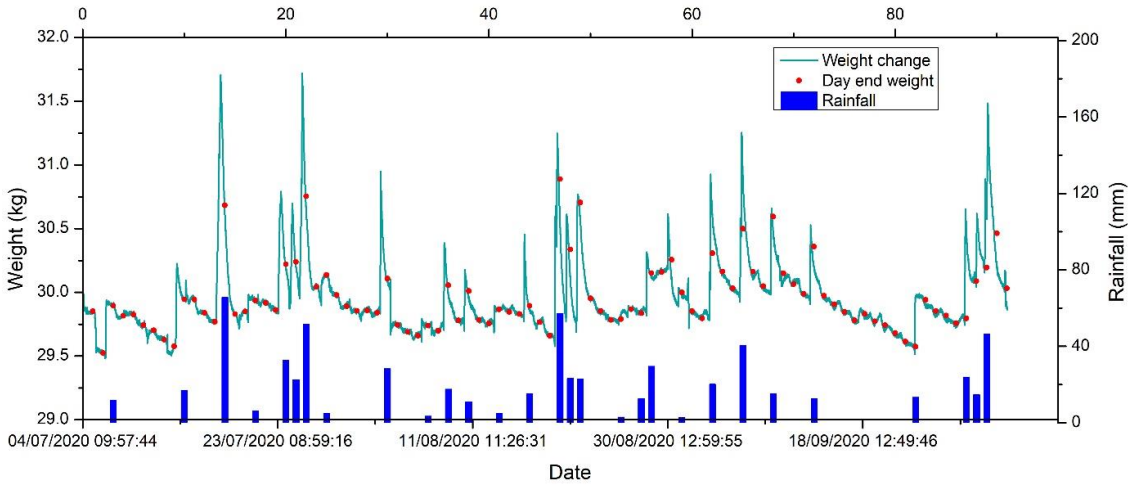

Figure 3.17. The weight changes of lysimeter (kg) obtained from load cell measurement, day end average lysimeter weight (kg) and rainfall (mm) during the experimental period.

The potential evapotranspiration was estimated using the FAO-56 version of the Penman-Monteith equation (Allen et al., 1998). Agreement between observed (ETo) and estimated evapotranspiration (ETe) was moderate throughout the experimental period (Figure 3.18 and Table 3.4). The cumulative ETo and ETe were 122.38 ± 45 and 104.96 mm, respectively. Although the ETo value was within the ETe value, the average observed ET was 17.42 mm (equivalent to 546.9 ml) higher than the estimated value and ETo always showed a higher trend than ETe (Figure 3.18). This could be attributed to the temperature variation in the growing space. The total number of matched, underestimated and overestimated ET events were 13, 10 and 5, respectively (Table 3.4). The number of underestimated events were higher in the first two months; 3 and 6, respectively, whereas overestimated events (2) were higher in the last month. The cumulative ETo in the first and third months was within the estimated range (Figure 3.19). However, ETo was greater than ETe in the second month. These observations are linked with the temperature of the growing space where the temperature of the second month deviated more when compared to the other two months. Other possible causes for deviation of ETo from ETe; ETo was influenced by the outside environment and underestimation of ET by the Penman-Monteith equation. Many other studies also reported the under or overestimation

of ET by the FAO-56 Penman-Monteith approach during the high and low evaporative demand periods (López-Urrea et al., 2006).

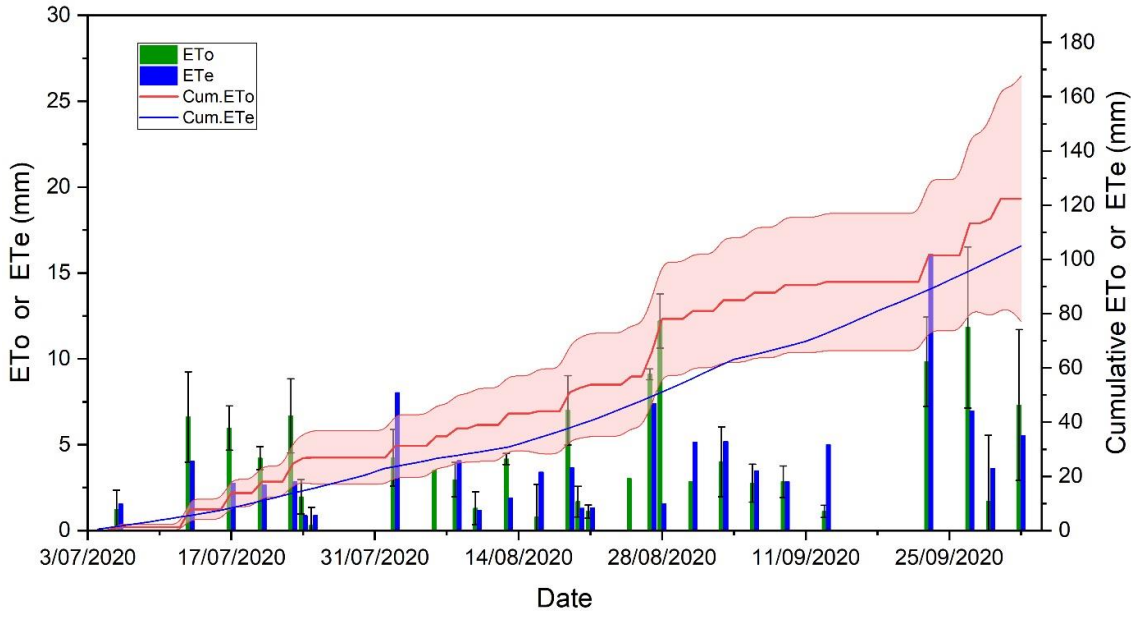

Figure 3.18. The sequential (ETo & ETe) and cumulative changes of observed (Cum.ETo) and estimated (Cum.ETe) evapotranspiration over the experimental period of 91 days. The red shaded area of cumulative ETo and error bars of ETo represent SD (n = 40).

Table 3.4. Summary of monthly estimated and observed evapotranspiration.

	Within range				Underestimated				Overestimated			
Month	**No of events**	**ETo**	**SD**	**ETe**	**No of events**	**ETo**	**SD**	**ETe**	**No of events**	**ETo**	**SD**	**ETe**
		(mm)	(mm)	(mm)		(mm)	(mm)	(mm)		(mm)	(mm)	(mm)
1	4	10.13	5.77	7.33	3	16.86	4.12	8.27	1	4.24	1.65	8.03
2	4	7.08	3.22	7.91	6	39.01	4.23	14.55	2	3.66	1.90	8.56
3	5	18.62	12.28	20.68	1	11.83	4.69	6.97	2	10.95	2.95	21.1
Total	13	35.83	21.27	35.92	10	67.7	13.04	29.79	5	18.85	6.51	37.69

SD – standard deviation (n = 40).

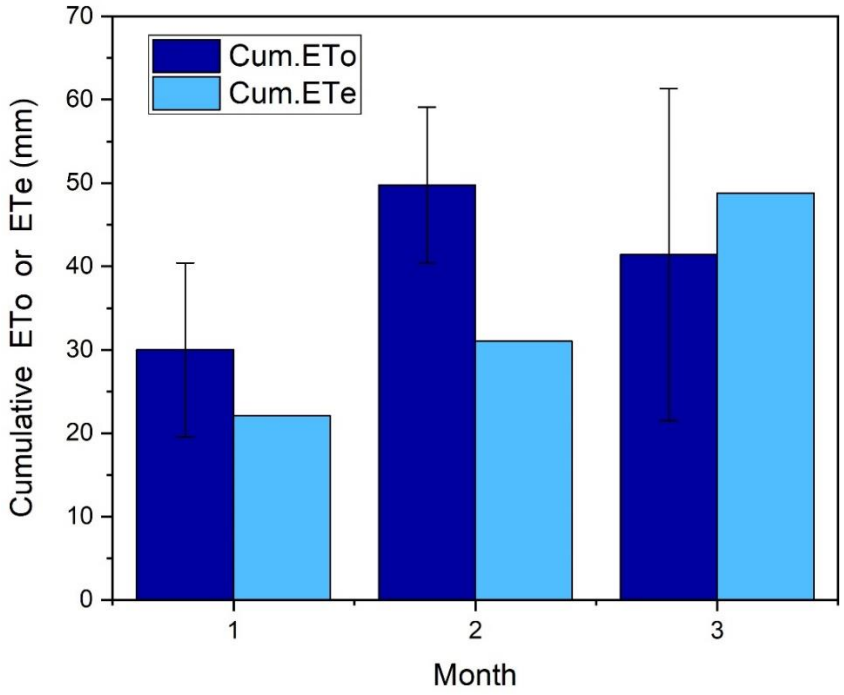

Figure 3.19. Monthly cumulative observed (Cum.ETo) and estimated (Cum.ETe) evapotranspiration.

3.3.4. Dry matter yield

The predicted DM yield using estimated evapotranspiration was compared with the observed DM yield in the lysimeter experiment. The DM yield decreased with time and it was significantly ($P<0.05$) higher for the first month and lower for the third month (Figure 3.20). The DM yields for the first two months were within the estimated value (Figure 3.20). However, the third month DM yield was lower than the estimation. Decreasing yield with time suggests that growth was limited by one or more factors (Figure 3.20). For a better prediction of DM yield using the ET approach, other factors such as water, nutrient and light should not be limiting the growth of the plant (Moir et al., 2000). In this study, plant available water was always above 50% of field capacity thus was not a limiting factor. The light was not a limiting factor since the LED provides sufficient light throughout the experimental period. Nevertheless, soil nitrogen level could be a limiting factor since the ryegrass received a single application of urea (200 kg-N ha^{-1}) at the

commencement of the experiment. The major portion of the applied nitrogen was attenuated by the plants in the first two months (67.1 kg-N ha^{-1}), and a portion of that was leached (72.9 kg-N ha^{-1}) since the subsoil (sand). Therefore, insufficient soil nitrogen potentially limited ryegrass growth in the third month. However, the total observed DM yield was within the estimated value (Figure 3.20). Overall, the ryegrass DM yield was satisfactorily produced in the new lysimeter system as estimated.

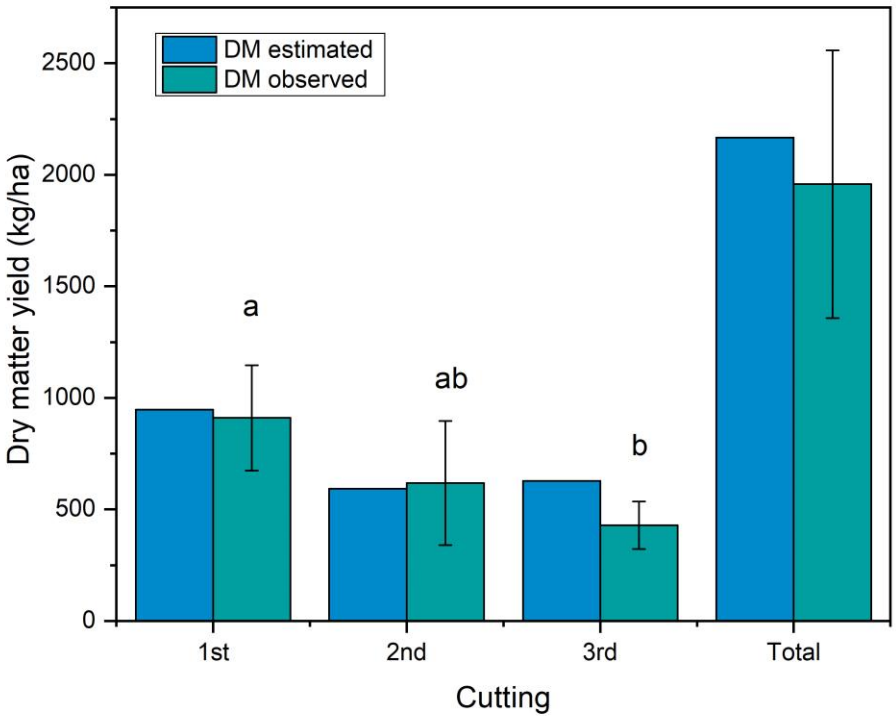

Figure 3.20. The observed (DMo) and estimated (DMe) DM yield of ryegrass for three months (1^{st}, 2^{nd} and 3^{rd}) and total DM yield. Vertical bars show the standard deviation (n=8). Letters show significant difference in monthly observed DM yield at $p<0.05$ using a Tukey HSD post-hoc test.

3.3.5. The correlation analysis

The correlation analysis was performed for observed and estimated values of drainage, evapotranspiration and DM yield. The observed drainage values were significantly ($P<0.05$) and positively correlated ($r = 0.97$) with estimated drainage

values (Figure 3.21). The lower RMSE (3.19) and MBE (0.12) confirm the good fit between observed and estimated values of drainage. The observed evapotranspiration showed significant ($P<0.05$) and positive correlation ($r = 0.757$) with estimated values (Figure 3.21). The correlation between observed and estimated DM yield was significant ($P<0.05$) and positively correlated ($r = 0.882$) (Table 3.5).

Table 3.5. Comparison of observed and estimated values of cumulative drainage, evapotranspiration (ET) and dry matter (DM) yield, root mean squared error (RMSE), mean bias error (MBE) and linear regression statistics over 91 days of the experimental period.

Parameter	Observed	Estimated	RMSE**	MBE**	R^2	Slope	Pearson r
Drainage	536±65*	525.15	3.19	0.12	0.94	0.05	0.97
ET	122±45*	104.97	1.83	0.21	0.57	0.22	0.76
DM yield	1957±599*	2167	117.34	-69.75	0.97	258	0.98

* Mean ± standard deviation of 40 replicates for drainage and ET, and 8 for DM yield.

** Units of RMSE and MBE for drainage, ET and DM yield are mm day^{-1}, mm day^{-1} and kg ha^{-1} $month^{-1}$, respectively.

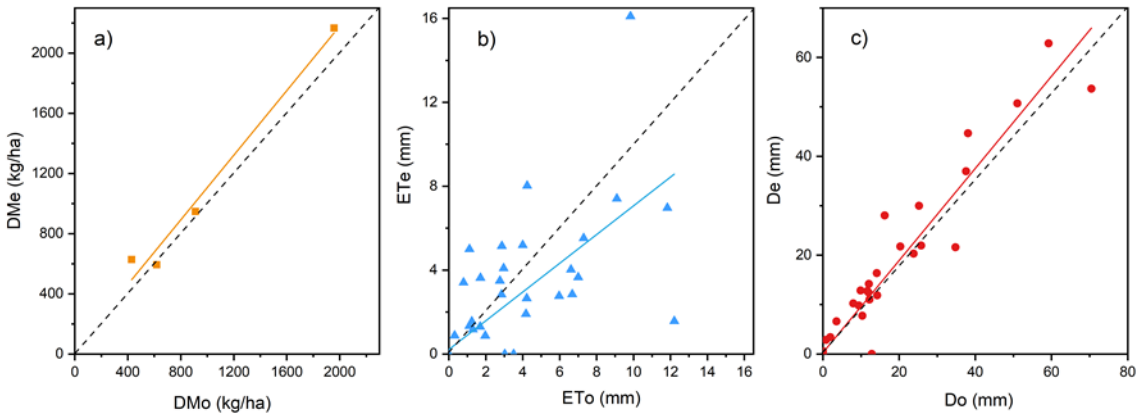

Figure 3.21. The correlation analysis; (a) observed DM yield (DMo) and estimated DM yield (DMe), (b) observed evapotranspiration (ETo) and estimated

evapotranspiration (ETe), and (c) observed drainage (Do) and estimated drainage (De). The broken line indicates the 1:1 line.

The correlation analysis suggests that drainage, evapotranspiration and DM yield were significantly ($P<0.05$) correlated with respective estimated values. The selected Taranaki climate model for this study was satisfactorily emulated in the newly developed lysimeter system design. Therefore, a challenging climate condition of a field study can be nearly imitated in a laboratory using this climate-controlled lysimeter system.

3.4. Conclusions

A climate-controlling lysimeter system design was required for iterative testing of newly developed CRF formulations. A lysimeter system coupled with an environment controlling unit was developed and the Taranaki climate model was emulated. The performance of this lysimeter system for imitating the climate model was investigated by comparing the observed temperature and RH with targeted values and comparing observed drainage, evapotranspiration and dry matter yield with estimated values from the climate model.

After 91 days of the experiment, the new lysimeter system design was able to imitate a climate model to a satisfactory level. The observed-average temperature and RH values were significantly ($P<0.05$) correlated with the targeted values. However, the RMSE of observed average temperature was higher than the allowable fluctuation limit (AFL), and the night-time temperature values were more deviated than day-time temperature. Although the RMSE of the day time observed-average RH value was within the AFL, RMSE of night time RH value was higher than the AFL. These observations are attributed to the use of a centralised environment controlling unit, with a single-low-capacity chiller and single humidification column. To overcome these issues, an individual humidification column coupled with a high-capacity chiller is required. A thermally insulated enclosure around the lysimeter bank for maintaining a consistent ambient temperature is recommended for future design.

The observed average drainage, evapotranspiration and dry matter yield were within the estimated values. However, observed evapotranspiration showed a higher trend compared to estimated values which could be partly associated with the observed higher temperature in the growing space compared to targeted values. An underestimation of potential evapotranspiration by the Penman-Monteith equation could also be another possible reason for this. Although observed DM yields in the first two months were within the estimated values, the third month was lower than estimated value which was possibly due to nutrition depletion in the soil. Nevertheless, the total observed DM yield was within the estimation. In general, the environmental control lysimeter design emulates a climate model well and produced drainage, evapotranspiration and DM yield within the estimated values.

Chapter 4

A low-cost simple lysimeter soil retriever design for retrieving soil from mini and small lysimeters

4.1. Introduction

A lysimeter on the simplest level is a container filled with either disturbed or undisturbed soil columns. Lysimeters are used for a range of applications in agricultural and environmental studies, including; movement of chemicals in the vadose zone, measuring hydrological components, movement of microbes in soil and environmental pollution studies. It is the standard method for estimating crop evapotranspiration (Howell et al., 1995) and is the only tool to measure all forms of hydrological components (Goss and Ehlers, 2009). The lysimeters are categorized into four groups based on weight; large (>5000 kg), medium (1000 – 5000 kg), small (100 - 1000 kg) and mini (<100 kg) lysimeters (Bello and Van Rensburg, 2017). The choice of type, size, and design of the lysimeters is based on the research question being studied.

On completion of a lysimeter experiment, the soil column is generally retrieved from the lysimeter to destructively test for properties such as chemical composition (as an indicator of chemical movement) through the soil profile and soil root density with depth. This is traditionally achieved by manual sectioning of the entire soil column or taking sub-sample soil cores at different depths. Occasionally, the soil column was sectioned along with the PVC lysimeter body using a reciprocating saw (Sung et al., 2003). These manual methods are appropriate only for a soil core sampling or for a small soil column in terms of weight and dimensions. However, complete incremental reclamation of soil either from a large lysimeter or a small lysimeter in large numbers is laborious and time-consuming using these manual methods. Therefore, a system that applies mechanical force to lift and slice the soil core could be used to ease the process.

There are mechanical soil retrievers and their functional features in experiments published in the literature. Two examples from the literature Seyfarth and Reth (2008) introduced a lysimeter soil retriever (LSR) which uses a telescopic hydraulic cylinder to retrieve the soil from a large lysimeter (2 m^3). This system uses a vertical-wire saw to loosen the soil from the lysimeter wall and a horizontal wire saw to section the soil block at a height of 20 cm each as it is pushed out of the lysimeter body. In this design, the lysimeter was placed on a platform in the vertical position and the hydraulic cylinder pushes the soil upward. Virtanen et al. (2013) reported another simple design based on a stationary piston and a winch system. The lysimeter body is clamped in the horizontal position with a piston at one end. The winch pulls the lysimeter body backwards off the soil column which is restrained in place by the stationary piston. The soil type retrieved was sulfic cryaquepts which has high silt and clay content; so, a horizontal retrieval design was possible in this study. The experiments pertaining to this paper used 80 mini lysimeters that were too small for coring and sufficiently cumbersome to make manual retrieval difficult. Existing LSR designs are complicated in design features and have a higher cost of production for the application in a mini to small size lysimeter that consists of low cohesive soil. Therefore, a low-cost simple LSR design is required to retrieve the soil with more precision in soil block sectioning.

The electric linear actuator can be useful in soil retriever design for performing soil lifting. It is cheaper and more efficient than hydraulic telescopic cylinders. It can overcome the most common issue of oil leaking in hydraulic systems and shows minimal performance variation under thermal expansion and contraction. The gears and lead screw lifting mechanism allows smooth operation and precise control of movement speed and height. Further, the electric motor facilitates the automation of the soil lifting process. An electric linear actuator was chosen for this soil retriever design. This design was used to retrieve the total soil block from 200 lysimeters from 40 lysimeters in 5 cycles.

This chapter introduces a soil retriever for a mini to small lysimeter, describing design considerations, fabrication and performance testing. In this study, we investigate; (a) suitability of a linear actuator for lifting the soil, (b) influence of soil moisture on soil retrieval, and (c) structural stability of lysimeter and design components.

4.2. Materials and methods

4.2.1. The lysimeter and soil profile

This work was part of a lysimeter study conducted to test the performance of different nitrogen fertilisers on ryegrass under a controlled environment. For this purpose, five banks of 40 capped lysimeters were designed and fabricated with each lysimeter body being 20 cm diameter and 45 cm height. These lysimeters were filled with a repacked soil column comprising Manawatu fine sandy loam in the top 10 cm layer, and the subsoil layer (30 cm) of builder's sand (Figure 4.1 – a). The total weight of each lysimeter was approximately 25 kg; 20 kg of soil column and 5 kg of lysimeter PVC body.

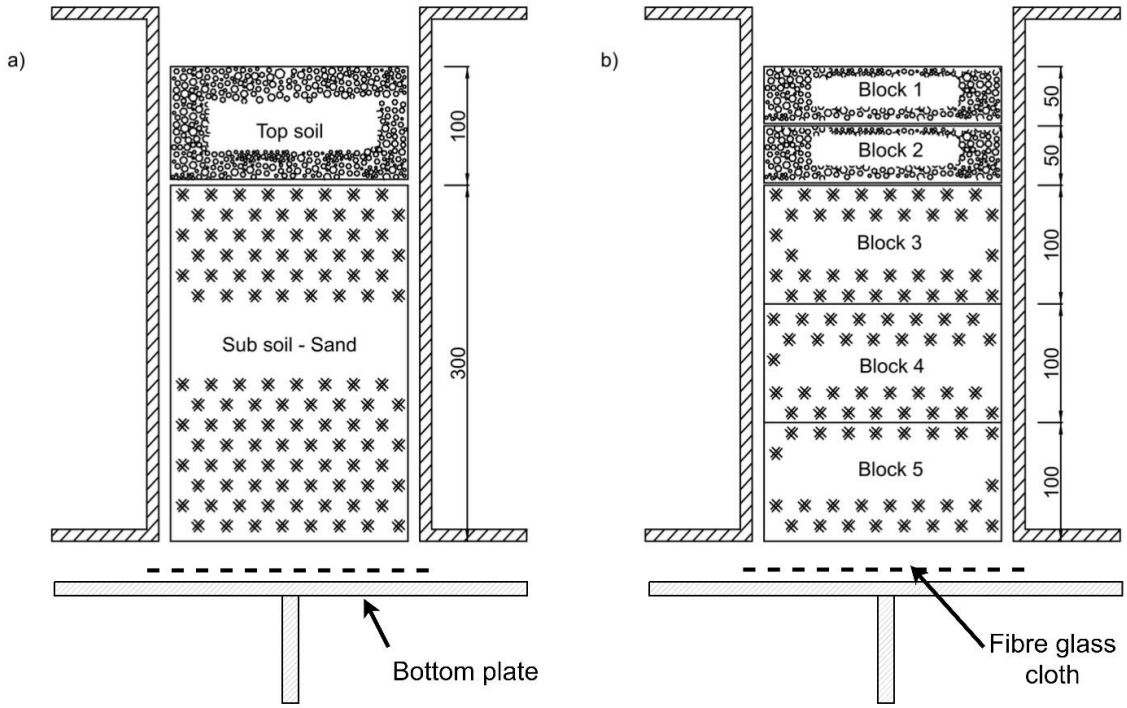

Figure 4.1. (a) The top and sub-soil layer of soil packing in lysimeter, and (b) different soil block sizes retrieved by the soil retriever. All the dimensions are in mm. The figure is not drawn to the scale.

Ryegrass tillers (*Lolium perenne*) were transplanted in the uncapped lysimeters and grown for three months under artificial lights. The lysimeters were then capped and different types and rates of fertiliser treatments were tested for three months, and therefore, the soil remained in the lysimeter for nearly six months. The experimental parameters required to be measured at the end of this trial included the residual nitrogen level and root density of ryegrass at different depths of the soil profile. More details of the lysimeter design and soil packing method employed in this study can be referred to (Gunaratnam et al., 2019);(Gunaratnam et al., 2020). The basic physical properties of the top and sub-soil were measured and are shown in Table 4.1.

Table 4.1. The basic soil physical properties.

Soil Type	**Grain Size distribution (Clay: Silt: Sand)**	**soil textural classes**	**Bulk density (g cm^{-3})**	**Porosity**	**Specific gravity**
Top-soil	20: 25: 55	Sandy clay loam	1.14	0.57	2.65
Sub-soil	06: 13: 81	Sand	1.65	0.38	2.65

4.2.2. The design of the lysimeter soil retriever

The parameters for designing the LSR in this study are based on the properties of the mini lysimeters developed for the fertiliser study. A key property considered in this design is the soil properties, as the sandy soil used in the lysimeter study has limited cohesion. Based on this property, a horizontal LSR was ruled out and a vertical system that pushed soil out the top of the lysimeter was chosen. In addition, containment (guide for soil) was included where the soil exits the lysimeter body to prevent the sandy soil layers from spilling out (Figure 4.2).

A 3D model and sectional view of the LSR design is shown in Figure 4.2. This comprises a metal frame, two wooden platforms, a soil/cutting guide and cutting

plate, and a piston attached to a linear actuator. The soil/cutting guide and piston are fabricated using PVC. The legs of the frame were made of a 40 mm steel square hollow section, and the crossbars were made of 20 mm equal angle welded to the legs. The wooden sheets were 20 mm thick melamine coated MDF boards that were bolted to the crossbars (Figure 4.2) labelled wooden table and top-wood sheet.

The wooden table provides the platform to place the lysimeter on. Marked lines on the wooden table are used to place the lysimeter in the correct position of the lysimeter compartment. The top-wood sheet restrains the lysimeter in place when the soil is pushed out by the linear actuator. A 220 mm diameter circular hole in both sheets provides space for soil and actuator movement. The guide for soil is 100 mm tall and has marks at 50- and 100-mm heights to allow soil retrieval at these heights. The guide is attached to the top-wood sheet with hinged brackets for access during the soil collection and cleaning after retrieving the sample. Plastic sheets attached to either side of the cap on the top-wood sheet provide a guide for the cutting plate movement. Therefore, the cutting plate moving straight which focuses the shear force directly on the soil block. The cutting plate fabricated with a cast-iron sheet has the dimensions of 425 x 250 x 10 mm. A metal handle facilitates the cutting process, and the 45° chamfer at the cutting end of the plate provides the shear force to the soil column. The cutting end was sharpened after soil retrieval from each lysimeter.

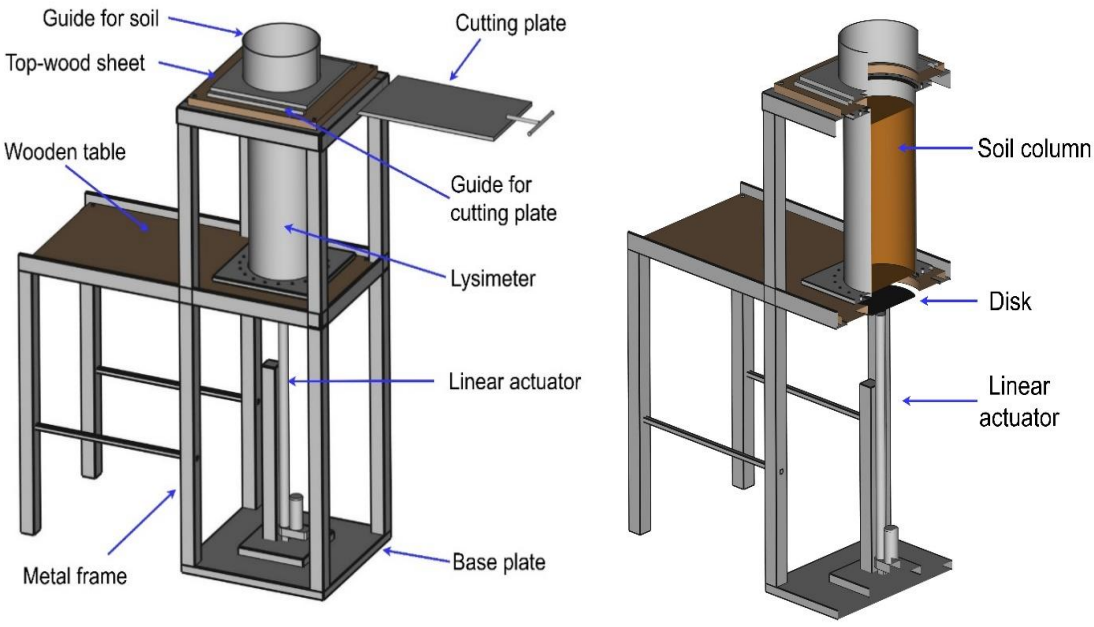

Figure 4.2. The three dimensional (left) and split view (right) of the soil retriever design.

The linear actuator (Instant Panel, New Zealand) used in this design is telescopic and has a 500 mm stroke length to push the soil out of the 450 mm long lysimeter. For performing this function, a linear actuator which has the minimum load capacity of approximately 40 kg (double the weight of the soil column) is required. The specifications of the selected linear actuator are given in Table 4.2. In this design, the actuator is attached to a vertical column and a heavy metal base plate. A 192 mm diameter metal disk is fixed at the top end of the linear actuator to push the soil column up (Appendix I). The metal disk has a 45° chamfer on the top edge to allow the disk to automatically align with the lysimeter and minimise the friction with the lysimeter wall (Appendix I). The direction of the linear actuator was controlled with a double-pole-double-throw (DPDT) rocker switch connected to the power line. The voltage applied to the linear actuator was reduced to 19 V from 24 V since the speed at zero loads under 24 V supply voltage (13 mm s^{-1}) was too fast for precise control of soil movement at the 50 mm and 100 mm

marks. After several iterations, it was found that 19 V supply gave a slower speed at zero loads of 11.6 mm s^{-1}.

The material cost of the LSR design was US$ 294 (NZ$ 407). Of that, the linear actuator cost was US$ 126 (NZ$ 174).

Table 4.2. The specifications of the linear actuator.

Specification	**Value**
Initial length of actuator	650 mm
Shaft diameter	15 mm
Stroke length	500 mm
Supply voltage	24 V
Speed at zero load	13 mm s^{-1}
Maximum load capacity	90 kg
Power rating - peak	30 W
Power rating – continuous	20 W
Current rating	2.5 A
Limit switches	At both ends
Noise level	<42 dB

4.2.3. The influence of soil moisture levels in soil retrieval

The influence of soil moisture on retrieval was studied using soil columns having two different soil moisture levels. Eight replicates were used for both soil moisture levels. The soil moisture of each level was measured by oven drying the sub-samples at 105 °C for 24 hours or until a constant weight was attained. The moisture content of high moisture (HM) and low moisture (LM) soils were 28.3 ± 3.6% and 12.6 ± 2.4%, respectively. Soil block height and weight were measured at the end of each block retrieval. The height was measured using a ruler at 4 opposite positions on the periphery of the soil block and averaged. The time taken to lift each soil block to either 50 or 100-mm mark was measured using a stopwatch.

4.2.4. The steps involved in soil retrieving

After the bottom plate and fibreglass cloth were removed from the lysimeter, it was placed on the wooden table bottom down and slid into the lysimeter compartment. Marked lines were used to place the lysimeter exactly in the middle position of the circular cut of the wooden table. The guide for soil was put in place. The linear actuator was moved upward until the soil column surface reached the required height (50 or 100 mm). The soil was then manually sliced using the cutting plate. The soil guide was then opened, and the soil was removed from the metal plate. This process was repeated until the entire soil column was sliced. For this experiment, the first two soil blocks (block 1 & 2) were sectioned at 50 mm height and the next three (block 3, 4 & 5) at 100 mm.

4.2.5. Finite element model and analysis

The LSR and the lysimeter body are subject to stress when the system is operated. In normal operation, this stress comes from the force required to overcome friction and cohesive forces between the soil column and the lysimeter wall. In the event of a jam, then the lysimeter body and the top wooden plate are subjected to the maximum upward force from the linear actuator. Maximum force was determined by stalling the LSR against a load cell and a dynamometer was used to measure frictional and cohesive forces during operation. The forces acting on the LSR and lysimeter under normal and jammed events are shown in Figure 4.3. This experimental data feeds into the analysis of stress and strain using finite element modelling (FEM).

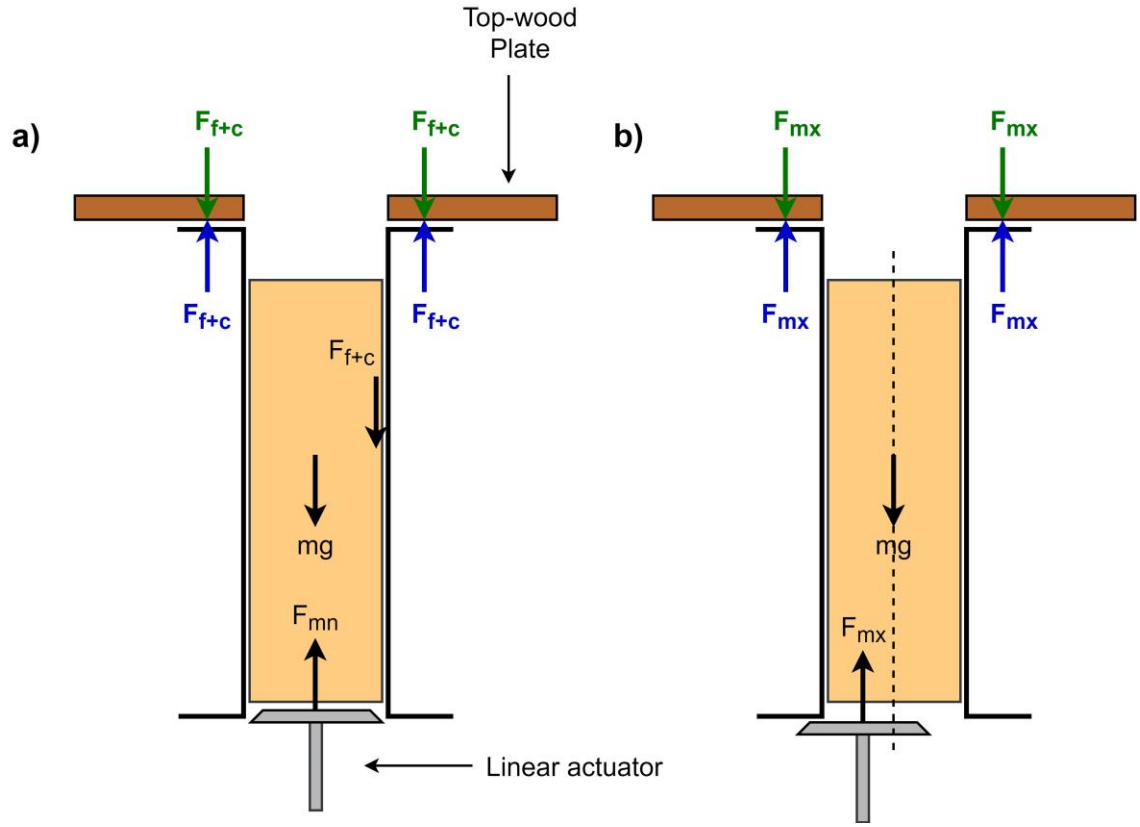

Figure 4.3. The forces acting on the lysimeter, soil and top-wood plate when the soil is lifted. (a) The forces acting on normal operation where the linear actuator is in alignment with the soil column and (b) the forces acting when the linear actuator misaligned and jammed. F_{mn} and F_{mx} are the minimum and maximum forces given by the linear actuator. The weight of the soil column is mg and the frictional (f) and cohesive (c) forces is F_{f+c}. The opposite and equal forces acting on the lysimeter and top-wood plate are shown in green and blue colour, respectively.

4.2.5.1. *Maximum force measurement of linear actuator*

The maximum force given by the linear actuator at different extended positions was investigated using the setup shown in Figure 4.4. A strain gauge load cell with 80 kg full-rated capacity was used in this design to measure the force. The configuration of the load cell accurately measures 50 g increments. In the setup, one end of the load cell was affixed to the fixed pillar using two L-brackets. A square metal block was attached to the other end of the load cell to avoid single point contact with the disk attached to the actuator and to avoid torsion to the

load cell when the actuator is lifted. Five extended positions were selected to study the maximum force; 0, 100, 200, 300 and 400 mm and the heights of these points were measured from the initial lowest position of the actuator. The load cell was driven with an HX711 (Adafruit Industries, New York, NY) module connected to an Arduino Mega (Adafruit Industries, New York, NY). The HX711 module converts the analogue output from the load cell to digital signals and these values are referred to as random values, which are proportional to the output voltage. The load cell was calibrated using nine-points and the calibration equation was used to calculate the maximum force. Force measurements are recorded every 0.1 seconds to capture shuttle changes in the force using a data logger shield (Adafruit Industries, New York, NY) with an SD card attached to Arduino Mega.

The maximum force was determined in two ways; first, when the disk is in contact with the load cell at the determined height and second, when the actuator moved from the zero position (lowest position of actuator). In the first case, the actuator has zero velocity when the experiment starts and in the latter case, it contacts the load cell with 11.6 mm s^{-1} velocity. The force at which the movement of the linear actuator was stopped was deemed as the maximum force.

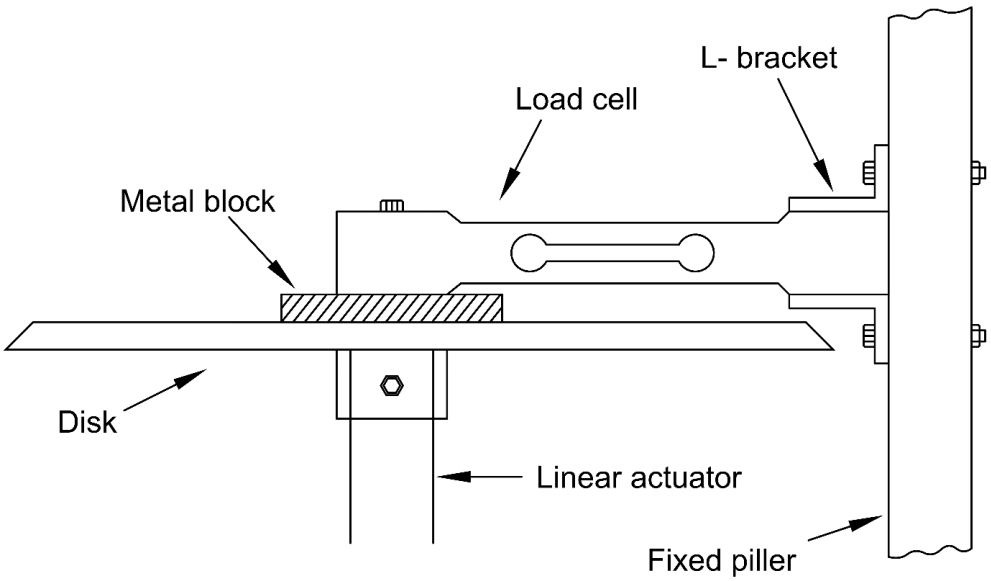

Figure 4.4. The experimental setup used to measure the maximum force of the linear actuator.

4.2.5.2. *Measurement of frictional and cohesive forces*

Frictional and cohesive forces acting between soil and lysimeter body are soil moisture dependent and increase with increasing soil moisture level. Therefore, the higher frictional and cohesive forces experience in high moisture soil column and it was taken for the frictional and cohesive forces study. A dynamometer was used to measure the maximum frictional and cohesive forces. The lysimeter with a high soil moisture column was placed on a PVC cylinder that had a diameter of 192 mm (equal diameter of the disk attached to the linear actuator), which allowed the lysimeter body to move freely downward when a force was applied, while the soil column was retained on the PVC cylinder. A downward force was applied on the lysimeter body using the dynamometer and maximum force was measured for five replicate soil columns. The average force value was fed into FEM analysis.

4.2.5.3. *Finite element modelling*

The structural stability of the lysimeter body and top-wood plate under normal operational and jam conditions was analysed using finite element analysis. ANSYS 19.2 software professional version (Ansys, Inc., Canonsburg, Pennsylvania, U.S.) (ANSYS, 2018) was used to create the physical model and to investigate the load-deformation responses. The 3D model was developed with ANSYS Design Modular (DM). The overall geometries of the lysimeter body and top-wood plate are shown in Figure 4.5.

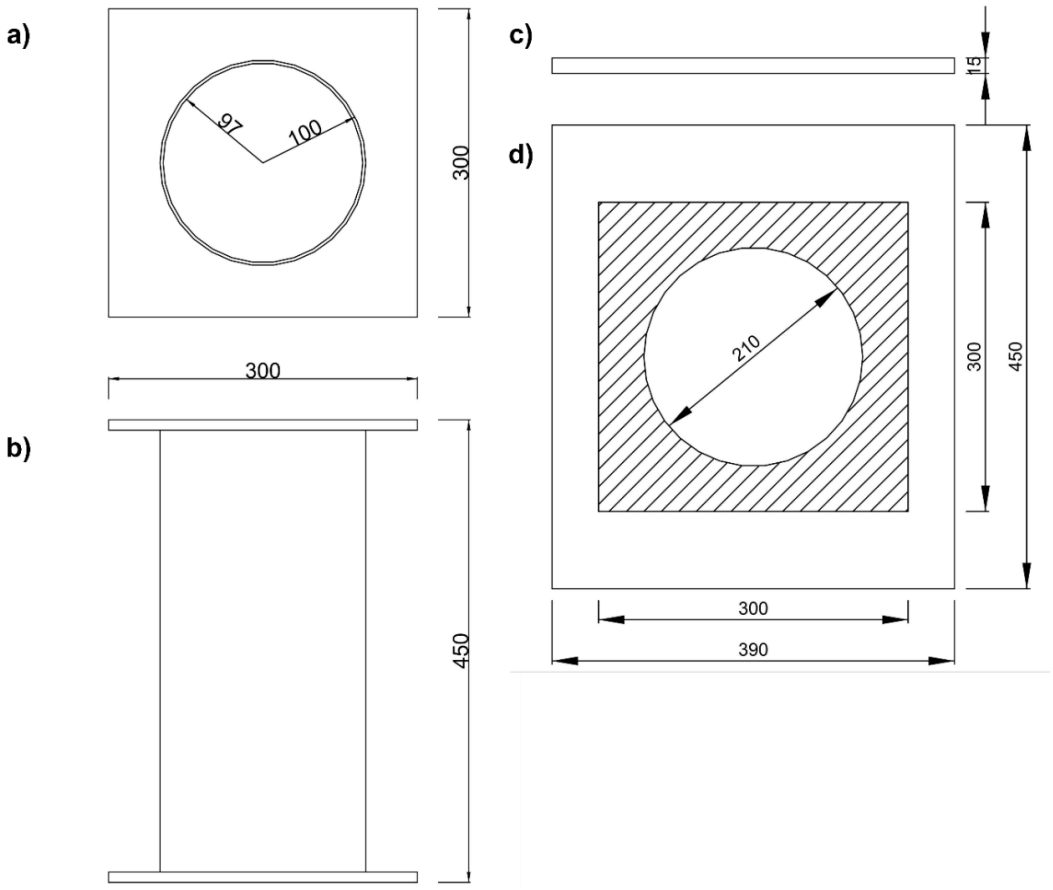

Figure 4.5. The schematic diagram of the lysimeter; (a) top and (b) side view. The schematic diagram of the top wood plate; (c) side view and (d) top view (shaded area shows the contact area of the top wood plate with the lysimeter flange when soil is lifted. It was the area where the force was applied for the FE analysis). All dimensions are in mm.

4.2.5.4. *Structural stability of the lysimeter body and top-wood plate*

The lysimeter body and top-wood plate undergo compression and bending when the soil is lifted. The actuator pushes the soil column and lysimeter against the top-wood plate. Therefore, both lysimeter body (on the top-flanges) and top-wood plate give equal and opposite forces on each other. The default parameters for un-plasticised PVC were used for the analysis of the lysimeter body (Table 4.3). For the top-wood plate, the particleboard properties (Kyvelou, 2017) were used (Table 4.3).

The auto-mesh function with refinement was used to generate SHELL181 elements for both the lysimeter body and top-wood plate. Mesh was optimized through a mesh convergence study and was used for the analysis (Appendix II). This yields a total of 157209 nodes and 99341 elements for the lysimeter body and 87341 nodes and 16971 elements for the top-wood plate.

Table 4.3. Material characteristics of PVC and particle board used for numerical analysis.

Material	Young's modulus in tension	Young's modulus in compression	Poisson's ratio	Tensile yield strength	Compressive yield strength
	GPa	GPa	-	MPa	MPa
PVC	2.86	-	0.4	46.7	-
Particle board	2.1	2.3	0.2	5.8	12.9

The lysimeter bottom flange and one end of the top-wood plate were fully constrained for translational motion. A 530 and 178 N of ramped forces from 0 N for 0.6 seconds was applied on the surface of the top-flange of the lysimeter body. A similar force was applied on the inward face of the wooden plate only to the contacted area with the lysimeter flange, not to the whole surface as shown in Figure 4.5-d (shaded area in top-view). It was deemed that the structure failure takes place when the stress exceeds the ultimate compressive and tensile stress of the board material and lysimeter body, respectively.

The maximum allowable lateral deformation was calculated using the following equation (Morassi et al., 2018);

$$\delta_0 = \left(\frac{1}{500}\right) \times L$$

Where δ_0 is the maximum allowable lateral deformation (mm) and L is the largest span of the geometry (mm).

4.2.6. Statistical analysis

Data analysis was performed using Minitab 16 statistical software (Minitab LLC, State College, Pennsylvania, USA) (Minitab, 2010). The results were tested with a one-way analysis of variance (ANOVA) at $P<0.05$ significance level. Where a significant ($P<0.05$) main effect was detected, the difference between treatment means was tested using a Tukey HSD posthoc test.

4.3. Results and Discussion

4.3.1. Influence of soil moisture on soil retrieval

4.3.1.1. *Disturbance of the soil block*

The soil moisture level impacted the slicing process with higher moisture content soils performing better than lower moisture content soils. The difference was most distinct in the topsoil, where the high moisture soil exhibited a sharp flat cut between blocks (Figure 4.6 - a). In comparison, the sliced face of low moisture topsoil blocks was crooked and uneven (Figure 4.6 - b), and it was observed that the low moisture soil presented more resistance to the movement of the slicer than the high moisture soil (i.e., the cutting movement speed of the high moisture soil was more uniform).

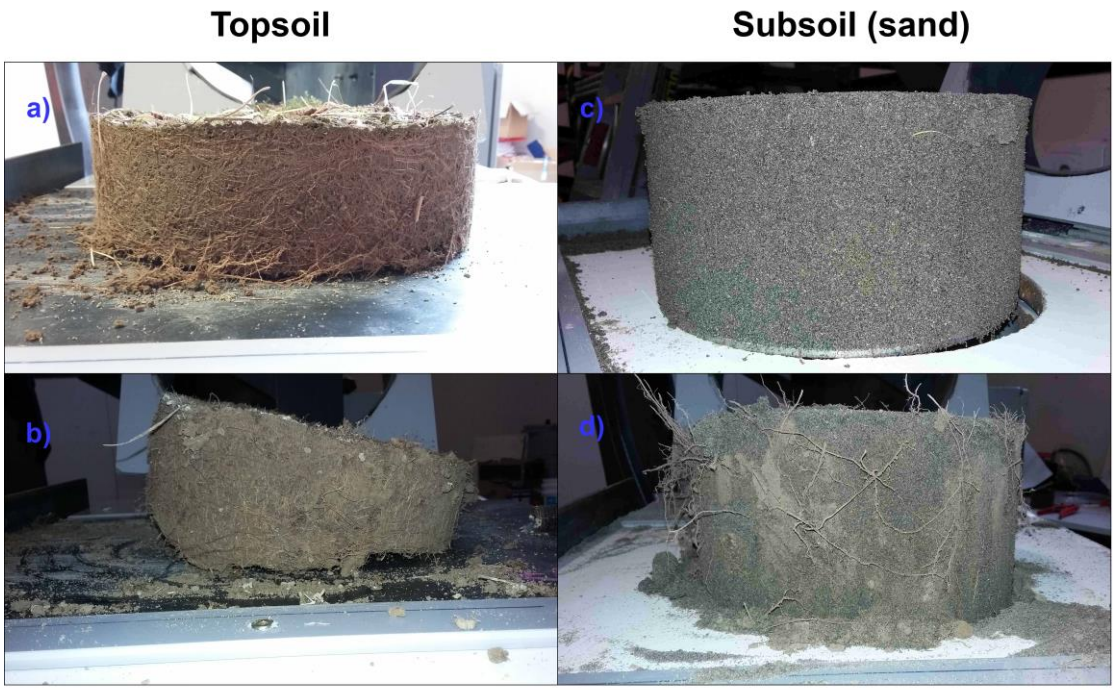

Figure 4.6. The soil blocks retrieved from soil columns with two different soil moisture levels. (a) Topsoil from high moisture, (b) topsoil from low moisture, (c) subsoil from high moisture, and (d) subsoil from low moisture soil columns.

The soil slicing process was smoother for subsoil (sand) compared to topsoil due to the lower resistance of sand for cutting plate movement. The retrieved soil column from the high moisture soil retained the shape of the lysimeter body whereas low moisture subsoil was less uniform and partially collapsed in some places (Figure 4.6 – d). This could be due to the low cohesion between sand particles at low soil moisture level (Rajaram and Erbach, 1999). Grass roots were pulled out of the soil during slicing in low moisture subsoil (Figure 4.6 – d), whereas these were cut through in the high moisture subsoil (Figure 4.6 – c).

4.3.1.2. *Average height and weight of soil blocks*

The average height and weight for soil blocks retrieved from high and low moisture soils are shown in Table 4.4. Statistically, there was no significant difference in soil height and weight of soil blocks between high and low moisture

soils. However, the soil block height and weight were more uniform for the high moisture soil compared to low moisture soil. This was attributed to the sliced bottom face of the topsoil block, where it was flatter for high moisture soil and crooked for low moisture soil. The high variation in subsoil was associated with the soil losses during retrieval; larger for low moisture and smaller for high moisture soil.

Table 4.4. The average weight and height of soil blocks retrieved from the high moisture (HM) and low moisture (LM) soil columns.

	Average height (mm)		**Average Weight (g)**	
	LM Soil	**HM Soil**	**LM Soil**	**HM Soil**
Block 1	51 ± 5	51 ± 2	2606 ± 121	2516 ± 81
Block 2	53 ± 5	52 ± 2	2461 ± 112	2491 ± 83
Block 3	100 ± 3	101 ± 2	4470 ± 148	4566 ± 72
Block 4	98 ± 2	100 ± 2	4454 ± 113	4547 ± 96
Block 5	99 ± 2	101 ± 3	4471 ± 113	4512 ± 148

4.3.1.3. *The soil block retrieval time*

The linear actuator took 43 seconds to complete the full stroke (500 mm) at the zero-load condition and the velocity of the actuator was uniform throughout the stroke. However, the average total time for retrieving low and high moisture soil were 48.3 and 52.1 seconds, respectively, which was longer than the time consumed at zero-load. The retrieval time was significantly higher ($P<0.05$) for high moisture soil than the low moisture soil (Figure 4.7). The low moisture soil retrieval for topsoil (blocks 1 & 2) was much quicker when compared to high moisture soil. This could be attributed to the visible gap created between the soil column and lysimeter body, as the topsoil had shrunk due to moisture loss. Hence, when soil is lifted upward, it moved freely in the lysimeter body which

reduced the friction between lysimeter and soil column surfaces and decreased the retrieval time. Whereas in high moisture soil, the cylindrical surface of topsoil had more contact with the lysimeter body. This possibly increased the friction and retrieval time. However, retrieval time for subsoil (blocks 3, 4 & 5) was not significantly different between low moisture and high moisture soil. As the subsoil was composed of sand, it did not undergo marked volume changes with moisture variations (Fredlund and Houston, 2013), thus may not alter the retrieval time.

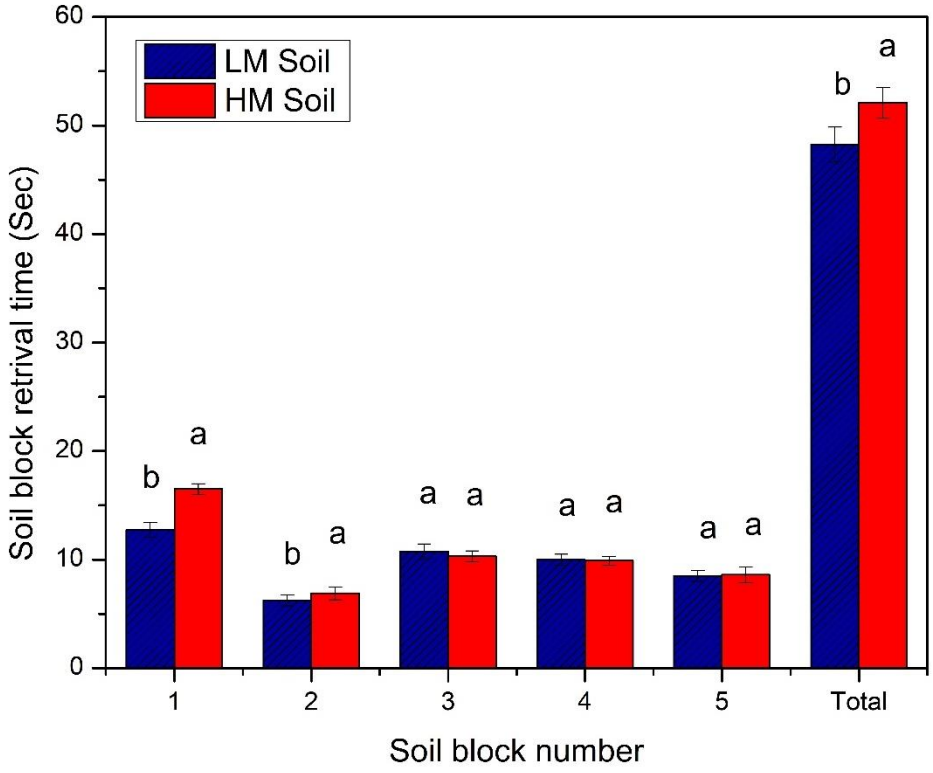

Figure 4.7. The individual and total soil blocks retrieval time for low moisture (LM) and high moisture (LM) soil columns. The different letters show significant difference between HM and LM for a particular soil block number ($p<0.05$). Vertical bars show the standard deviation (n = 8).

4.3.2. Force measurements

A relationship between actual weight and load cell reading (random values) was linear with a correlation coefficient value of 1 (Appendix III). The linear regression equation which was developed to predict the force is given below;

$$\text{Force (N)} = \frac{(\text{Load cell reading} + 6952.74) \times 10^{-2}}{55.768}$$

The force applying to and being removed from the load cell by the linear actuator in the event of a jam is shown in Figure 4.8. The force increased and reached the maximum force of 530 N. The maximum force did not change with extended height levels of the linear actuator or the linear actuator starting position. This observation is attributed to the mechanism of a linear actuator in which a lead screw lifts the actuator arm. Therefore, it moves with constant speed and gives constant force regardless of the position of the actuator. The time taken to reach the maximum force applied by actuator was 0.6 seconds. This maximum force of 530 N in 0.6 seconds (Figure 4.8) was used in the FEM analysis for linear actuator jammed situation.

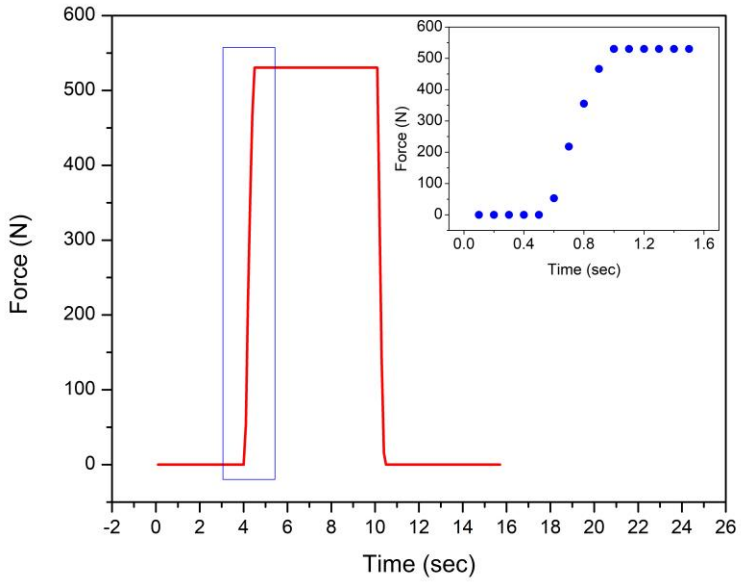

Figure 4.8. The force applied by the linear actuator changes with time in the event of a jam (red line). The inset plot with blue data points shows the magnified portion of the graph section shown in a blue rectangular box.

The maximum frictional and cohesive force was measured using a dynamometer and it was 178 ± 15.3 N. This force acts on the lysimeter body and top-wood plate in normal operational conditions. It was used for the FEM analysis to measure the structural stability of the lysimeter body and top-wood plate.

4.3.3. FE model and analysis

The Von-Mises stress and Mohr-Coulomb stress are being used in failure theories in ductile (PVC lysimeter body) and brittle material (particle wood-wood plate), respectively. This stress value of a material is the threshold value which the material can withstand when stress is applied. Under the normal operational conditions, the maximum equivalent stress acting on the lysimeter body and top-wood plate were 2.18 and 0.32 Mpa, respectively (Figure 4.9 & 4.10). These stress values are much less than the yield strength of PVC (46.7 Mpa) and the ultimate tensile strength of particle wood (5.8 Mpa). The maximum allowable lateral deformation for the lysimeter body and the top-wood plate are 0.6 and 0.98 mm, respectively. The corresponding maximum deformations were 0.38 and 0.12 mm, respectively (Figure 4.9 & 4.10). Therefore, both the lysimeter body and top-wood plate are unlikely to suffer structural failure under normal operational conditions.

In the event of a linear actuator jam, the lysimeter body and top-wood plate undergo high stress and deformation compared to the normal operational condition. The maximum equivalent stress applied on the lysimeter body and top-wood plate were 6.48 and 0.96 Mpa, respectively (Figure 4.9 & 4.10). Although these values were higher than normal operational conditions, they are still under the limit of the safety factor of both bodies and they retain their structural stability. The total deformation of the lysimeter body and the top-wood plate were 1.12 and 0.36 mm, respectively (Figure 4.9 & 4.10). The total deformation of the top-wood plate is less than the permitted lateral deformation level. However, the total deformation of the lysimeter body exceeds the permitted value. Nevertheless, only the four corners of the lysimeter flange experienced this high deformation for a short period and therefore, it does not greatly impact the structural stability.

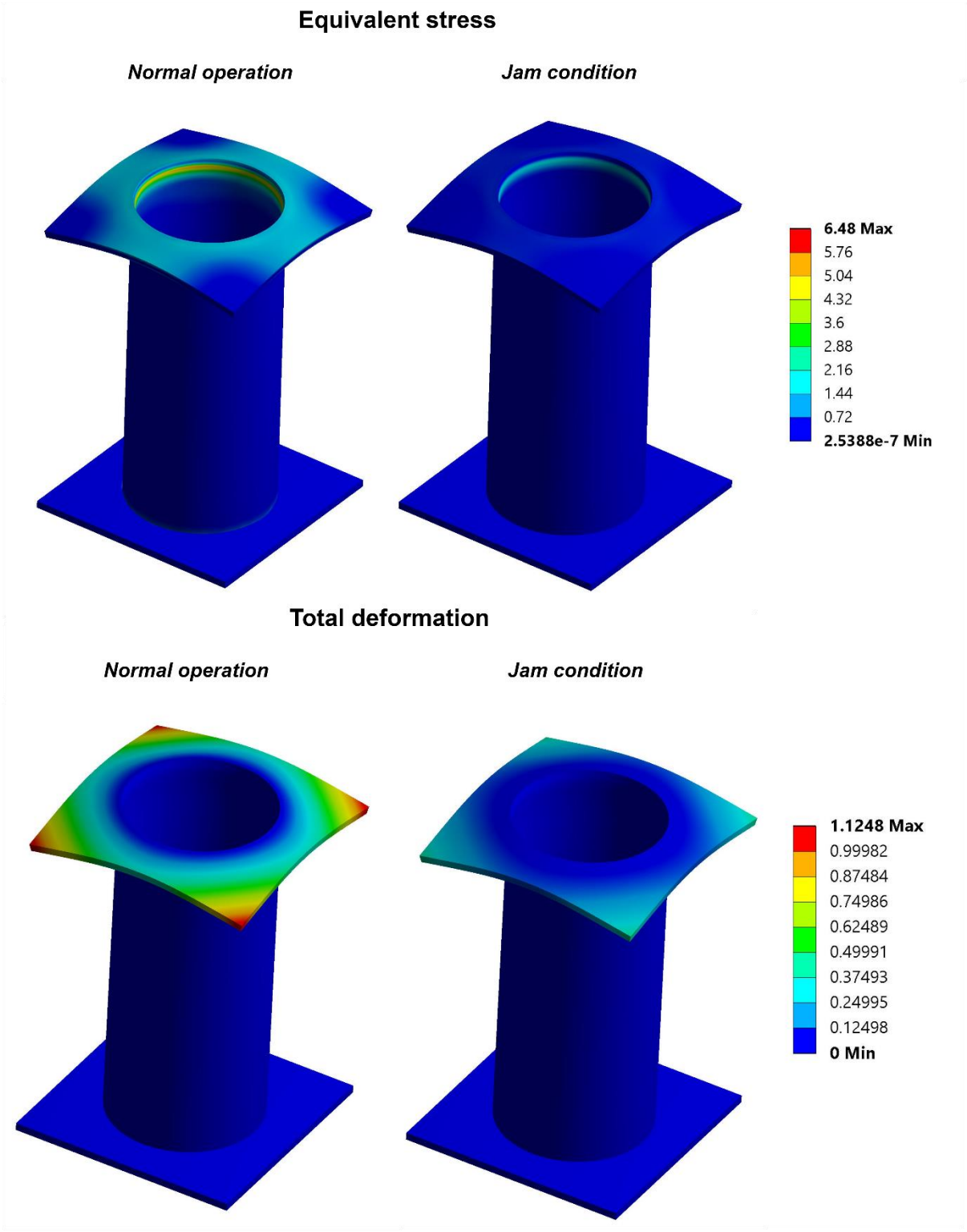

Figure 4.9. Three-dimensional view of lysimeter body; Von Mises equivalent stress (MPa) and total deformation (mm) under normal operating condition and event of a jam.

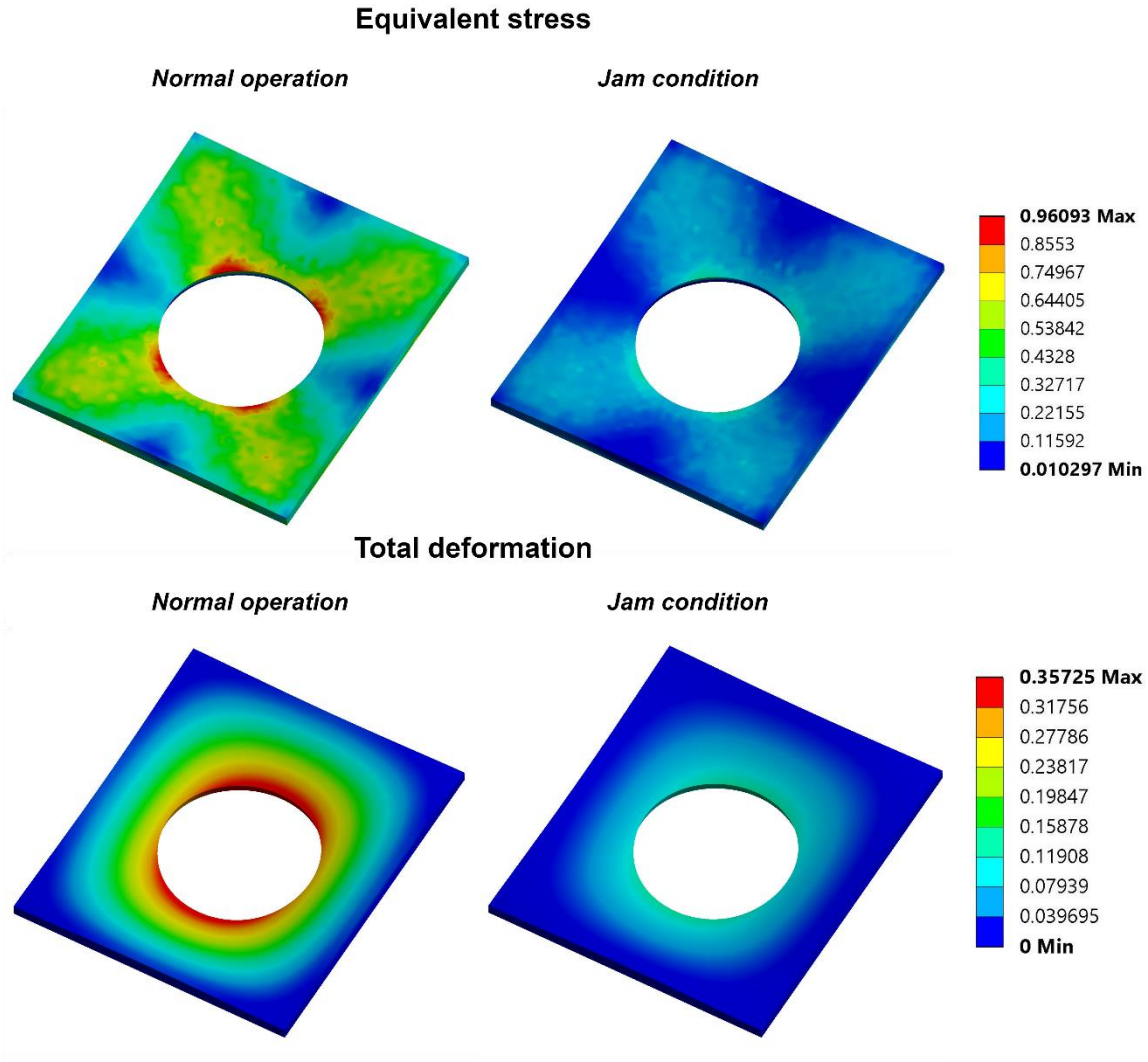

Figure 4.10. Three-dimensional view of top-wood plate; Von Mises equivalent stress (MPa) and total deformation (mm) under normal operating condition and event of a jam.

4.3.4. Summary and implication of new LSR for the agriculture experimental process

4.3.4.1. *The application of a linear actuator for other lysimeters*

The linear actuator was fit for the purpose of the current application. The linear actuator appears suitable for long term and continuous soil retrieval. It did not heat up during experiments even after four hours of continuous use. No performance losses were observed after 80 soil columns were retrieved, with the time taken for the full stroke remaining at 43 seconds and maximum force remained at 530 N.

A linear actuator in the configuration used here may not be suitable for other applications, especially for larger diameter lysimeters. A key design consideration when applying a linear actuator to a different LSR application is to have the maximum force generated by the linear actuator specified that is:

1. Greater than the force required to overcome the soil weight and soil column friction and cohesion, and
2. Less than the force required to damage the lysimeter body in the event of a jam.

With larger lysimeters, consideration must be given to the connection between the linear actuator shaft and the disk. The linear actuator has a small diameter shaft and a high pressure can be generated at the end of the shaft when a large load is applied. In this experiment, the total pressure applied by the soil weight is exerted on a 15 mm diameter shaft. For the average soil column weight of 20 kg, the pressure exerted on the shaft was 283×10^3 N m^{-2}. The pressure could be much higher with larger lysimeters. The disk must be designed to handle the point load at the centre and distribute the load evenly out from the centre to maintain stability. Positioning the lysimeter at the dead centre of disk movement is critical. An off-centre disk is likely to become misaligned and jam against the lysimeter, potentially damaging the lysimeter and linear actuator.

The automation of linear actuator incremental movement to predetermined heights is possible in many ways; using an encoded motor, limiting switches and

optical or acoustic sensors. This allows more precise control of soil column increment than manual control using a rocker switch. For fine incremental height movement, the encoded motor is better than other techniques.

4.3.4.2. *The design consideration for different types of soil*

In this study, a layered soil column comprised of sandy loam and sand was retrieved by the LSR. These soils are comparatively less compressible and therefore, the design does not need a mechanism to loosen the soil from the lysimeter wall. However, highly compressive and sticky soils (e.g. Peat, clay) need to be loosened to avoid compaction. Seyfarth and Reth (2008) used a vertical wire saw which runs between soil column and lysimeter inner wall which separates the soil and avoids compaction. A gentle tapping force with a rubber hammer can be applied to the lysimeter body to detach the soil from the lysimeter wall.

This study considered a cutting method which is slicing the soil using a cutting blade. The selection of cutting force and mechanism depends on the characteristics of the root system of the plant, soil type, soil moisture level and foreign materials in the soil such as gravel or stones. The reconstructed soil column used in this study is free of foreign materials like stones and pebbles, thus easy to slice without deformation of the soil block shape when the soil moisture is high. A minimal force is required to slice the roots, as the ryegrass used in this study had a fibrous root system. Therefore, a sharp metal plate was sufficient to slice the soil and roots without damage. Nevertheless, a saw cutting mechanism or angle cutting plate would be better for dry soil, hard root systems like taproots and soil with a high degree of foreign materials. A thin wire saw can be used for a thinner slice of a soil block.

4.4. Conclusions

This study was undertaken with the objective of designing and fabricating a simple and low cost lysimeter soil retriever. Soil moisture content influences the soil retrieving and slicing process. Higher soil moisture decreased the disturbance of the soil block, disturbance of the roots, soil losses in the retrieving process and variation in soil block weight and height. Therefore, it is suggested to retrieve the soil soon after the termination of the experiment before the soil dries. This lifting and slicing mechanism is sufficient for sandy loam and sandy soil with a fibrous root system. The linear actuator is ideal for lifting the soil and can be used in soil retriever designs. It gave consistent performance even after 80 soil columns were retrieved. The force given by the actuator is sufficient for lifting the soil, yet not too great to damage the LSR and lysimeter body.

Chapter 5

Formulation and characterisation of polymer-lignite composite coated controlled-release fertilisers

5.1. Introduction

Controlled-release fertilisers (CRFs) are being used successfully as an effective way to control nitrogen losses by increasing the release duration to synchronise with plant demand (Trenkel, 2010). Polymer coated fertilisers are the most widely used CRFs since the release rate can be predefined at the formulation stage (Trenkel, 2010). The direct physical contact of the active ingredient (N fertiliser) with water is prevented by applying a coating around the granule as a barrier. The diffusion of water into the coating membrane dissolves the nutrient and releases it slowly out of the membrane. Several inorganic and organic polymer coating membranes have been employed in CRF formulation and reported in literature such as epoxy, polyester, linseed oil, calcium carbonate, sulphur, etc. (Azeem et al., 2014). Cured epoxy and polyester resins have desirable characteristics such as better mechanical, chemical and heat resistance properties (Haque et al., 2003; Dutta and Karak, 2018).

The cured epoxy resins are used as coating materials in CRFs; either bio-based (Li et al., 2018) or petroleum-based epoxy (Lu et al., 2013; Tian et al., 2019). For example, Lu et al. (2013) used epoxy in pure and additive form for coating urea and Tian et al. (2019) used epoxy as a sealant for providing greater physical strength and prolonged N release in a urea-based composite coating. Unsaturated polyester (UP) is a thermosetting polymer with excellent abrasion resistance, hydrophobic and mechanical properties. Different types of petroleum and bio-based polyester resins have been used for CRF formulation. For example, Dutta and Karak (2018) synthesized a waterborne polyester using a poly-condensation technique from citric acid, glycerol, and dimer acid that was used for coating urea. This polyester coating showed high tensile strength, impact

resistance, fracture strain, thermal stability and good control over urea release. However, these polymers (epoxy and polyester) use is limited by long curing times, high cost and they are not environmentally friendly materials (Gopinath et al., 2014).

Developing composite polymer coatings could be a solution to overcome the limitations of both epoxy and polyester resins. These composite polymers are made by mixing additives with the polymers to reduce the polymer content, cost of coating material and increase biodegradability, while sustaining the beneficial properties of the polymer as a coating material (Lu et al., 2013). In this regard, lignite can be used as an organic additive or filler in polymer composite for coating.

In agriculture, lignite has been used as a soil amendment for various purposes; increases soil pH and decreases aluminium solubility (Yazawa et al., 2000), reduces the solubility and plant availability of heavy metals by binding them on the active sites (Karczewska et al., 1996; Simmler et al., 2013), improves soil fertility through adding organic matter (Kwiatkowska et al., 2008), increases water retention capacity, decreases moisture loss (Qin and Leskovar, 2018), decreases the ammonia losses from cattle feedlots (Chen et al., 2015), and improves pasture growth (Little et al., 2014). Moreover, lignite was employed in the formulation of CRFs. For instance, Tang et al. (2017) developed a granular slow-release fertiliser by mixing the urea-formaldehyde polymer with KOH-activated lignite which prolonged the N release up to 90 days. Rose et al. (2016) developed a brown coal-urea blended granular CRF using the pan granulation method and it decreased the ammonium and nitrate losses by 40% and 20%, respectively, compared to urea.

Although lignite was employed in the CRF synthesis in different ways, the polymer-lignite composite has not been tested as a coating material. Therefore, the present work attempts to (a) develop different new polymer-lignite composites (epoxy-lignite and polyester-lignite), (b) characterise the physical and chemical properties of synthesised coating material, and (c) investigate the slow-releasing behaviour of newly developed CRFs.

5.2. Materials and Methods

Lignite and two different polymer resins (epoxy and polyester) were used to prepare the coating for urea-based CRFs. For each resin, two different CRFs were made which differ in coating thickness. The lignite from Kai Point mine (Clutha District, Otago), New Zealand was used for the study and the basic physiochemical properties of the lignite are described in Table 5.1. Fine lignite powder was prepared by sifting ground lignite through a 200-micron sieve. In preparation of both composite polymers, lignite was used as an organic amendment and conditioner to overcome the surface stickiness of viscous polymers. The viscosity of the epoxy and polyester resins was not decreased using any solvents as it can cause unpleasant odours and therefore, was used in its original high viscous form.

Table 5.1. The general physiochemical properties of Kai Point lignite.

Property	**Value (%)**
Moisture	29.5
Ash	4.6
Volatiles	35.4
Fixed carbon	30.5
Sulphur	1.94
C: H: O: N	47.7: 3.4: 11.7: 0.5

5.2.1. Controlled-release fertiliser preparation

5.2.1.1. *Preparation of epoxy-lignite coated CRF*

Epoxy resin (4 g) was applied on urea (200 g) in a rotating drum coater (30 rpm) and lignite powder (3 g) was sprinkled on the mixture. The mixture was allowed to cured for 30 minutes on a flat tray. A similar coating was applied two more times. A 100 g portion of three times coated fertiliser was separated and coated two more times with 2 g of epoxy and 2 g of lignite at each time. Finally, both, the three coatings (Epox3) and five coatings (Epox5) were allowed to cure overnight.

5.2.1.2. *Preparation of polyester-lignite coated CRF*

Urea (100 g) was mixed with polyester resin (1 g) in a rotating drum coater (30 rpm), and fine lignite powder (1.5 g) was sprinkled on top of the mixture. Lignite powder can easily bind to the surface as the polyester resin is sticky. The mixture was allowed to cure for 30 minutes on a flat tray at room temperature. A similar coating was repeated three times and this CRF is referred to as Poly3. In a similar method, another 100 g urea was coated five times with polyester resin and lignite composite and it is referred to as Poly5. In the Poly5 formulation, 3.5 g lignite was applied (instead of 3 g) in the last coating only. A 50 g portion of Poly5 was coated with linseed oil (2 g) as a sealant to improve the release characteristics and it is referred to as Poly5-linseed.

5.2.2. Coating percentage, coating efficiency, nitrogen percentage and composition of the fertiliser

The theoretical coating percentage of the CRF was calculated by the weight ratio of the coating material used for the coating to the total weight of the CRF. The actual coating percentage of CRF was measured by the following method: A 10 g portion (Mt) of triplicate samples were crushed and kept in 100 ml water at room temperature. After complete dissolution of urea, the polymer coating was filtered

using a 0.45-micron filter paper and washed carefully with distilled water to remove the urea. The coating was dried at 40°C for approximately 6 hours and the residual was weighed (Mc). The coating percentage, coating efficiency and nitrogen percentage were calculated using the following equations.

$$\text{Actual coating percentage} = \frac{M_c}{M_t} \times 100\%$$

Where Mt and Mc are CRF sample taken and residual sample, respectively.

$$\text{Coating efficiency} = \frac{\text{Actual coating weight}}{\text{Theoretical coating weight}} \times 100\%$$

$$\text{Nitrogen \%} = \left[\frac{(M_t - M_c) \times 46}{M_t}\right] \times 100$$

The actual composition (ratio of polymer and lignite) in the coating was determined by the elemental analysis. The nitrogen level of both polymer and lignite is a constant. The nitrogen level in the coating membrane, polymer and lignite were measured and the composition was calculated by the following equation.

$$M_L = \frac{M_S(N_S - N_P)}{N_L - N_P}$$

Where M_L and Ms are the weight of lignite in the membrane and sample taken for elemental analysis, respectively. N_P, N_L and N_S are the nitrogen percentage of polymer, lignite and sample measured in elemental analysis, respectively.

5.2.3. Analysis of static urea releasing in water

The dissolution test was carried out to measure the urea release from the uncoated and coated CRF urea. A 20 g sample of uncoated and coated urea was weighed and placed in 250 ml distilled water separately. Another 20 g of coated and uncoated urea were crushed and put into 250 ml distilled water to measure the available urea in each. The uncoated urea was used as the control. All the

treatments were conducted in triplicate. An aliquot of samples (1 ml) was collected at different time intervals and nitrogen content was measured using an auto analyser for total nitrogen. The urea releasing percentage was calculated using the following equation.

$$\text{Urea release } \% = \frac{\text{N in noncrushed sample}}{\text{N in crushed sample}} \times 100$$

5.2.4. Characterization of the coating

5.2.4.1. *Morphological features*

The surface and cross-section of the coated urea CRFs were analysed using a scanning electron microscope (SEM) at different magnifications. Randomly selected CRFs were cut into half and samples were sputter-coated with gold in an IB-5 ion coater and SEM images were obtained.

The images of surface and cross-sectional view of CRFs were taken under a polarized light microscope (PLM) to visualize the relative distribution of the lignite and polymer in the coating. The SEM image of the cross-section at 250 magnification was used to measure the coating thickness. The thickness was measured at 25 random points of the coating and the average was calculated.

An image processing method was employed for further analysis of the coating surface morphology using ImageJ software (Schneider et al., 2012). The SEM (x 500) and PLM (x 100) images were selected to visualize the smooth and coarse regions of the coating, respectively. Both images were converted to 32-bit colour depth mode and an Interactive 3D Surface Plot plug-in was deployed in the selected region of the images. The 5% smoothness was applied for SEM images whereas a higher level of smoothness (50%) was applied to PLM images to visualise the large undulation of the surface. The outputs were saved as surface plot images.

5.2.4.2. *Fourier transform infrared spectroscopy (FTIR) analysis*

The Fourier transform infrared (FTIR) is a technique used to identify the bonds in a compound. The bond formation between polymer and lignite was characterised using a FTIR spectrophotometer with a wavenumber range from 4000 to 500 cm^{-1}.

5.2.4.3. *Thermogravimetric analysis (TGA)*

The thermal stability of the coatings was analysed using TGA (Discovery TGA 55, New Castle, DE) under a nitrogen atmosphere (60 cm^3 min^{-1}). The samples were heated from room temperature to 600°C with a heating rate of 10°C min^{-1}.

5.2.5. Physical characteristics

5.2.5.1. *Particle size distribution and circularity*

The particle size distribution of the coated and uncoated urea was analysed using ImageJ software (Schneider et al., 2012). Five grams of coated CRF (Epox5 and Poly5) and uncoated urea were measured and uniformly spread on a flat surface to avoid contact between granules. Contrast colour sheets were used as the background; a white sheet for coated granules (since they are black colour) and a black colour board for uncoated urea granules. The images were taken using a 7.2 MP camera (Sony) in a dark place using flashlights. The colour images were converted to binary images and an Analyse Particle Function was used to measure the area of each granule. The 0.01-pixel threshold value was applied for the size to exclude the fine particulates that are not objects of interest. The circularity option was selected in full range (0 – 1) to include granules of different shapes. The diameter was calculated from the cross-sectional area of the particle

generated by the software assuming all the particles were spherical. For the same binary image, a range of circularity values with an increment of 0.1 from 0 to 1 were applied and the number of particles belonging to each range was recorded. The particle count for each circularity value was plotted.

5.2.5.2. *Abrasion resistance*

The strength of the coating material for the abrasion was measured by a modified method from Timmons (1987). A 10 g portion of coated urea granules was placed in a No 6 sieve (3.36 mm) with 10 metal balls (1.5 cm diameter and 16 g weight each) and a pan was kept underneath it to collect the sieved particles. The sample was shaken for 10 minutes and the weight of the sample remaining in the sieve and collected in the pan were weighed. The abrasion resistance was measured using the following equation.

$$\text{Abrasion resistance } \% = \frac{\text{Weight of the sample remaining on No 6 sieve}}{50 \text{ g}} \text{ x } 100$$

5.2.5.3. *Water absorbance of coated fertiliser*

One and a half gram of coating material (Mo) in triplicate was kept in 100 ml of water for 90 minutes at room temperature. The water-soaked sample was filtered carefully using a 177-micron sieve to remove the surface water and the final weight (M) was measured. The water absorbency was calculated using the following equation.

$$\text{Water absobancy } (\%) = \left[\frac{M - M_O}{M_O}\right] \times 100$$

5.2.5.4. *Coating porosity measurement*

The amount of water absorbed by the coating was used to measure the coating porosity using the modified method from Liu et al. (2017). Ten similar size

granules were selected and soaked in water until the urea completely released out of the granule. Thereafter, surface-bound water on the coating was removed using blotting paper and wet weight was measured (Mw). The coating was dried in the oven at 30 °C until a constant weight was gained (Md). The volume of coating (Vc) was calculated using the thickness of coating obtained from the SEM images and it was assumed that the coating was spherical and the coating thickness was uniform. The porosity (Ɛ) was calculated using the following equation. The density of water (ρ_w) is 1 g cm^{-3}.

$$\varepsilon = \frac{\frac{M_w - M_d}{\rho_w}}{V_c} \times 100\%$$

5.2.6. Modelling of release kinetics

Nutrient release can be governed by various mechanisms such as dissolution, diffusion, portioning, osmosis, swelling and erosion. Mathematical modelling helps to understand the nutrient releasing mechanism from a coated CRF. Therefore, experimental results were fitted with selected mathematical models; Korsmeyer–Peppas model and Peppas–Sahlinmode model.

5.2.6.1. *Korsmeyer–Peppas Model*

This semi-empirical model (Korsmeyer et al., 1983) explains the nutrient release behaviour of a polymer coating for an unknown or a complex-releasing mechanism (Bruschi, 2015).

$$Q_t = k\, t^n$$

Where Qt is the fraction of solvent released at time t, K is a distinctive constant for the filler–polymer system, and n is the diffusion exponent. The n value determines the releasing mechanism; n < 0.45 indicates a Fickian diffusion mechanism, 0.45 < n < 0.89 shows non- Fickian transport, n = 0.89 belongs to Case II (relaxation) transport, and n > 0.89 to super case II transport (Dash et al., 2010).

5.2.6.2. *Peppas–Sahlin Model*

This Peppas–Sahlin model (Peppas and Sahlin, 1989) describes the contribution of diffusion, and coating matrix swelling and relaxation in the anomalous nutrient release process.

$$Q_t = k_1 t^m + k_2 t^{2m}$$

Where Q_t is the fraction of nutrient release at time t, k_1 and k_2 are Fickian diffusion contribution coefficient and relaxation contribution coefficient, respectively and m is the Fickian diffusion exponent.

The first and second terms of the equation describe the diffusion contribution and relaxation contribution, respectively. If k1 > k2, the dominant factor in nutrient release is Fickian diffusion and vice-versa also true. When k1 = k2, both contribute equally to the nutrient release. The initial diffusion coefficient (Df) was calculated using the following equation (El Assimi et al., 2020). The thickness of the coating is denoted by *l* and time by t.

$$Q_t = 4\sqrt{\frac{D_f \times t}{\pi l^2}}$$

5.2.7. Statistical analysis

Minitab 18 was used for the statistical analysis. The results were tested at 0.05 significance level with one-way analysis of variance (ANOVA) and the results are presented as mean ± standard deviation. The significant difference between mean values was tested with Tukey honest significant difference (HSD) post hoc test at 0.05 probability level. The model fitting of urea release from the CRFs was performed using Origin 8.5 software (OriginLab Corporation, Northampton, MA, USA). Non-linear curve fitting was performed to fit the experimental results with the model.

5.3. Results and Discussion

5.3.1. Coating characteristics

Increasing the number of coating (from 3 to 5) significantly (P<0.05) increased the coating percentage by 6% and 8% and coating efficiency by around 6% and 12%, respectively for epoxy-lignite and polyester-lignite composite coatings (Table 5.2). Even though the coating thickness was increased by 1% for Poly5-linseed fertiliser, the application of linseed oil decreased the coating efficiency by 2% in comparison to Poly5, however this decrease was insignificant. All CRFs showed a high nitrogen percentage ranging from 36 - 42% (Table 5.2). In both polymer composite coatings, the nitrogen content of the CRF significantly (P<0.05) decrease with increasing the coating thickness, as the coating materials (polymer or lignite) have low nitrogen content. For example, the N content significantly (P<0.05) decreased by 2% for Epox5 in relation to Epox3 (Table 5.2).

Table 5.2. The coating percentage, coating efficiency, nitrogen percentage, composition of coating membrane.

CRF	Coating %	Coating Efficiency %	Nitrogen %	lignite: polymer in coating
Epox3	7.8±0.6 [d]	82±6 [a]	42.4±0.3 [a]	4.0±1.4[a]
Epox5	13.7±0.6 [b]	88±4 [a]	39.7±0.3 [c]	2.1±0.6[b]
Poly3	10.6±1.1 [c]	81±8 [a]	41.1±0.5 [b]	5.3±0.1[A]
Poly5	19.3±2.0 [a]	94±10 [a]	37.1±0.9 [d]	5.0±1.6[A]
Poly5-Linseed	20.4±1.6 [a]	92±7 [a]	36.7±0.8 [d]	-

Mean value with different letters within a column are significantly different (P<0.05). CAPITAL letters indicate the significant difference of lignite: polymer ratio in Poly3 and Poly5 coating (P<0.05).

The N content of the lignite and polymer used to find out the composition of the coating membrane. Lignite: polymer ratio of Epox3 and Epox5 coatings were 4.0

and 2.1, respectively (Table 5.2). Increasing the number of epoxy-lignite coatings (from 3 to 5) significantly decreased ($P<0.05$) the lignite content by 50%. Lignite: polymer ratio of Poly3: Poly5 were 5.3 and 5.0, respectively. The lignite and polymer content were not significantly changed by increasing the polyester-lignite coating number from 3 to 5.

5.3.2. Urea release in static water

5.3.2.1. *Release characteristics of epoxy-lignite coated urea*

Both epoxy-lignite composite coatings significantly ($P<0.05$) prolonged the urea release compared to the uncoated urea (UU), that was completely dissolved in water within 3 hours (Figure 5.1). Increasing coating thickness significantly ($p<0.05$) increased the time take to release urea. The urea release longevity of Epox3 and Epox5 CRFs were 144 and 408 hours, respectively. The corresponding values for the 75% urea release were 110 and 145 hours, respectively.

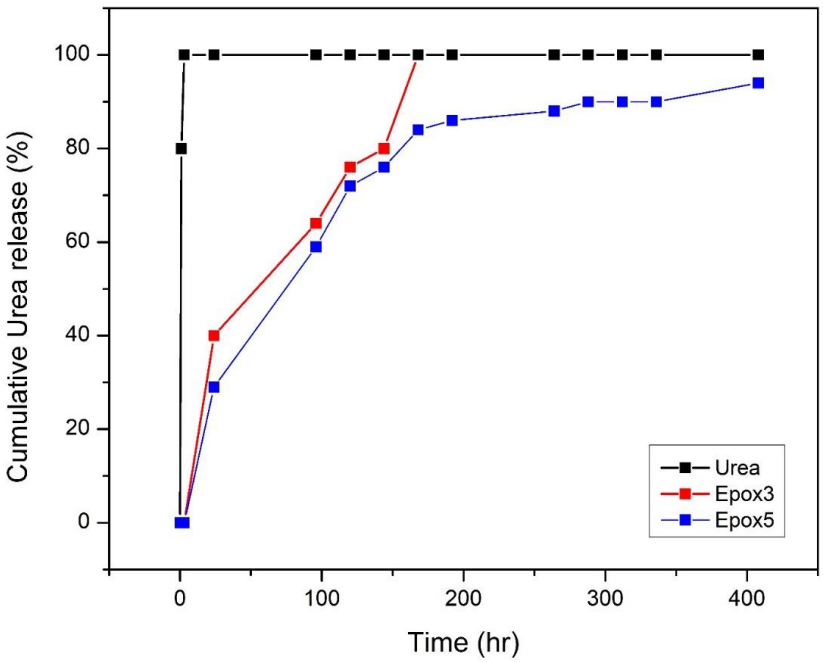

Figure 5.1. The cumulative urea release of uncoated and controlled-release fertilisers (Epox3 & Epox5).

The epoxy-lignite coating results showed that only around 6% increment of the coating thickness increased the controlled release by three-fold. The relative quick release of Epox3 could be attributed to the burst effect wherein the coating burst due to osmotic pressure exerted on the coating membrane (Figure 5.1). The coating ruptures when the osmotic pressure exceeds the threshold value of membrane tensile strength. However, Epox5 did not show a failure release that may be due to increased coating thickness which gave more resistance against the osmotic pressure.

The epoxy resin based controlled release fertilisers found in literature showed better urea release characteristics compared to this study. For example, a product of bio-based epoxy resin made from ethanol, Bisphenol-A Di glycidyl ether and liquefied bagasse showed very quick release of urea (up to 60%) in 5 days and then controlled the release up to 70 days (Li et al., 2018). A multilayer coating of urea with epoxy resin controlled the release of urea where 19% of the urea was released in 72 hours (Hansen, 1966). The better controlled release of these fertilisers probably ascribed to the high polymer content in the coating compared to this study.

5.3.2.2. *Release characteristics of polyester-lignite coated urea*

The urea dissolution behaviour of UU and two polyester-lignite coated CRFs (Poly3 & Poly5) were tested in distilled water. Both CRFs significantly ($P<0.05$) extended the urea release compared to UU. The complete urea dissolution took place at 120 and 175 hours for Poly3 and Poly5, respectively, while urea was completely dissolved at 3 hours (Figure 5.2). The corresponding values for 75% release of urea from these two CRFs were 30 and 125 hours, respectively. Results showed that around 9% increment of the polyester-lignite coating thickness doubles the controlled release of urea. The poly5 showed a rapid release after 120 hours (green shaded area), and the last 25% urea release occurred in just 10 hours, suggested that the coating membrane possibly ruptured and exhibited failure release.

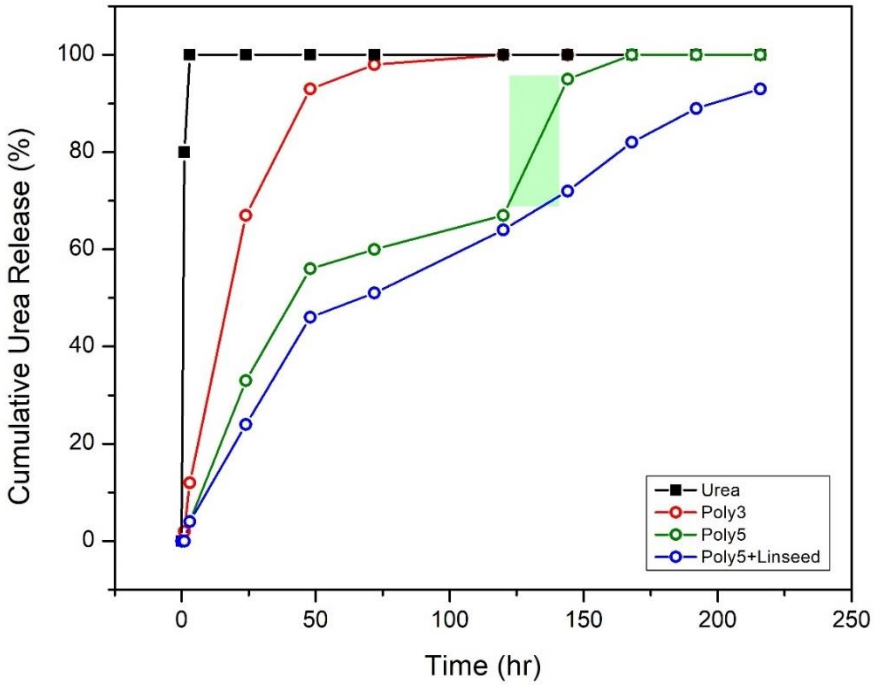

Figure 5.2. The cumulative release of urea from uncoated urea, two polyester-lignite coated CRFs; Poly3 and Poly5, and linseed sealant coated CRF (Poly5+Linseed).

A double layer linseed coating was applied for the Poly5 as a sealant to overcome the failure release. The sealant has prevented the failure release and significantly ($P<0.05$) improved the urea release rate. The 75% release time was increased by 25 hours after the addition of linseed coating (Figure 5.2).

5.3.3. Morphology of CRFs

5.3.3.1. *Epoxy-lignite coated CRF*

The morphology of the Epox5 coatings were investigated using SEM and PLM microgram images. The surface of the Epox5 coating was very coarse and lignite particles were protruding from the coating (Figure 5.3-a & f). The surface roughness can be more clearly visible in PLM than SEM images. Fine lignite particles formed agglomerates with epoxy resin and showed as irregular clumps on the surface.

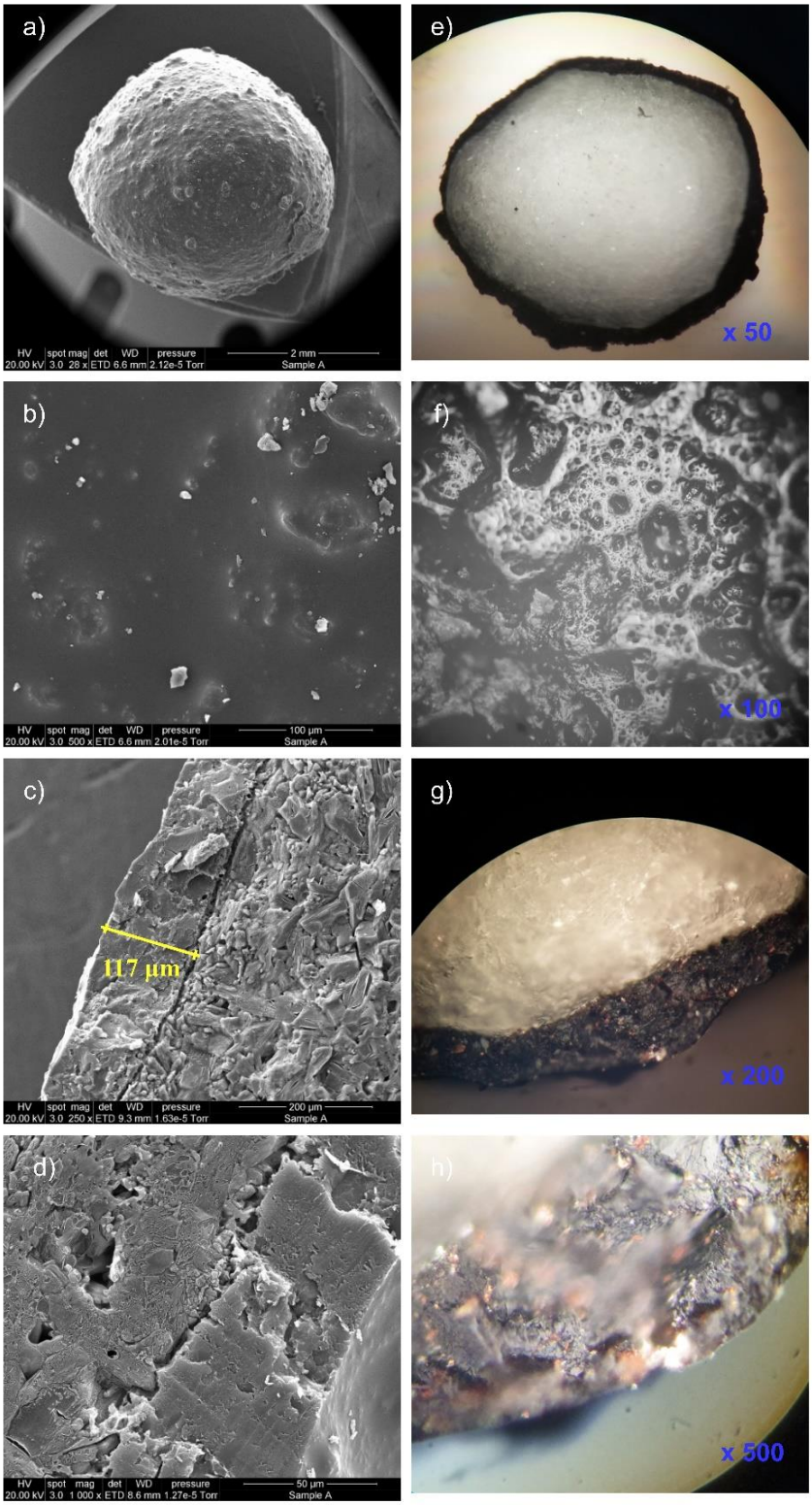

Figure 5.3. The SEM (a - d) and PLM images (e - h) of Epox5 CRF. Images a, b and f show the surface of the coating and c, d, e, g and h are the cross-section of the CRF at different magnifications.

The coating can be clearly distinguished from the urea core as there was clear depression at the interface of the coating (Figure 5.3-c). However, part of the coating intruded into the urea in a few regions and made the coating more intact with the core. Easily distinguishable prominent layers similar to an onion layer structure was expected in the cross-sectional view of the coating as multiple layers of coatings were applied one over the other. Nevertheless, ring formation was not visible as multiple coatings were fused. This was due to the successive coatings being applied before complete curing of the previous coating. The average coating thickness was 117 µm (Figure 5.3-c). The coating was fairly uniform and compact. The PLM images show that lignite was the primary compound of the coating compared to the epoxy resin (Figure 5.3 - g & h). The lignite was entrapped within the three-dimensional polymer structure of the epoxy resin and formed a matrix. Epoxy resin was spread all over the coating and also can be seen in some localized areas.

Although a few parts of the coating surface looked smooth in the SEM images, the 3D-surface plot images suggested that very fine roughness existed (Figure 5.4 - a & b). The surface regions covered with epoxy were found to be smoother than regions with lignite particles (Figure 5.4 - a & b). The protrusions of sharp lignite edges (Figure 5.4 - a & c) and irregular clumps attributed to the unevenness of the coating surface (Figure 5.4 - d & e). There were no cracks or weak coated regions found both in SEM and PLM images. Fine pinholes and cavities were visible on the surface under high magnification (not shown). However, the extension of the hole for the entire width of the coating cannot be confirmed from the cross-sectional images of Epox5.

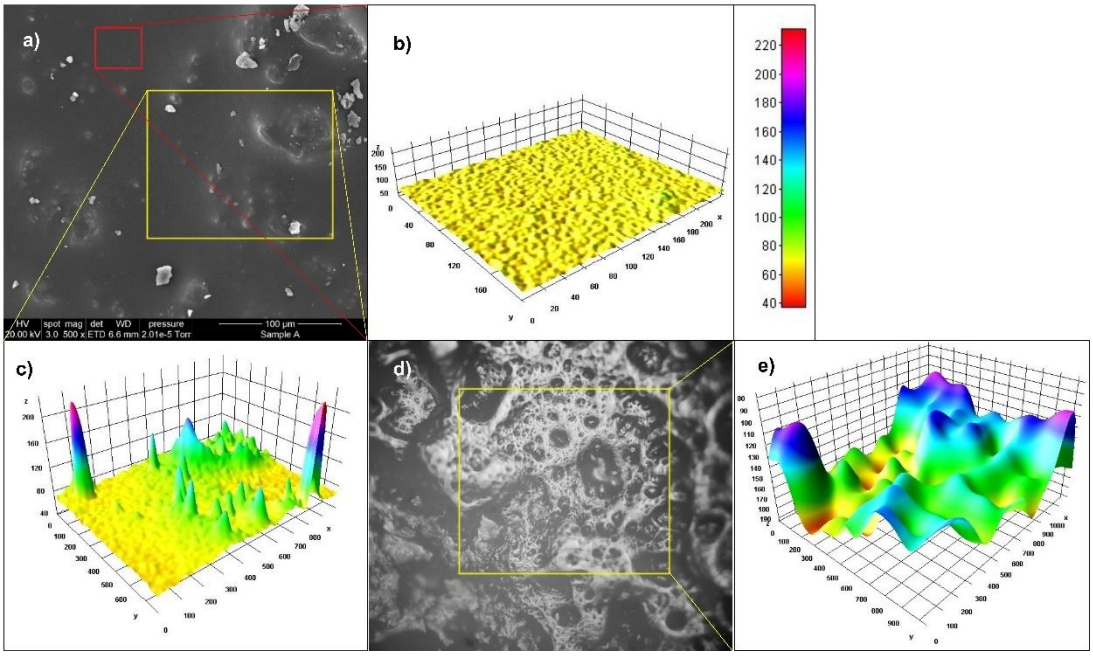

Figure 5.4. The 3D-surface plots of Epox5 obtained from (a) SEM and (d) PLM images. The obtained surface undulations were from (b) smooth, (c) coarse region of SEM images and (e) uneven region of PLM image.

5.3.3.2. *Polyester-lignite coated CRF*

The coating surface and cross-section were investigated using SEM and PLM images under different magnifications. The surface of the polyester-lignite coating was coarse and grainy (Figure 5.5 – a, b, e & f). The fine lignite particles were stuck to the surface and fully covered it. The coating made good physical contact with the urea core with no obvious boundary separation in cross-sectional view (x 250 magnification) (Figure 5.5 - c). However, there were minute gaps and pockets that can be seen under high magnification (x 1000) (Figure 5.5 - d). The average thickness of the coating was 167.2 ± 15 µm (Figure 5.5 - c) and the coating thickness was reasonably uniform throughout the granule.

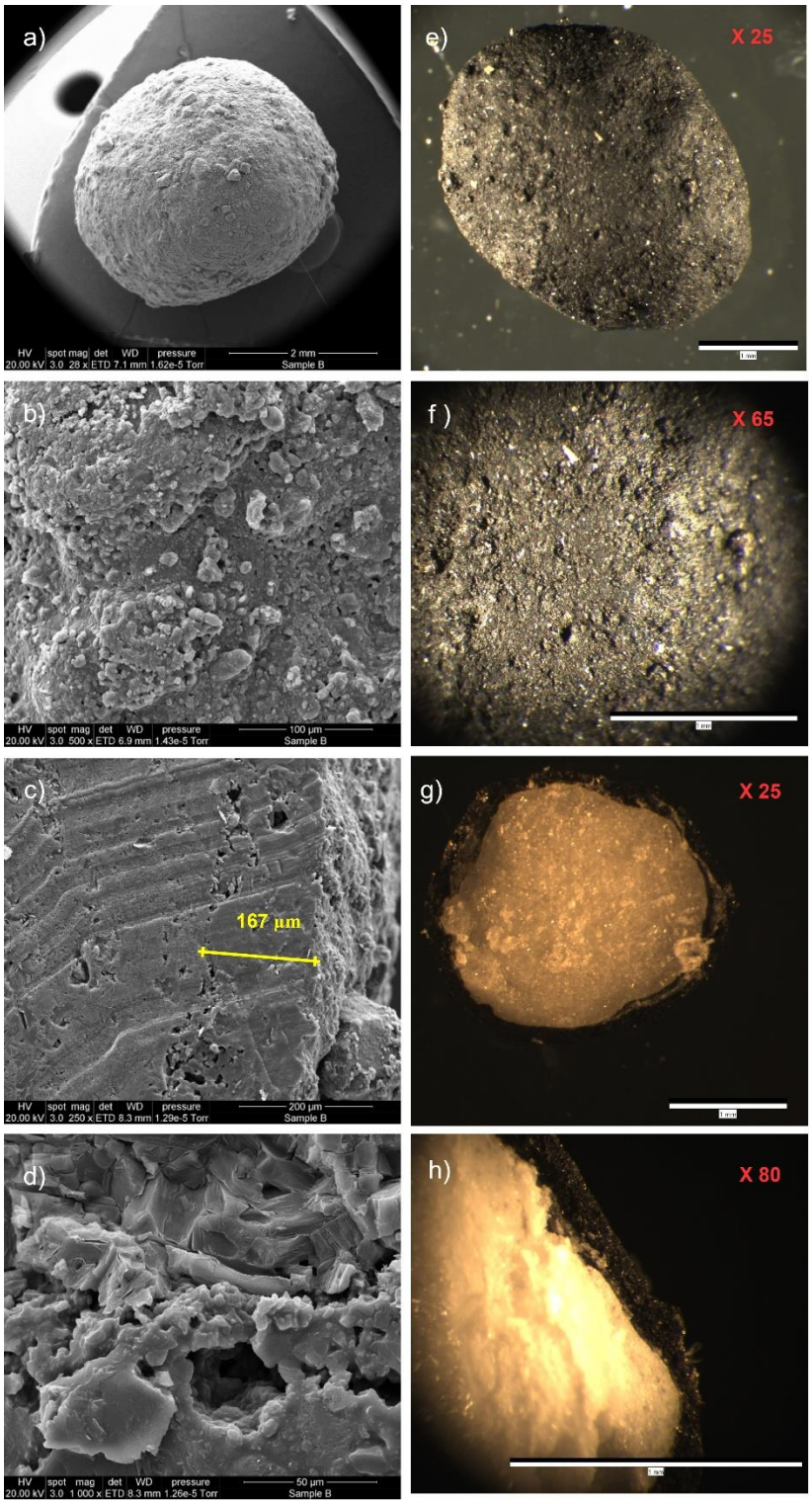

Figure 5.5. The SEM (a - d) and PLM images (e - h) of Poly5 CRF. Images a, b, e and f show the surface of the coating and c, d, g and h are the cross-section of Poly5 at different magnifications.

The 3D-surface image obtained from SEM image (x 500) showed that surface irregularity exists all over the coating surface and ranged from 60 – 220 pixels (Figure 5.6). However, the majority of the coating was between 60 – 120 and only a small portion in 200 – 220 pixels range.

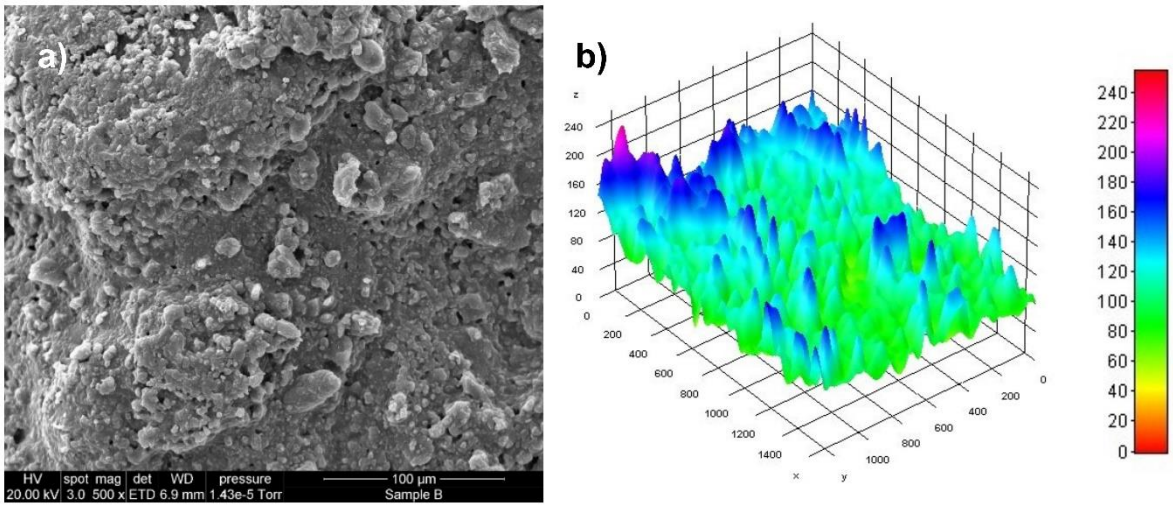

Figure 5.6. (a) The SEM image of Poly5 CRF surface at x 500 magnification and (b) 3D-surface image of the surface obtained from the image analysis using ImageJ software.

5.3.4. FTIR analysis of coating membrane

5.3.4.1. *FTIR analysis of epoxy-lignite coatings*

There are four major regions of coal and its derivatives that can be classified by FTIR spectrum analysis; aromatic substitution region (900 – 700 cm^{-1}), O-containing group (1800 – 1000 cm^{-1}), aliphatic structures (3000 – 2800 cm^{-1}) and hydrogen bond region (3700 – 3000 cm^{-1}) (Wang et al., 2017). The broad strong peak found in 3400 cm^{-1} wavelength region was attributed to hydroxyl group (–OH stretching) (Figure 5.7). The weak sharp peaks around 2900 cm^{-1} wavelength belong to the aliphatic group (-CH2). The aromatic sp^2 hybridized carbon-carbon

bond was characterised by the sharp peak at 1621 cm^{-1} wavelength (Xu et al., 2017). The weak absorption peaks at 1440 and 1369 cm^{-1} were hydroxyl stretching of carboxylic functional group and sp3 hybridized carbon stretching, respectively (Xu et al., 2017) (Figure 5.7). Ether bond C – O stretching was ascribed by the small peak at 1106 cm^{-1} wavelength. Sulphur can be found as an impurity in the lignite (Bayraktar and Lawson, 1984). Absorption at 1031 cm^{-1} wavelength corresponded to sulphur-oxygen bonding suggested that sulphur was found in this lignite. The strong absorption in 900 – 700 cm^{-1} regions is attributed to the aromatic ring structures of lignite (Figure 5.7).

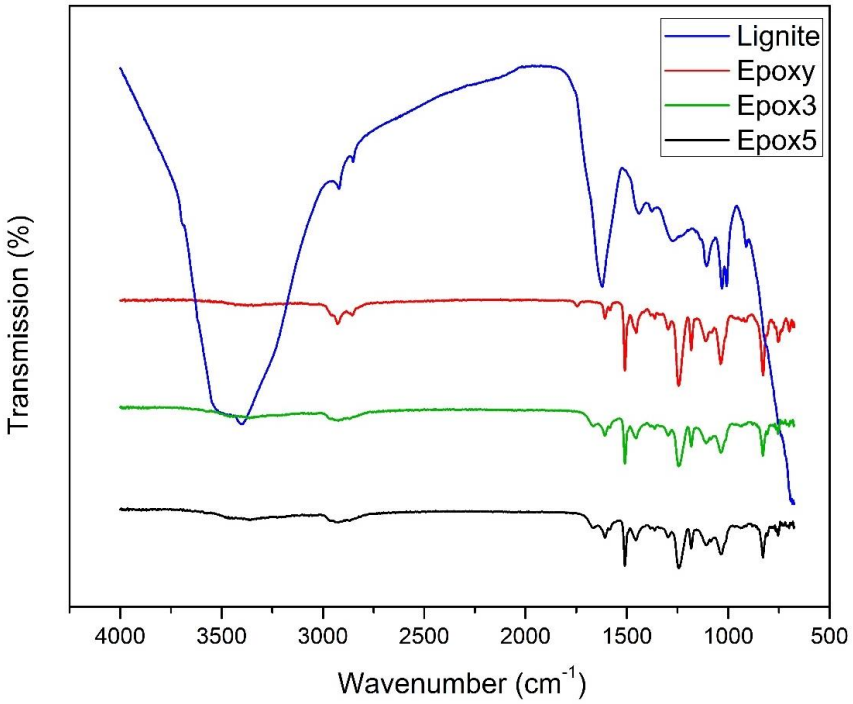

Figure 5.7. The FTIR spectrum of lignite, epoxy resin, Epox3 and Epox5 CRF coating membranes.

The characteristic peaks of epoxy resin were hydroxyl group, epoxy group and ester bonds. This epoxy resin matches the typical absorption spectrum of epichlorohydrin and bisphenol, an epoxy resin (Fernandes et al., 2018). However, the peak at 3400 cm^{-1} wavelength was not prominent (short) as epoxy contains a low number of hydroxyl groups (Fernandes et al., 2018) (Figure 5.7). The sharp peaks at 2927 and 2854 cm^{-1} due to the aliphatic carbon and hydrogen bond

stretching; -CH_2 and -CH, respectively (Francis, 1950). The sharp and strong absorption around 1500 cm^{-1} was attributed to the benzene ring structure and the peaks around 1600 cm^{-1} belongs to aromatic sp^2 hybridized carbon-carbon bond (Li et al., 2018) (Figure 5.7). The very sharp and strong peak at around 1250 cm^{-1} was ascribed to C – O – C bond of ether. The higher number of ether bonds formed due to the reaction of epoxy group with bisphenol-A and it was found to be the dominant type of bond in epoxy resin (Figure 5.8). The epoxy group (oxirane group) was characterised by the small peaks around 916 cm^{-1} (Romão et al., 2006). The absorption peaks at 1181 cm^{-1} represents the C – O bond stretching of the aromatic rings. The different types of C – H bond absorptions were in between 680 – 850 cm^{-1} wavelengths. The aromatic ester bonds were represented by peaks at 1037 and 1108 cm^{-1} (Figure 5.7).

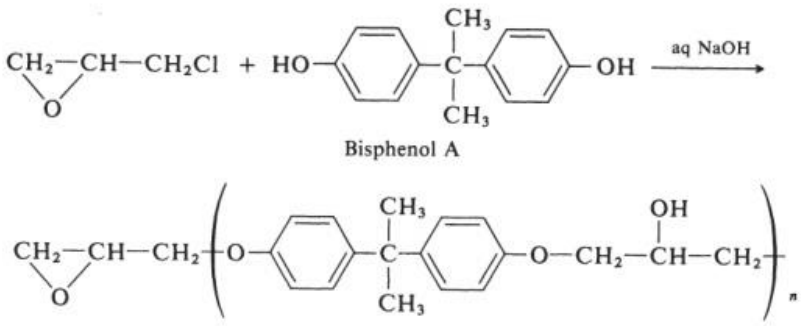

Figure 5.8. The reaction mechanism of epoxy resin.

The coating membrane showed a modified FTIR spectrum of epoxy that did not reflect the lignite component since a large portion of the coating surface was composed of epoxy resin. The mixing of lignite has not hindered the epoxy curing reaction which can be confirmed by the formation of C – O – C bond (peak at 1250 cm^{-1}) and small peaks of the epoxy group (at 916 cm^{-1}). However, the absorbance values of all peaks, especially characteristic regions of epoxy such as ester and epoxy functional groups, decreased in the coating membrane compared to pure epoxy resin. This was possibly due to the decreased amount of epoxy when blended with lignite. In addition, hydrogen bonds stretching such as - CH_2 and – CH become weak and broad (between 2850 and 2950 cm^{-1}). The

shift of the C-O region at 1743 cm^{-1} towards the right side suggests that the bond became stronger. The FTIR spectrum of coating membrane suggests that lignite and epoxy not only physically blended but also chemically interacted. The low availability of hydroxyl groups in the blended mixture of epoxy-lignite possibly decreases the water interaction with the coating. Although modified spectra were observed in epoxy-lignite blends, there was no clear evidence to show new covalent bond formation. Comparable observations were made in many similar composite mixtures (Fernandes et al., 2018; Sathishkumar et al., 2018).

5.3.4.2. *FTIR analysis of polyester-lignite coatings*

The absorbance at around 3500 cm^{-1} was not prominent which suggests that the hydroxyl group was rarely present in polyester (Figure 5.9-b). The weak absorbance at 2916 and 2844 cm^{-1} were attributed to -CH_2 and -CH stretching, respectively (Francis, 1950). The characteristic functional group of polyester resin was an ester bond. The sharp peak at 1726 cm^{-1} belongs to the C=O bond stretching of ester and peak at 1378 cm^{-1} was represented by COO^- bonds. The C – O – C peaks were identified at 1281, 1163 and 1121 cm^{-1} (Figure 5.9-b). The aromatic ring structure stretching was caused by the peaks at 1600 and 1452 cm^{-1} wavelengths (Sahari and Maleque, 2016). The band at 1069 cm^{-1} was due to unsaturated in-plane deformation which indicates it was an unsaturated polyester (Sahari and Maleque, 2016). Out-of-plane stretching of aromatic C-H bonds was represented by 744 cm^{-1} (Wang et al., 2015; Sahari and Maleque, 2016). The absorption of aromatic groups can be assigned to the peak at 700 cm^{-1}.

The polyester-lignite coating showed a modified spectrum of polyester wherein the influences of lignite also can be noticed. The overall absorbance of the coating decreased compared to polyester resin. A new peak appeared around the 3000-3500 cm^{-1} region, possibly the hydroxyl group due to interactions between the lignite and polyester (Figure 5.9-c). The weak –CH_2 and –CH peaks of polyester resin disappeared in the coating. Further, a new broad peak appeared at around 1500 – 1700 cm^{-1} belongs to the aromatic stretching of sp^2 hybridized carbon, possibly from the lignite (Xu et al., 2017). A sharp peak at 700

cm^{-1} was missing in the coating spectra (Figure 5.9-c). All these suggested that polyester made chemical interactions with lignite in coating membrane synthesis, and more interactions were observed in polyester-lignite coating than epoxy-lignite coating.

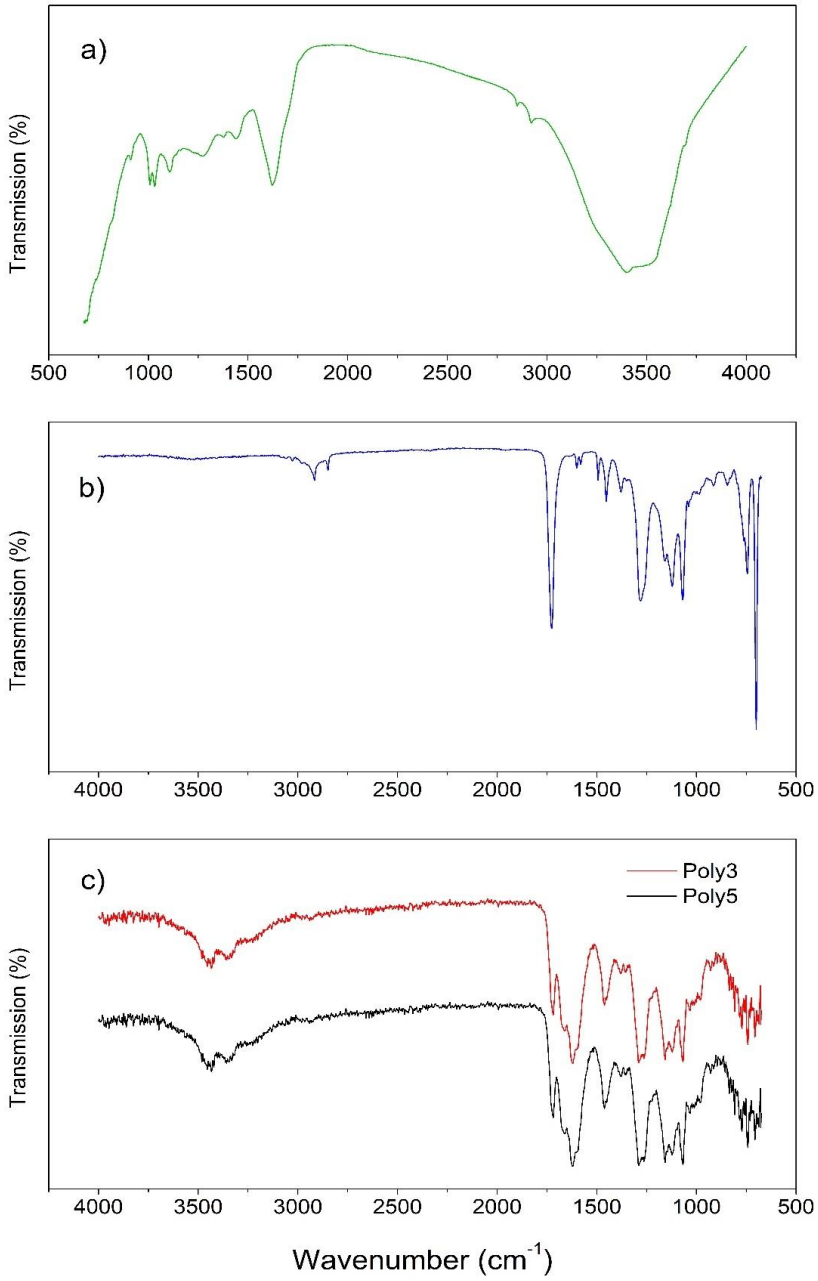

Figure 5.9. The FTIR spectrum of (a) Lignite, (b) polyester resin, (c) Poly3 (red) and Poly5 (black) CRFs.

5.3.5. Thermogravimetric analysis (TGA)

5.3.5.1. *TGA analysis of epoxy-lignite composite coatings*

The TGA and derivative thermogravimetric analysis (DTG) were performed to study the thermal properties of the lignite, epoxy resin and epoxy-lignite composite coating materials; Epox3 and Epox5 (Figure 5.10).

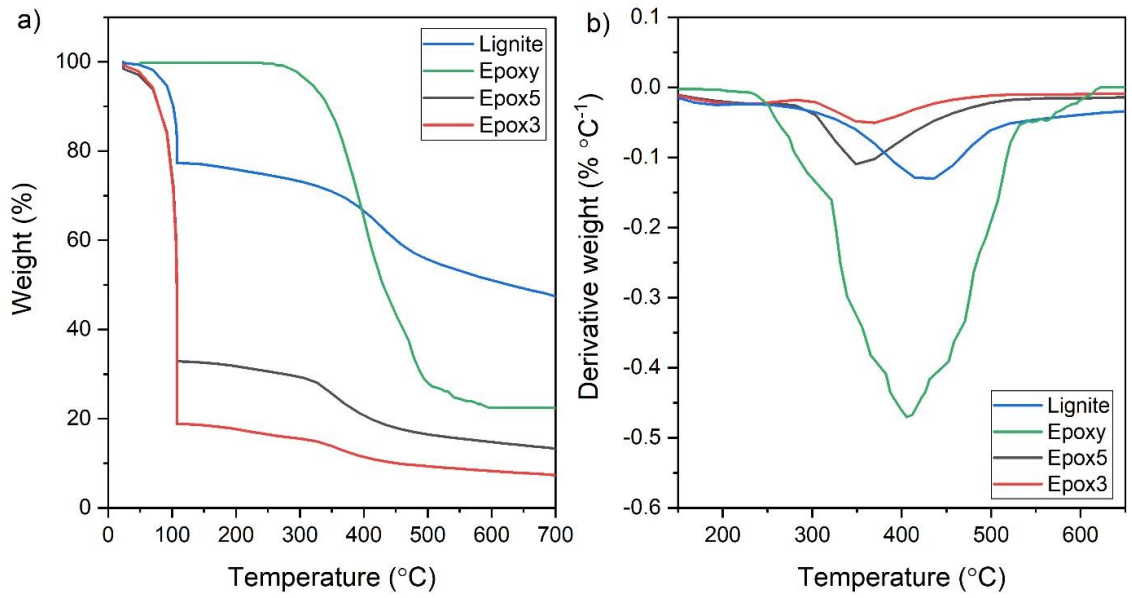

Figure 5.10. (a) The TGA and (b) Derivative thermogravimetry (DTG) curves of lignite, epoxy and epoxy-lignite composite coating materials; Epox3 and Epox5.

All the materials underwent thermal mass losses at an elevated temperature. The first mass loss took place at around 100 °C that corresponded to the losses of moisture and volatile material (Figure 5.10-a). The mass losses were 22%, 67% and 81% for lignite, Epox3 and Epox5, respectively, while epoxy resin didn't exhibit any mass loss at this stage. The washed coating membranes of Epox3 and Epox5 fertilisers were used for TGA analysis, which was attributed to the high moisture loss of these samples. The second mass loss initiated at around 250 °C for all samples. The mass losses per unit changes of temperature were in the following order; epoxy > lignite > Epox5 > Epox3 (Figure 5.10-b). The maximum

decomposition temperature (T_{max}) was 427, 407, 350 and 364 °C for lignite, epoxy, Epox3 and Epox5, respectively (Figure 5.10-b). The T_{max} values of epoxy-lignite composites were lower than lignite and epoxy resin (Figure 5.10-b) which suggest that these composites had lower thermal stability than raw materials. Although the coating thickness was higher for Epox5 than Epox3, the T_{max} value of Epox3 was higher than Epox5. The possible reason for this was the epoxy content in Epox5 higher than Epox3, which lowered the T_{max} value.

5.3.5.2. *TGA analysis of polyester-lignite composite coatings*

The TGA and derivative thermogravimetric analysis (DTG) showed the thermal degradation of lignite, polyester resin and polyester-lignite composite coating materials; Poly3 and Poly5 under elevated temperature in nitrogen atmosphere (Figure 5.11).

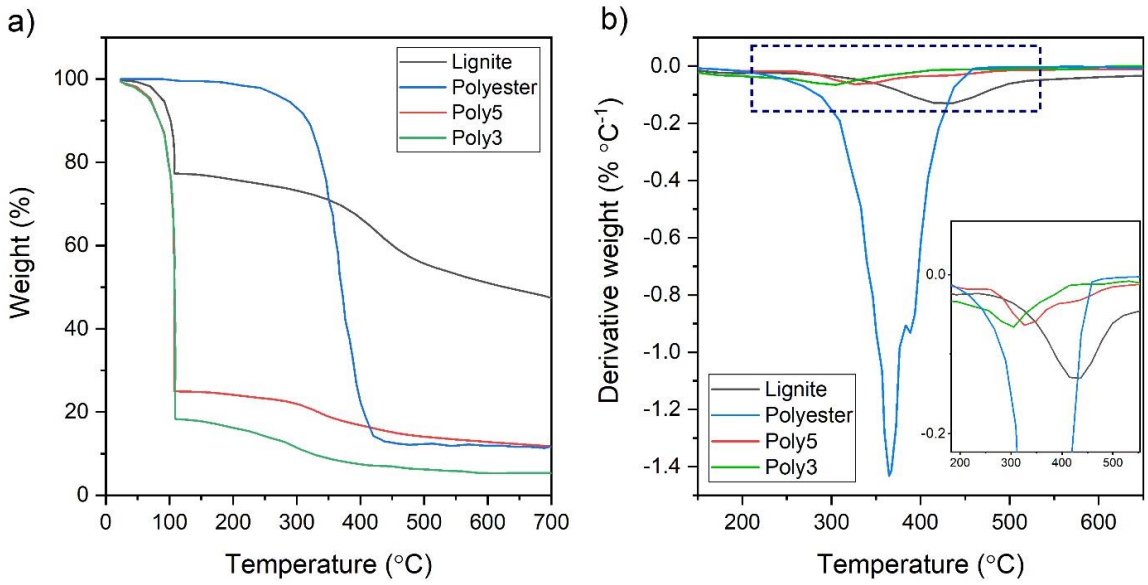

Figure 5.11. (a) The TGA and (b) Derivative thermogravimetry (DTG) curves of lignite, polyester and polyester-lignite composite coating materials; Poly3 and Poly5 (inset graph shows magnified view of the graph in dashed rectangle).

All the samples lost mass with increasing temperature in two stages; at 100 °C and 220 - 265 °C. The first mass losses were 22%, 81% and 75% for lignite, Poly3 and Poly5 samples, respectively, which corresponded to losses of moisture and volatile substances. However, polyester resin didn't show a considerable mass loss at this stage (Figure 5.11-a). The observed high moisture losses in samples Poly3 and Poly5 were due to moisture absorbed by coating during the washing process on urea removal. The second mass losses were 30%, 88%, 14% and 13% for lignite, polyester, Poly3 and Poly5 samples, respectively (Figure 5.11-a). The mass loss for unit temperature change in the following order; polyester > lignite > Poly3 = Poly5. The T_{max} values for lignite, polyester, Poly3 and Poly5 were 430, 365, 326 and 305 °C, respectively (Figure 5.11-b). This suggests that composite coatings had lower thermal stability than raw materials. Poly3 showed a lower T_{max} value than Poly5 which could be attributed to the high polyester content in Poly3 coating. These findings are consistent with epoxy-lignite composites.

5.3.6. Physical properties

5.3.6.1. *Particle size distribution and circularity of the coated and uncoated urea*

The particle size distribution and circularity of urea and CRFs were analysed using images of these fertilisers by ImageJ software. The d50 values of Epox3, Epox5, Poly3, Poly5 and urea were 1.63, 1.7, 1.78, 1.85 and 1.8 mm, respectively. The uncoated urea particle size distribution was closer to the d50 value, whereas Epox5 showed a skewed distribution, and Poly5 showed a broad distribution around the d50 value (Figure 5.12 - a, b & c). The obvious changes in particle size possibly changed the distribution of coated CRFs.

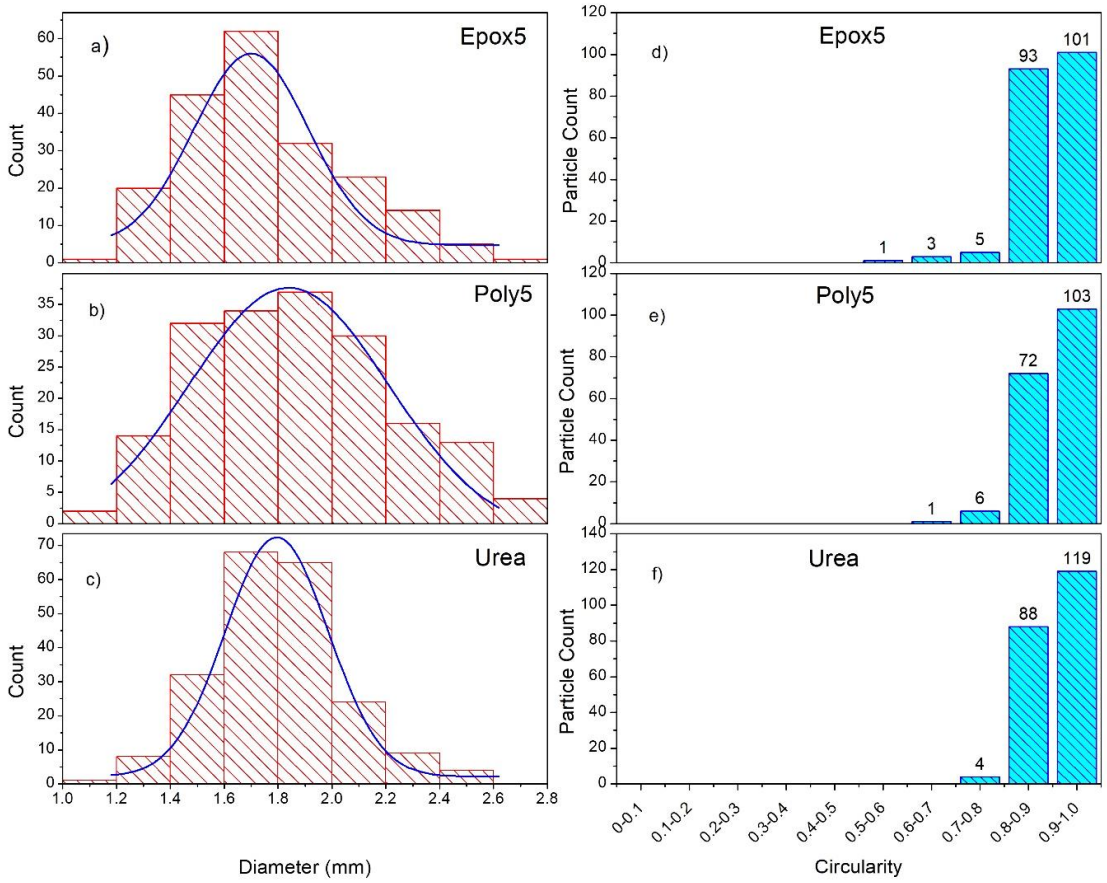

Figure 5.12. The particle size distribution (a-c) and circularity (d-f) of the uncoated and coated (Epoxy5 and Poly5) urea granules.

The particle circularity is an important shape parameter that influences the spreading of fertilisers onto the field (Bouwman et al., 2004). The circularity range between 0.8 – 1.0 shows the high circular shape of the granules. The percentage of granules in this range were 93%, 96%, 95%, 96% and 98% for Epox3, Epox5, Poly3, Poly5 and urea, respectively (Figure 5.12 - d, e & f). Circularity value decreased only by a small percentage for the CRFs compared to uncoated urea. This small decrease was attributed to many reasons such as fusion of particles, protruded lignite edges on the surface, and polymer-lignite clumps stick to the surface of the coating.

5.3.6.2. *Water absorbency and coating porosity*

The water absorbency was significantly ($p<0.05$) influenced by the coating thickness for both CRF types. The greater the coating thickness, the lower the water absorbency; Epox5 > Epox3 and Poly5 > Poly3 (Table 5.3). The water absorbency decreases with increasing hydrophobicity, the elasticity of polymer and polymer crosslinking density (Liang et al., 2007). The lower water absorbency in thick coatings was associated with the amount of polymer which was higher in the thick coating which resists water diffusion into the coating material. Other studies also reported that increased polymer content and coating thickness decreased the water absorbency (Novillo et al., 2001; Qiao et al., 2016). For the same number of coating the epoxy-lignite mixture showed significantly ($p<0.05$) lower water absorbency than the polyester-lignite mixture (Epox5 < Poly5 and Epox3 < Poly3). Epoxy resin has higher elasticity compared to polyester resin (Reis, 2012). Therefore, it has more resistance to water diffusion into the coating matrix. However, there was no significant ($p>0.05$) difference between Epox3 and Poly5.

Table 5.3. The water absorbency and coating porosity of CRFs.

CRF	Water absorbency (%)	Effective porosity (%)	Abrasion resistance (%)
Epox3	2.00 ± 0.67^{b}	12.28 ± 0.53^{b}	97.2
Epox5	0.44 ± 0.38^{c}	2.35 ± 0.39^{c}	98.7
Poly3	4.00 ± 0.67^{a}	15.85 ± 2.30^{a}	97.8
Poly5	2.00 ± 0.67^{b}	2.95 ± 0.49^{c}	98.5

The different letters within a column shows the statistically significant values (LSD method, n = 3, $p<0.05$).

The effective porosity (EP) of a coating directly influences the nutrient releasing characteristics of a CRF. The EP only includes the pores in which the water can penetrate. Increased EP facilitates water diffusion into the CRF granule and reduces the controlled release behaviour. Therefore, a low level of EP is preferred for a coating material to improve the nutrient releasing property. Increasing

coating thickness significantly ($p<0.05$) decreased the EP for both types of coatings; Poly5 < Poly3 and Epox5 < Epox3 (Table 5.3). The EP decreased by 10% and 13% for epoxy-ignite and polyester-lignite coating, respectively. This finding is in agreement with a study that reported the porosity decreased by 8% when the polymer concentration was increased (Jarosiewicz and Tomaszewska, 2003). The EP of Epox3 was significantly ($p<0.05$) lower than Poly3, but there was no significant difference between Epox5 and Poly5. This suggests that the polymer composite type has no clear relation to EP.

Increasing coating thickness improved the abrasion resistance for both polymer composites. The abrasion resistance increased by 2% and 1% for epoxy-lignite and polyester-lignite composite coatings, respectively, when the coating thickness was increased (Table 5.3).

5.3.7. Modelling of release kinetics

The urea release data were fitted against the Korsmeyer-Peppas and Peppas–Sahlin models (Figure 5.13 & 5.14) and the derived values are summarized in Table 5.4. Although many studies suggest only 60% release shows the best fit with these models (Bruschi, 2015), the data in this study used 100% release as it improved the model fit with the observed values (Figure 5.13 & 5.14).

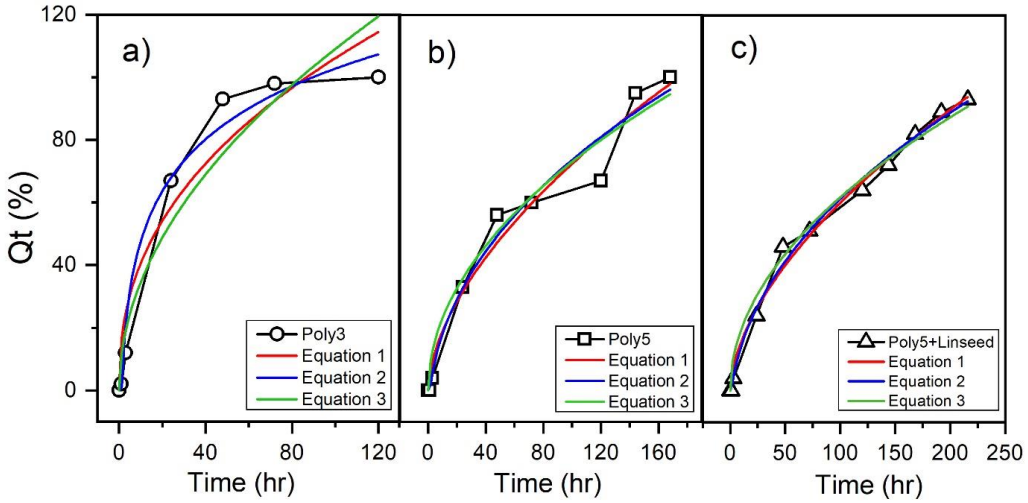

Figure 5.13. Model fitting of urea release from (a) poly3, (b) poly 5, and (c) poly5+linseed CRFs. The equation 1, 2 and 3 stands for Korsmeyer–Peppas model, Peppas–Sahlin model and initial coefficient of diffusion (Df) equations.

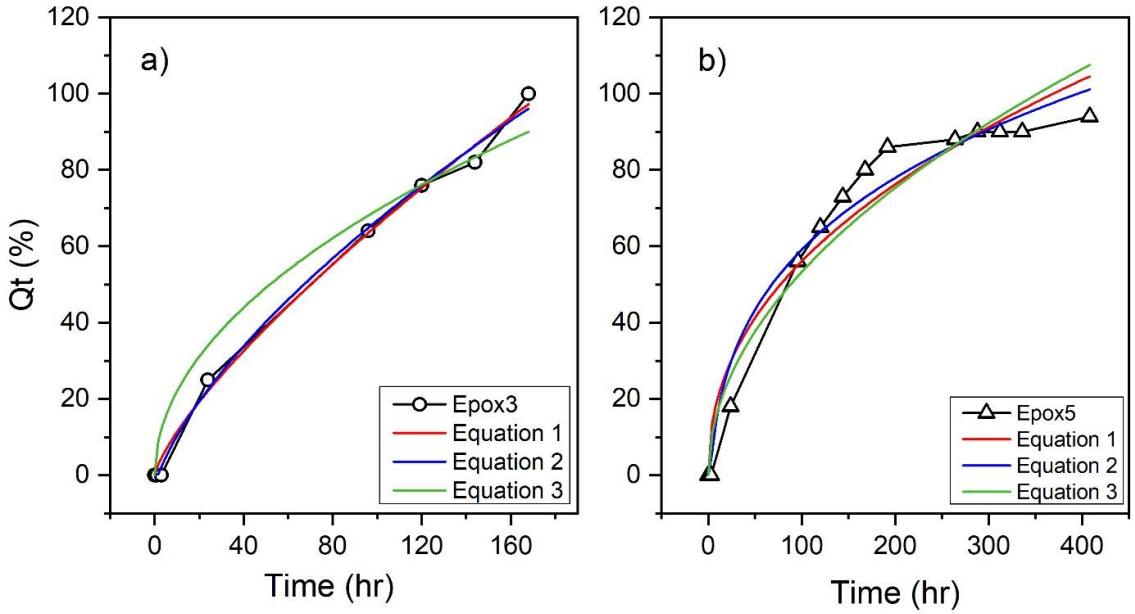

Figure 5.14. Model fitting of urea release from (a) Epox3 and (b) Epox5 CRFs. The equation 1, 2 and 3 stands for Korsmeyer–Peppas model, Peppas–Sahlin model and initial coefficient of diffusion (Df) equations.

The n values of Epox3, Epox5, Poly5 and Poly5+Linseed were 0.76, 0.44, 0.58 and 0.58, respectively, suggesting that the nutrient release was non-Fickian anomalous transport ($0.45 < n < 0.89$). Whereas, Poly3 showed Fickian diffusion release ($n = 0.42$) according to the Korsmeyer-Peppas model (Table 5.4).

The values of $k_1 < k_2$ (Peppas–Sahlin model) for all CRFs indicated that the primary nutrient releasing mechanism was erosion and relaxation (Bruschi, 2015). Except for Poly3, the results obtained from Peppas–Sahlin model agreed with the results of the Korsmeyer-Peppas model. For Poly3, the former model suggested the Fickian release and the latter model suggested polymer coating relaxation. A similar contradicting prediction between these models was reported in other studies (de Matos et al., 2018; Llive et al., 2019). This could be ascribed to multiple mechanisms involved in the nutrient release, other than those investigated by these models (Xiaoyu et al., 2013).

Table 5.4. Kinetic parameters of the newly developed CRFs.

		Controlled-release fertiliser				
	Parameter	**Epox3**	**Epox5**	**poly3**	**Poly5**	**Poly5-Linseed**
Equation 1	**k**	1.96	7.28	15.50	4.95	4.12
	n	0.76	0.44	0.42	0.58	0.58
	R^2	0.99	0.95	0.92	0.97	0.99
Equation 2	**k_1**	-6.78	-74.70	-1580.68	-21.88	-15.01
	k_2	6.02	68.95	1577.74	21.42	14.76
	m	0.30	0.10	0.01	0.19	0.21
	R^2	0.99	0.97	0.97	0.97	0.99
Equation 3	**D_f**	1.35	0.89	0.32	0.29	0.21
	l	0.377	0.4	0.12	0.17	0.17
	R^2	0.97	0.95	0.92	0.97	0.99

The initial coefficient of diffusion (Df) was linked to the coating thickness and decreased with increasing thickness for all CRFs. The increment of actual coating percentage by 5.9% and 8.7% for epoxy-lignite and polyester-lignite coating has decreased the Df by 0.46 and 0.03 hr^{-1}, respectively (Table 5.4). Increasing the coating thickness was not effective for Poly5 as only a small increment in Df (0.03 hr^{-1}) was observed. This must be associated with the burst effect and subsequent quick release of urea. The addition of linseed sealant coating decreased the Df by 0.07 hr^{-1} when compared to Poly5.

5.4. Conclusions

This study focused to develop new controlled-release fertilisers and characterise the physiochemical performances. Four different controlled-release fertilisers (CRFs) were developed by coating the granular urea with polymer-lignite composite; epoxy-lignite and polyester-lignite. The physiochemical properties and urea releasing behaviours were studied. The lignite acted as a filler or conditioner and it decreased the polymer content of the coating membrane. The polymer-lignite coatings were dense and physical and chemical integrations were

observed within the compositions of the coatings. The urea releasing behaviour was coating thickness-dependent for all CRFs where release rate decreased with increasing coating thickness. The epoxy-lignite composite coating showed superior urea releasing property when compared to the polyester-lignite composite. The Epox5 prolonged the urea releasing period (nearly 400 hours) compared to other fertiliser formulations. The nutrient release kinetic models suggest that the primary mechanism governing the nutrient releases were erosion and relaxation of the coating membrane.

Chapter 6

Evaluation of newly developed controlled-release fertilisers in Climate-Controlled Lysimeters

6.1. Introduction

A significant portion of applied nitrogen in agriculture is lost to the environment via leaching and gaseous losses. Therefore, controlled-release fertilisers (CRFs) are being used to improve nitrogen use efficiency while reducing the negative environmental effects. These fertilisers slowly release nutrients with the aim of synchronising release with the plant demand.

In a previous study (Chapter 5) the newly developed CRFs; Epox5 and Poly5 showed better controlled release characteristics than Epox3 and Poly3 in static water. These CRFs were trialled in the soil to compare their performance to conventional nitrogen fertilisers (urea and diammonium phosphate – DAP) on ryegrass in a climate-controlled lysimeter system under a simulated climate regime. The parameters measured in respect to N losses were leaching and nitrous oxide emission, and impact of fertilisers on dry matter yield and herbage nitrogen recovery.

6.2. Materials and Methods

6.2.1. Lysimeter setup and ryegrass establishment

Forty climate-controlled lysimeters were employed in this study and all of them were packed with Manawatu fine sandy loam soil (topsoil) and washed builders' sand (subsoil). The general physicochemical properties of top and subsoil were measured and are summarised in Table 6.1. A more detailed description of the lysimeter design is described in Chapter 3 and the soil column packing method referred to in Gunaratnam et al. (2020). Perennial ryegrass (*Lolium perenne* L.)

swards were grown in lysimeters for four months under artificial lights to reach the mature stage. At the end of each month, ryegrass swards were clipped at 5 cm height to simulate natural grazing. The grass swards were fertilized in the second month with 'Nitrophoska (Ravensdown®)' fertiliser at a rate of 25 kg-N ha^{-1}. In the last two weeks of the establishment period, the soil column was leached with nearly 5 pore volume changes of water to eliminate the residual fertiliser effect on the experiment.

Table 6.1. The basic physical and chemical properties of soils.

Parameter	**Unit**	**Topsoil**	**Subsoil**
Bulk Density	(g cm^{-3})	1.14	1.65
Soil texture class	-	Sandy clay loam	Sand
pH	-	5.6	7.6
Olsen Phosphorus	mg L^{-1}	18	-
CEC	me $100g^{-1}$	12	5
Anion Storage Capacity	%	15	-
C: N	%	1.21: 0.13	0.03: 0.04
Nitrate-N	kg ha^{-1}	43	3
Ammonium-N	kg ha^{-1}	3	0.2

6.2.2. Treatments and climate model

The experimental design consists of five treatments with eight replicates; control (with 0 N), urea, diammonium phosphate (DAP), Epox5 and Poly5. The Epox5 and Poly5 are newly developed CRFs in this research programme and the preparation processes and characteristics are detailed in Chapter 5. All fertilisers were applied as a single surface application at the start of the experiment at a rate equivalent to 50 kg-N ha^{-1}. The treatments were arranged in a completely randomized design (CRD) in the lysimeters. The lysimeters were covered with caps after the fertiliser application to control the microclimatic environment. The spring season (year 2013) of the Taranaki region was selected as the climate

model for this study to emulate in the climate-controlled lysimeter system. The artificial rainfall events were created according to the climate model. More details of the climate model and control of climate variables are described in Chapter 3 and McCurdy et al. (2019). The performance of fertilisers on ryegrass yield and losses to the environment were studied for 91 days.

6.2.3. Grass cutting and analysis

6.2.3.1. *Leaf and stubble dry matter (DM) yield*

The grass swards were clipped at the end of each month at 5 cm height. The stubbles were cut at the ground level at the end of the experiment. The grass and stubble DM were determined by weighing the oven-dried samples at 65°C until a constant weight is attained. Above-ground total biomass DM was calculated by summing the total grass and stubble DM.

6.2.3.2. *Herbage nitrogen (HN)*

The dried grass samples were ground to a fine powder using a coffee grinder. One gram of ground sample was digested using the micro-Kjeldahl digestion method and the total nitrogen was analysed using an Auto analyser (Blakemore et al., 1987).

6.2.3.3. *Agronomic use efficiency*

The agronomic use efficiency (AUE) is the measure of DM yield increment from fertiliser application compared to control treatment and was calculated using the following equation.

$$\mathrm{AUE} = \frac{\mathrm{DM\ yield\ of\ N\ treatment} - \mathrm{DM\ yield\ of\ control}}{\mathrm{Applied\ N}}$$

6.2.3.4. *Apparent recovery efficiency*

The apparent recovery efficiency (ARE) refers to additional N taken up in plants from the N treatments compared to the control. ARE was calculated using the following equation where HN stands for herbage nitrogen.

$$\text{ARE} = \frac{\text{HN of N treatment} - \text{HN of control treatment}}{\text{Applied N}}$$

6.2.4. Root dry matter distribution

Soil blocks were incrementally retrieved at the end of the experiment using a newly designed lysimeter-soil-retriever (LSR). The topsoil and subsoil were sliced into 5 and 10 cm sections, respectively. This yielded 2 topsoil and 3 subsoil blocks from each soil column. The detailed LSR design and retrieval process are described in Chapter 4. The retrieved soil blocks were air-dried, rolled to break soil clods and sent through a 1 mm sieve to extract the roots from the soil. The extracted roots were washed in water on a sieve and foreign materials were manually removed. The dry weight was obtained after oven-drying the root samples at 65°C until a constant weight was achieved. The root DM in the last 10 cm of the soil profile is negligible compared to other depths and therefore, it was omitted in the DM calculation.

6.2.5. Nitrous oxide collection and analysis

A similar approach to the static chamber method (Collier et al., 2014) was employed to collect N_2O gas from each lysimeter. In this study, the lysimeter cap used for climate control was also used as the chamber for gas collection. A valve at the air-inlet port was closed and the air-exit port was sealed using a rubber bung to create an air-sealed environment for collecting the gas in the lysimeter cap (Figure 6.1). During the gas collection, the air blower was shut down to avoid damage to the airline. The gas sampling was undertaken weekly throughout the experimental period. The gas samples were collected at 0, 1 and 1.5 hours for

the first 2 months and 0, 1.5 and 2 hours during the last month. The N_2O accumulation decreases with time and therefore, the gas collection period increased in the third month to collect a sufficient amount of N_2O. A 60 ml syringe was connected to the gas collection port, and the plunger was pressed four times to homogenise the gas before a 35 ml sub-sample was taken. Collected sub-samples were injected into a 12 ml pre-evacuated screw-cap septum glass vial. The N_2O gas concentration was measured using a gas chromatograph (GC-2010, Shimadzu, Tokyo, Japan) coupled with an electron capture detector. Oxygen-free nitrogen gas was used as the carrier gas. The nitrous flux on a particular day was calculated using the following equation;

$$F = \frac{d_C}{d_t} \times \rho \times H$$

Where F is nitrous oxide flux (µg-N m^{-2} hr^{-1}), d_C/d_t is the nitrous oxide flux increment in the headspace in one hour (µL L^{-1}), ρ is nitrous oxide gas density (g m^{-3}) and H is lysimeter cap-height (m).

The total nitrous oxide emission was calculated by integrating the daily flux to the total experimental period.

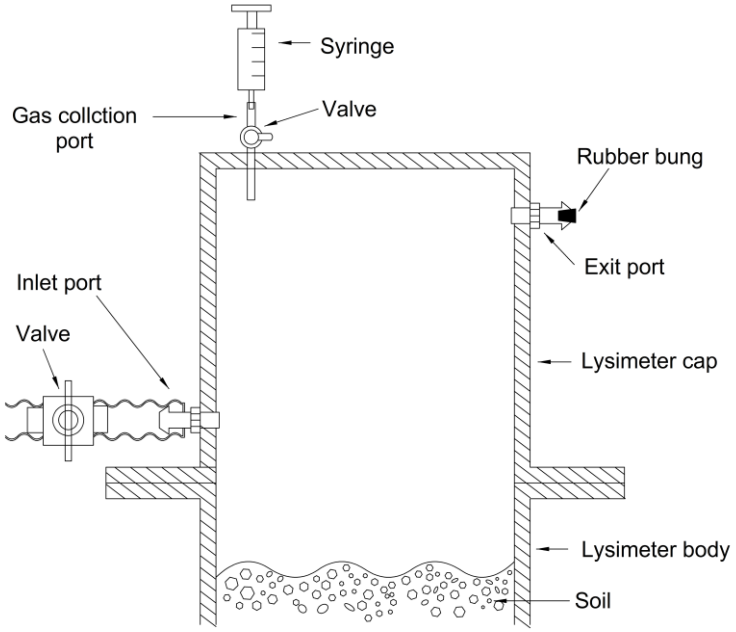

Figure 6.1. The schematic diagram of the experimental setup of nitrous oxide gas collection.

6.2.6. Leachate collection and analysis

The leachates were collected, and the volume was measured after every drainage event. A sub-sample of 50 mL was kept in the freezer until taken for analysis. Before analysis, leachates were thawed and filtered through 0.45 µm cellulose acetate filter papers. The mineral nitrate (NO_3^-) and ammonium (NH_4^+) ions were analysed by a Technicon Auto analyser, Series 2 (Blakemore et al., 1987).

6.2.7. Residual nitrogen in the soil

A 200 g soil sub-sample was collected from each retrieved soil block and frozen at - 4°C until it was analysed. The soil samples were thawed and mineral-N species (NO_3^- & NH_4^+) were extracted from 3 g of soil with 25 ml of 2 M KCl solution on an end-over-end shaker for 1 hour. The extractant was centrifuged at 9000 rpm (107,100 g) for 10 minutes, followed by filtering through Whatman No. 42 filter paper. The filtrate was then analysed for mineral-N using a Technicon Auto analyser, Series 2 (Blakemore et al., 1987). The moisture content of each soil sample was measured by oven-drying the sample at 105°C for 48 hours and moisture was calculated. The total residual mineral-N was calculated for a hectare of dry soil.

6.2.8. Nitrogen budgeting

The nitrogen balance for each treatment was calculated by the difference in total N inflow and outflow.

$$N\ Balance = F_N + M_N + IM_N - FM_N - H_N - L_N - G_N$$

The net soil nitrogen mineralisation (M_N) over the experimental period was calculated from the control treatment as follows. Other N gas species were not measured and therefore, not considered for N balance calculation.

$$\text{Net soil N mineralisation } (\mathrm{M_N}) = H_N + L_N + G_N + FM_N - IM_N$$

Where F_N is fertiliser N, M_N is soil mineralised N, IM_N is initial soil mineral N at the start of the experiment, FM_N is final soil mineral N at the end of the experiment, H_N is N accumulated in herbage, L_N is N lost via leaching and G_N is N lost in nitrous oxide form.

6.2.9. Data analysis

All data are presented as mean ± standard deviation. The one-way ANOVA was performed to determine the significant difference between treatment mean values using Minitab 18 (Minitab, USA). Two-way multiple factor ANOVA was employed for the investigation study to access the impact of sand type (main-factor), N levels and interaction effect of both these factors. The Tukey honest significant difference (HSD) was calculated when the treatment effect was significant, $P<0.05$.

6.3. Results and Discussion

6.3.1. Soil and Climate variables

The selected Taranaki climate regime has an intense and high rainfall pattern (Figure 6.2-a), and around 50% of the total experimental days (44 days) received rainfall. The highest rainfall received in a day and cumulative rainfall were 80 and 687 mm, respectively.

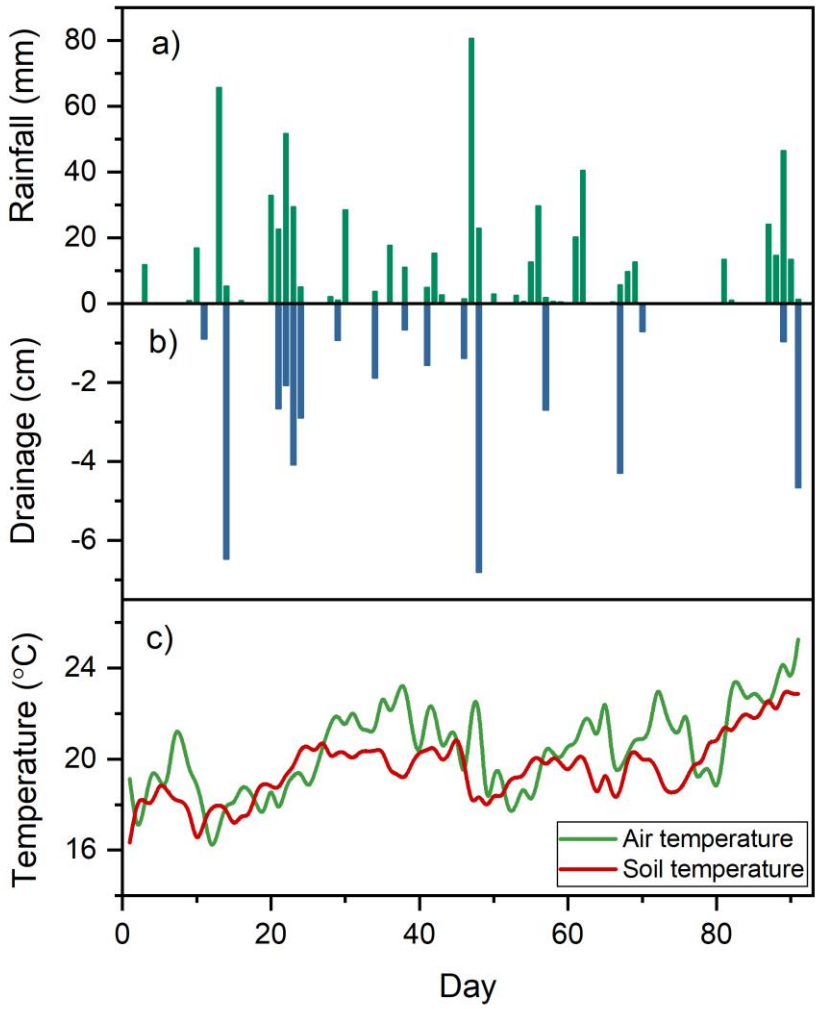

Figure 6.2. The soil and climate variables change over the experimental period; (a) rainfall, (b) drainage (cm), and (c) air and soil temperature. The drainage values are shown in negative.

The number of drainage events beyond 40-cm soil depth were 17 and cumulative drainage was 45 cm (Figure 6.2-b). The air and soil temperature at 10 cm depth showed an increasing trend over the time of the experiment (Figure 6.2-c). During the experimental period, the air temperature changed from 19°C to 25°C, whereas soil temperature increased from 16°C to 22°C.

6.3.2. Grass and above ground DM yield

The grass DM yield was influenced by the fertiliser type. In all three months, the control treatment has provided a significantly ($p<0.05$) lower yield compared to all N fertiliser treatments (Figure 6.3-a). Urea and Poly5 showed a significantly ($p<0.05$) higher yield than Epox5 for the first month. The DM yield was not significantly different between N treatments in the last two months (Figure 6.3-a). The yield continued to decline over time for all N treatments. The total grass DM yields were 768, 2195, 2151, 2062 and 2118 kg-DM ha^{-1} for control, urea, DAP, Epox5 and Poly5 treatments, respectively. Even though the total grass DM was significantly higher for N treatments compared to control ($p<0.05$) (Figure 6.3-b), the DM yield differences among N treatments were not significant.

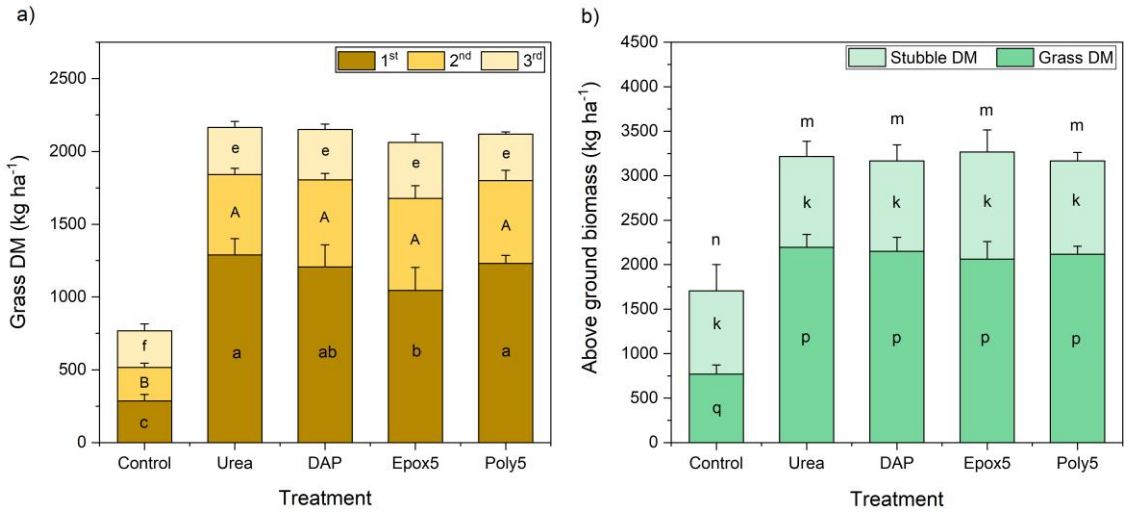

Figure 6.3. (a) The DM of monthly (1st, 2nd & 3rd) ryegrass cuttings and (b) above-ground biomass DM for different treatments. Vertical bars represent +SD (n=8). The letters show significant differences between treatments ($p<0.05$).

Only the Epox5 coating showed a significantly lower yield in the first month from urea (Figure 6.3-a). The significantly lower yield for the first month in Epox5 treatment could be attributed to the slow-releasing rate of nitrogen from the coating. However, the DM yield of Epox5 did not significantly different from DAP. The DM yield of Poly5 treatment was comparable with urea and DAP in all three months (Figure 6.3-a). This showed that N released from Epox5 was much slower

than Poly5. These findings confirmed the results obtained from the dissolution study in Chapter 5 where the release was controlled better in Epox5 than Poly5.

The stubble DM did not significantly different between treatments. The stubble DM values were 13.6, 25.7, 25.3, 26.1 and 25.3 MT-DM ha^{-1} for control, urea, DAP, Epox5 and Poly5 treatments, respectively (Figure 6.3-b). Even though the above-ground total biomass (AGTBM) was not significantly different between N treatments, they were significantly higher than the control treatment ($p<0.05$).

6.3.3. Herbage nitrogen and Nitrogen utilization efficiencies

The nitrogen utilised by ryegrass and stubble, and nitrogen utilisation efficiencies are shown in Table 6.2. The agronomic use efficiency (AUE) and apparent recovery efficiency (ARE) were calculated for treatments in relation to the control treatment. The N content of cuttings significantly decreased ($p<0.05$) with time for all nitrogen treatments, except for control (Table 6.2). Herbage N continued to significantly decrease ($p<0.05$) throughout the experiment in all N treatments except for DAP. The herbage N in DAP treated ryegrass in the second month was significantly lower ($p<0.05$) than the first month, and did not significantly differ till the end of the experiment.

The herbage N of the control treatment was significantly ($p<0.05$) lower than N treatments in the first month (Table 6.2). The Epox5 treatment showed significantly lower ($p<0.05$) herbage N (28.6 kg-N ha^{-1}) in the first month compared to other N treatments. Although herbage N was significantly higher ($p<0.05$) for N treatments than control in the second month, they were not significantly different between N treatments. The herbage N of Epox5 treatment was significantly ($p<0.05$) higher than urea and control in the third month (Table 6.2). This observation could be attributed to the slow release of urea from Epox5 coating, which may lower the available N for the plant in the first month but continued to supply in the last two months.

Table 6.2. The herbage nitrogen and nitrogen utilization efficiencies of different treatments.

Treatment	TN in 1st cutting	TN in 2nd cutting	TN in 3rd cutting	TN in Stubble	Total Herbage N	AUE	ARE
	kg-N ha^{-1}	kg-N ha^{-1}	kg-N ha^{-1}	kg-N ha^{-1}	kg-N ha^{-1}	kg-DM kg-N^{-1}	
Control	5.7 ± 1.6 cA	4.5 ± 1.2 bA	4.7 ± 1.2 cA	2.3 ± 0.6 b	14.9 ± 2.9 b	-	-
Urea	34.9 ± 5.5 aA	9.6 ± 1.5 aB	6.0 ± 0.8 bcC	2.6 ± 0.6 ab	50.5 ± 5.7 a	28.5 ± 2.9 a	0.7 ± 0.1 a
DAP	36.8 ± 5.5 aA	9.9 ± 0.9 bB	7.1 ± 1.1 abB	2.7 ± 0.5 ab	53.7 ± 5.8 a	27.6 ± 3.2 a	0.8 ± 0.1 a
Epox5	28.6 ± 4.6 bA	11.3 ± 2.2 aB	7.8 ± 1.6 aC	3.4 ± 0.9 a	47.6 ± 5.6 a	25.9 ± 4.0 a	0.7 ± 0.1 a
Poly5	37.2 ± 2.0 aA	9.1 ± 1.6 aB	6.3 ± 0.6 abC	2.8 ± 0.3 ab	52.5 ± 3.3 a	27.0 ± 1.8 a	0.8 ± 0.1 a

Data are mean ± standard deviation error of eight replicates. Values followed by different lower-case letters within a column for each treatment are significantly different at $P<0.05$ ($n = 8$). Values followed by different upper-case letters within a row for each treatment indicate the significant difference between cuttings at $P<0.05$ ($n = 8$). Total herbage N includes the first three-month cuttings. AUE and ARE refer to agronomic use efficiency and apparent recovery efficiency, respectively.

The total herbage N was significantly ($p<0.05$) higher for N treatments compared to control treatment, but it was not significantly different between N treatments. The total herbage N recoveries were 14.9, 50.5, 53.7, 47.6 and 52.5 kg-N ha^{-1} for control, urea, DAP, Epox5 and Poly5, respectively. The N recovered by stubble was lower than N recovered by herbage for the respective treatments. The stubble N recovery was significantly ($p<0.05$) higher for Epox5 in comparison to control (Table 6.2). There was no significant treatment effect on AUE and ARE. This was due to a non-significant DM yield difference between nitrogen treatments (Table 6.2). The AUE and ARE values ranged between 25.9 – 28.5 and 0.7 – 0.8 kg-DM ha^{-1}, respectively.

6.3.4. Root dry matter distribution

The root DM distribution in the soil profile was not significantly different between treatments. The root DM percentage at 0-5, 5-10, 10-20 and 20-30 cm soil layers were 56-72%, 10-18%, 12-18% and 3-9%, respectively (Figure 6.4). This result aligns with a previous New Zealand study which reported around 75% of the root dry weight distributed in the top 7 cm soil layer and a similar decrement of root dry weight in consequent soil layers (Wedderburn et al., 2010). The total root DM did not significantly differ among treatments and it varied from 477 to 833 kg ha^{-1}. Cougnon et al. (2017) reported a similar finding for ryegrass root biomass between two fertiliser rates. This observation suggests that all ryegrass seedlings were at a similar maturity level. Therefore, grass DM yield and N leaching losses may not be influenced by the root distribution.

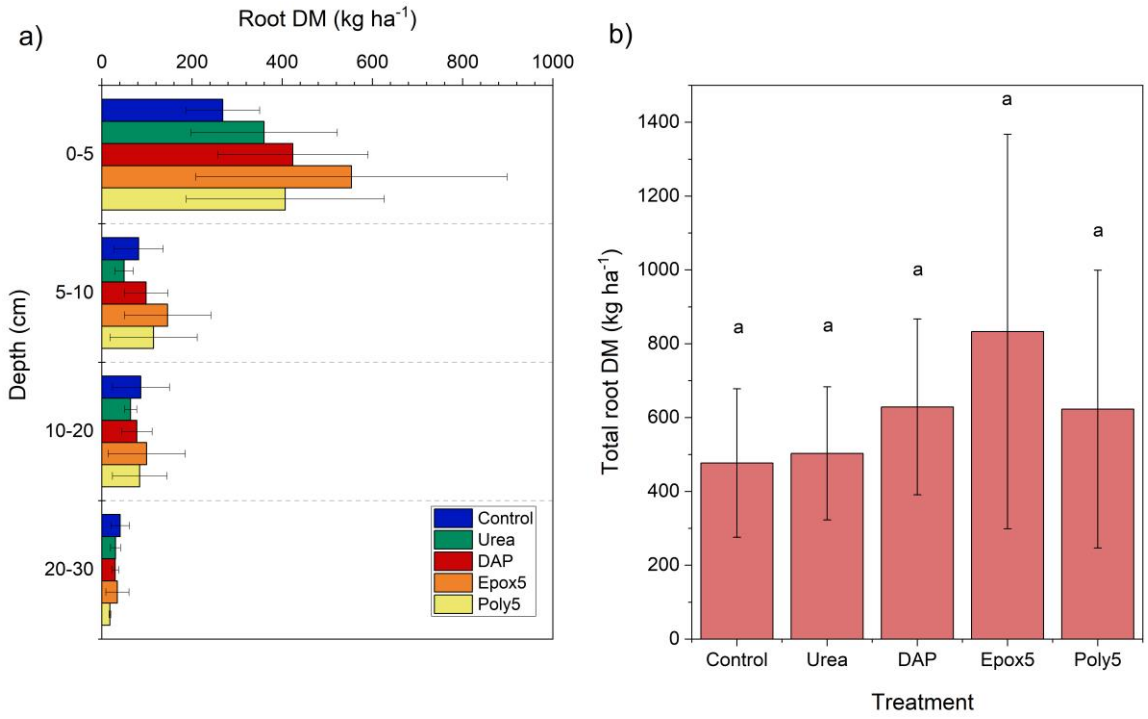

Figure 6.4. The root DM yield; (a) root DM distribution in the soil profile and (b) total root DM yield. Error bars show the standard deviation of 8 replicates. The same letters indicate the non-significance between treatments ($p<0.05$).

6.3.5. Nitrous oxide emission

The nitrous oxide flux was close to zero on the first day of the experiment for all treatments but gradually increased from the 4th day after a rainfall event (Figure 6.5). The nitrous oxide fluxes were higher for the next three weeks and then started to decline for all treatments. Again, the flux was close to a zero level from 43rd day. The maximum emission rate of 7.99 µg-N m^{-2} hr $^{-1}$ was observed 8 days after the urea fertiliser application. The control treatment showed significantly ($p<0.05$) lower nitrous oxide compared to other nitrogen treatments on both the 15th and 21st day.

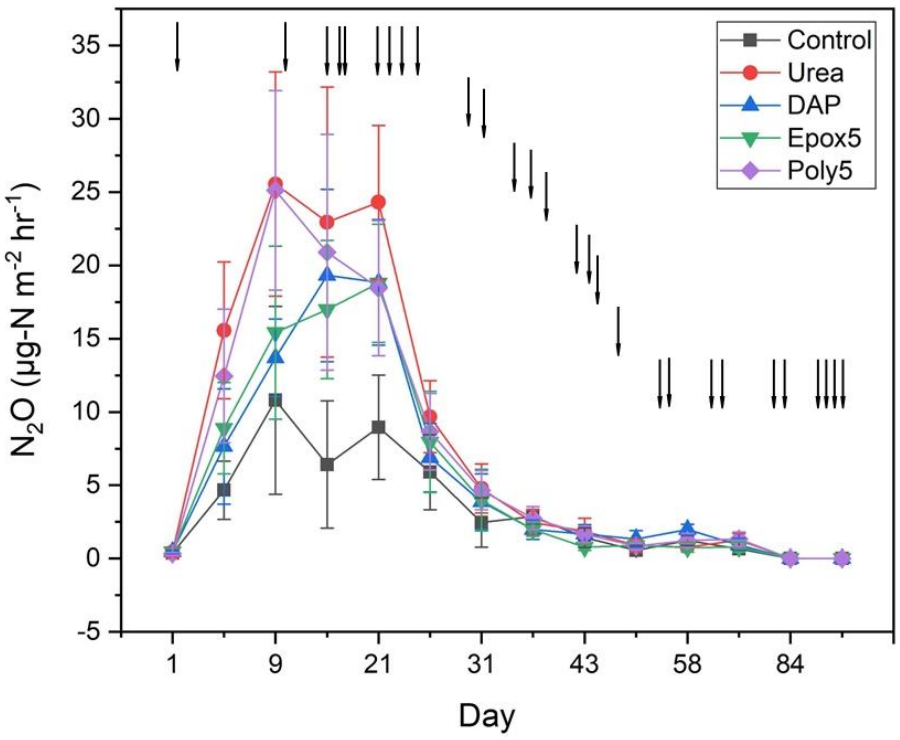

Figure 6.5. The temporal variation of nitrous oxide flux of control and nitrogen treatments for the total span of the experimental period. Data points represent the mean ± standard deviation of the mean (n=8). The downward arrows indicate the rainfall events.

The total nitrous oxide fluxes during the experimental period were 0.063, 0.146, 0.106, 0.102 and 0.133 kg-N ha^{-1} for control, urea, DAP, Epox5 and Poly5 treatments, respectively. The accumulated nitrous oxide emission was significantly ($p<0.05$) lower for the control compared to other treatments, but not significantly different between nitrogen treatments. Nitrous oxide emission from nitrogen treatments observed throughout the experimental period in this study was lower than other reported New Zealand studies in the spring season (Luo et al., 2007; Smith et al., 2008).

6.3.6. Leaching losses of mineral nitrogen

The total nitrate and ammonium leaching losses were not significantly different between any treatments (Figure 6.6). The total nitrate leaching losses were low for all treatments and in between 1.23 and 1.63 kg-N ha^{-1}. This suggests that the nitrate in the soil could have undergone chemical reaction/s which possibly decreased the leaching losses.

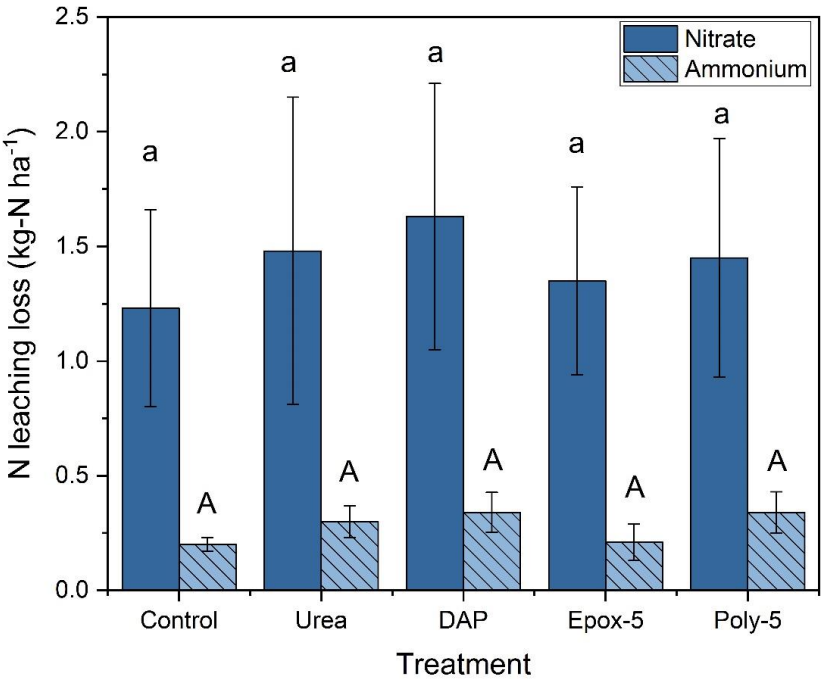

Figure 6.6. Total nitrate and ammonium leaching losses of all treatments. The data present as mean ± standard deviation (n=8). The lower and upper letters indicate the significant difference in nitrate and ammonium leaching losses, respectively, at $p<0.05$.

6.3.7. Residual soil nitrogen

The residual soil nitrate and ammonium were measured at five different depths; 0-5, 5-10, 10-20, 20-30, and 30-40 cm, at the completion of the experiment (Table 6.3). The total mineral nitrogen was calculated by summing nitrate and ammonium ions.

Table 6.3. The distribution of residual nitrate, ammonium and total mineral N in the soil profile at end of the experiment.

Soil residual N	Depth	Treatment				
		Control	**Urea**	**DAP**	**Epox5**	**Poly5**
	(cm)			(kg-N ha^{-1})		
Nitrate-N	0 - 5	40.4 ± 9.0 [a]	30.0 ± 5.8 [ab]	30.7 ± 5.7 [ab]	29.0 ± 4.2 [b]	32.6 ± 6.5 [ab]
	5 - 10	13.6 ± 3.2 [ab]	7.0 ± 2.5 [b]	16.0 ± 1.9 [a]	13.5 ± 4.0 [ab]	16.2 ± 4.9 [a]
	10 - 20	3.0 ± 1.0 [a]	3.1 ± 0.3 [a]	4.1 ± 1.5 [a]	4.3 ± 1.2 [a]	4.1 ± 0.6 [a]
	20 - 30	2.7 ± 0.9 [b]	2.8 ± 0.4 [ab]	3.7 ± 1.3 [ab]	4.4 ± 1.0 [a]	4.3 ± 0.9 [a]
	30 - 40	3.9 ± 2.1 [a]	2.7 ± 0.2 [a]	2.9 ± 0.4 [a]	3.7 ± 1.4 [a]	3.8 ± 1.3 [a]
	Total	**63.2 ± 6.1** [a]	**45.6 ± 17.0** [b]	**56.8 ± 5.9** [ab]	**55.0 ± 9.5** [ab]	**61.0 ± 9.0** [ab]
Ammonium-N	0 - 5	2.5 ± 1.0 [a]	2.9 ± 1.5 [a]	2. 9 ± 2.0 [a]	4.3 ± 3.2 [a]	4.3 ± 3.6 [a]
	5 - 10	1.7 ± 0.7 [a]	2.5 ± 1.3 [a]	2.6 ± 1.8 [a]	3.1 ± 1.9 [a]	3.6 ± 3.4 [a]
	10 - 20	3.1 ± 1.8 [a]	1.9 ± 1.4 [a]	4.5 ± 3.3 [a]	6.0 ± 3.9 [a]	3.7 ± 3.2 [a]
	20 - 30	3.4 ± 2.5 [a]	1.7 ± 0.9 [a]	3.1 ± 2.9 [a]	5.3 ± 3.6 [a]	3.7 ± 2.6 [a]
	30 - 40	3.9 ± 2.4 [a]	3.2 ± 0.6 [a]	3.6 ± 2.7 [a]	6.2 ± 3.7 [a]	4.7 ± 3.7 [a]
	Total	**13.7 ± 7.7** [a]	**12.2 ± 0.4** [a]	**11.3 ± 2.4** [a]	**29.2 ± 15.4** [a]	**20.1 ± 16.4** [a]
Total mineral-N	0 - 5	42.9 ± 9.8 [a]	33.0 ± 5.1 [ab]	33.5 ± 4.9 [ab]	33.3 ± 2.4 [b]	37.0 ± 4.4 [ab]
	5 - 10	15.2 ± 3.3 [a]	9.6 ± 3.6 [a]	18.6 ± 3.4 [a]	16.6 ± 5.2 [a]	19.8 ± 10.2 [a]
	10 - 20	6.1 ± 2.5 [a]	5.0 ± 1.3 [a]	8.7 ± 4.7 [a]	10.3 ± 5.0 [a]	7.8 ± 3.3 [a]
	20 - 30	6.1 ± 2.7 [a]	4.4 ± 1.3 [a]	6.9 ± 3.9 [a]	9.8 ± 3.3 [a]	8.0 ± 3.2 [a]
	30 - 40	7.7 ± 2.7 [a]	5.8 ± 0.8 [a]	6.5 ± 3.0 [a]	9.9 ± 4.7 [a]	8.5 ± 4.9 [a]
	Total	**76.6 ± 13.0** [a]	**57.7 ± 17.0** [a]	**73.0 ± 14.5** [a]	**79.9 ± 18.0** [a]	**81.1 ± 19.0** [a]

Data are presented as mean ± standard deviation of five replicates. The lower-case letters within a row indicate the significant difference of N components between treatments at $p<0.05$ (n=5).

The residual nitrate significantly varied depth-wise within a treatment and between treatments at a particular depth ($p<0.05$). The residual nitrate of Epox5 treatment at 0-5 cm depth was significantly ($p<0.05$) lower than the control treatment, but not significantly different from other nitrogen treatments. The urea treatment showed significantly lower residual nitrate at 5-10 cm depth compared to DAP and Poly5 treatments, however not significantly different between other treatments (Table 6.3). At 10-20 and 30-40 cm depths, there was no significant difference between treatments for residual nitrate. Both CRFs (Epox5 and Poly5) showed significantly ($p<0.05$) higher nitrate at 20-30 cm depth compared to the control treatment, but not significantly different from other treatments (Table 6.3). Unexpectedly, the total residual nitrate was significantly ($p<0.05$) lower for urea by 28% compared to the control treatment. Soil nitrogen mineralisation increases with soil temperature (Nadelhoffer et al., 1991). In this study, soil temperature increased over the experimental period (Figure 6.2-c), which could have increased the mineralisation over time. However, the slow growth rate of ryegrass in the control treatment may not have utilised the mineralised nitrate possibly causing the higher residual nitrate in the soil.

The residual ammonium was not significantly different between treatments at all depths (Table 6.3). Similarly, the total residual ammonium was also not significantly different between treatments, although there was a nominal increase by 113% and 47% for Epox5 and Poly5 treatments, respectively, in relation to control. A significant difference in total mineral nitrogen was observed only at 0-5 cm depth wherein control treatment was significantly higher ($p<0.05$) by 29% than Epox5 treatment. However, other treatments; urea, DAP and Poly5 were not significantly different from control and Epox5 treatments at this depth. Although there was no significant difference in total mineral nitrogen between treatments, a 25% reduction was noticed in the urea treatment compared to the control.

6.3.8. Nitrogen budget

The mineralisation that took place during the experimental period was calculated from the control treatment and it was 49.3 kg-N ha^{-1}. The final soil mineral nitrogen of all treatments was higher than the initial soil mineral nitrogen. The N balance of all N treatments was positive, which suggests that outflow was lower than the inflow of N components (Table 6.4).

Table 6.4. The nitrogen balance for different treatments.

Parameter	**Treatment**				
	Control	**Urea**	**DAP**	**Epox5**	**Poly5**
	kg-N ha^{-1}				
Fertiliser N	0.0	50.0	50.0	50.0	50.0
Mineralized N	49.3	49.3	49.3	49.3	49.3
SIMN*	46.0	46.0	46.0	46.0	46.0
Herbage N	-14.9	-50.5	-53.7	-47.6	-52.5
Stubble N	-2.3	-2.6	-2.7	-3.4	-2.8
Leaching N	-1.4	-1.8	-2.0	-1.6	-1.8
Nitrous oxide N	-0.1	-0.1	-0.1	-0.1	-0.1
SFMN*	-76.6	-57.7	-73.0	-79.9	-81.1
N balance	0.0	32.6	13.8	12.7	7.0

The inflow and outflow components of the N balance indicated by positive and negative signs in front of the values, respectively. *SIMN & SFMN stand for soil initial and final mineral nitrogen, respectively.

This positive N-balance was attributed to the lower N leaching and nitrous oxide emission. These observations suggest that nitrate could have undergone chemical reactions and therefore, an investigation study was conducted to identify the cause/s for these results.

6.3.9. Investigative study to identify the reason for lower nitrogen losses in fertilised treatments

In this fertiliser testing study, the nitrate leaching and nitrous oxide emission were exceptionally low when compared with other lysimeter studies available in the New Zealand context. Different hypothesises were tested to identify the reason/s for this observation. They are; (1) the LED light which was in operation during the gas collection has an impact on nitrous oxide accumulation, (2) the mixing of gas in the headspace using a peristaltic pump would increase the nitrous oxide detection in the sample, and (3) a considerable amount of urea converted to ammonia which decreased the nitrous oxide and nitrate leaching losses. All of these hypotheses did not show a relationship with the observed lower nitrate level and N_2O emission.

At the end of the experiment, the sand matrix shown gleying (turned to grey to black in colour). It was suspected that the iron content of the soil and sand could be high which may have promoted the dissimilatory nitrate reduction (DNR) pathway. Therefore, extractable total iron (Fe^{2+} & Fe^{3+}) in topsoil and sand was measured as described by Keeney and Nelson (1983). It was found that extractable total iron in the sand used for the experiment was high, 92.8 ± 3.5 mg-Fe kg^{-1} sand. To investigate this, a leaching column study was conducted for nearly 3 weeks with different possible hypotheses that could have caused the deviated results. The tested hypotheses were; (a) the fertilisation rate (50 kg-N ha^{-1}) was insufficient to produce sufficient nitrate level in leachate and nitrous oxide in the gas samples and (b) abundance of total iron in the sand could have promoted the DNR.

For this investigation, two different types of sand were selected; one with high iron content (92.8 ± 3.5 mg-Fe kg^{-1}) and another with low iron content (12.1 ± 0.4 mg-Fe kg^{-1} sand). The origin of both sand types was unknown. However, the topsoil remained the same in this study. A 2 x 4 factorial experimental design was employed with types of sand (low and high total Fe sands) and rates of nitrogen applications (control - 0, 50, 100 and 200 kg-N ha^{-1}). The experiment was conducted with triplicates, and the experimental set-up was maintained in the

same environmental condition. The leachates and gas samples were collected and measured for nitrate-nitrogen and nitrous oxide, respectively.

The leachate and gas samples from the low and high-iron sand treatments were measured for nitrate and nitrous oxide emission. Sand types, fertiliser application levels and combined effect of these two factors showed significant ($P<0.05$) impact on nitrate level in leachate. The total nitrate leaching losses from high-iron sand was significantly ($p<0.05$) lower than low-iron sand at all N levels, except for the 0 kg-N ha^{-1} treatment (Figure 6.7).

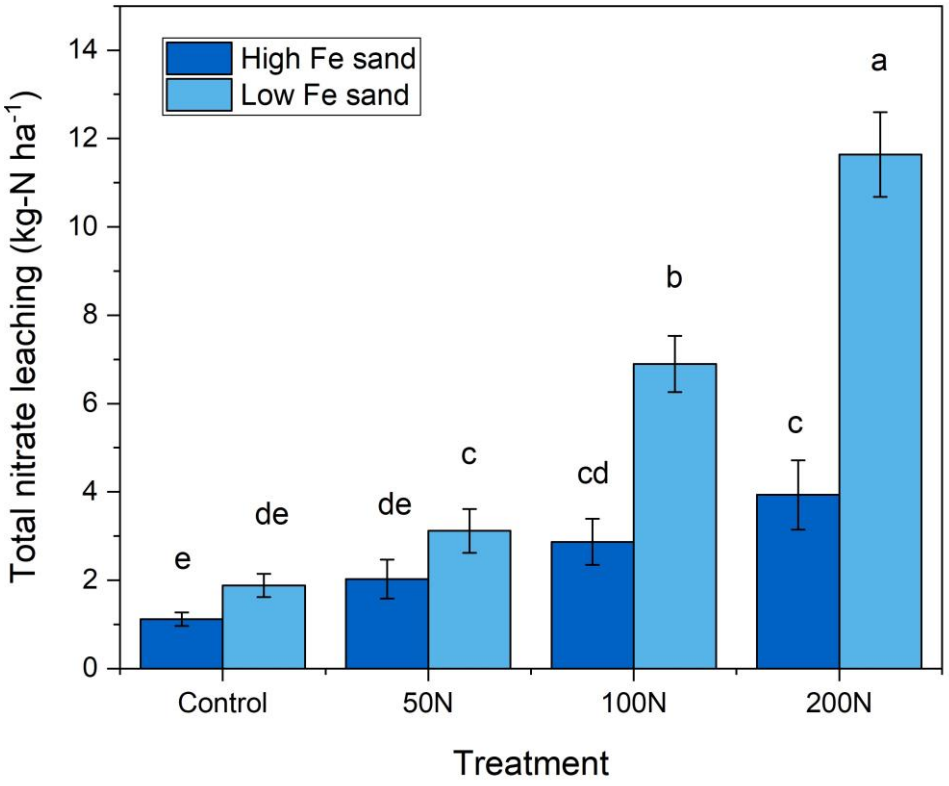

Figure 6.7. The total nitrate leaching losses of low and high-iron sand under different N application levels. The error bars indicate the standard deviation (n=3). Means with different letters are significantly different ($p<0.05$).

The difference in leached nitrate amount between low and high-iron sand increased with increasing N application rate. The increase of total nitrate in leachate between low and high-iron sand were 1.6, 1.5, 2.4 and 3.0 for N application rates increased from 0 N to 200 N. These results confirmed that the

50 kg-N ha^{-1} application rate was sufficient to produce detectable nitrate differences in leachate between two-types of sand. The difference between the iron content of the sands significantly ($P<0.05$) influences the denitrification process, possibly via the iron-coupled DNR pathway. It was observed that drainage was interrupted and the flow rate decreased due to the thickness of the fibreglass wick in the fertiliser testing trial, which may have created an anaerobic condition in the subsoil. Under the anaerobic-non-sulphatic condition, Fe^{3+} reduces to Fe^{2+} and it reacts with nitrate (Matocha et al., 2012). Nitrate acts as an electron donor for the oxidation of Fe^{2+} back to Fe^{3+} ion and nitrate undergoes rapid complete denitrification through to N_2 under anoxic conditions (Matocha et al., 2012). This high iron level with the prevailing anaerobic condition may have promoted the DNR pathway and decreased the nitrate leaching losses in high-iron sand.

The nitrous oxide accumulation was significantly ($P<0.05$) affected by sand types, N levels and interaction of sand types-N levels. The total nitrous oxide emission increased with an increasing application rate for both types of sand (Figure 6.8). The nitrous oxide flux did not significantly differ between low and high-iron sand at 0 N, 50 N and 100 N application levels. However, low-iron sand showed significantly ($p<0.05$) higher nitrous oxide emission compared to high-iron sand in the 200 N treatment. In this investigation, a significantly higher level of N_2O was expected for high-iron sand, as denitrification of nitrate could have released more nitrous oxide. However, a similar level of emission was observed for all treatments except for the 200 N application level. This suggested that the denitrified nitrates were converted to other nitrogen forms; most likely nitrogen gas or ammonia. A similar low nitrous oxide emission was observed in iron-rich soils (Wang et al., 2016) and activated sludge (Nielsen and Nielsen, 1998) as it further reduced to nitrogen gas.

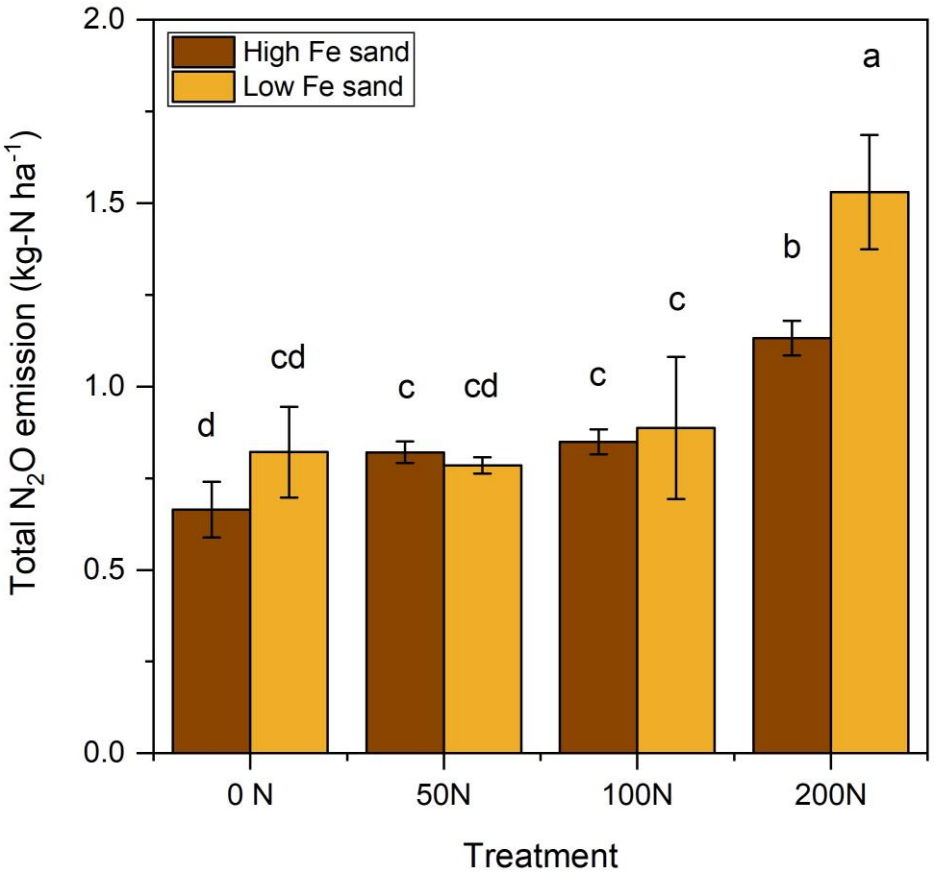

Figure 6.8. The comparison of total nitrous oxide emission between low and high iron sand treatment at different N application levels (mean ± SD, n=3).

The significantly ($p<0.05$) lower nitrate leaching losses and lower level of nitrous oxide emission in high-iron sand compared to low-iron sand in this investigative leaching column study confirmed that nitrate has denitrified by iron possibly through a DNR pathway.

6.4. Conclusions

This study designed to measure the performance of new controlled-release fertiliser formulations against standard N fertilisers. The comparative nitrogen release behaviour of granular urea and two CRFs (Epox5 and Poly5) were tested on ryegrass in a controlled environment lysimeter system. Although Epox5

showed significantly ($p<0.05$) lower grass DM yield compared to other N treatments in the first month, the total DM yield did not significantly differ. The total nitrate leaching loss in all treatments was exceptionally low and was not significantly different between treatments. Nitrous oxide emission was not significantly different between N treatments; however, they were significantly higher than the control ($P<0.05$). Therefore, a leaching column study was conducted for 3 weeks with two different types of sands (high-iron and low-iron sand) and four different nitrogen application levels (0, 50, 100 and 200 N) to identify the reason for the low level of nitrate in leachate and nitrous oxide emission. The results revealed that the nitrate level in leachate was significantly ($P<0.05$) lower for the high-iron sand compared to low-iron sand at all N application levels, other than control. However, nitrous oxide flux did not significantly differ between low and high-iron sand for the first three N application levels, except for 200 N. These observations support the involvement of iron in the denitrification process and the possible pathway of nitrogen transformation was dissimilar nitrate reduction.

Chapter 7

Testing the performance of new CRFs and the effect of iron on nitrate reduction

7.1. Introduction

The soil mineralogy and biology have direct involvement in the nitrogen cycle, which determines the final product of an N transformation pathway. Iron, one of the prevalent metallic elements in soil, may affect the nitrogen cycle and its transformational pathways. The role of ferrous (Fe^{2+}) and ferric (Fe^{3+}) ions in nitrogen cycles is not fully understood (Liu et al., 2019) and is a topic being greatly studied in recent times. This involvement of iron is referred to as dissimilatory iron-reduction (DIR) wherein microbial and chemical reactions take part in the denitrification process. In the non-sulfidic environment, the dissimilatory iron-reducing bacteria (DIRB) involves in reducing Fe^{3+} to Fe^{2+} in cytochrome by oxidizing the organic carbon (Mehta et al., 2005; Matocha et al., 2012). The resulting Fe^{2+} ion coupled to nitrate reduction by this DIRB under anaerobic conditions yields Fe^{3+} and reduced forms of N, predominantly N_2 (Matocha et al., 2012; Kiskira et al., 2017). This DIR process is reported in many agricultural soils under anoxic condition (Ratering and Schnell, 2001; Wang et al., 2009).

In a previous experiment discussed in Chapter 5, it was found that a high concentration of iron in subsoil under anaerobic conditions has decreased nitrate in leachate and nitrous oxide emission, possibly due to Dissimilatory Nitrate Reduction (DNR). However, the effect of Fe^{2+} application under aerobic conditions on the nitrate reduction pathway was not examined in the previous study. The present study investigates the impact of iron surface application on nitrate reduction. This study also investigates two new CRF formulations and the influence of lignite in controlling N losses on ryegrass under a simulated climate condition.

7.2. Materials and Methods

7.2.1. Experimental design

Most of the experimental conditions maintained were similar to the conditions discussed in Chapter 6.2.1. The following experimental conditions were altered in the present study to overcome low nitrate level in leachate observed in the previous study (Chapter 6); (a) the thickness of the wick was reduced to avoid the interruption to drainage which may create an anaerobic condition, (b) a low iron sand (12.1±0.4 mg-Fe kg^{-1} of sand) was employed in subsoil packing to avoid the possible DNR pathway, and (c) the nitrogen application rate was increased to 200 kg-N ha^{-1} to increase the detectable nitrate concentration in leachate. The low iron sand bags were purchased from Mitre 10, Lower Hutt, New Zealand and the origin of the sand is unknown.

7.2.2. Treatments and climate model

The experiment was conducted in climate control lysimeters with eight treatments of negative control (NC), control, urea, Fe 7.5, Fe 15, Epox5, Ver-c and Ver-1. The NC treatment was a bare soil-sand matrix without ryegrass, but the control was planted with ryegrass, and both NC and control treatments did not receive N fertilisers. All other treatments were amended with urea, equivalent to 200 kg-N ha^{-1} soil. The Fe 7.5 and Fe 15 treatments received 478 and 239 kg-$FeSO_4$ ha^{-1}, respectively (equivalent to 7.5 and 15 mg $FeSO_4$ kg^{-1} of soil, respectively). The Epox5 and Ver-1 were two different types of controlled-release fertilisers. The treatment Ver-c was a blend of 1200 kg-lignite ha^{-1} (particle size <1 mm) and granular urea (compositions and rates were equivalent to Ver-1). The treatments were replicated five times, and the experimental setup was arranged in a completely randomised design (CRD). All other conditions and climate model were the same as discussed in Chapter 6.2.2.

7.2.3. Grass analysis

The methods followed for the analysis of grass and stubble DM, herbage nitrogen, agronomic use efficiency (AUE) and apparent recovery efficiency (ARE) were described in Chapters 6.2.3 and 6.2.4, respectively.

7.2.4. Root analysis

The method followed to measure the ryegrass root DM distribution in the soil profile was described in Chapter 6.2.4.

7.2.5. Nitrogen losses

The method followed for the measurement of nitrous oxide emission, and nitrate and ammonium leaching losses were detailed in Chapters 6.2.5 and 6.2.6, respectively.

7.2.6. Lock-off nitrogen in controlled-release fertiliser

The Epox5 granule shells were collected at the end of the experiment to measure the lock-off (unreleased) nitrogen. The shells were visually tested for unreleased urea and ground to powder. The powdered fertiliser shells were washed with deionised water several times to remove the urea from the coating membrane and filtered using 45- micron filter paper. The filtrate was measured for total nitrogen using the micro-Kjeldahl digestion method (Blakemore et al., 1987). The lock-off nitrogen in Ver-1 fertiliser was not measured since it was in powder form that made it difficult to completely retrieve from the soil.

7.2.7. Residual nitrogen in soil

The method followed to measure the soil residual nitrate and ammonium ions is described in Chapter 6.2.7.

7.2.8. Nitrogen budget

The procedure followed for the nitrogen budget model is described in Chapter 6.2.8.

7.2.9. Data analysis

Statistical analysis was performed using Minitab 18 (Minitab, USA). The treatment effect on different parameters was analysed using the one-way ANOVA test, followed by Tukey honest significant difference (HSD) post hoc test for mean separation at a 5% significance level. The data are presented as mean ± standard deviation of five replicates.

The hierarchical clustering was performed to group the similar fertiliser treatments based on the following parameters; nitrate leaching reduction, total N leaching reduction, N_2O emission reduction, total DM yield, herbage N and soil residual N and was conducted using Origin 2019 Pro (Origin Lab Corporation, Northampton, MA, USA). The measured result of each parameter was normalised by calculating the percentage to avoid bias. In this way, the treatment which had the maximum value for a parameter received 100% and other treatments were reported as a percentage proportionally.

7.3. Results and discussion

7.3.1. Climate data

The climate emulated in the lysimeter had 28 rainfall events in which 26 of them created drainage (Figure 7.1). The cumulative monthly rainfalls were 380, 409 and 443 mm, respectively, for the first three months, and the corresponding cumulative drainage values were 199, 189 and 147 mm. The air temperature in the lysimeter cap fluctuated between 7 and 16°C, whilst the soil temperature varied between 10 and 17°C (Figure 7.1).

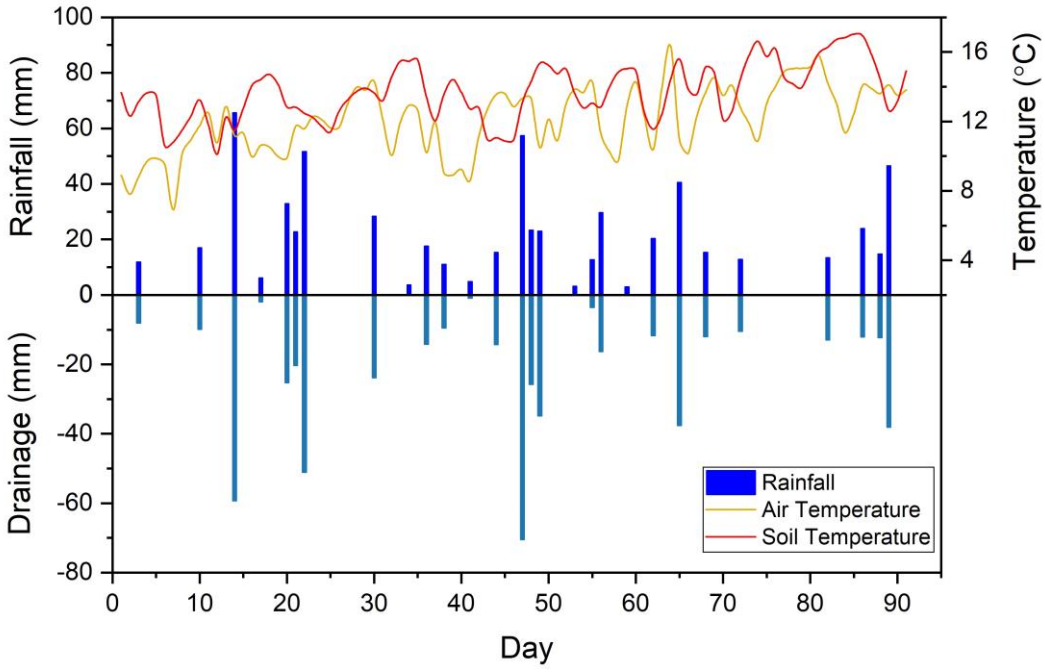

Figure 7.1. The climate data for the experimental period.

7.3.2. DM yield

The control treatment showed significantly ($P<0.05$) lower DM yield in the first month than other treatments, except for Fe 15 (Figure 7.2-a). Although N treatments were significantly ($P<0.05$) higher than the control in the 2nd month, there was no significant difference among them (Figure 7.2-b). All N treatments

showed significantly (P<0.05) higher DM than control in the 3rd month, except for Ver-c (Figure 7.2-c). DM yield of ryegrass declined with time for all treatments since the soil nutrient level depleted with time. Total DM yield was significantly (P<0.05) lower for control, compared to other treatments. Total DM grass yields were 672, 1958, 2083, 1798, 1543, 1614 and 1992 kg ha^{-1} for control, urea, Fe 7.5, Fe 15, Epox5, Ver-C and Ver-1 treatments, respectively (Figure 7.2-d). The stubble DM was not significantly different between treatments (Figure 7.2-e). Although above-ground total biomass (AGTBM) was significantly (P<0.05) higher for all N treatments relative to the control, they were not significantly different among them (Figure 7.2-f).

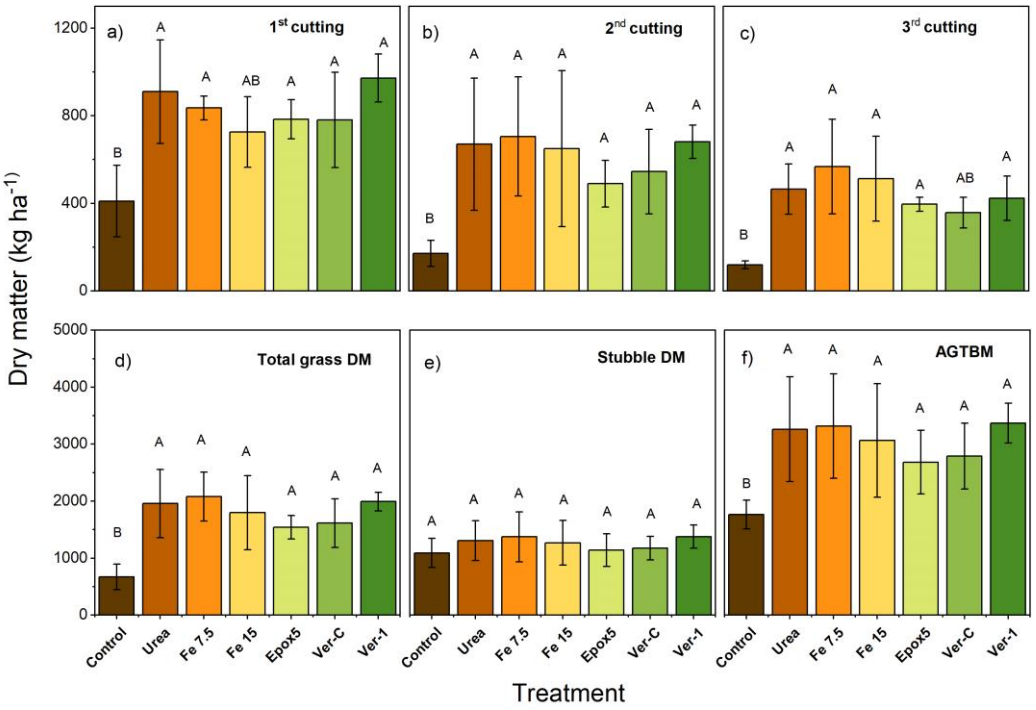

Figure 7.2. (a, b & c) Monthly and (d) total grass DM, (e) stubble DM and (f) above-ground total biomass (AGTBM) DM. The upper-case letters show the significant difference between treatments at p<0.05 (n=5). The error bar indicates the standard deviation (n=5).

Although the Epox5 treatment did not show a significant difference in total grass DM compared to urea, the observed DM reduction in Epox5 was 21% lower than urea. Similarly, Epox5 showed a 6% insignificant DM yield reduction compared

to urea at an application rate of 50 kg-N ha^{-1} in a previous experiment (Chapter 6). Ver-1 also showed a non-significant grass DM yield compared to the urea treatment. The iron treatments (Fe 7.5 & Fe 15) were non-significantly different in total grass DM yield compared to urea. Iron application at these levels (7.5 & 15 mg $FeSO_4$ kg^{-1} of soil) has not significantly impaired the DM yield. In contrast, Wong and Bradshaw (1982) reported a significant reduction of ryegrass DM yield (24%) at 15 mg-$FeSO_4$ L^{-1} of solution level in a hydroponic study.

7.3.3. Herbage N and N utilisation efficiencies

The herbage N recovery by ryegrass cuttings of each month and stubble cuttings at the end of the experiment are tabulated in Table 7.1. The total herbage N was calculated by summing the N recovery of monthly grass cuttings.

Table 7.1. The herbage nitrogen and nitrogen utilization efficiencies of different treatments.

Treatment	TN in 1st cutting	TN in 2nd cutting	TN in 3rd cutting	TN in Stubble	Total Herbage N	AUE	ARE
	(kg-N ha^{-1})					(kg-DM kg-N^{-1})	
Control	10.8±4.7^{d}	3.3±1.1^{c}	1.5±1.1^{b}	9.5±3.7^{b}	15.6±6.2^{b}	-	-
Urea	44.1±12.4^{ab}	23.0±10.7^{ab}	6.4±3.6^{a}	18.0±2.8^{a}	73.5±25.8^{a}	6.4±3.0^{a}	0.29±0.13^{a}
Fe 7.5	35.9±2.7^{abc}	22.1±8.7^{ab}	6.6±2.1^{a}	15.3±7.7^{ab}	66.7±5.5 ^{a}	7.1±2.1^{a}	0.26±0.03^{a}
Fe 15	34.0±8.2^{bc}	29.7±9.2^{a}	10.0±2.0^{a}	16.1±2.7^{ab}	77.3±20.1^{a}	5.6±3.2^{a}	0.31±0.10^{a}
Epox5	33.8±6.3^{c}	17.9±3.2^{b}	7.6±3.9^{a}	17.8±6.9^{a}	56.7±12.5^{a}	5.0±1.0^{a}	0.21±0.06^{a}
Ver-C	38.2±11.5^{abc}	18.3±6.0^{b}	5.8±2.6^{a}	17.8±2.8^{a}	62.3±13.8^{a}	4.7±2.1^{a}	0.23±0.07^{a}
Ver-1	44.8±3.7^{a}	20.7±3.3^{ab}	8.5±3.3^{a}	17.5±6.6^{a}	77.1±2.5^{a}	6.6±0.8^{a}	0.30±0.03^{a}

Data are mean ± standard deviation error of five replicates. Values followed by different lower-case letters within a column for each treatment are significantly different at $P<0.05$ ($n = 8$). TN, AUE and ARE refer to total N, agronomic use efficiency and apparent recovery efficiency, respectively. AUE and ARE are additional DM yield and additional N accumulation of an N treatment compared to control for a unit kg-N application, respectively.

The control treatment showed significantly (P<0.05) lower herbage N compared to other treatments in all three cuttings (Table 7.1). The herbage N in the first grass cutting was significantly (P<0.05) higher for Ver-1 treatment compared to the control, Fe 15 and Epox5 treatments, but not significantly different from other treatments (Table 7.1). In the second cutting, Fe 15 treatment showed significantly (P<0.05) higher herbage N compared to control, Epox5 and Ver-c, however did not significantly differ from other treatments (Table 7.1). The third cutting and total herbage N were significantly lowest (P<0.05) for the control, whereas other treatments did not show significant variation from each other (Table 7.1). The N content of stubble was significantly (P<0.05) lower for the control compared to urea, Epox5, Ver-c and Ver-1, but did not significantly different from both iron treatments. Both AUE and ARE were not significantly (P<0.05) different between any treatments. All the treatments showed very low ARE values ranged between 0.21–0.31. These observed lower ARE values were possibly due to the high amount of N leaching losses.

The Epox5 provided significantly (P<0.05) lower nitrogen recovery than Ver-1 in the 1st month, but didn't significantly different in the last two months. Both CRFs didn't significantly increase the AUE and ARE compared to urea treatment (Table 7.1). Total herbage N was decreased by 27% in comparison to Ver-1, but this reduction was insignificant. Other studies have reported that CRF application lowered the herbage N recovery (Bishop et al., 2008; Van Eerd et al., 2017). Both iron treatments did not significantly alter the N recovery in relation to urea treatment.

7.3.4. Root dry matter distribution

The root DM was measured at 5 different depths; 0-5, 5-10, 10-20, 20-30, and 30-40 cm. The root DM did not significantly differ among treatments along with the soil profile except for a few treatments in 0-5 cm depth (Figure 7.3-a). Only urea and Ver-1 showed significantly (P<0.05) higher root DM compared to Epox5 at 0-5 cm depth. The percentages of root DM distribution were 60-65%, 14-18%, 12-14%, 5-8% and 3-4% for incremental depths from the top of the soil, and this was similar to the previous study (Chapter 6). The total root DM (TRDM) was

significantly (P<0.05) higher for Urea and Ver-1 treatments relative to Epox5, but there was no significant difference among other treatments (Figure 7.3-b). This lower TRDM for Epox5 can be explained using the root plasticity. It is documented that plant root biomass and extensions are inhibited by high N application and vice versa (Jiang et al., 2016; Wang et al., 2019), including perennial ryegrass (Wang et al., 2019). A continuous supply of nitrogen by Epox5 could have decreased the demand for nitrogen and impaired the root growth and extension compared to other treatments.

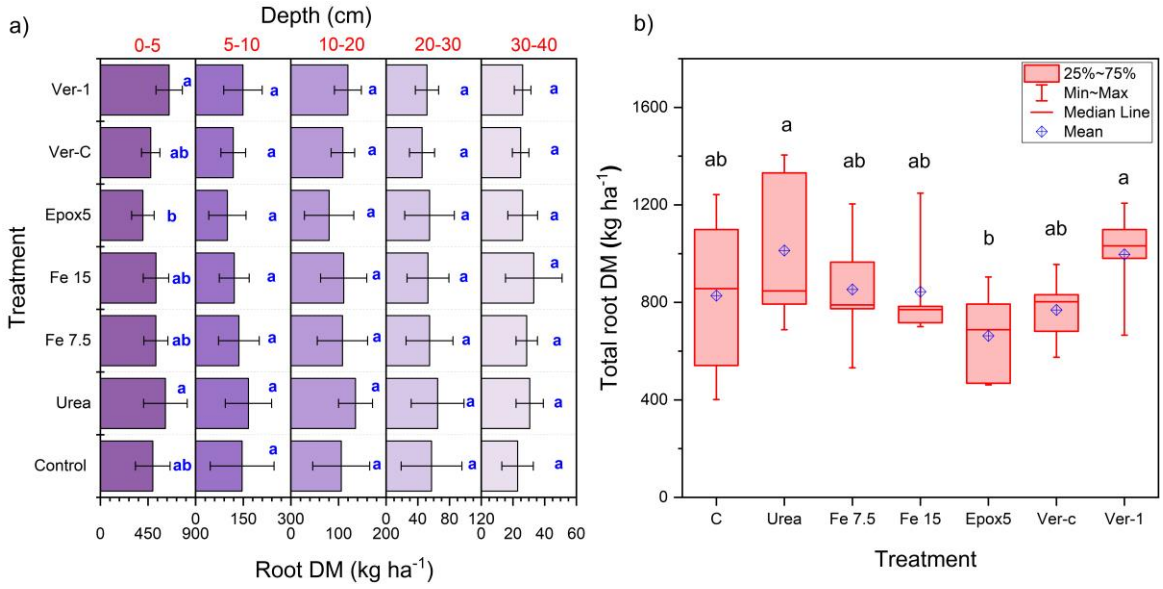

Figure 7.3. (a) Depth-wise root DM distribution; error bars show the standard deviation (n=5) and (b) total root DM (TRDM) for different treatments. Different letters indicate the significant difference between treatment within a depth in figure 7.3-a, and total root DM in figure 7.3-b, at P<0.05 (n=5).

7.3.5. Nitrous oxide emission

The N_2O emission of the NC treatment was the lowest among all the treatments. However, it was higher than other treatments on the day one gas collection (Figure 7.4-a). This observation may be due to the absence of ryegrass which led to non-utilisation of the soil residual mineral N. This condition probably favoured the denitrification process and released higher N_2O compared to other treatments. However, in the following days, N_2O emission was close to zero in the NC treatment. A similar observation was reported by Hénault et al. (1998) in

a field study where the N_2O emissions were high in the initial days and declined in subsequent days in bare soil.

In general, the peak N_2O emission was reached in 15-25 days after fertiliser application, which is consistent with our previous finding (Chapter 6). After 45 days, the emission was close to zero for all treatments, except for Epox5 since mineral N was unavailable on topsoil layers for the denitrification process (Figure 7.4-a). In contrast, Epox5 treatment continued to release N_2O to the last gas collection day (88th day) (Figure 7.4-a). At the end of the experiment, Epox5 fertiliser coating shells were collected and analysed for residual nitrogen. It was found that 9.7±0.3 kg-N ha^{-1} amount of unreleased N remained in the coating, which supports the reason for continuous N_2O release measured.

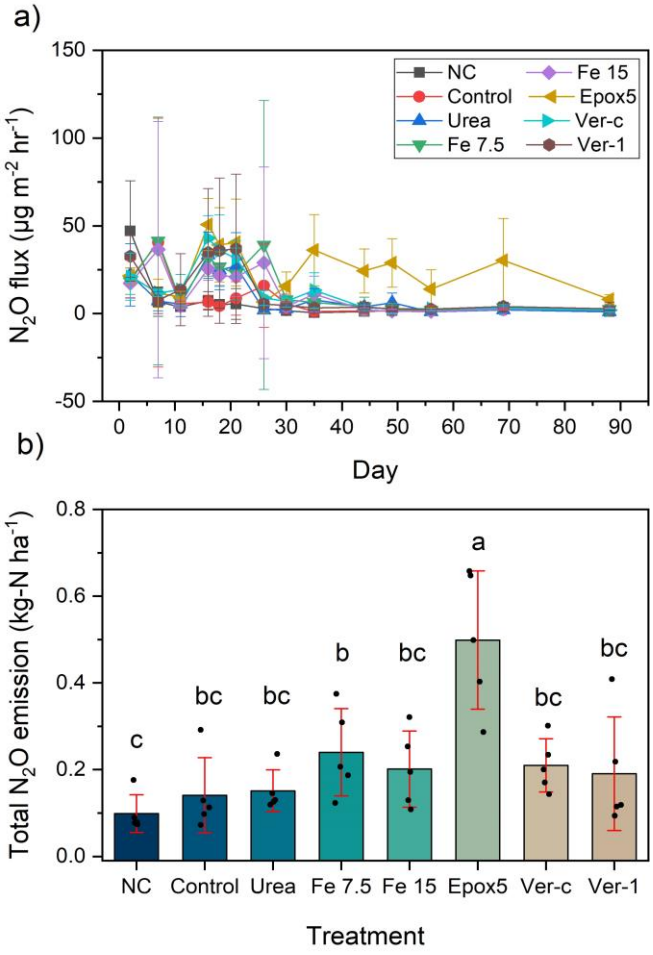

Figure 7.4. (a) The temporal variation of N_2O flux and (b) bar chart with individual points comparing the total N_2O emission between treatments (error bars show standard deviation and letters show a significant difference at $P<0.05$ (n=5)).

The total N_2O emission was significantly ($P<0.05$) lower for the NC treatment compared to Epox5 and Fe 7.5 treatments, but not significantly different from other treatments (Figure 7.4-b). The Epoxy5 exhibited the highest N_2O emission of 0.5 kg-N ha^{-1}, which was 0.35 kg-N ha^{-1} (233%) higher than the urea treatment. This difference might be explained through the slow release of N by Epox5, which continued to supply N available for the denitrification process that has increased the emission. Although this is a new finding for ryegrass, a similarly higher N_2O emission from sulphur-polymer coated urea, when compared with granular urea, was reported on sugarcane in a Brazilian study (Soares et al., 2015). The N_2O emission of Ver-1 was not significantly different from any other treatments, except Epox5 (Figure 7.4-b). The lack of significant N_2O emission differences between most treatments is possibly due to the high leaching conditions existing in all treatments of this study due to the climate model with high rainfall events and sandy subsoil.

The Fe^{2+} acts as an electron donor for the denitrification of nitrate and enhances the N_2O emission in the chemodenitrification process (Jamieson et al., 2018). However, the application of $FeSO_4$ did not significantly increase the nitrous oxide emission in this study, which suggests that chemodenitrification was not pronounced. Meanwhile, iron treatments did not significantly decrease the N_2O emission compared to urea, which shows DNR was also not prominent in this study.

7.3.6. Nitrate and ammonium leaching losses

The nitrate leaching losses were higher in the first two months compared to the third month (Figure 7.5-a). Control and NC treatments showed lower nitrate leaching losses throughout the experimental period. The peaks of nitrate loss for most treatments (except the control and NC treatments) were observed on 15, 23 and 48 days after fertiliser application which followed the high rainfall events.

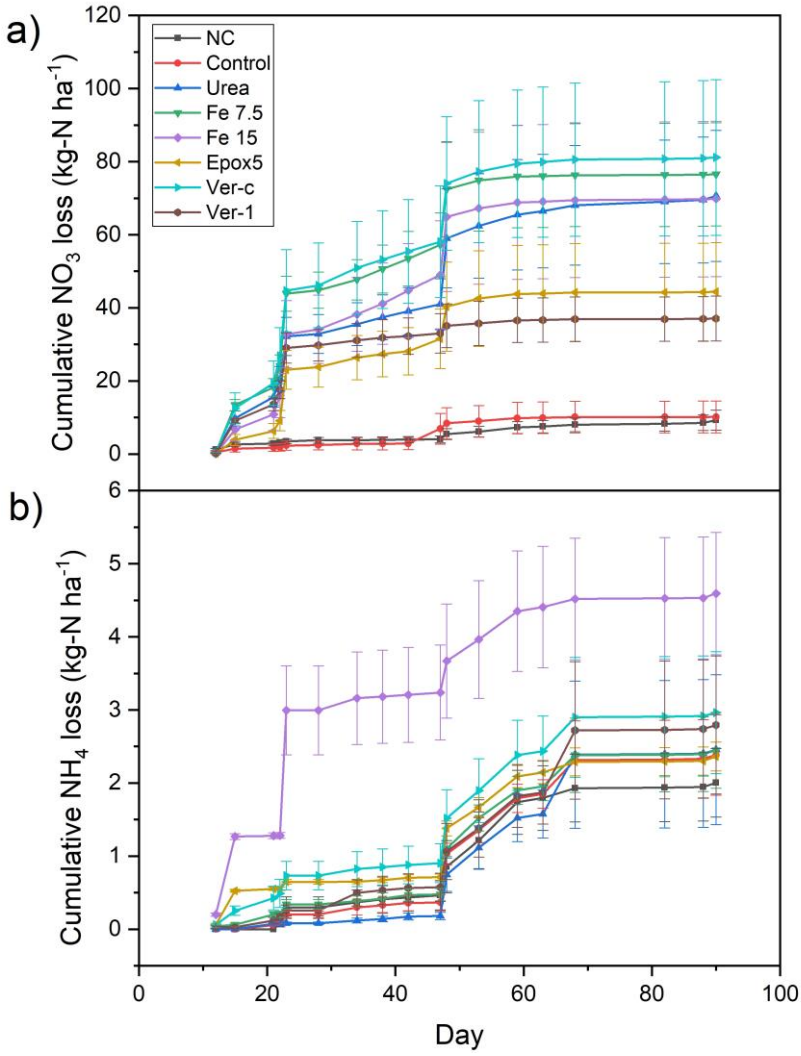

Figure 7.5. The cumulative (a) nitrate and (b) ammonium ion leaching losses. The error bars represent the standard error of 5 replicates.

The cumulative nitrate leaching losses in the 1st month were 34, 25 and 30 kg-N ha^{-1} for urea, Epox5 and Ver-1, respectively (Figure 7.5-a). The corresponding values for the 2nd month were 65, 44 and 37 kg-N ha^{-1} and they remained nearly constant in the 3rd month. This suggests that not enough nitrate is left in the soil for leaching losses in the 3rd month. Ammonium leaching occurred right through the experimental period with intermittent leaching peaks (Figure 7.5-b). The highest ammonium losses were recorded from 48 to 68 days of leaching events for all treatments. This showed that ammonium ions moved slower in the soil profile than nitrate ions as the soil has a negative surface charge which attracts positive ammonium ions that slow down the movement.

The total nitrate leaching was significantly (P<0.05) lower in control and NC treatments compared to any other N treatments (Figure 7.6-a). Among N treatments, total nitrate leaching was significantly (P<0.05) lower in Ver-1 and Epox5 treated soils. A 16% nominal reduction in nitrate loss was observed in Ver-1 treated soil in comparison to Epox5, but it was insignificant. The total ammonium losses did not make up the major form of N loss, which ranged from 1.6 to 2.6 kg-N ha^{-1}, and it was not significantly different between treatments (Figure 7.6-a).

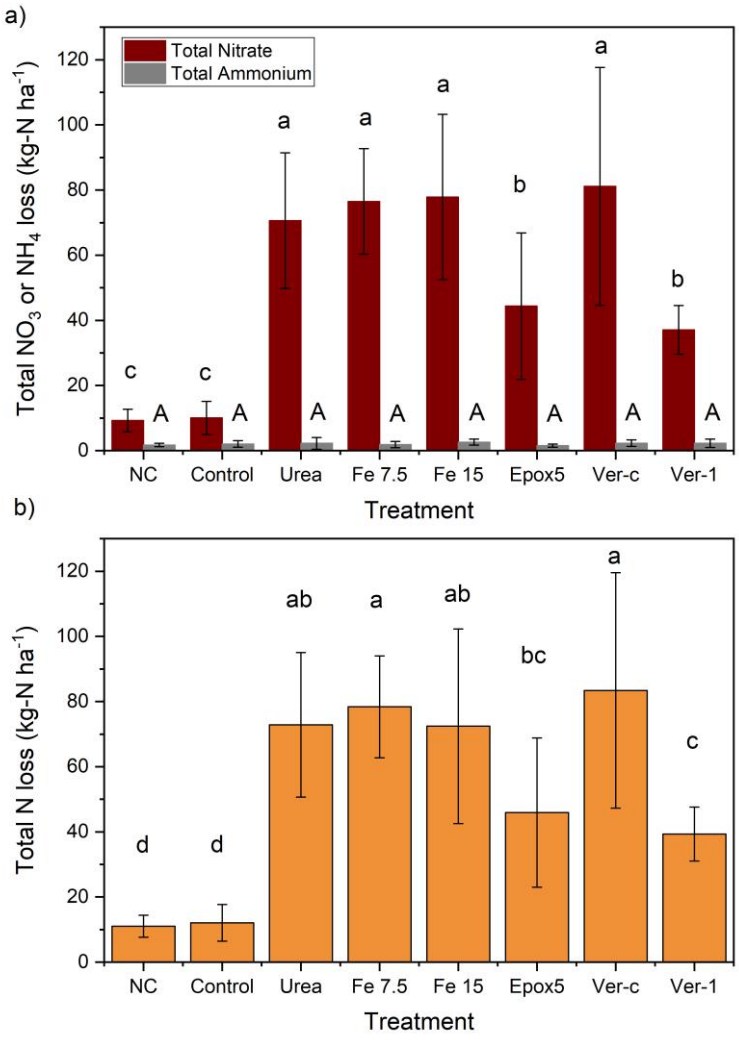

Figure 7.6. (a) Total nitrate and ammonium losses and (b) total N losses of different treatments. Error bars indicate standard deviation (n=5). The letters show significant difference between treatments at P<0.05 (n=8).

The total N leaching loss is the sum of both nitrate and ammonium losses. It was significantly ($P<0.05$) lower for the control and NC treatments compared to all N treatments (Figure 7.6-b). The soil treated with Ver-1 showed significantly ($P<0.05$) lower total N loss compared to other N treatments, except for Epox5.

Nitrate leaching is the predominant pathway for N losses through an agriculture system (Huang et al., 2017). The results in this study showed that both CRFs (Epox5 and Ver-1) were effective in controlling nitrate-N leaching loss by 37% and 47%, respectively compared to urea, and it is evident that both CRFs slowly release N and prolong the N release duration. These nitrate leaching loss reduction values were higher than the average leaching reduction value of 10% reported for polymer-coated CRFs applied in many grasslands (Li et al., 2018). Both chemodenitrification and DNR pathways involve denitrifying the nitrate (Jamieson et al., 2018), which could have decreased the nitrate in leachate. However, iron ($FeSO_4$) application with urea did not control the nitrate and ammonium leaching losses, which implies that both these pathways were not prominent in this study. The Ver-1 significantly ($P<0.05$) lowered the nitrate and total mineral N losses compared to Ver-c. This shows that this effect was due to the formulation of CRF (Ver-1), not the mere interactions between lignite and urea (Ver-c). Application of lignite with urea (Ver-c) did not significantly decrease the N leaching losses and therefore, lignite application can't be used as an effective leaching control measure. This result supports a New Zealand study that reported that lignite was ineffective in controlling nitrate leaching from urea and biosolids (Paramashivam et al., 2016).

7.3.7. Residual soil nitrogen

The residual mineral nitrogen (nitrate and ammonium) in the soil were measured at 5, 10, 20, 30 and 40 cm depths (Table 7.2). The total mineral nitrogen was calculated by summing the nitrate and ammonium content in the respective depths.

Table 7.2. The residual mineral nitrogen in soil profile at different depths.

Parameter	Depth (cm)	Treatment							
		NC	Control	Urea	Fe 7.5	Fe 15	Epox5	Ver-c	Ver-1
		----------	----------	----------	kg-N ha^{-1}	----------	----------	----------	----------
NO_3-N	0-5	28.5±6.7 [a]	33.7±10.7 [a]	43.2±13.7 [a]	36.2±11.6 [a]	39.3±14.1 [a]	34.0±23.8 [a]	36.3±12.6 [a]	38.8±23.1 [a]
	5-10	21.1±5.4 [a]	32.7±7.9 [a]	31.7±7.3 [a]	29.5±9.4 [a]	34.5±4.2 [a]	32.6±11.2 [a]	33.4±8.7 [a]	33.0±7.3 [a]
	10-20	1.4±0.6 [a]	2.9±0.7 [a]	3.3±1.1 [a]	2.8±0.4 [a]	3.4±1.8 [a]	2.7±0.4 [a]	2.9±0.9 [a]	3.5±1.4 [a]
	20-30	1.7±0.5 [a]	2.2±0.9 [a]	2.1±0.9 [a]	1.8±0.8 [a]	2.1±0.7 [a]	2.1±1.3 [a]	1.9±1.1 [a]	2.5±1.3 [a]
	30-40	0.8±0.3 [a]	1.8±1.0 [a]	2.2±1.7 [a]	2.4±1.7 [a]	2.3±1.7 [a]	1.9±1.2 [a]	1.4±0.6 [a]	1.5±0.9 [a]
	Total	**53.5±12.4 [a]**	**73.2±18.5 [a]**	**82.5±20.6 [a]**	**72.7±21.7 [a]**	**81.5±20.4 [a]**	**80.3±24.3 [a]**	**76.0±20.7 [a]**	**79.3±30.5 [a]**
NH_4-N	0-5	2.4±1.2 [a]	3.8±2.3 [a]	3.9±2.2 [a]	3.2±1.7 [a]	3.3±1.2 [a]	3.0±3.0 [a]	3.1±1.9 [a]	3.8±5.5 [a]
	5-10	2.1±0.9 [a]	2.5±1.1 [a]	2.8±1.1 [a]	2.7±1.5 [a]	3.1±1.5 [a]	2.3±1.2 [a]	2.2±1.5 [a]	2.6±2.3 [a]
	10-20	1.1±1.1 [a]	1.9±1.2 [a]	1.3±1.8 [a]	0.9±1.0 [a]	1.9±1.8 [a]	2.2±2.3 [a]	1.6±2.4 [a]	1.5±1.5 [a]
	20-30	0.5±0.8 [a]	1.8±1.6 [a]	1.3±2.0 [a]	0.2±0.4 [a]	1.4±1.4 [a]	1.0±1.0 [a]	0.7±1.3 [a]	0.9±0.9 [a]
	30-40	0.4±0.7 [a]	1.9±1.7 [a]	1.7±2.2 [a]	1.1±1.4 [a]	1.4±1.7 [a]	1.1±1.0 [a]	0.5±1.0 [a]	1.2±1.9 [a]
	Total	**6.5±2.8 [a]**	**14.4±1.7 [a]**	**13.3±6.3 [a]**	**6.5±3.3 [a]**	**11.1±6.7 [a]**	**11.5±5.9 [a]**	**9.4±7.9 [a]**	**12.0±9.6 [a]**
Total-N	0-5	30.9±8.5 [a]	37.5±12.2 [a]	47.0±15.7 [a]	39.4±12.2 [a]	42.6±15.1 [a]	46.3±19.2 [a]	39.4±14.4 [a]	42.6±28.2 [a]
	5-10	23.2±5.8 [a]	35.2±8.8 [a]	34.5±8.1 [a]	32.3±10.8 [a]	37.6±4.7 [a]	34.9±11.8 [a]	35.6±9.4 [a]	35.6±8.6 [a]
	10-20	2.5±1.6 [a]	4.8±1.8 [a]	4.6±2.6 [a]	3.6±0.7 [a]	5.3±3.3 [a]	5.0±2.5 [a]	4.5±2.5 [a]	4.9±2.6 [a]
	20-30	2.2±1.3 [a]	3.9±2.3 [a]	3.4±2.9 [a]	1.9±1.1 [a]	3.4±2.0 [a]	3.1±2.0 [a]	2.6±2.4 [a]	3.3±1.5 [a]
	30-40	1.2±1.5 [a]	3.7±2.6 [a]	3.9±3.8 [a]	3.5±3.1 [a]	3.7±3.4 [a]	3.0±2.1 [a]	1.9±1.6 [a]	2.7±2.3 [a]
	Total	**60.0±14.3 [a]**	**93.2±16.8 [a]**	**104.4±8.9 [a]**	**77.1±27.2 [a]**	**92.6±25.6 [a]**	**91.8±28.1 [a]**	**84.1±26.6 [a]**	**100.5±31.7 [a]**

Data presented as mean ± standard deviation of five replicates. Mean values with the same lower-case letters within a row are not significantly different between treatments ($P<0.05$, $n=5$).

The residual nitrate, ammonium and total nitrogen content were not significantly different between any treatments at any depth (Table 7.2). Total residual nitrate and ammonium were between 53.5-82.5 and 6.5-14.4 kg-N ha^{-1}, respectively. The residual nitrate made up a larger portion of the residual N compared to ammonium. The residual nitrate decreased with depth for all treatments and the major portion resided in the first 10 cm depth of soil profile (Table 7.2). In this study, the top 10 cm of the soil profile is composed of topsoil that has a higher anion storage capacity than the sandy subsoil. Similarly, residual ammonium decreased with depth, but the decrease was not as prominent as nitrate (Table 7.2).

7.3.8. Nitrogen budget

The mineralisation during the experimental period was calculated using the nitrogen balance model. The N mineralisation calculated for the control treatment was 84.6 kg-N ha^{-1}, and was assumed as the N mineralisation value for all other treatments (Table 7.3). All the treatments showed a surplus N balance, in which the highest value was observed in Epox5 treatment (Table 7.3). The surplus N balance in this study could be attributed to the following reasons; unmeasured N components such as root N, ammonia volatilisation, immobilisation, and denitrification. In addition, using the N mineralisation value calculated for control could be an overestimation for using all other treatments. The rate of mineralisation of a fertilised soil is lower than the unfertilised soil in cultivated land use (control) (Bremer and Kuikman, 1997).

Table 7.3. The N balance of different treatments.

Variable	Treatment							
	NC	**Control**	**Urea**	**Fe 7.5**	**Fe 15**	**Epox5**	**Ver-c**	**Ver-1**
	Kg-N ha^{-1}							
Fertiliser N	0	0	200	200	200	200	200	200
Mineralised N	84.6	84.6	84.6	84.6	84.6	84.6	84.6	84.6
SIMN*	46	46	46	46	46	46	46	46
Herbage N	-	-15.6	-73.5	-66.7	-77.3	-56.7	-62.3	-77.1
Stubble N	-	-9.5	-18	-15.3	-16.1	-17.8	-17.8	-17.5
Leaching N	-11.0	-12.1	-72.9	-78.4	-80.5	-45.9	-83.4	-39.3
N_2O-N	-0.1	-0.1	-0.2	-0.2	-0.2	-0.5	-0.2	-0.2
SFMN*	-60.0	-93.2	-104	-77.1	-92.6	-91.8	-84.1	-100.5
Unreleased N	0	0	0	0	0	9.7	0	0
N Balance	**59.4**	**0.0**	**61.6**	**92.8**	**63.8**	**108.1**	**82.8**	**95.9**

Inflow and outflow variables are indicted in positive and negative sign, respectively. *SIMN & SFMN stand for initial and final soil mineral nitrogen, respectively.

7.3.9. Hierarchical clustering of fertiliser treatments

The hierarchical clustering was used to identify the best and closely related fertiliser treatment/s based on overall performances of nitrate leaching loss reduction, total N leaching loss reduction, N_2O emission reduction, total DM yield, herbage N and soil residual N. The nitrate leaching loss reduction, total N leaching loss reduction and N_2O emission reduction were the distinct variables between treatments that mainly influenced the cluster method. Other variables showed low variation between treatments, and therefore, their influences in the clustering were not substantial (Figure 7.7). Ver-1 was the best treatment based on overall performances, which showed the highest values for nitrate and total N leaching loss reductions, and second-highest N_2O emission reduction. Both CRFs (Ver-1 and Epox5) showed better performances than other treatments and their performances were more closely associated for reducing nitrate and N leaching losses (Figure 7.7). For example, nitrate leaching loss reductions were

84% and maximum (100%) for Epox5 and Ver-1 treatments, respectively. The urea treatment was grouped separately from any other fertiliser treatments. Fe 15 and Ver-c treatments were more associated with each other since both treatments showed a similar N loss profile. For example, nitrate leaching loss reductions were 53% and 46% for Fe 15 and Ver-c, respectively.

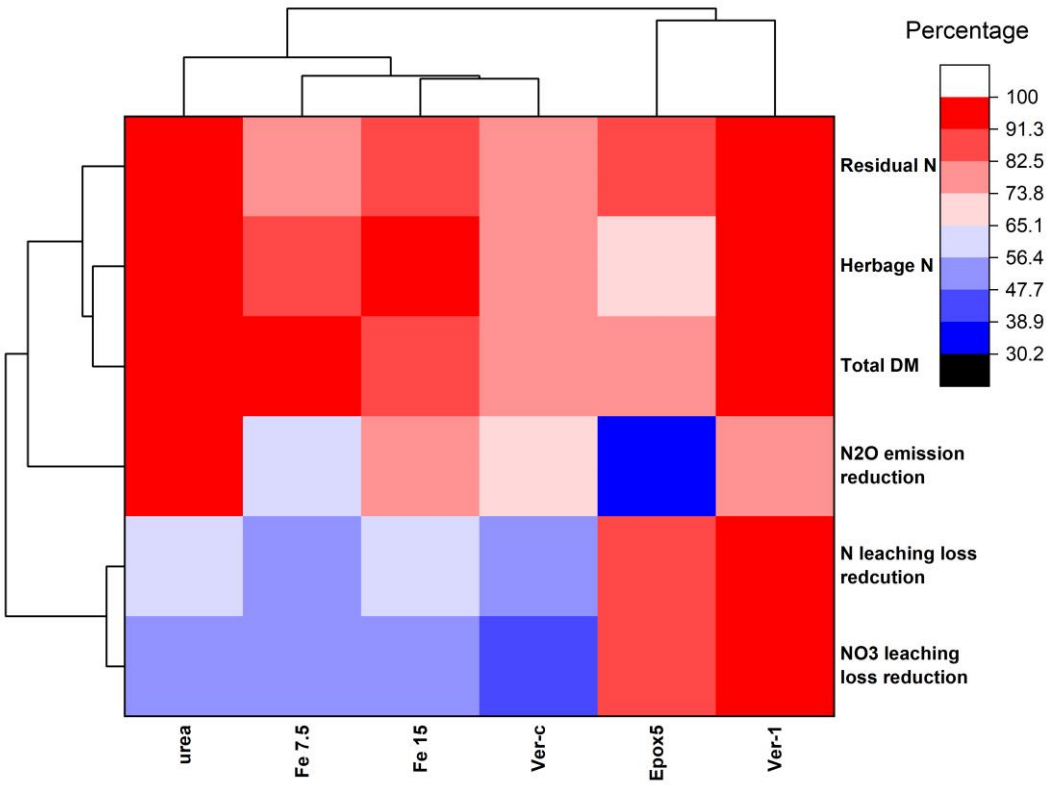

Figure 7.7. The hierarchical clustering heatmap for classification of N treatments based on the nitrate leaching loss reduction, total N leaching loss reduction, total DM yield, herbage N, and soil residual N. The values of all variables are in percentage (not absolute values).

7.3.10. Overview of the N fertiliser testing

In general, the newly developed CRF formulations controlled the leaching losses without a significant loss of DM yield compared to the urea treatment. The insignificant effect of these formulations on DM yield was a positive response when compared to the 50% DM yield reduction reported for CRFs on various grasslands (Li et al., 2018). Although Ver-1 showed insignificant N_2O emission, Epox5 has increased the emission significantly ($P<0.05$) compared with other treatments. However, Epox5 provided a net benefit of minimising N losses since N leaching control was 90 times higher than increased N_2O emission.

Despite both CRFs significantly ($P<0.05$) decreasing the N leaching losses, it was not used by the ryegrass. Both CRFs showed an insignificant ($P<0.05$) herbage N recovery compared to urea and therefore, leaching control does not always improve the nitrogen utilisation efficiencies. This observation could be due to the mismatches between the N demand of ryegrass and N supply by the CRFs.

The Ver-c treatment (a blend of raw lignite with urea) was used to test whether the outcome of Ver-1 treatment is the effect of formulation or only the interaction of urea with lignite. The superior performance of Ver-1 over Ver-c distinctly separated each other in the clustering (Figure 7.7), which showed that the formulation has an impact on the performance rather than the mere interaction of lignite with urea.

Both iron treatments have not shown major differences from the urea treatment on overall performances (Figure 7.7). The N leaching losses and nitrous oxide emission of iron treatments were non-significantly different from the urea treatment. This suggests that both DNR and chemodenitrification were not prominent in denitrifying the nitrate in this study. This may be due to the oxidation of ferrous ions to ferric ions. These results confirmed that surface iron application is not an effective control method for N losses.

7.4. Conclusions

This lysimeter study tested different types of controlled-release fertilisers and different iron application levels on controlling the N losses. The following hypotheses were tested; (a) the performances of new CRF formulations were better than urea, (b) lignite application with urea decreases N losses and (c) iron application (with urea) under aerobic conditions promotes the dissimilatory nitrate reduction. Both CRFs decreased N leaching losses, whereas Epox5 increased the N_2O emission compared to the urea treatment. These CRFs didn't significantly increase the DM yield and nitrogen utilisation efficiency (NUE) compared to urea. The overall performance analysis using the hierarchical clustering method revealed that Ver-1 performed better than other treatments, followed by Epox5. Lignite surface application (Ver-1) did not significantly decrease N losses or improved NUE. The better performance of Ver-1 on controlling N losses than Ver-c implied that fertiliser formulation impacts the performance. Iron treatments were ineffective in controlling N losses as they showed similar N loss profiles to urea. The application of Fe^{2+} with urea has not altered the dissimilatory nitrate reduction and chemodenitrification pathways under aerobic conditions. Further studies are recommended to test the effect of Fe^{2+} on promoting the aforementioned pathways on different types of soil.

Chapter 8

Integrated discussion - Key research findings, implications and future recommendations

8.1. Key research findings

- Polymer-Lignite composite coatings prolonged the urea release and showed good chemical and thermal properties.

Polymer-Lignite composite (epoxy-lignite & polyester-lignite) coated urea CRF formulations were developed and their physiochemical properties were tested [Chapter 5]. The core idea of using lignite as a filler was to decrease the polymer content significantly in coating while retaining the properties of a good coating membrane for the formulation of CRFs. The dissolution test in water at room temperature revealed that epoxy-lignite (Epox5) and polyester-lignite (Poly5) CRFs prolonged the urea release up to 400 and 170 hours, respectively. The FTIR analysis showed that lignite interacted with epoxy and polyester resins and, strengthened the composite. Although the composites showed lower thermal stability compared to their raw materials, the degradation temperatures were 350 and 305 °C, respectively for Epox5 and Poly5. These temperatures are high enough to be used as a coating membrane for fertilisers, and will not undergo thermal degradation in soil under natural conditions.

- The new climate control lysimeter imitates a climate model to a satisfactory level and allows the control of environmental variables in a small confined space.

The lysimeter was permanently capped and coupled to an environmental control unit in the lysimeter cap [Chapter 3]. The Taranaki region's spring season (year 2013) was emulated and the performance of the new design was evaluated by comparing observed climate variables (temperature and RH) with targeted

values, and observed drainage, evapotranspiration and ryegrass dry matter (DM) yield, against the estimated values derived from the climate model.

Both temperature and RH of the climate model were satisfactorily achieved in this study. The actual temperature and RH values were positively and significantly ($P<0.05$) correlated with the targeted values. However, the root-mean-square error (RMSE) value of night temperature exceeded the targeted fluctuation limit of 1°C, unlike the day temperature values. Similarly, the RMSE value of day RH was within the targeted fluctuation limit of 5% whereas the night RH value exceeded this limit. These deviations were noticed on the day, where targeted temperature values were well below ambient temperature. This suggests that the environmental control unit (ECU) was not able to control very low night-time temperatures.

The centralised climate control unit used in this study comprised of a humidification column and a chiller, which were insufficient to maintain the lower night temperature on days that had a high ambient temperature. This could be overcome by using a high-capacity chiller, and separate humidification columns for each lysimeter bank. Another issue was the influence of ambient temperature on climate control. A thermally insulated chamber with an air conditioning unit is required to maintain a consistent ambient temperature.

The observed cumulative drainage, evapotranspiration and DM yield were within the estimated values and showed a significant ($P<0.05$), and positive correlation with estimated values. The evapotranspiration showed higher variation than other parameters which were linked to the temperature deviation. In general, the new lysimeter system design emulates a climate regime well. It is a creative alternative, which is able to emulate climate variables of a field study in the laboratory. Further performance improvement can be achieved by incorporating the identified solutions for the problems encountered.

- Iron-rich subsurface sand possibly promotes the dissimilatory nitrate reduction (DNR) under anaerobic conditions which decreased the nitrate in leachate and N_2O gas emissions.

In testing of newly formulated CRFs, it was noticed that nitrate in leachate and N_2O emission were very low compared to other reported New Zealand studies [Chapter 6]. To identify the possible cause/s for these observations, different hypotheses were tested; (a) LED lights which were in operation while gas samples were collected may have significantly lowered the N_2O emission, (b) mixing of gas in the headspace before sub-sampling, could increase the N_2O in sub-sample, (c) a significant amount of urea converted to ammonia gas, (d) the low N application rate of 50 kg-N ha^{-1} was insufficient to produce nitrate in leachate and (e) high-iron concentration (92.8 ± 3.5 mg-Fe kg^{-1} of sand) in the sand could have promoted the DNR, under anaerobic conditions, which could have decreased nitrate levels, in leachate and N_2O emission. Only the last hypothesis showed a significant influence on observed results.

In testing of the last hypothesis, two different types of sand one with high-iron (92.8 ± 3.5 mg-Fe kg^{-1} of sand) and another with low-iron (12.1 ± 0.4 mg-Fe kg^{-1} of sand) were applied, with four levels of nitrogen fertiliser; 0, 50, 100 and 200 kg-N ha^{-1}. All other conditions were similar between the two sets of experiments other than sand type. The nitrate in leachate was significantly ($P<0.05$) lower for the high-iron sand treatment, compared to the low-iron sand at all N levels, and the difference between the two treatments increased with increasing N levels. The N_2O emission was significantly ($P<0.05$) different, between the two iron treatments, when the N level was 200 kg-N ha^{-1}, but not in the other N levels. This suggested that the nitrate in high-iron sand, possibly underwent DNR under anaerobic conditions, which decreased the nitrate in leachate and N_2O emission.

- Controlled-release fertiliser (Epox5) conversely increased the N_2O emission.

One of the aims of using CRF is to minimise N_2O emissions. However, the Epox5 treatment significantly ($P<0.05$) increased N_2O emissions, three times higher than urea [Chapter 7]. This observation was linked to nitrate leaching losses

wherein Epox5 controlled the leaching losses by 1.5 times compared to the urea treatment since Epox5 lowered the urea release rate. More N was available in the soil top layers due to the slow release of urea from Epox5, which has increased the chance of denitrification losses, which resulted in high N_2O emissions. The analysis of the coating membrane at the end of the experiment revealed that unreleased (lock off) urea was found on the coating inner surface, which supports the above observation. This suggests that controlling N leaching could increase the likelihood of N_2O emission.

- Urea-impregnated lignite (Ver-1) and Epox5 CRFs significantly decreased N leaching loss.

Urea impregnated lignite (Ver-1) and Epox5 were tested against urea in a climate control lysimeter under simulated climate conditions [Chapter 7]. The results revealed that Ver-1 and Epox5 fertilisers have significantly ($P<0.05$) decreased the nitrate leaching losses by 46% and 37%, respectively compared to the urea treatment. This provided evidence that Ver-1 and Epox5 could effectively be used as a CRF for mitigating N leaching losses.

- The surface application of lignite as an amendment along with urea has not decreased the urea leaching losses and nitrous oxide emission.

To underpin the effect of lignite in controlling nitrate leaching and N_2O emissions, lignite at a rate of 1200 kg ha^{-1} was applied along with urea (200 kg-N ha^{-1}) as a surface application and this treatment is referred to as “Ver-c” [Chapter 7]. There was no significant difference in nitrate leaching between Ver-c and the urea treatment. This suggests that lignite (in its native form) cannot be used to control N leaching losses. The treatment Ver-c was ineffective in controlling N_2O emission and was not significantly different from the urea treatment.

- Lysimeter soil retriever (LSR) design retrieved soil blocks with minimum disturbance using a linear actuator with enough power for soil retrieval.

A low cost and simple LSR design to retrieve the soil blocks from mini (<100 kg) and small (100 – 1000 kg) size lysimeters are unavailable commercially. Therefore, this study was undertaken to design and fabricate an LSR design with simple features and a low cost [Chapter 4]. An electric linear actuator was chosen to push the soil out of the lysimeter and a metal plate was used to manually section the soil column. The design was found to be ideal to retrieve soil blocks that have high moisture content (28.3 ± 3.6%) with minimum shape distortion and disturbance for roots. The linear actuator was powerful enough for the soil retrieval process and allowed for precision control of soil block height, as the movement speed of the column can be controlled. The linear actuator gave a consistent performance for all soil columns retrieved from 80 lysimeters (400 soil blocks).

- Controlling N losses does not necessarily increase plant N uptake or DM yield.

The treatments Ver-1 and Epox5 significantly lowered mineral N losses compared to urea. Nevertheless, both treatments showed insignificant differences in total DM yield and total herbage N compared to urea. Therefore, controlling N losses was beneficial in terms of offsetting environmental contamination, but not for improving nitrogen utilisation efficiency [Chapter 7]. This could be due to mismatches between nutrient delivery from CRF and plant demand, and/or lock-off nutrients in CRF.

8.2. Implication of this study for New Zealand Agriculture

The N losses from pastoral farming contribute to contamination of water bodies and greenhouse gas emissions. One of the greatest challenges for pastoral farming is mitigating N losses, while sustaining productivity. The CRFs are being applied as an effective way to control N losses and improve NUE. The CRFs

formulated in this study decreased N leaching losses, with no effect on DM yield and NUE. Therefore, these fertilisers can be used in pastoral farming as an option to control N leaching losses. Although Ver-1 fertiliser showed comparable N_2O emission to urea, Epox5 fertiliser has increased N_2O emission which limits its year-round and wider application. The Epox5 fertiliser is more suitable for the areas and/or seasons receiving lower rainfall to minimise denitrification in anaerobic conditions which correspond to N_2O emission. In addition, these lignite-based CRFs may bring other advantages of lignite such as binding heavy metals and organic carbon source as a soil amendment.

The technique used for impregnation of urea in lignite was inexpensive, under standard temperature and pressure, and did not require the use of sophisticated equipment. However, the methodology was labour intensive and was used to produce small quantities for experimentation. Therefore, this technique paves the way for a new alternative application for lignite, which provides one solution for two problems; minimising environmental contamination and finding a non-combustion use for lignite.

The climate-controlled lysimeter design is novel and necessary to conduct a study under a controlled environment. This climate-controlled lysimeter design emulates a climate scenario and, therefore, imitates a field condition. This allows conducting a study that is difficult to run in a field. Moreover, a past or future climate scenario can be emulated using this design which might be helpful for climate change studies.

The new simple and low-cost lysimeter soil retriever (LSR) design can be an alternative for the existing complete manually operated design. This new design provides benefits such as fast soil retrieval, required fewer labour hours, more precise soil block height, fine adjustment of soil block height, and less disturbance for roots, and the soil monolith structure. In addition, this partly automated design reduces the muscle fatigue of the operator.

8.3. Future recommendations

This study identified iron-rich subsurface sand under anaerobic conditions may lead to DNR, whereas iron application to low-iron sand has no effect on nitrate levels in leachate. Further studies are recommended, to identify the underlying mechanism responsible for nitrate reduction with iron-rich sand.

The new climate control lysimeter design satisfactorily emulated a challenging climate regime of the Taranaki region. A thermally insulated chamber with an air-conditioning facility, is proposed to minimise the influence of the ambient environment on climate control. However, the impact of this modification needs to be tested in a future study. In addition, testing the performance of this design under moderate to extreme dry climate conditions would enable this design for wider application.

The native form of lignite used in this study was ineffective in controlling nitrate leaching. Activated or modified lignite can improve the sorption properties (Huang et al., 2019), thus it may increase the potential for nitrate leaching control. Therefore, studies focusing on the influence of activated or modified lignite on N losses (leaching and gaseous losses) control are recommended.

The LSR design presented in this study was tested on non-compressive soils and therefore, testing and modification of the design need to be considered when it is used to retrieve compressive and sticky soils (e.g., Peat, clay). This design can be fully automated by the following modifications; (a) replacing an existing motor with an encoder motor or adding positioning sensors that control the incremental movement of soil blocks with high precision and (b) replacing the manual cutting blade with a wire saw cutter to slice the soil block.

References

Abdou, H. and M. Flury (2004). Simulation of water flow and solute transport in free-drainage lysimeters and field soils with heterogeneous structures. European Journal of Soil Science. 55(2): 229-241.

Abdulkareem, J., A. Abdulkadir and N. Abdu (2015). A review of different types of lysimeter used in solute transport studies. Int. J. Plant Soil Sci. 8(3): 1-14.

Allen, R. G., L. S. Pereira, D. Raes and M. Smith (1998). Crop evapotranspiration-Guidelines for computing crop water requirements-FAO Irrigation and drainage paper 56. Fao, Rome. 300(9): D05109.

ANSYS, C. (2018). Release 19.2, 2018. Ansys. Inc., Canonsburg, PA.

Anzecc, A. (2000). Australian and New Zealand guidelines for fresh and marine water quality. Australian and New Zealand Environment and Conservation Council and Agriculture and Resource Management Council of Australia and New Zealand, Canberra: 1-103.

Azeem, B., K. KuShaari, Z. B. Man, A. Basit and T. H. Thanh (2014). Review on materials & methods to produce controlled release coated urea fertilizer. Journal of Controlled Release. 181: 11-21.

Bayraktar, K. and G. Lawson (1984). Properties and potential of formed cokes derived from two Turkish lignites by carbonization of binderless briquettes. Fuel. 63(9): 1221-1225.

Bell, M., J. Cloy, C. Topp, B. Ball, A. Bagnall, R. Rees and D. Chadwick (2016). Quantifying N_2O emissions from intensive grassland production: the role of synthetic fertilizer type, application rate, timing and nitrification inhibitors. The Journal of Agricultural Science. 154(5): 812-827.

Bello, Z. A. and L. D. Van Rensburg (2017). Development, calibration and testing of a low-cost small lysimeter for monitoring evaporation and transpiration. Irrigation and Drainage. 66(2): 263-272.

Bishop, P., H. Liu, M. Hedley and P. Loganathan (2008). New zealand made controlled release coated urea increases winter growth rates of Italian ryegrass with lower N leaching than uncoated urea. Proceedings of the New Zealand Grasslands Association. 70: 85-89.

Bishop, P. and M. Manning (2010). Urea volatilisation: the risk management and mitigation strategies. Palmerston North, New Zealand: Fertilizer and Lime Research Centre, Massey University: 1-13.

Blakemore, L., P. Searle and B. Daly (1987). Methods for chemical analysis of soils. New Zealand soil Bureau scientific report 80. New Zealand, Lower Hutt: New Zealand Society of Soil Science, p103.

Blight, L., B. Currell, B. Nash, R. Scott and C. Stillo (1978). Preparation and properties of modified sulfur systems, ACS Publications.

Boulding, J. R. and J. S. Ginn (2003). Practical handbook of soil, vadose zone, and ground-water contamination: assessment, prevention, and remediation, CRC Press.

Bouwman, A. M., J. C. Bosma, P. Vonk, J. H. A. Wesselingh and H. W. Frijlink (2004). Which shape factor (s) best describe granules? Powder Technology. 146(1-2): 66-72.

Bowman, D. and J. Paul (1991). Absorption of three slow-release nitrogen fertilizers by perennial ryegrass turf. Fertilizer research. 29(3): 309-316.

Bremer, E. and P. Kuikman (1997). Influence of competition for nitrogen in soil on net mineralization of nitrogen. Plant and Soil. 190(1): 119-126.

Brock, J., J. Caradus and M. Hay (1989). Fifty years of white clover research in New Zealand. Proceedings of the New Zealand Grassland Association. 50**:** 25-39.

Bruschi, M. L. (2015). Strategies to modify the drug release from pharmaceutical systems, Woodhead Publishing.

Bucklin, R., R. W. Henley and D. B. McConnell (1993). Fan and pad greenhouse evaporative cooling systems. Circular (Florida Cooperative Extension Service)(USA).

Burden, R. (1982). Nitrate contamination of New Zealand aquifers: a review. New Zealand journal of science. 25(3): 205-220.

Cameron, K., H. Di and L. Condron (2002). 17 Nutrient and Pesticide Transfer from Agricultural Soils to Water in New Zealand. Agriculture, hydrology and water quality, CABI Publishing**:** 373-393.

Cameron, K., H. J. Di and J. Moir (2013). Nitrogen losses from the soil/plant system: a review. Annals of applied biology. 162(2): 145-173.

Chen, D., J. Sun, M. Bai, K. B. Dassanayake, O. T. Denmead and J. Hill (2015). A new cost-effective method to mitigate ammonia loss from intensive cattle feedlots: application of lignite. Scientific reports. 5(1): 1-5.

Chen, X., Z. Zhang, X. Zhang, Y. Chen, M. Qian and S. Peng (2008). Estimation of groundwater recharge from precipitation and evapotranspiration by lysimeter measurement and soil moisture model. Journal of Hydrologic Engineering. 13(5): 333-340.

Chirinda, N., D. Kracher, M. Lægdsmand, J. R. Porter, J. E. Olesen, B. M. Petersen, J. Doltra, R. Kiese and K. Butterbach-Bahl (2011). Simulating soil N2O emissions and heterotrophic CO2 respiration in arable systems using FASSET and MoBiLE-DNDC. Plant and Soil. 343(1-2): 139-160.

Collier, S. M., M. D. Ruark, L. G. Oates, W. E. Jokela and C. J. Dell (2014). Measurement of greenhouse gas flux from agricultural soils using static chambers. Journal of visualized experiments: JoVE(90): 1-8.

Cougnon, M., T. De Swaef, P. Lootens, J. Baert, P. De Frenne, R. Shahidi, I. Roldán-Ruiz and D. Reheul (2017). In situ quantification of forage grass root biomass, distribution and diameter classes under two N fertilisation rates. Plant and Soil. 411(1-2): 409-422.

Crush, J., S. Woodward, J. Eerens and K. Macdonald (2006). Growth and milksolids production in pastures of older and more recent ryegrass and white clover cultivars under dairy grazing. New Zealand Journal of Agricultural Research. 49(2): 119-135.

Czigány, S., M. Flury, J. B. Harsh, B. C. Williams and J. M. Shira (2005). Suitability of fiberglass wicks to sample colloids from vadose zone pore water. Vadose Zone Journal. 4(1): 175-183.

Dash, S., P. N. Murthy, L. Nath and P. Chowdhury (2010). Kinetic modeling on drug release from controlled drug delivery systems. Acta Pol Pharm. 67(3): 217-223.

De Datta, S., A. Trevitt, J. Freney, W. Obcemea, J. Real and J. Simpson (1989). Measuring nitrogen losses from lowland rice using bulk aerodynamic and nitrogen-15 balance methods. Soil Science Society of America Journal. 53(4): 1275-1281.

de Klein, C. A. and S. F. Ledgard (2005). Nitrous oxide emissions from New Zealand agriculture–key sources and mitigation strategies. Nutrient cycling in Agroecosystems. 72(1): 77-85.

de Matos, M., B. D. Mattos, B. L. Tardy, O. J. Rojas and W. L. Magalhães (2018). Use of Biogenic Silica in Porous Alginate Matrices for Sustainable Fertilization with Tailored Nutrient Delivery. ACS Sustainable Chemistry & Engineering. 6(2): 2716-2723.

Dell, P. (2006). The Rotorua Lakes Protection and Restoration Action Programme, Proposals, Costs, Progress. Wonderful Lakes–What Value?–Who Pays? Rotorua, New Zealand, The Royal Society of New Zealand (Rotorua Branch) 45-69.

Di, H. and K. Cameron (2000). Calculating nitrogen leaching losses and critical nitrogen application rates in dairy pasture systems using a semi-empirical model. New Zealand Journal of Agricultural Research. 43(1): 139-147.

Diez, J., R. Roman, M. Cartagena, A. Vallejo, A. Bustos and R. Caballero (1994). Controlling nitrate pollution of aquifers by using different nitrogenous controlled release fertilizers in maize crop. Agriculture, Ecosystems & Environment. 48(1): 49-56.

Dutta, G. K. and N. Karak (2018). One-Pot Synthesis of Bio-Based Waterborne Polyester as UV-Resistant Biodegradable Sustainable Material with Controlled Release Attributes. ACS Omega. 3(12): 16812-16822.

Dymond, J., A.-G. Ausseil, R. Parfitt, A. Herzig and R. McDowell (2013). Nitrate and phosphorus leaching in New Zealand: a national perspective. New Zealand Journal of Agricultural Research. 56(1): 49-59.

Easton, Z. M. and A. M. Petrovic (2004). Fertilizer source effect on ground and surface water quality in drainage from turfgrass. Journal of Environmental quality. 33(2): 645-655.

Edmeades, D. C. (2015). The evaluation of a controlled release nitrogen fertiliser. Journal of New Zealand Grasslands. 77: 147-152.

El Assimi, T., O. Lakbita, A. El Meziane, M. Khouloud, A. Dahchour, R. Beniazza, R. Boulif, M. Raihane and M. Lahcini (2020). Sustainable coating material based on chitosan-clay composite and paraffin wax for slow-release DAP fertilizer. International Journal of Biological Macromolecules. 161(2020): 492-502.

Fares, A., S. K. Deb and S. Fares (2009). Review of vadose zone soil solution sampling techniques. Environmental reviews. 17: 215-234.

Fenemor, A. and C. Robb (2001). Groundwater management in New Zealand. Groundwaters of New Zealand: 273-289.

Fernandes, I. J., R. V. Santos, E. C. A. D. Santos, T. L. A. C. Rocha, N. S. Domingues Junior and C. A. M. Moraes (2018). Replacement of commercial silica by rice husk ash in epoxy composites: a comparative analysis. Materials Research. 21(3): 1-10.

Fertilizer Association - New Zealand (2019). The fertilizer use in New Zealand. Retrieved 13 April 2019, from http://www.fertiliser.org.nz/Site/about/fertiliser_use_in_nz.aspx.

Francis, S. (1950). Absolute Intensities of Characteristic Infra-Red Absorption Bands of Aliphatic Hydrocarbons. The Journal of Chemical Physics. 18(6): 861-865.

Franzen, D. (2011). Nitrogen extenders and additives. SF-1581. North Dakota State Univ. and NCERA-103 Committee. North Dakota State Univ. Ext. Serv., Fargo.

Fredlund, D. and S. Houston (2013). Interpretation of soil-water characteristic curves when volume change occurs as soil suction is changed. Advances in unsaturated soils. 1: 15-31.

Frisbee, M. D., F. M. Phillips, A. R. Campbell, J. M. Hendrickx and E. M. Engle (2010). Modified passive capillary samplers for collecting samples of snowmelt infiltration for stable isotope analysis in remote, seasonally inaccessible watersheds 2: field evaluation. Hydrological Processes: An International Journal. 24(7): 834-849.

Ganguly, A. and S. Ghosh (2011). A review of ventilation and cooling technologies in agricultural greenhouse application. Iranica Journal of Energy & Environment. 2(1): 32-46.

Garcia, C., L. Garcia, A. Vallejo, M. Cartagena and J. Díez (1998). Forecasting by laboratory tests of nitrogen leached and absorbed in soil-plant system with urea-based controlled-release fertilizers coated with lignin. Communications in soil science and plant analysis. 29(15-16): 2479-2491.

Garcia, C., A. Vallejo, J. A. Diéz, L. García and M. C. Cartagena (1997). Nitrogen use efficiency with the application of controlled release fertilizers coated with kraft pine lignin. Soil Science and Plant Nutrition. 43(2): 443-449.

Gee, G. W., A. L. Ward, T. G. Caldwell and J. C. Ritter (2002). A vadose zone water fluxmeter with divergence control. Water Resources Research. 38(8): 1-7.

Goertz, H. M. (2000). Controlled release technology, agricultural. Kirk-Othmer Encyclopedia of Chemical Technology.

Goh, K. and G. Bruce (2005). Comparison of biomass production and biological nitrogen fixation of multi-species pastures (mixed herb leys) with perennial ryegrass-white clover pasture with and without irrigation in Canterbury, New Zealand. Agriculture, Ecosystems & Environment. 110(3-4): 230-240.

Gopinath, A., M. S. Kumar and A. Elayaperumal (2014). Experimental investigations on mechanical properties of jute fiber reinforced composites with polyester and epoxy resin matrices. Procedia Engineering. 97: 2052-2063.

Goss, M. and W. Ehlers (2009). The role of lysimeters in the development of our understanding of soil water and nutrient dynamics in ecosystems. Soil Use and Management. 25(3): 213-223.

Goyne, K. W., R. L. Day and J. Chorover (2000). Artifacts caused by collection of soil solution with passive capillary samplers. Soil Science Society of America Journal. 64(4): 1330-1336.

Graham, S. L., J. Laubach, J. E. Hunt, A. Eger, S. Carrick and D. Whitehead (2019). Predicting soil water balance for irrigated and non-irrigated lucerne on stony, alluvial soils. Agricultural water management. 226: 105790.

Greer, F. R. and M. Shannon (2005). Infant methemoglobinemia: the role of dietary nitrate in food and water. Pediatrics. 116(3): 784-786.

Grossmann, J. and P. Udluft (1991). The extraction of soil water by the suction-cup method: a review. Journal of soil science. 42(1): 83-93.

Gunaratnam, A., M. Grafton, P. Jeyakumar, P. Bishop, C. Davies and M. McCurdy (2020). Study the influence of soil moisture and packing incremental level on soil physical and hydraulic properties. Nutrient Management in Farmed Landscapes. 33**:** 1-6.

Gunaratnam, A., M. McCurdy, M. Grafton, P. Jeyakumar, P. Bishop and C. Davies (2019). Assessment of nitrogen fertilizers under controlled environment–a lysimeter design. 32**:** 1-8.

Hahn, J. and C. Junge (1977). Atmospheric nitrous oxide: A critical review. Zeitschrift fuer Naturforschung A. 32(2): 190-214.

Hähndel, R. and S. Jürgens-Gschwind (1986). Langsamwirkende Stickstoffdünger-ihre Eigenschaften und Vorteile, Landwirtschaftl. Versuchsstation.

Hansen, E. A. and A. R. Harris (1975). Validity of soil-water samples collected with porous ceramic cups. Soil Science Society of America Journal. 39(3): 528-536.

Hansen, L. I. (1966). Slow release fertilizer granule having a plurality of epoxy resin coatings, Google Patents.

Haque, A., M. Shamsuzzoha, F. Hussain and D. Dean (2003). S2-glass/epoxy polymer nanocomposites: manufacturing, structures, thermal and mechanical properties. Journal of Composite materials. 37(20): 1821-1837.

Harris, S. and D. Clark (1996). Effect of high rates of nitrogen fertiliser on white clover growth, morphology, and nitrogen fixation activity in grazed dairy pasture in northern New Zealand. New Zealand Journal of Agricultural Research. 39(1): 149-158.

Harris, S., E. Thom and D. Clark (1996). Effect of high rates of nitrogen fertiliser on perennial ryegrass growth and morphology in grazed dairy pasture in northern New Zealand. New Zealand Journal of Agricultural Research. 39(1): 159-169.

Haygarth, P. M. and S. C. Jarvis (2002). Agriculture, hydrology, and water quality, CABI Pub.

Hénault, C., X. Devis, S. Page, E. Justes, R. Reau and J. Germon (1998). Nitrous oxide emissions under different soil and land management conditions. Biology and Fertility of Soils. 26(3): 199-207.

Höring, H. and D. Chapman (2004). Nitrates and Nitrites in Drinking Water in: World Health Organization Drinking Water Series IWA Publishing, London.

Howell, T., A. Schneider, D. Dusek, T. Marek and J. Steiner (1995). Calibration and scale performance of Bushland weighting lysimeters. 38(4): 1019-1024.

Howell, T., J. Steiner, A. Schneider and S. Evett (1995). Evapotranspiration of irrigated winter wheat—Southern High Plains. Transactions of the ASAE. 38(3): 745-759.

Huang, B., G. Liu, P. Wang, X. Zhao and H. Xu (2019). Effect of nitric acid modification on characteristics and adsorption properties of lignite. Processes. 7(3): 167.

Huang, T., X. Ju and H. Yang (2017). Nitrate leaching in a winter wheat-summer maize rotation on a calcareous soil as affected by nitrogen and straw management. Scientific reports. 7(1): 1-11.

Hubbard, R., G. Newton and G. Hill (2004). Water quality and the grazing animal. Journal of animal science. 82(suppl_13): E255-E263.

Humphreys, E., J. Freney, W. Muirhead, O. Denmead, J. Simpson, R. Leuning, A. Trevitt, W. Obcemea, R. Wetselaar and C. Gui-Xin (1988). Loss of ammonia after application of urea at different times to dry-seeded, irrigated rice. Fertilizer research. 16(1): 47-57.

Irfan, M., M. B. Khan Niazi, A. Hussain, W. Farooq and M. H. Zia (2018). Synthesis and characterization of zinc-coated urea fertilizer. Journal of Plant Nutrition. 41(13): 1625-1635.

Islam, M. R., S. Mao, A. S. Alam, A. E. Eneji, Y. Hu and X. Xue (2011). A lysimeter study for leaching losses, sustainable fertilization, and growth responses of corn (Zea mays L.) following soil amendment with a water-saving superabsorbent polymer. Applied Engineering in Agriculture. 27(5): 757-764.

Jamieson, J., H. Prommer, A. H. Kaksonen, J. Sun, A. J. Siade, A. Yusov and B. Bostick (2018). Identifying and quantifying the intermediate processes during nitrate-dependent iron (II) oxidation. Environmental science & technology. 52(10): 5771-5781.

Jarosiewicz, A. and M. Tomaszewska (2003). Controlled-release NPK fertilizer encapsulated by polymeric membranes. Journal of agricultural and food chemistry. 51(2): 413-417.

Jemison, J. M. and R. H. Fox (1992). Estimation of zero-tension pan lysimeter collection efficiency. Soil Science. 154(2): 85-94.

Jiang, Y., Y. Li, G. Nie and H. Liu (2016). Leaf and root growth, carbon and nitrogen contents, and gene expression of perennial ryegrass to different nitrogen

supplies. Journal of the American Society for Horticultural Science. 141(6): 555-562.

Jordan, C. F. (1968). A simple, tension-free lysimeter. Soil Science. 105(2): 81-86.

Karczewska, A., T. Chodak and J. Kaszubkiewicz (1996). The suitability of brown coal as a sorbent for heavy metals in polluted soils. Applied Geochemistry. 11(1-2): 343-346.

KC, B., M. Mohssen, H. W. Chau, A. Curtis, R. Cuenca, J. Bright, M. Srinivasan, W. Hu and K. Cameron (2018). Impact of rotational grazing systems on the pasture crop coefficient for irrigation scheduling. Irrigation and Drainage. 67(3): 441-453.

Keeney, D. R. and D. W. Nelson (1983). Nitrogen—inorganic forms. Methods of soil analysis: Part 2 chemical and microbiological properties. 9: 643-698.

Kiskira, K., S. Papirio, E. Van Hullebusch and G. Esposito (2017). Fe (II)-mediated autotrophic denitrification: a new bioprocess for iron bioprecipitation/biorecovery and simultaneous treatment of nitrate-containing wastewaters. International Biodeterioration & Biodegradation. 119: 631-648.

Knutson, J., S. Lee, W. Zhang and J. Selker (1993). Fiberglass wick preparation for use in passive capillary wick soil pore-water samplers. Soil Science Society of America Journal. 57(6): 1474-1476.

Knutson, J. and J. S. Selker (1994). Unsaturated hydraulic conductivities of fiberglass wicks and designing capillary wick pore-water samplers. Soil Science Society of America Journal. 58(3): 721-729.

Korsmeyer, R. W., R. Gurny, E. Doelker, P. Buri and N. A. Peppas (1983). Mechanisms of solute release from porous hydrophilic polymers. International journal of pharmaceutics. 15(1): 25-35.

Kreith, F. (1999). Handbook of solid waste management, McGRAW-HILL.

Kwiatkowska, J., M. Provenzano and N. Senesi (2008). Long term effects of a brown coal-based amendment on the properties of soil humic acids. Geoderma. 148(2): 200-205.

Kyvelou, P. (2017). Structural behaviour of composite cold-formed steel systems. Department of Civil and Environmental Engineering, Imperial College London. PhD.

Lantinga, E., P. Deenen and H. Van Keulen (1999). Herbage and animal production responses to fertilizer nitrogen in perennial ryegrass swards. II. Rotational grazing and cutting. NJAS wageningen journal of life sciences: 243-261.

Ledgard, S., M. Sprosen, G. Brier, E. Nemaia and D. Clark (1996). Nitrogen inputs and losses from New Zealand dairy farmlets, as affected by nitrogen fertilizer application: year one. Plant and Soil. 181(1): 65-69.

Li, T., W. Zhang, J. Yin, D. Chadwick, D. Norse, Y. Lu, X. Liu, X. Chen, F. Zhang and D. Powlson (2018). Enhanced-efficiency fertilizers are not a panacea for resolving the nitrogen problem. Global Change Biology. 24(2): e511-e521.

Li, Y., C. Jia, X. Zhang, Y. Jiang, M. Zhang, P. Lu and H. Chen (2018). Synthesis and performance of bio-based epoxy coated urea as controlled release fertilizer. Progress in Organic Coatings. 119: 50-56.

Liang, R., M. Liu and L. Wu (2007). Controlled release NPK compound fertilizer with the function of water retention. Reactive and Functional Polymers. 67(9): 769-779.

Litaor, M. I. (1988). Review of soil solution samplers. Water Resources Research. 24(5): 727-733.

Little, K. R., M. T. Rose, W. R. Jackson, T. R. Cavagnaro and A. F. Patti (2014). Do lignite-derived organic amendments improve early-stage pasture growth and key soil biological and physicochemical properties? Crop and Pasture Science. 65(9): 899-910.

Liu, C., W. Ren, B. Zhang and C. Lv (2011). The application of soil temperature measurement by LM35 temperature sensors. Proceedings of 2011 International Conference on Electronic & Mechanical Engineering and Information Technology, IEEE. 4**:** 1825-1828.

Liu, L., G. Hoogenboom and K. Ingram (2000). Controlled-environment sunlit plant growth chambers. Critical reviews in plant sciences. 19(4): 347-375.

Liu, T., D. Chen, X. Li and F. Li (2019). Microbially mediated coupling of nitrate reduction and Fe (II) oxidation under anoxic conditions. FEMS microbiology ecology. 95(4): fiz030.

Liu, T., D. Fan, X. Zhang, J. Chen, C. Li and C. Cao (2015). Deep placement of nitrogen fertilizers reduces ammonia volatilization and increases nitrogen

utilization efficiency in no-tillage paddy fields in central China. Field Crops Research. 184: 80-90.

Liu, X., Y. Yang, B. Gao, Y. Li and Y. Wan (2017). Environmentally friendly slow-release urea fertilizers based on waste frying oil for sustained nutrient release. ACS Sustainable Chemistry & Engineering. 5(7): 6036-6045.

Llive, L., E. Bruno, A. D. Molina-García, A. Schneider-Teixeira and L. Deladino (2019). Biodegradation of Yerba Mate Waste Based Fertilizer Capsules. Effect of Temperature. Journal of Polymers and the Environment. 27(6): 1302-1316.

López-Urrea, R., F. M. de Santa Olalla, C. Fabeiro and A. Moratalla (2006). Testing evapotranspiration equations using lysimeter observations in a semiarid climate. Agricultural water management. 85(1-2): 15-26.

Lu, P., M. Zhang, Q. Li and Y. Xu (2013). Structure and properties of controlled release fertilizers coated with thermosetting resin. Polymer-Plastics Technology and Engineering. 52(4): 381-386.

Luo, J., S. Ledgard and S. Lindsey (2007). Nitrous oxide emissions from application of urea on New Zealand pasture. New Zealand Journal of Agricultural Research. 50(1): 1-11.

Luo, J., S. Saggar, T. van der Weerden and C. de Klein (2019). Quantification of nitrous oxide emissions and emission factors from beef and dairy cattle excreta deposited on grazed pastoral hill lands. Agriculture, Ecosystems & Environment. 270: 103-113.

MacGibbon, R., J. Turner and C. Tozer (2010). Wetland feasibility for nutrient reduction to Lake Rotorua, Bay of Plenty Regional Council.

Mantovani, D., M. Veste, A. Badorreck and D. Freese (2013). Evaluation of fast growing tree water use under different soil moisture regimes using wick lysimeters. iForest-Biogeosciences and Forestry. 6(4): 190.

Matocha, C., P. Dhakal and S. Pyzola (2012). The role of abiotic and coupled biotic/abiotic mineral controlled redox processes in nitrate reduction. Advances in Agronomy. 115: 181-214.

McCurdy, M., C. Davies, A. Gunaratnam, M. Grafton, P. Bishop and P. Jeyakumar (2019). Instrumentation of a bank of lysimeters: Sensors and sensibility. Chemeca 2019: Chemical Engineering Megatrends and Elements: 425.

McLay, C., R. Dragten, G. Sparling and N. Selvarajah (2001). Predicting groundwater nitrate concentrations in a region of mixed agricultural land use: a comparison of three approaches. Environmental Pollution. 115(2): 191-204.

McLenaghen, R., K. Cameron, N. Lampkin, M. Daly and B. Deo (1996). Nitrate leaching from ploughed pasture and the effectiveness of winter catch crops in reducing leaching losses. New Zealand Journal of Agricultural Research. 39(3): 413-420.

Mehta, T., M. V. Coppi, S. E. Childers and D. R. Lovley (2005). Outer membrane c-type cytochromes required for Fe (III) and Mn (IV) oxide reduction in Geobacter sulfurreducens. Applied and environmental microbiology. 71(12): 8634-8641.

Mertens, J., J. Diels, J. Feyen and J. Vanderborght (2007). Numerical analysis of passive capillary wick samplers prior to field installation. Soil Science Society of America Journal. 71(1): 35-42.

Ministry for the Environment (2018). New Zealand's Climate Change Programme. Retrieved 20 April 2019, from http://www.mfe.govt.nz/climate-change/what-government-doing/new-zealands-climate-change-programme.

Minitab, I. (2010). Minitab 16 statistical software.

Misra, R., J. Padhi and J. Payero (2011). A calibration procedure for load cells to improve accuracy of mini-lysimeters in monitoring evapotranspiration. Journal of Hydrology. 406(1-2): 113-118.

Mitchell, K. (1963). Production potential of New Zealand pasture land. New Zealand Institute of Agricultural Science Proc**:** 80-86.

Moir, J., D. Scotter, M. Hedley and A. Mackay (2000). A climate-driven, soil fertility dependent, pasture production model. New Zealand Journal of Agricultural Research. 43(4): 491-500.

Monaghan, R., R. Paton, L. Smith and C. Binet (2000). Nutrient losses in drainage and surface runoff from a cattle-grazed pasture in Southland. Proceedings of the Conference-New Zealand Grassland Association**:** 99-104.

Monaghan, R., L. Smith and S. Ledgard (2009). The effectiveness of a granular formulation of dicyandiamide (DCD) in limiting nitrate leaching from a grazed dairy pasture. New Zealand Journal of Agricultural Research. 52(2): 145-159.

Morassi, S. A., J. L. R. da Silva and A. Ortenzi (2018). Comparative result between standard requirements and finite element analysis of wood-frame panels. Journal of Building Engineering. 15: 78-84.

Mueller, L., A. Saparov and G. Lischeid (2013). Novel measurement and assessment tools for monitoring and management of land and water resources in agricultural landscapes of Central Asia, Springer Science & Business Media.

Nadelhoffer, K., A. Giblin, G. Shaver and J. Laundre (1991). Effects of temperature and substrate quality on element mineralization in six arctic soils. Ecology. 72(1): 242-253.

Naz, M. Y. and S. A. Sulaiman (2016). Slow release coating remedy for nitrogen loss from conventional urea: a review. Journal of Controlled Release. 225: 109-120.

Nielsen, J. L. and P. H. Nielsen (1998). Microbial nitrate-dependent oxidation of ferrous iron in activated sludge. Environmental science & technology. 32(22): 3556-3561.

Nolz, R., G. Kammerer and P. Cepuder (2009). Wind influence on lysimeter measurements in Gross-Enzersdorf. Bericht. 13. Gumpensteiner Lysimetertagung**:** 17-20.

Novillo, J., M. I. Rico and J. M. Alvarez (2001). Controlled release of manganese into water from coated experimental fertilizers. Laboratory characterization. Journal of agricultural and food chemistry. 49(3): 1298-1303.

Novoa, R. and R. Loomis (1981). Nitrogen and plant production. Plant and Soil. 58(1-3): 177-204.

Oenema, O. (2006). Nitrogen budgets and losses in livestock systems. International Congress Series, Elsevier. 1293**:** 262-271.

Paramashivam, D., T. J. Clough, A. Carlton, K. Gough, N. Dickinson, J. Horswell, R. R. Sherlock, L. Clucas and B. H. Robinson (2016). The effect of lignite on nitrogen mobility in a low-fertility soil amended with biosolids and urea. Science of the Total Environment. 543: 601-608.

Peppas, N. A. and J. J. Sahlin (1989). A simple equation for the description of solute release. III. Coupling of diffusion and relaxation. International journal of pharmaceutics. 57(2): 169-172.

Petersen, S. O., S. Stamatiadis and C. Christofides (2004). Short-term nitrous oxide emissions from pasture soil as influenced by urea level and soil nitrate. Plant and Soil. 267(1-2): 117-127.

Plummer, M. A., L. C. Hull and D. T. Fox (2004). Transport of carbon-14 in a large unsaturated soil column. Vadose Zone Journal. 3(1): 109-121.

Pütz, T., B. Brumhard, J. Dressel, R. Kaiser, A. Wüstemeyer, K. Scholz, H. Schäfer, T. König and F. Führ (1998). FELS: a comprehensive approach to studying the fate of pesticides in soil at the laboratory, lysimeter and field scales, ACS Publications.

Qiao, D., H. Liu, L. Yu, X. Bao, G. P. Simon, E. Petinakis and L. Chen (2016). Preparation and characterization of slow-release fertilizer encapsulated by starch-based superabsorbent polymer. Carbohydrate polymers. 147: 146-154.

Qin, K. and D. I. Leskovar (2018). Lignite-derived humic substances modulate pepper and soil-biota growth under water deficit stress. Journal of plant nutrition and soil science. 181(5): 655-663.

R Core Team (2019). R: A Language and Environment for Statistical Computing (Version 3.5. 2, R Foundation for Statistical Computing, Vienna, Austria, 2018). There is no corresponding record for this reference.[Google Scholar].

Radulovich, R. and P. Sollins (1987). Improved performance of zero-tension lysimeters. Soil Science Society of America Journal. 51(5): 1386-1388.

Rajaram, G. and D. Erbach (1999). Effect of wetting and drying on soil physical properties. Journal of Terramechanics. 36(1): 39-49.

Ratering, S. and S. Schnell (2001). Nitrate-dependent iron (II) oxidation in paddy soil. Environmental Microbiology. 3(2): 100-109.

Reid, D. (1972). The effects of the long-term application of a wide range of nitrogen rates on the yields from perennial ryegrass swards with and without white clover. The Journal of Agricultural Science. 79(2): 291-301.

Reis, J. M. L. d. (2012). Effect of temperature on the mechanical properties of polymer mortars. Materials Research. 15(4): 645-649.

Robison, W., E. Stone and T. Hamilton (2004). Large plate lysimeter leachate collection efficiency for water being transported from soil to ground water. Soil Science. 169(11): 758-764.

Romão, B., M. F. Diniz, M. F. Azevedo, V. L. Lourenço, L. C. Pardini, R. C. Dutra and F. Burel (2006). Characterization of the curing agents used in epoxy resins with TG/FT-IR technique. Polímeros. 16(2): 94-98.

Rose, M. T., E. L. Perkins, B. K. Saha, E. C. Tang, T. R. Cavagnaro, W. R. Jackson, K. P. Hapgood, A. F. Hoadley and A. F. Patti (2016). A slow release nitrogen fertiliser produced by simultaneous granulation and superheated steam drying of urea with brown coal. Chemical and Biological Technologies in Agriculture. 3(1): 10.

Ruark, M. (2012). Advantages and disadvantages of controlled-release fertilizers. University of Wisconsin-Madison.

Saggar, S., N. Bolan, R. Bhandral, C. Hedley and J. Luo (2004). A review of emissions of methane, ammonia, and nitrous oxide from animal excreta deposition and farm effluent application in grazed pastures. New Zealand Journal of Agricultural Research. 47(4): 513-544.

Sahari, J. and M. A. Maleque (2016). Mechanical properties of oil palm shell composites. International Journal of Polymer Science. 2016.

Sahoo, P. K., K. Kim and M. Powell (2016). Managing groundwater nitrate contamination from livestock farms: implication for nitrate management guidelines. Current Pollution Reports. 2(3): 178-187.

Sathishkumar, G., G. Rajkumar, K. Srinivasan and M. Umapathy (2018). Structural analysis and mechanical properties of lignite fly-ash-added jute–epoxy polymer matrix composite. Journal of Reinforced Plastics and Composites. 37(2): 90-104.

Scarsbrook, M. and A. Melland (2015). Dairying and water-quality issues in Australia and New Zealand. Animal Production Science. 55(7): 856-868.

Schipper, L. A., R. Parfitt, C. Ross, W. T. Baisden, J. Claydon and S. Fraser (2010). Gains and losses in C and N stocks of New Zealand pasture soils depend on land use. Agriculture, Ecosystems & Environment. 139(4): 611-617.

Schneider, C. A., W. S. Rasband and K. W. Eliceiri (2012). NIH Image to ImageJ: 25 years of image analysis. Nature methods. 9(7): 671-675.

Sear, D., W. Damon, D. Booker and D. Anderson (2000). A load cell based continuous recording bedload trap. Earth Surface Processes and Landforms. 25(6): 659-672.

Sempeho, S. I., H. T. Kim, E. Mubofu and A. Hilonga (2014). Meticulous overview on the controlled release fertilizers. 2014: 1-16.

Seyfarth, M. and S. Reth (2008). Lysimeter soil retriever (LSR)—an application of a new technique for retrieving soils from lysimeters. Water, Air, & Soil Pollution: Focus. 8(2): 227-231.

Shaviv, A. (1996). Plant response and environmental aspects as affected by rate and pattern of nitrogen release from controlled release N fertilizers. Progress in nitrogen cycling studies, Springer**:** 285-291.

Shaviv, A. (2001). Advances in controlled-release fertilizers. Advances in Agronomy. 71: 1-49.

Shaviv, A. and R. Mikkelsen (1993). Controlled-release fertilizers to increase efficiency of nutrient use and minimize environmental degradation-A review. Fertilizer research. 35(1-2): 1-12.

Shoji, S., A. Gandeza and K. Kimura (1991). Simulation of crop response to polyolefin-coated urea: II. Nitrogen uptake by corn. Soil Science Society of America Journal. 55(5): 1468-1473.

Shuford, J., D. Fritton and D. Baker (1977). Nitrate-nitrogen and chloride movement through undisturbed field soil. Journal of Environmental quality. 6(3): 255-259.

Shukla, S. and A. Saxena (2018). Global status of nitrate contamination in groundwater: its occurrence, health impacts, and mitigation measures. Handbook of environmental materials management: 869-888.

Silva, R., K. Cameron, H. Di and E. Jorgensen (2005). A lysimeter study to investigate the effect of dairy effluent and urea on cattle urine N losses, plant uptake and soil retention. Water, Air, and Soil Pollution. 164(1-4): 57-78.

Simmler, M., L. Ciadamidaro, R. Schulin, P. Madejón, R. Reiser, L. Clucas, P. Weber and B. Robinson (2013). Lignite reduces the solubility and plant uptake of cadmium in pasturelands. Environmental science & technology. 47(9): 4497-4504.

Simonne, E. H. and C. M. Hutchinson (2005). Controlled-release fertilizers for vegetable production in the era of best management practices: Teaching new tricks to an old dog. HortTechnology. 15(1): 36-46.

Singh, G., G. Kaur, K. Williard, J. Schoonover and J. Kang (2018). Monitoring of water and solute transport in the vadose zone: A review. Vadose Zone Journal. 17(1): 1-23.

Smith, L., C. deKlein and W. Catto (2008). Effect of dicyandiamide applied in a granular form on nitrous oxide emissions from a grazed dairy pasture in Southland, New Zealand. New Zealand Journal of Agricultural Research. 51(4): 387-396.

Soares, J. R., H. Cantarella, V. P. Vargas, J. B. Carmo, A. A. Martins, R. M. Sousa and C. A. Andrade (2015). Enhanced-efficiency fertilizers in nitrous oxide emissions from urea applied to sugarcane. Journal of Environmental quality. 44(2): 423-430.

Soni, P., V. Salokhe and H. Tantau (2005). Effect of screen mesh size on vertical temperature distribution in naturally ventilated tropical greenhouses. Biosystems Engineering. 92(4): 469-482.

Spalding, R. F. and M. E. Exner (1993). Occurrence of nitrate in groundwater—a review. Journal of Environmental quality. 22(3): 392-402.

Stats NZ (2018). Agricultural and horticultural land use. Retrieved 24 June 2020, from http://archive.stats.govt.nz/browse_for_stats/environment/environmental-reporting-series/environmental-indicators/Home/Land/land-use.aspx#:~:text=At%202016%3A,for%20agricultural%20and%20horticultural%20use.&text=Sheep%20and%20beef%20farming%20was,9.8%20percent%20of%20total%20land.

Steele, K. and T. Dawson (1980). Nitrogen as an aid to pasture establishment and renovation in Northland. New Zealand journal of experimental agriculture. 8(2): 123-129.

Stevenson, B. A., R. Parfitt, L. A. Schipper, W. T. Baisden and P. Mudge (2010). Relationship between soil δ15N, C/N and N losses across land uses in New Zealand. Agriculture, Ecosystems & Environment. 139(4): 736-741.

Strong, W., P. Saffigna, J. Cooper and A. Cogle (1992). Application of anhydrous ammonia or urea during the fallow period for winter cereals on the Darling Downs, Queensland. II. The recovery of 15N by wheat and sorghum in soil and plant at harvest. Soil Research. 30(5): 711-721.

Sung, K., C. Munster, R. Rhykerd, M. Drew and M. Y. Corapcioglu (2003). The use of vegetation to remediate soil freshly contaminated by recalcitrant contaminants. Water Research. 37(10): 2408-2418.

Tang, Y., X. Wang, Y. Yang, B. Gao, Y. Wan, Y. C. Li and D. Cheng (2017). Activated-lignite-based super large granular slow-release fertilizers improve apple tree growth: synthesis, characterizations, and laboratory and field evaluations. Journal of agricultural and food chemistry. 65(29): 5879-5889.

Teitel, M., M. Atias and M. Barak (2010). Gradients of temperature, humidity and CO2 along a fan-ventilated greenhouse. Biosystems Engineering. 106(2): 166-174.

Thompson, M. L. and R. L. Scharf (1994). An improved zero-tension lysimeter to monitor colloid transport in soils. Journal of Environmental quality. 23(2): 378-383.

Thomson, A. J., G. Giannopoulos, J. Pretty, E. M. Baggs and D. J. Richardson (2012). Biological sources and sinks of nitrous oxide and strategies to mitigate emissions, Philosophical Transactions of the Royal Society. 367(1593)**:** 1157-1168.

Tian, H., Z. Liu, M. Zhang, Y. Guo, L. Zheng and Y. C. Li (2019). Biobased Polyurethane, Epoxy Resin, and Polyolefin Wax Composite Coating for Controlled-Release Fertilizer. ACS applied materials & interfaces. 11(5): 5380-5392.

Timmons, R. J. (1987). Sulfur-based encapsulants for fertilizers, Google Patents.

Trenkel, M. E. (2010). Slow-and controlled-release and stabilized fertilizers: an option for enhancing nutrient use efficiency in agriculture, IFA, International fertilizer industry association.

Vallejo, A., M. C. Cartagena, D. Rodriguez and J. Diez (1993). Nitrogen availability of soluble and slow release nitrogen fertilizers as assessed by electroultrafiltration. Fertilizer research. 34(2): 121-126.

Van der Weerden, T., J. Luo, H. Di, A. Podolyan, R. Phillips, S. Saggar, C. de Klein, N. Cox, P. Ettema and G. Rys (2016). Nitrous oxide emissions from urea fertiliser and effluent with and without inhibitors applied to pasture. Agriculture, Ecosystems & Environment. 219: 58-70.

Van Eerd, L., J. Turnbull, C. Bakker, R. Vyn, A. McKeown and S. Westerveld (2017). Comparing soluble to controlled-release nitrogen fertilizers: storage cabbage yield, profit margins, and N use efficiency. Canadian Journal of Plant Science. 98(4): 815-829.

Virtanen, S., A. Simojoki, O. Knuutila and M. Yli-Halla (2013). Monolithic lysimeters as tools to investigate processes in acid sulphate soil. Agricultural water management. 127: 48-58.

Volk, G. and G. Horn (1975). Response Curves of Various Turfgrasses to Application of Several Controlled-Release Nitrogen Sources 1. Agronomy Journal. 67(2): 201-204.

Wachendorf, M., M. Büchter, H. Trott and F. Taube (2004). Performance and environmental effects of forage production on sandy soils. II. Impact of defoliation system and nitrogen input on nitrate leaching losses. Grass and Forage Science. 59(1): 56-68.

Wang, C. F., X. Fan, F. Zhang, S.-Z. Wang, Y.-P. Zhao, X.-Y. Zhao, W. Zhao, T.-G. Zhu, J.-L. Lu and X.-Y. Wei (2017). Characterization of humic acids extracted from a lignite and interpretation for the mass spectra. RSC advances. 7(33): 20677-20684.

Wang, H., D. J. Grant, P. C. Burns and C. Na (2015). Infrared Signature of the Cation− π Interaction between Calcite and Aromatic Hydrocarbons. Langmuir. 31(21): 5820-5826.

Wang, M., R. Hu, J. Zhao, Y. Kuzyakov and S. Liu (2016). Iron oxidation affects nitrous oxide emissions via donating electrons to denitrification in paddy soils. Geoderma. 271: 173-180.

Wang, X.-J., J. Yang, X.-P. Chen, G.-X. Sun and Y.-G. Zhu (2009). Phylogenetic diversity of dissimilatory ferric iron reducers in paddy soil of Hunan, South China. Journal of Soils and Sediments. 9(6): 568-577.

Wang, Y., X. Zhang, J. Chen, A. Chen, L. Wang, X. Guo, Y. Niu, S. Liu, G. Mi and Q. Gao (2019). Reducing basal nitrogen rate to improve maize seedling growth, water and nitrogen use efficiencies under drought stress by optimizing root morphology and distribution. Agricultural water management. 212: 328-337.

Water Research Center (2020). Nitrates and Nitrites in Drinking Water Groundwater and Surface Waters. Retrieved 12th December 2020, from https://www.water-research.net/index.php/nitrate.

Way, T., J. Lamba and P. Srivastava (2011). A method for installing zero-tension pan and wick lysimeters in soil. Applied Engineering in Agriculture. 27(5): 747-755.

Wedderburn, M., J. Crush, W. Pengelly and J. Walcroft (2010). Root growth patterns of perennial ryegrasses under well-watered and drought conditions. New Zealand Journal of Agricultural Research. 53(4): 377-388.

Weihermüller, L., J. Siemens, M. Deurer, S. Knoblauch, H. Rupp, A. Göttlein and T. Pütz (2007). In situ soil water extraction: a review. Journal of Environmental quality. 36(6): 1735-1748.

Wild, A. and K. Cameron (1980). Soil nitrogen and nitrate leaching. In'Soils and Agriculture'.(Ed. PB Tinker.) pp. 35-70, Blackwell: Oxford.

Wilson, L. G., L. G. Everett and S. J. Cullen (2018). Estimating the transport and fate of contaminants in the vadose zone based on physical and chemical properties of the vadose zone and chemicals of interest. Handbook of vadose zone characterization & monitoring, CRC Press.

Wong, M. H. and A. Bradshaw (1982). A comparison of the toxicity of heavy metals, using root elongation of rye grass, Lolium perenne. New Phytologist. 91(2): 255-261.

Xiaoyu, N., W. Yuejin, W. Zhengyan, W. Lin, Q. Guannan and Y. Lixiang (2013). A novel slow-release urea fertiliser: Physical and chemical analysis of its structure and study of its release mechanism. Biosystems Engineering. 115(3): 274-282.

Xu, F., S. Pan, C. Liu, D. Zhao, H. Liu, Q. Wang and Y. Liu (2017). Construction and evaluation of chemical structure model of Huolinhe lignite using molecular modeling. RSC advances. 7(66): 41512-41519.

Yazawa, Y., M. Wong, R. Gilkes and T. Yamaguchi (2000). Effect of additions of brown coal and peat on soil solution composition and root growth in acid soil from wheatbelt of Western Australia. Communications in soil science and plant analysis. 31(5-6): 743-758.

Zaman, M., M. Nguyen, J. Blennerhassett and B. Quin (2008). Reducing NH3, N2O and $${\text {NO}} _3^-$$–N losses from a pasture soil with urease or nitrification inhibitors and elemental S-amended nitrogenous fertilizers. Biology and Fertility of Soils. 44(5): 693-705.

Zaman, M., M. Nguyen, J. Blennerhassett and B. Quin (2008). Reducing NH3, N2O and NH3-N losses from a pasture soil with urease or nitrification inhibitors and elemental S-amended nitrogenous fertilizers. Biology and Fertility of Soils. 44(5): 693-705.

Zvomuya, F., C. J. Rosen, M. P. Russelle and S. C. Gupta (2003). Nitrate leaching and nitrogen recovery following application of polyolefin-coated urea to potato. Journal of Environmental quality. 32(2): 480-489.

Appendix

Appendix 1.

The chamfer of the metal disk and lysimeter body alignment to the moving axis.

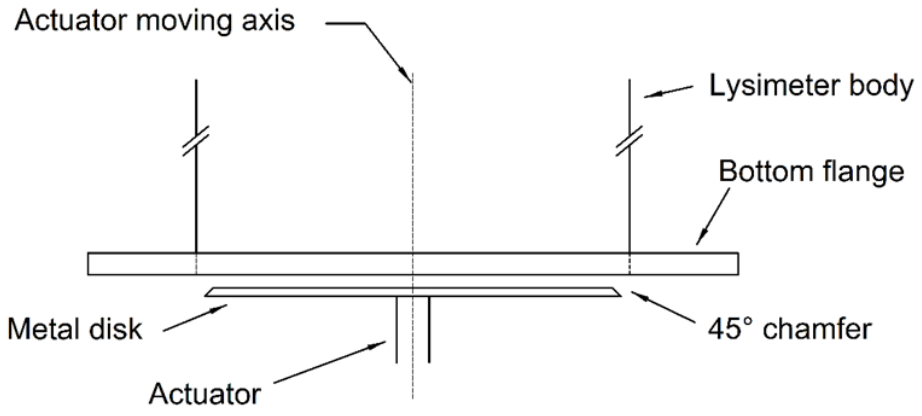

Appendix II.

The finite element mesh used for numerical analysis; (a) top-wood plate and (b) lysimeter body.

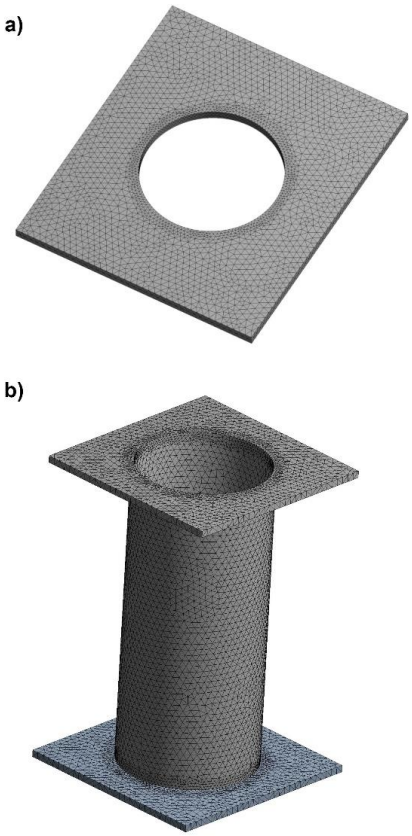

Appendix III.

The calibration curve of the load cell. The black square and red triangle points shows loading and unloading of known weights, respectively. Y axis is load cell reading in random values (RV). Black line is the linear regression line.